On the analysis of singly-propped diaphragm walls.

Li, Shing Foon

ON THE ANALYSIS OF SINGLY-PROPPED DIAPHRAGM WALLS

by

Shing Foon Li

A Dissertation submitted for the

Degree of Doctor of Philosophy

at

University of London

Civil Engineering Department

King's College

May 1990

To my Wife

ABSTRACT

This thesis reports a study of the behaviour of diaphragm walls in over-consolidated clay, singly-propped at either the crest or formation level.

Initially, the analysis of walls propped rigidly at the crest was considered. The limitations of a finite element program and the soil parameters adopted were investigated with reference to the results of a centrifuge test, which modelled the events from excavation of the soil in front to collapse. The calculated and measured soil movements, pore water pressure distributions, bending moments and prop loads were compared. The program was then used to investigate the behaviour of deeper walls under working conditions.

A different approach to the limit equilibrium method, based on mobilising full passive pressure in front of the wall, was used to calculate the bending moments under working conditions for over-consolidated soil and the inconsistency of the methods currently used was highlighted. A simple method based on idealised deformation patterns was also used to assess the serviceability of relatively rigid walls propped at the crest. The applicability of this simple approach was investigated with reference to the soil:wall stiffness and compared with numerical analyses and previous experimental results.

For walls propped rigidly at formation level, a rigorous treatment of soil:structure interaction is often considered necessary because of their remoteness from collapse. Finite element analyses were carried out for walls of different stiffness and embedment ratios. Bending moments, prop loads and movements were calculated.

Finally a series of analyses was carried out to investigate some factors affecting the practical design of walls propped at final formation level. The effect of installing a temporary prop during excavation was evaluated. More realistic prop behaviour was investigated by modelling a reinforced concrete slab at formation level so that both wall movement and heave of the excavated soil surface were allowed. The effects of different soil stiffness and pre-excavation earth pressure conditions were discussed.

ACKNOWLEDGEMENT

The work in this dissertation was carried out at a time just prior to the closure of the Civil Engineering Department at King's College. During this turbulent period, numerous problems were encountered and solved, often with the advice and help from other colleagues. I would first like to thank my supervisor, Dr W Powrie, for his continuous interest and enthusiasm throughout the project. His support extended beyond the academic work by offering constant encouragement and stimulation, and the arrangement of the financial support at the final stage was particularly helpful. I am also grateful for his reading and correcting the manuscripts with his usual thoroughness.

I would also like to express my thanks to Dr R H Bassett for initiating my interest in research during my undergraduate studies at King's College, and supervision at the early stage of this project. I am grateful to Dr A M Britto of Cambridge University for permission to use the program CRISP and the helpful discussion when problems arose. Thanks are also due to Mr R Postolowsky of Newcastle-Upon-Tyne City Council for providing the information for the Cradlewell Bypass project.

I am grateful to Dr P Payne and Mrs M O'Hara of the Croucher Foundation Scholarship for providing the financial support, without which my work will not be possible.

Although mere thanks are grossly inadequate, I must acknowledge my wife Isabelle. Her encouragement from the beginning and the tender care throughout were my main steam when I was down. She also provided the professional typing for the manuscripts in this dissertation.

Finally I would like to say thank you to all my colleagues, Jackson, David, Eddie and Jessie, in the Soil Mechanics group for their helpful discussions and innovative ideas.

TABLE OF CONTENTS

LIST OF TABLES

NOTATION

A,B,C,D	Constants defined in text
C_u	Undrained shear strength
E	Young's modulus
E_o	1-dimensional modulus of elasticity
E_u	Undrained modulus of elasticity
EI	Flexural rigidity for wall
F	Force in the prop Factor of safety (usually with subscript defined in text)
G	Shear modulus
G^*	Rate of increase in shear modulus with depth ($G^*=G/z$)
H	Total length of retaining wall
I	Second moment of area of wall
K	Bulk modulus Earth pressure coefficient
K_o	Pre-excavation earth pressure coefficient
K_a	Active earth pressure coefficient
K_p	Passive earth pressure coefficient
K_{nc}	Earth pressure coefficient after 1-dimensional normal consolidation
M	Wall bending moment
N	Specific volume on isotropic consolidation line at p'=1 kPa
OCR	Over-consolidation ratio (calculated based on effective vertical stress, σ'_{vmax}/σ'_v)
P	Flexibility ratio ($=wH^4/EI$)
PI	Plasticity index
R	Resultant force defined in text
V	Specific volume ($V=1+e$)
V_κ	Specific volume on swelling line at p'=1 kPa
W	Weight of Coulomb soil wedge
Z	Depth

bgl	Below ground level
c	Cohesion intercept
d, d_o	Depth of embedment for diaphragm wall
e	Void ratio
e_o	Void ratio on critical state line at p'=1 kPa ($e_o = \Gamma-1$)
g	Slope intercept for Hvorslev surface
h	Slope for Hvorslev surface Retained height for diaphragm wall
k	Soil permeability (usually with subscript)
m	Retained height ratio (retained height to total wall length)
n	Gravity scaling factor
p	Mean normal stress (= $(\sigma_1+\sigma_2+\sigma_3)/3$)
p_c'	Equivalent stress: value of p' at the point on the normal consolidation line at the same specific volume
p_{cs}'	Value of p' at the point on the critical state line at the same specific volume
q	Deviatoric stress ($=(\sigma_1-\sigma_3)$ for triaxial plane)
s	Slope of no tension cut-off in Schofield soil model
u	Pore water pressure
w	Unit weight of soil (used alternatively to avoid confusion with shear strain)
wc	Water content
x	Linear dimension
y	Linear dimension Horizontal wall displacement
z	Depth

α,β	Plane of maximum shear stress in stress field analysis
γ	Unit weight of soil Shear strain
γ_{sat}	Saturated unit weight of soil
γ_w	Unit weight of water
δ	Angle of friction at soil/wall interface Displacement Incremental change
ϵ	Strain (usually with subscript)
ϵ_s	Shear strain
ϵ_v	Volumetric strain
M	Slope of critical state line in p'-q plane
λ	Slope of critical state line in V-$\log_e$p' plane
κ	Slope of swelling line in V-$\log_e$p' plane
ν	Poisson's ratio
ϱ	Rowe's flexibilty number (=H^4/EI)
σ	Stress (usually with subscript)
τ	Shear stress
ϕ'	Angle of soil friction (usually with subscript)
ϕ_H'	Angle of soil friction for Hvorslev surface

The following subscripts are often used in conjunction with the symbols listed in previous pages:

a	Active
p	Passive
v	Vertical
h	Horizontal
x,y	X-Y plane
a,b	Arbitrary A-B plane
o	Initial
u	Undrained value
cri	Critical
mob	Mobilised
peak	Peak
1,2,3	Principal planes

Symbol with prime (') denotes its equivalent effective value

CONVENTION

1. Except otherwise specified, compressive normal stress and anti-clockwise shear stress are taken as positive.

2. Bending moments are drawn on tensile side.

3. All quantities used throughout this dissertation are in SI unit, unless otherwise stated.

CHAPTER 1

GENERAL INTRODUCTION

CHAPTER 1 - GENERAL INTRODUCTION

1.1 Introduction

As inner-city building land becomes scarcer and more expensive, there is an increasing demand for the construction of deep basements in office blocks and other urban developments. In addition, when improvements to existing transport corridors through city centres are needed, or sometimes to reduce the environmental impact, roads are often required to run in cuttings and cut-and-cover tunnels. The advancement in piling and slurry trench construction methods during last two decades and the improved understanding of soil behaviour have resulted in the increasing use of free or propped embedded insitu retaining walls in these situations.

The construction of diaphragm walls generally involves the digging of a trench to the desired depth under re-circulating bentonite slurry. A steel reinforcing cage is lowered into the trench and the slurry is then replaced by the concrete. The soil in front of the wall will be excavated once the concrete is set. These walls serve to maintain stability of the cutting or tunnel sides, preventing excessive movements and reducing water seepage into the excavation.

Recent studies of diaphragm-type retaining walls have found that their behaviour is influenced by many factors, including the geometry and stiffness of the wall, the soil properties, the stress history of the ground, the ground water regime and the method of construction. In this dissertation, the finite element method will be employed to examine the effects of some of the factors outlined. Results from experiments and other methods of analysis will be compared with the findings of the numerical analyses.

1.2 Review of Current Practice in the Analysis of Retaining Walls

In engineering practice, soil is considered as a continuum consisting of soil particles and void filled with water and air. In 1936, Terzaghi presented an important theory that the total stress for a saturated soil is made up of two parts - effective stress and pore water pressure - which are related by equation 1.1.

$$\text{Effective stress} = \text{Total stress} - \text{Pore water pressure}$$
$$\sigma' = \sigma - u \quad \ldots\ldots\ldots\ldots\ldots\ldots \quad (1.1)$$

He further stated that the deformation of a soil skeleton is exclusively determined by the change in the effective stress σ' and the shear stress τ. This is the most important concept in the understanding of soil mechanics. The following discussions are confined to the effective stress analysis of soil having a failure envelope governed by $\tau = \sigma' \tan\phi'$ where τ and σ' are respectively the normal and shear components of stress on the plane of maximum stress ratio and ϕ' is the soil friction angle.

1.2.1 Collapse Limit Analysis

The conventional design of a diaphragm wall generally involves investigating the wall stability by assuming that the adjacent soil is on the verge of failure, and applying a lumped factor of safety both to account for uncertainties and to limit the wall movement under working conditions. Therefore it is appropriate to consider first the limit analysis where the soil is on the verge of collapse.

In 1773, Coulomb introduced perhaps the earliest method for determining the stability of a retaining wall. He calculated the thrust on the wall by considering the equilibrium of a wedge of soil bounded by the wall, the

free ground surface and an assumed rupture surface. Although he realised that the failure plane might be curved, he applied the method to plane rupture surfaces only (fig. 1.1). This was essentially an upper bound approach. In this method it is necessary to search for the worst failure mechanism, i.e. the inclination of the failure plane, which results in the least stable condition. For a smooth wall, the solution can be found fairly easily by differentiation of the thrust with respect to the slope. However, the solution for a rough non-vertical wall with an inclined ground surface is not so straightforward and is normally solved graphically (Bolton, 1979).

The main problem associated with Coulomb's method is the assumption of a plane failure surface. This might result in an unsafe mechanism which over-estimates the resisting force under passive conditions, particularly when the mobilised wall friction is large. Later, Fellenius (1927) and Rendulic (1935) improved Coulomb's approach by investigating different failure mechanisms, such as a circular rupture for undrained failure and a logarithmic spiral for dilatant soil. However none of these methods provide any information on the stress state of the soil.

In 1857, Rankine introduced a contrasting method of retaining wall analysis, in which the earth pressures acting on the wall were calculated. He assumed that the wall was smooth and that movement would be sufficient to cause a state of passive failure in the soil in front of the wall and active failure in the soil behind (fig. 1.2). This was essentially a lower bound approach based on a system of stresses which was everywhere in equilibrium and did not violate the failure condition at any location. At failure, the horizontal stress on either side of the wall can be calculated with reference to Mohr's circle of stress

as shown in fig. 1.3. However to be a true lower bound, the stress field should be extended to infinity with the failure condition not violated anywhere.

If the wall surface is rough, the soil near the wall will be sheared by the friction, resulting in a rotation of the principal stress direction. Rankine's solution can, in principle, be modified to deal with such a situation as shown in fig. 1.4. However, the solution is only straightforward if the weight of the soil is ignored.

In 1965, Sokolovskii proposed the method of characteristics, which was essentially an extension of Rankine's solution. It enabled the self-weight of the soil to be inlcuded in the calculation. His idea was based on the planes of maximum stress ratio (α and β planes) in the Mohr's circle of stress which lie at angles of $\pm(45°+\phi'/2)$ to the plane on which the major principal stress acts. By considering every point for which the Mohr's circle touches the failure envelope throughout a region of failing soil, it is possible to construct familes of α and β characteristics. In theory, once the boundary conditions are defined, it is possible to obtain a solution by finding the stress conditions at every point within the soil.

1.2.2 Overall Stability

Generally, in the design of a retaining wall, the stability against horizontal, vertical and rotational movement has to be considered. At present, it is assumed that the wall thickness is small in comparison with other dimensions, and that the bearing capacity of the soil at the toe is not a controlling criterion. However, for a load bearing concrete diaphragm wall, it is necessary to check the potential failure in this mode. Also, it is customary in

current practice to ignore the shear resistance acting on the base of the wall in considering horizontal equilibrium.

For diaphragm walls propped near the crest or cantilevered, two methods are commonly used, namely fixed earth support and free earth support methods. The difference between these two methods lies in the assumption of fixity near the lower half of the wall. The free earth support method assumes that the toe of the wall is free to rotate and there is no passive resistance to the backward movement of the bottom of the wall. The idealised wall deflection and earth pressure distribution are shown in fig. 1.5. The depth of embedment is then determined by taking moments about the position of the prop. Obviously this method can only be applied to propped walls for which the lateral equilibrium is provided by the prop.

In contrast, the fixed earth support method assumes that the base of the wall is prevented from rotation by the passive resistance behind it. Fig. 1.6 shows the deflected shape and pressure distributions for a cantilevered wall (Padfield & Mair, 1984). For limit equilibrium analysis, the pressure distribution is idealised by introducing smooth stress discontinuities at the level of rotation. In the full analysis, the calculation of the depth of embedment involves equating the horizontal forces and taking moments about point of rotation. If pore water pressures are taken into account, this results in two equations which are quartic and simultaneous in the two unknowns, d and z. The iterative solution of these equations by hand is tedious, but may be easier with the aid of a micro-computer. Nevertheless, because of the complexity of the full solution, a simplified version is commonly used, in which a horizontal force R at the toe is taken to represent the resultant pressure which provides the fixity. By taking moments about the toe, the depth of embedment can be obtained. The final depth of embedment is

increased empirically, normally by 20%, to reflect the additional length of the wall required to develop the passive force R. This method is applicable to both propped and cantilevered retaining walls. However, for a rigid wall which is adequately propped, there is no failure mechanism corresponding to the fixed earth support assumption and its use is not recommended by Padfield & Mair (1984).

For walls propped nearer dredge level, provided the prop does not fail, the sense of wall rotation is not obvious. Bolton (1979) used an example of rigid sheets retaining dry sand to demonstrate that the failure mechanism would depend on the position of prop. This approach may be used for retaining walls propped at dredge level, for which the wall rotation is also dependent on the relative retained height to embedment ratio. This will be discussed in more detail in chapter 5.

1.2.3 Factors of Safety

The methods outlined in previous section concern only the stability of the wall on the verge on collapse. In design, it is traditional to incorporate a factor of "safety" to account for uncertainties in the soil parameters and the design philosophy. Also, the factor of safety is intended to restrict the soil and wall movements to within the limit required for serviceability.

There are at least three distinct ways in which the factor of safety might be applied in designing the diaphragm wall; namely factor on embedment, factor on strength and factor on bending moment. Burland et al (1981) compared these methods and found that there was considerable inconsistency under different conditions. They subsequently proposed a new method based on the bearing capacity analogy. The use

of these methods and the recommended values for the factor of safety are detailed by Padfield & Mair (1984) and Bica & Clayton (1989).

All the methods used currently assume that the soil mobilises the full active strength with only small wall movement, whereas the full passive strength will require a comparatively large deformation. However, for over-consolidated clay, the insitu horizontal effective stress is likely to be larger than the vertical effective stress (i.e. $K_o > 1$) and the stress state is closer to passive failure than is the case for a normally consolidated soil. Therefore the assumptions used in the conventional limit equilibrium calculations may not be appropriate to over-consolidated clays. In Chapter 4, an alternative approach, based essentially on the mobilisation of full passive pressure in front of the wall, is outlined. Although strictly this may not be the real situation, it at least represents an upper bound to the magnitude of the bending moments.

1.2.4 Wall Bending Moments

The bending moment under working condition can be estimated by either of the following methods (Padfield & Mair, 1984):

i) Using the unfactored soil parameters to determine the depth of embedment required and then calculating the bending moments corresponding to this wall length. The additional depth for safeguarding the wall under working conditions is ignored.

ii) Postulating a permissible stress distribution which is in moment and force equilibrium over the actual wall length. The bending moments are then calculated accordingly. Sometimes, the stress distribution will be difficult to assess.

Throughout this dissertation, whenever the limit equilibrium calculation is employed, the latter method is used to find the bending moments. The stress distributions at working conditions are estimated by applying factors of safety, either on bending moment equilibrium (CP2, 1951) or on strength.

1.2.5 Limitations of Current Design Practice

The main disadvantage of many current design methods is the lack of information on soil and wall deformations. In addition, there is no consideration of the insitu stress condition, which is sometimes critical to the wall behaviour prior to collapse. Furthermore, Rowe (1952) pointed out that the wall bending moments are normally a function of the wall flexibility ($\varrho = H^4/EI$), which is not accounted for in the limit equilibrium analysis. The last, but not the least, is that the time taken for excess pore water pressure dissipation is currently ignored, and either an undrained or a drained analysis is performed. In the next few chapters, some of these factors will be investigated using either the finite element analysis or a simplified method taking due account of the stress-strain behaviour of the soil.

1.3 Finite Element Method

Finite element methods were first generally used in the early 1940's by aircraft engineers. With the fast development of computer technology, the use of finite element methods became more popular. The principle of this method is to divide the structure or material being considered into large number of elements joined by a number

of nodes. Interpolating polynomials are then used to describe the variation of a field variable (e.g. stresses and strains in solid mechanics) within an element.

The displacement approach of finite element method involves expressing the displacement inside each discrete element as a polynomial function of the displacement at the nodal points and the position of the element (Zienkiewicz, 1967). The condition of compatibility is then used to obtain the strains inside the element by means of the nodal displacements. The next step is to apply the stress-strain relationship (D-matrix) for the material to determine the stresses inside the elements in terms of the nodal displacement. Finally the principle of virtual work is used to find the equivalent nodal forces which are in equilibrium with this state of internal stresses. These nodal forces should balance the loads due to self-weight and boundary stresses. The details of the finite element method can be found in many books, such as Irons & Ahmad (1980).

In theory, any irregular geometry can be discretised into small elements of regular shape, usually triangles and quadrilaterals. Hence using finite element methods it is possible to solve nearly all kinds of boundary value problems, even though closed-form analytical solutions may not be available. A particular advantage of finite element methods is the comparative ease with which a non-homogeneous and anisotropic material, such as soil, can be handled. Also the accuracy can be improved with the use of higher-order elements at the expense of additional computer resources.

Although the finite element method may have many merits, its use is not without reservations (Irons and Ahmad, 1980). Firstly there is no guarantee of accuracy without careful justification of input information. Secondly,

although the linear elastic modelling is fairly well understood, the development of non-linear elastic behaviour and the application of plasticity theory to the finite element method are still not yet fully explored. Therefore there may sometimes be difficulties in relating stress and strain using simple polynomials.

1.3.1 Finite Element Program CRISP

CRISP (CRItical State Programs) is a set of finite element programs used principally for soil mechanics. It has been written and developed by research workers in the Cambridge University Engineering Department Soil Mechanics Group since 1975 (Britto and Gunn, 1987). This program was one of the first programs to implement the critical state model of soil mechanics into the finite element analysis.

The program, at present, can perform drained, undrained or fully-coupled consolidation analyses of two-dimensional plane strain or axi-symmetric and three-dimensional analyses. The soil models which can be used include anisotropic elasticity, non-homogeneous elasticity (Young's Modulus E varies with depth), critical state soil models and elastic-perfectly plastic models incorporating various failure criteria. For a general linear strain approximation, 6 noded triangles (LST) and 8 noded quadrilaterals (LSQ) are available. 15 noded cubic strain triangles (CuST) can be used for a higher order approximation. For three dimensional analyses there is a 20 noded linear strain brick element (LSB). To cater for some special situations, slip, beam and bar elements were recently included.

It is well known that soil has a non-linear stress-strain response under most circumstances, and the implementation of this in finite element programs is not straightforward. CRISP uses a incremental or tangent stiffness approach.

The loadings are divided into a number of small increments and the program applies each of these incremental loads in turn. In each increment the stiffness properties appropriate to the current stress level are used in the computation. The main disadvantage of this approach is that if too few increments are used, it produces a weaker response for a strain-hardening model and displacements are subsequently over-estimated. In contrast, an alternative approach is based on iterations, which can use a larger size of increments. To correct for the error, iterations are carried out within each increment until convergence to the non-linear load-displacement curve is obtained. Sometimes convergence may not be achieved by this approach with the critical state soil models (Britto and Gunn,1987).

There are two special features in CRISP which facilitate the modelling of some geotechnical problems. First, the program is capable of modelling problems in which soil is excavated or added. CRISP allows the element stiffness to be added to or removed from the mesh when backfilling or excavation occurs. The implied loadings for both cases are then calculated automatically and incorporated into the increment.

Secondly, CRISP allows consolidation to be included in the analysis. As already mentioned in the previous section, soil mechanics problems should generally be analysed by using the effective stresses acting on the soil skeleton. This introduces the pore water pressure as an extra unknown. Hence some types of element in CRISP have additional nodes to deal with this further degree of freedom (fig. 1.7).

This program has been used successfully in the past to model various kinds of geotechnical problems, such as

ground movements associated with tunnels (Taylor, 1984), reinforced embankments on soft foundations (Guest, 1990) and axisymmetric shaft excavations (White, 1987).

CRISP was first brought to King's College London in 1986. The program was substantially the 1984 version. The program was installed to run on the VAX computers (models 8600 & 8700) at King's and to provide a graphical output facility using the GINO graphic package (version 2.7c). During the period of this research, various new developments were incorporated into the program. Also some bugs and deficiencies came to light: these are inevitable in such a large and sophisticated program. Generally, these problems were discussed with Dr. A. Britto of Cambridge University and the necessary remedial work was carried out. Some of them will be mentioned in the appropriate sections.

1.4 Critical State Soil Mechanics

In order to apply the finite element method successfully, a mathematical model that can describe the behaviour of soil as closely as possible has to be established. It is generally accepted that the stress-strain relationship of soil depends on its current stress state and previous stress history, and also on the stress-strain paths to which it is subjected. In modelling the behaviour of diaphragm walls, it is anticipated that the changes in stress may be large - particularly when the soil starts yielding. The stress variation is even more severe in modelling the centrifuge test when the gravity level is increased to 125g. Among all the options available in CRISP, only the critical state soil models are able to satisfy the criterion of varying stiffness with stress level and therefore just these models are considered in the analyses in the next few chapters.

In this section, a brief description of Cam-clay models and the definitions of various parameters will be given. It is intended to provide a frame of reference for the rest of the dissertation. For a complete discussion for Critical State Soil Mechanics, see Schofield & Wroth (1968) or Atkinson & Bransby (1978).

1.4.1 Plasticity

The theory of critical state soil mechanics was originated from the application of plasticity theory. To describe completely the stress-strain relationship for an elasto-plastic material, three different properties have to be specified:-

a) **Yield function:** this is a surface in stress space which separates two types of soil behaviour. When the stress state is described by a point within this surface, the material is in some way elastic and the soil exhibits a reversible response to loading. When the stress state is on the yield surface, it exhibits large irrecoverable deformation, i.e. yielding, in response to continued loading. Stress states outside the yield surface are not permissible.

b) **Hardening law:** this determines the increase in size of the yield surface when the material is undergoing yielding. For a strain softening material, the yield surface will contract instead of expand.

c) **Flow rule:** this gives the ratios of the plastic strain increments when the material is yielding in a particular stress state. A plastic potential is often defined in principal stress space and then the plastic strain increment vector is normal to this

surface. If the plastic potential is the same as the yield surface, the material is said to have an associated flow rule.

1.4.2 Cam-clay

Cam-clay is the name given to an elasto-plastic soil model: it is not a natural clay. The model uses three parameters - effective mean normal stress p′, deviatoric stress q and the specific volume V - to describe the state of a soil. It can be used to model the behaviour of many real soils if appropriate parameters are chosen. The basic assumptions for Cam-clay are:-

a) the equations for various lines in V-$\log_e$ p′ space:

isotropic normal consolidation:

$$V = N - \lambda \log_e p' \quad \ldots\ldots\ldots\ldots\ldots \quad (1.2)$$

critical state:

$$V = \Gamma - \lambda \log_e p' \quad \ldots\ldots\ldots\ldots\ldots \quad (1.3)$$

isotropic swelling:

$$V = V_\kappa - \kappa \log_e p' \quad \ldots\ldots\ldots\ldots\ldots \quad (1.4)$$

The definitions of the various parameters are shown in fig. 1.8

b) the plastic work done (and flow rule) when yielding is governed by the expression:

$$p' \delta v^p + q \delta \epsilon^p = M p' \delta \epsilon^p \quad \ldots\ldots\ldots\ldots \quad (1.5)$$

c) elastic shear strains are zero.

Assuming that the normality condition applies, the yield surface for Cam-clay model can be found by applying the

flow rule and the normality condition of plasticity theory (i.e. plastic strain increment vector is normal to the plastic potential) and the equation is (see fig. 1.9a):

$$q = Mp' \log_e(p_c'/p') \quad \ldots\ldots\ldots\ldots\ldots\ldots \quad (1.6)$$

1.4.3 Modified Cam-clay

Modified Cam-clay changes the assumed plastic work done to:

$$p' \delta v^p + q \delta \epsilon^p = p' \sqrt{[(\delta v^p)^2 + (M \delta \epsilon^p)^2]} \quad \ldots\ldots \quad (1.7)$$

and subsequently the yield surface becomes:

$$q^2 = M^2 p'(p_c' - p') \quad \ldots\ldots\ldots\ldots\ldots\ldots \quad (1.8)$$

The modified Cam-clay yield locus is elliptical in shape as shown in fig. 1.9b.

1.4.4 Schofield Model

For the reasons stated in section 2.2.1, a hybrid soil model called the Schofield model is used for the finite element analyses in this dissertation. This model incorporates a three-part yield surface (Schofield,1980) as shown in fig. 1.9c:

a) yielding: this is identical to the Cam-clay yield surface when $(q/p') < M$,

b) rupture: this region is governed by the Hvorslev failure criterion (Hvorslev surface) (see fig. 1.9c for notations of variables):

$$\frac{q}{p_c'} = g + h \left(\frac{p'}{p_c'}\right) \quad \ldots\ldots\ldots\ldots\ldots\ldots (1.9)$$

The Hvorslev surface intersects the Cam-clay yield surface and the critical state line at the critical state appropriate to the specific volume under consideration, and therefore the yield function of this surface can be found:

$$q = (M-h)\exp\left(\frac{\Gamma-V}{\lambda}\right) + hp' \quad \ldots\ldots\ldots\ldots \quad (1.10)$$

However, the program CRISP, in common with many continuum finite element programs, cannot model rupture behaviour and interprets this surface as a distorted yield surface. When the stress state reaches this boundary, the soil yields instead of ruptures as would occur in reality.

c) no tension cut-off: this results from the inability of the soil to support tensile stresses. If the stress in a soil reaches a state where the minor principal stress is zero, any further reduction in stress would result in the development of a tension crack.

1.5 Outline of This Dissertation

In the following chapters, a study of the post-excavation behaviour of diaphragm walls, singly-propped either at the crest or at dredge level, will be presented. The effects of the installation of the wall represent an important but separable problem, and will not be considered.

In chapter 2, a brief description of the work carried out by Powrie (1986), which formed the basis of some of the finite element analyses which follow, will be presented. The numerical model will be discussed with reference to the analysis of a wall of shallow embedment propped at the crest, which served in effect to calibrate the details of the modelling procedure and the soil parameters employed.

A study of walls of deeper embedment with different flexural stiffness is presented in chapter 3. The wall behaviour prior to collapse was investigated, with particular emphasis on the variation in earth pressures, wall bending moments and prop loads.

In chapter 4, the applicability of various limit equilibrium-based techniques is assessed. A simple method which takes account of the stress-strain behaviour of the soil and enables the estimation of soil and wall deformations for stiff walls propped at the crest, is then discussed.

In chapter 5, the behaviour of walls propped at dredge level is considered. Limit equilibrium calculations based on different failure mechanisms are first presented. Finite element analyses and test results are then compared with these calculations. Finally, a series of analyses carried out to investigate the various factors affecting practical design and construction is describe in chapter 6.

The main points of this dissertation are summarised in chapter 7, where recommendations for further research are also made.

CHAPTER 2

NUMERICAL ANALYSIS OF WALL OF SHALLOW EMBEDMENT PROPPED AT THE CREST

CHAPTER 2 - NUMERICAL ANALYSIS OF WALL OF SHALLOW EMBEDMENT PROPPED AT THE CREST

Although the finite element program CRISP has been widely used to predict and investigate the behaviour of a variety of geotechnical structures, the applicability of the program and the input parameters still need to be justified for any specific problem. In this chapter, therefore an analysis is carried out on a diaphragm wall propped at the crest, and the results compared with the appropriate experimental data.

2.1 Description of Previous Work

An extensive investigation into the post-excavation behaviour of diaphragm walls in over-consolidated clay had been carried out by Powrie (1986). The aim of his study was to identify the factors which affect the behaviour both under working conditions and the collapse of diaphragm walls in heavily over-consolidated clay. These results formed a good basis for comparison with the finite element calculations. Powrie's work involved a series of centrifuge tests which modelled walls of 10m retained height with embedment depths of 5m, 10m, 15m and 20m. The walls were either cantilevered, propped at the crest or propped at dredge level. In his report, pore water pressures, bending moments, prop loads and soil and wall movements from each experiment were presented. He also calculated the bending moments and prop loads for the walls, based on an assumed equilibrium stress distribution. In all tests, the clay used was speswhite kaolin. The clay was first mixed under partial vacuum to a slurry of moisture content of 120%. Then the soil sample was one-dimensionally consolidated gradually in a chamber to an eventual vertical effective stress of 1250 kPa. After that the sample was unloaded to a vertical effective stress of

80 kPa, resulting in an over-consolidation ratio of 15.6. The estimated stress path is shown in fig. 2.1.

At a mean effective stress of just under 100 kPa, the clay was removed from the consolidation chamber and cut to receive the aluminium model diaphragm wall. The soil on the excavated side was removed at the same time and replaced by a rubber bag containing zinc chloride solution mixed to the same unit weight as the soil. By doing this, a pre-excavation lateral earth pressure coefficient of unity was imposed at least above formation level on the excavated side of the wall. A sheet of porous plastic was also placed at the bottom of the sample to provide bottom drainage and reduce the reconsolidation time in the centrifuge. The whole model was then taken up to a radial acceleration of 125g in the centrifuge, and sufficient time was allowed for the excess pore water pressure to dissipate. During this reconsolidation stage, the water level was maintained near the soil surface and the condition eventually became hydrostatic. The excavation process was modelled by the drainage of the zinc chloride solution to the pre-formed excavation level.

In most tests, the post-excavation water table on the excavated side was kept at soil surface. At the bottom, no water was allowed to drain, but the porous plastic acted as an internal drain and became an equipotential in the steady state. The pore water pressure regime is therefore different from that corresponding to an impermeable boundary at the same level. Flow nets for the two boundary conditions are shown in fig. 2.2.

Throughout the test, pore water pressures were monitored by transducers at various locations. The ground surface and lateral wall movements were recorded by standard linear variable differential transformers (LVDTs). In addition,

in-flight photographs were taken at intervals. After measuring the photographic negatives and processing the data, an overall pattern of soil movements around the wall could be obtained. In cases where the results from LVDTs and photographs were compared they were found to be in reasonable agreement. Strain gauges were fixed on the model wall so that bending moments could be calculated from the measured differential strains on both sides of wall at particular depths. For propped walls, load cells capable of reading axial forces were used to record the prop loads developed during the tests.

Powrie had in total carried out five tests on walls propped at the crest, as summarised in table 2.1.

Author's analysis reference	Powrie's test reference	Wall embedment (m)	Prop location	Wall stiffness EI ($\times 10^6$ kN/m^2)
R250	DWC11	5	Crest	9.8
R260	DWC10 & 15	10	Crest	9.8
R270	DWC14	15	Crest	9.8
R271	DWC16	15	Crest	1.2

All finite element analyses and centrifuge modelling tests were for a retained height of 10m at prototype scale.

Table 2.1 Summary of finite element analyses for walls propped at the crest

In particular, the test on the wall of 5m embedment (DWC11) modelled the events from excavation to collapse and was in this aspect different from the other tests, in which an outright collapse was not observed. This test was therefore the first to be investigated using the finite element analysis. The results from propped walls of deeper penetration will be presented in chapter 3. White (1987) had also analysed DWC11 by finite element program CRISP.

Although some boundary conditions in his study were not identical to those in the centrifuge model test, some of White's results will be compared with the current analysis.

2.2 Finite Element Modelling

The mesh used for the analysis of wall propped at the crest with a 5m embedment is shown in fig. 2.3.

2.2.1 Selection of Elements and Parameters

The diaphragm wall was modelled using linear strain quadrilateral elements for easy evaluation of bending moments. Beam elements had also been tried for the wall, which would yield bending moments directly. However, it was considered desirable to use slip interface elements between the wall and the soil, and also because the beam elements are incompatible with the slip elements, the linear strain quadrilateral elements were finally adopted. The properties of the wall were taken to be linearly elastic with Young's modulus E of 72×10^6 kN/m^2 and Poisson ratio ν of 0.33, since the wall was much stiffer than the soil and the stress was unlikely to exceed the elastic limit. This value of Young's modulus is typical value of aluminium alloy HE15w. The wall was assumed to be impermeable.

Regarding the soil, a mixture of linear strain triangle and quadrilateral elements was used. It was anticipated that shear strain and stress variation would be most significant near the ground surface and around the wall. Therefore many small elements (having regard to the element aspect ratio) were used in these regions.

On shearing, heavily over-consolidated soil will generally fail by the formation of thin rupture surfaces with

associated dilation and softening. Tests carried out by Hvorslev (1937) found that within a certain range of effective normal stress, the shear stress on these rupture planes increased approximately linearly with the effective normal stress. Both the Cam-clay and modified Cam-clay soil models over-predict the yield stress for soil in this over-consolidated region. Schofield and Wroth (1968) suggested that the Hvorslev surface defined a region of instability in the soil which cuts across the Cam-clay state boundary surface. Since the clay used by Powrie was heavily over-consolidated, the so-called Schofield model was used to represent the soil constitutional behaviour.

The Schofield model was a late development from Cambridge University and was incorporated into CRISP-84 at King's College London by the author. In the finite element representation of this soil model, the Hvorslev surface is interpreted as a yield surface. When the stress state reaches this boundary, the soil will yield instead of rupture as would occur in reality.

The soil parameters used for the analyses were essentially those adopted by White (1987). However, the value of κ, the slope relating the change in void ratio to the change in the logarithm of the effective mean normal stress during swelling, was taken as 0.035, implying an increased stiffness during unloading. Figs. 2.4 and 2.5 indicate that the value of κ is not constant but depends on the stress level and over-consolidation ratio. Therefore the choice of the lower κ value is justified, at least for small reductions in stress.

To establish the stiffness matrix in finite element analysis, two elastic parameters must be known, usually Young's modulus E and either Poisson's ratio ν or the shear

modulus G. CRISP calculates E from the Cam-clay parameters by the following equations:

$$K' = \frac{(1+e)p'}{\kappa} \qquad \ldots.(2.1)$$

$$E' = 3(1-\nu)K' \qquad \ldots.(2.2)$$

Where p' = effective mean normal stress
e = void ratio
K' = bulk modulus
ν = Poisson's ratio
κ = slope of swelling line

Concerning the second parameter (either ν or G), Britto and Gunn (1987) pointed out that from the standpoint of theoretical elasticity, a constant value of G is preferable. However since the shear modulus is dependent on the stress level, a single value of G is difficult to justify, especially as the stress during the centrifuge modelling will change significantly. It is therefore customary to specify a constant value of ν when the stress level and shear modulus are expected to vary substantially. The shear modulus is then calculated by the program using the elastic relationship,

$$G = \frac{E'}{2(1+\nu)} \qquad \ldots.(2.3)$$

This implies that the soil will have an elastic behaviour but is non-conservative (Gunn and Britto, 1984). Although this would not give a good prediction under conditions of cyclic loading, the assumption of exact elasticity for a soil is perhaps unrealistic in most circumstances.

The calculated stiffness profiles for the soil prior to acceleration in the centrifuge and after reconsolidation are shown in fig. 2.6.

From the results of pore water pressure against time graph (Bolton et al, 1985), it may be seen that the pore pressure

recovered very quickly after excavation, implying a relatively high permeability for soil of this nature. Therefore permeabilities of k_v = $5x10^{-9}$ m/sec and k_h = $7x10^{-9}$ m/sec were adopted which were higher than White's (1987) values but still within the limits for kaolin given by Al-Tabbaa (1987) (see fig. 2.7).

Regrettably there is little published information available on the value of s, the slope of the no tension cut-off in the Schofield model and the permeability of soil in the tensile fracture region. Atkinson and Bransby (1982) calculated a possible value for s of 3, based on the triaxial test and the criterion that soil could not sustain any tensile effective normal stress. In plane strain, s varies from 1.8 to 3.0, depending on the value of Poisson's ratio. All the analyses for the centrifuge modelling were based on s=3. One supplementary analysis was carried out with s=2 and it was found that the differences were insignificant and confined to very small zones near the soil surface adjacent to the wall. As a result, no attempt was made to repeat the analyses using different s values. The permeability for the tensile fracture region was arbitrarily taken as $1x10^{-6}$ m/sec in both vertical and horizontal directions. The soil parameters used are summarised in table 2.2 at the end of this section.

Results from Powrie's (1986) tests indicated that certain degree of friction was mobilised at the interface between the soil and the wall and thus a layer of slip elements was placed on this location. The basic principle of the slip element is that within the limiting stress condition given by the Mohr-Coulomb failure criterion, the element will behave like an elastic material. Once this limiting value is exceeded, the shear modulus will be reduced to a value specified by the user, usually between 100 and 1000 times

smaller and the shear stress in the next load increment will be set at this limiting value. If the normal stress is negative, i.e. tensile, then both the normal and shear modulus are reduced almost to zero. This effectively makes the interface element very stretchable and the normal stress will then be set to zero in the next increment.

Soil : (Schofield model)		Slip interface :	
κ = 0.035		c	= 0
λ = 0.25		ϕ	= 21.4°
Γ = 3.48	(e_o=2.48)	k_n	= 5320 kN/m^2
M = 0.65		k_s	= 2660 kN/m^2
ν = 0.33		k_{res}	= 27 kN/m^2
γ_w= 9.81	kN/m^3	t	= 0.001 m
γ_b= 17.34	kN/m^3		
k_v= 5 x 10^{-9}	m/sec	Diaphragm wall : (Elastic)	
k_h= 7 x 10^{-9}	m/sec	E	= 72 x 10^6 kN/m^2
ϕ_B'= 15.5°		G	= 27 x 10^6 kN/m^2
s = 3.0		ν	= 0.33
k_x= 1 x 10^{-6}	m/sec		
k_y= 1 x 10^{-6}	m/sec	Porous plastic : (Elastic)	
		E	= 1 x 10^{10} kN/m^2
		G	= 0.38 x 10^{10} kN/m^2
		ν	= 0.33
		k	= 1 x 10^{-4} m/sec

Table 2.2 Parameters used in the finite element analysis

The parameters (see fig. 2.8 for definition) for the slip interface element are based on the elastic properties of the adjacent soil and are summarised in table 2.2.

For the reasons mentioned in section 2.1, a layer of porous plastic was laid at the bottom of the soil such that this became an equipotential in the centrifuge model test. A thin layer of rigid elastic material of high permeability was therefore placed in the analysis to simulate this effect. The parameters used are arbitrary (see table 2.2). However, apart from the pore water pressure, the behaviour of this material should not affect the analysis.

2.2.2 Initial Stress Conditions

The effective stresses during the soil sample preparation can be estimated according to the stress history of the sample at any stage.

During one-dimensional normal consolidation, the simplified version of Jaky's (1944) equation was used to estimate the earth pressure coefficient, K_{nc}:

$$K_{nc} = 1 - \sin\phi' \qquad \ldots\ (2.4)$$

where ϕ' = soil friction angle

Wroth (1975) proposed the following relationship between K_o, K_{nc} and OCR for the soil subsequently unloaded:

$$m\left[\frac{3(1-K_{nc})}{(1+2K_{nc})}-\frac{3(1-K_o)}{(1+2K_o)}\right]=\ln\left[\frac{OCR(1+2K_{nc})}{(1+2K_o)}\right] \quad .... \quad (2.5)$$

Where K_o = current earth pressure coefficient

OCR= over-consolidation ratio based on vertical effective stresses

m = 0.022875 PI + 1.22

PI = plastic index in per cent

Based on a maximum vertical stress of 1250 kPa and unloading to a vertical stress of 80 kPa prior to making the model and m = 1.87, K_o was calculated to be 1.70 and the effective mean normal stress was 117 kPa. The estimated stress path during soil sample preparation, with associated over-consolidated ratios and earth pressure coefficients, is shown in fig. 2.1.

When the soil was removed from the consolidation chamber and cut to receive the model diaphragm wall, stress redistribution would inevitably occur. It is assumed in the analysis that there was no stress relief and the stresses attained the isotropic conditions at the end of this process. Consequently, the effective vertical, horizontal and mean normal stresses would all equal to 117 kPa and these were taken as the starting point of the analysis.

2.2.3 Boundary Conditions

In Powrie's experiment, all the vertical sides were greased to reduce friction and hence the vertical boundaries were modelled as simply supported so that the soil elements were free to move vertically (fig. 2.3). At the bottom, White

(1987) assumed that the soil was free to move horizontally so that a downward movement of the soil on the retained side would result in an upward movement of the soil on the excavated side. However there was no evidence of this in the centrifuge tests, indicating that the surface of the porous plastic was sufficiently rough to prevent sliding. It was therefore decided to model the bottom boundary as pinned. Careful examination of the results from the analyses indicated that the shear stresses in the elements close to this boundary were very small, justifying the this assumption.

In most tests, Powrie did not allow bottom drainage after the reconsolidation phase. Because of the presence of the porous plastic at the bottom, this boundary became an equipotential, for which the pore water pressure will depend on a number of factors including the geometry of the diaphragm wall, the clear distance between the toe of the wall and test box boundary and the ground water level on either side of the wall. In modelling centrifuge tests, the finite element program CRISP cannot calculate this potential which must therefore be input by the user.

Powrie installed a transducer to monitor the pore water pressure at the base and in general found that its value was approximately 265 kPa. This pore water pressure may also be estimated by drawing a seepage flownet or by carrying out a separate finite element seepage analysis at prototype scale (unfortunately, it is not possible by CRISP for centrifuge modelling at increasing gravity level (Britto, 1988)). In order to establish an approximate value for the pore water pressure at the bottom boundary, all three methods were tried and the results were within 10% to each other. A value of 265 kPa was finally adopted for all analyses.

White (1987) assumed that water was supplied to the base of the model and that the pore water pressure was hydrostatic with respect to a water table at the pre-excavation ground level. This implies a strong upward seepage in front of the wall into the excavation, which may in reality cause piping and flooding of the excavation. Powrie (1986) observed this problem in some of his tests. Although the implications of upward seepage are important to engineering design (Stewart 1990), especially with the increasing threat of rising water table in London, Birmingham and other cities, this effect is not the subject of this dissertation.

2.2.4 Simulation of Centrifuge Test

Before the test began, the effective stresses which in the centrifuge test resulted from a strong pore water suction within the clay were replicated in the finite element analysis by means of an equivalent surcharge applied at the soil surface. The lateral equilibrium of the diaphragm wall in the finite element analysis was maintained by a series of surface loads over the face representing the effect of the zinc chloride solution. The prop was modelled by fixing the corresponding node before the gravity level was increased, replicating the situation in the experiment. Once the centrifuge test had been started, water was fed at the piezometric level corresponding to the ground surface to both the ground surface and the porous plastic at the base. In the finite element analysis, the base pore water pressure was fixed to a value appropriate to the current gravity level and to zero at the retained soil surface.

In the analysis, the surface loads on the wall and on the pre-formed excavated surface were set equal to the self-weight of the zinc chloride solution which would give a

K_o=1 condition. As the gravity level was increased, these surface loads were increased accordingly to reflect the increase in the self-weight. The model was then kept at 125g for an average of 3 hours, equivalent to approximately 5½ years at prototype scale, to establish the equilibrium state in both the centrifuge test and the finite element analysis. The effect of this reconsolidation phase will be discussed more fully in section 2.3.1.

Just prior to excavation in the experiment, the water level in front of the wall was lowered to the pre-determined excavated surface. Water was not supplied to this surface afterwards. Hence in the subsequent excavation, by means of draining the zinc chloride solution, pore water suction was able to develop in the short term. The process of excavation was simulated in the analysis by the incremental reduction of the loads on both the wall and excavated surface. The time taken was in general 3 to 5 minutes, equivalent to approximately 40 days at prototype scale. Details of this stage will be discussed in section 2.3.2.

In both the experiment and the finite element analysis, the boundary conditions remained unchanged for a period of 7.38 years (prototype time) after excavation, in order to investigate the long term effects of pore water pressure dissipation. The results are discussed in section 2.3.3.

2.3 Results and Discussions

The finite element analysis of the wall of 5m embedment propped at the crest is presented in this section. Using a simple limit equilibrium method, Powrie (1986) showed that walls propped at crest of 10m retained height should require approximately 13.5m embedment below the dredge level to maintain equilibrium in the long term. In his

test DWC11, he observed clear indications of a rupture surface, which developed in an approximately logarithmic spiral pattern (see fig. 2.9). The purpose of this finite element analysis was primarily to demonstrate the ability of the finite element program to model the events up to and including the collapse limit state of the wall.

The results, unless otherwise specified, are presented at prototype scale. The relationships between finite element modelling and prototype scale of some quantities are listed in table 2.3

Quantities		Prototype Scale	Finite Element Scale
Gravity	(m/sec^2)	1	n
Length	(m)	1	1/n
Self-weight	(kN/m^3)	1	1
Stress	(kPa)	1	1
Strain		1	1
Young's Modulus	(kN/m^2)	1	1
Pore Pressure	(kPa)	1	1
Prop Force	(kN/m)	1	1/n
Time	(sec)	1	$1/n^2$

Table 2.3 Scale factors for centrifuge modelling

The analysis represented the complete centrifuge test (DWC11) from the starting of the machine to the end of the test. Three different result stages representing various loading conditions were obtained. These were the reconsolidation phase; immediately after excavation; and in the long term (7.38 years at prototype time after excavation).

2.3.1 Effects of Reconsolidation

Undoubtedly, the influence of the slurry trench phase of diaphragm wall construction is important, but the emphasis

of this dissertation is on the behaviour of the wall after excavation and hence the effect of construction will not be considered in detail.

In section 2.2.2 it was assumed that the soil was isotropic and having $p'=\sigma_v'=\sigma_v$=117 kPa. In the centrifuge test, these stresses were provided by the pore water suction whereas in the finite element analysis, they were maintained by the surcharge on the soil surface. The idealised vertical stresses and pore water pressure distributions at this stage are shown in fig. 2.10a. In the finite element analysis, after the gravity was increased to 125g and the surcharge was removed simultaneously, the pore water pressure was maintained at zero at the ground surface and a value of 314 kPa at the base (= γ_w.d, where γ_w = unit weight of water, d = depth of soil at prototype scale).

Fig. 2.10 shows that, although the initial total vertical stress states and pore water pressure distributions in the centrifuge model and in the finite element analysis are different, the initial effective vertical stress states are the same. The dissipation of excess pore water pressures during reconsolidation in the centrifuge is modelled correctly however, and at the end of reconsolidation, the stress states in the centrifuge model and in the finite element analysis are identical.

The change of effective vertical stresses during the reconsolidation process is shown in fig. 2.11. It can be seen that the soil close to the surface suffers a reduction in vertical effective stress from 117 kPa to nearly zero and therefore would swell. Near the bottom, the vertical effective stress has increased from 117 kPa to 240 kPa. Hence the soil near the bottom would settle.

Fig. 2.12a shows the displacement vector diagram at the end of the reconsolidation stage. It can be seen that the displacement was predominantly vertical especially away from the vicinity of the wall. This confirms that the soil was primarily undergoing consolidation. The uniformity was disturbed close to the wall, particularly near the toe. There are two main reasons. Firstly, the vertical effective stress below the base of the wall increased from approximately 117 kPa at 1g to 255 kPa at 125g: this alone would cause the wall to settle. Since the soil:wall interface was modelled as rough, the soil around the wall was dragged downwards as the wall moved. It can be seen in fig. 2.13a that the vertical displacement of the soil next to the wall was approximately constant and equal to that of the wall. Secondly, because of the kniematic restraint of the prop at the crest, the lateral stresses were higher than expected near the retained surface (see fig. 2.14), giving approximately K=4 at a depth of 1m.

Over the lower half of the wall, the pressures on both the retained and excavated sides were generally very close to the K=1 condition (fig. 2.15). In a similar analysis of an unpropped diaphragm wall, it can be seen from fig. 2.16 that the K=1 condition is able to develop on the retained side, confirming the effect of the restraint imposed by the prop. However, the larger forward movement of the wall into the excavation near the formation level in the unpropped case compresses the soil, leading to a higher lateral stresses and K values on the excavated side.

The resulting stress distributions for the propped wall were slightly different from the initial assumption of K_o=1 (at least above the formation level) and therefore it is not surprised to have small wall movement into the excavation (see fig. 2.13b - a maximum of 19mm at prototype

scale near the toe). Consequently, there was horizontal movement in the soil adjacent to the wall. As a result of the non-linear lateral pressure distribution at the end of reconsolidation, bending moments and prop forces were induced (see fig. 2.17). However these movements and bending moments should not affect the subsequent analyses significantly and the results presented thereafter are the incremental values with respect to the end of reconsolidation, unless otherwise specified.

2.3.2 Short Term Effects

The two significant consequences of the excavation of soil in front of the wall are the reduction of vertical pressure on the excavated surface and the removal of lateral support from the diaphragm wall. Generally, the short term behaviour is regarded as undrained, with the soil deforming at constant volume in response to a change in deviatoric stress.

Figs. 2.12b and 2.18a show respectively the cumulative displacement vector diagram and the associated deformed shapes of the mesh immediately after excavation. The wall movement was predominantly a rigid body rotation about the position of the prop, together with some vertical settlement due to the effect of reconsolidation, as explained in the previous section. The computed movements in the soil behind the wall were apparently compatible: at any level, the displacements were approximately parallel, with a steeper orientation in the upper region and flatter nearer the toe (fig. 2.10b). The soil in front moved horizontally, following the movement of the wall. Away from the wall, the tendency of the soil in front to swell as a result of the removal of the over-burden pressure was inhibited by the development of short term pore water suctions. On the retained side, there was generally a 80mm

or so settlement, giving the first indication of a problem with serviceability.

The lateral stresses and pore water pressure distributions immediately after excavation are shown in fig. 2.14. It is clear that there was considerable drop in pore water pressure on both sides. As commonly expected, negative pore water pressures were developed in front of the wall near the excavated soil surface due to the removal of the over-burden pressure. In the finite element analysis, the pore water pressure at the excavated surface was set to zero, i.e. acted as a source of water. In reality, with careful control of surface water, the amount of suction developed could be higher and take longer to dissipate. As a result, the rate of swelling on the excavated side should tend to be over-estimated in the finite element analysis. Comparing stresses at different times in fig. 2.14, it can be observed that there was little change in the total and effective lateral stresses over the upper half of the wall on the retained side wall due to excavation. This might again be because of the kinematic restraint of the prop which prevented the soil from moving forward and towards the active condition. Over the lower half, there was a 50% reduction in both total and effective stresses. Near the toe, where the movement and lateral stress reduction were most significant, the lateral earth pressure coefficient fell during excavation to approximately 0.4 indicating that the soil was moving towards the active state but that the ultimate condition had not yet been achieved. In front of the wall, the total lateral stress dropped, particularly near the surface, as a result of the reduction in over-burden pressure: however the effective lateral stress increased as a higher soil strength was mobilised. Both total and effective lateral stresses moved towards a linear distribution with depth as the soil approached the passive condition.

Normally, engineers calculate lateral earth pressure coefficients based on the long term nominal vertical effective stress ($\sigma_v' = \gamma_b z - u$). If calculated in this way, the passive pressure coefficient immediately after excavation was apparently larger than 5 and exceeded the Kp value (Caquot and Kerisel, 1948). However, because the excavation took place quickly, the transient pore water suction prevented the effective stresses from achieving the long term values: hence the actual vertical effective stress was higher. If calculated based on the actual vertical effective stress, the earth pressure coefficient in the soil in front of the wall varied from 1.3 to 1.6, except the region near the surface (see fig. 2.15).

Fig. 2.17 shows the bending moment diagrams and prop loads at various stages. These bending moments were derived from the internal stresses of wall elements; but other methods were also tried (see Appendix A) and results were compared to check the validity. The corresponding short and long term values measured from the centrifuge model test and calculated based on the idealised effective stress distribution and the measured ground water conditions by Powrie (1986) are also superimposed on the same figure.

In general the maximum bending moments in all cases occurred near the mid-height of the wall. The overall highest bending moment calculated in the complete finite element analysis was approximately 1800 kNm/m and occurred immediately after the completion of excavation. The bending moment then decreased as time went on. This result was at first surprising because it might be thought to imply that the wall would be more stable in the long term, contradicting the general expectation. This can be explained by examining the lateral pressures acting on the wall. Because the wall:soil stiffness ratio was high, wall

deformation happened mostly as a result of rigid body rotation, with bending effects being small. Thus in the short term the pore water pressure on the upper half of the retained side was unlikely to drop significantly immediately after excavation and remained broadly hydrostatic, as shown in fig. 2.14. Near the toe and on the excavated side, the pore water pressure dropped drastically and even became negative close to surface as a result of the simultaneous removal of the over-burden pressure, lowering of the water table and lateral movement of the toe of the wall. As time went on, pore water pressures tended to decrease on the retained side and to increase considerably on the excavated side as the steady seepage condition was approached. The total lateral pressure, which determines the bending moment and prop load, followed a similar trend and consequently the bending moment decreased with time. The prop loads behaved similarly and were compatible with the changes in total lateral stress.

It is however important to consider the soil stability in terms of the degree of shear strength being mobilised. It can be seen that the lateral pressures on either side of the wall moved towards the respective active and passive states, except for a localised region near the prop, and hence mobilised certain angles of soil friction. In fig. 2.19 which shows the calculated contours of shear strain, it can be observed that immediately after excavation there were three isolated regions of high shear strain, namely near the prop location, just below dredge level and around the toe. In practice, soil subjected to such high shear strain would probably have ruptured locally.

2.3.3 Long Term Effects and Collapse

In the longer term, the pore water suction developed by rapid excavation in front of the wall will gradually dissipate and result in soil heaving. At the steady state, the pore water pressure behind the wall would be below hydrostatic, resulting higher effective mean normal stress p'. Although the forward movement of the wall may lead to a lower p' value, the effect due to pore water pressure change would dominate resulting overall an increase in p'. The soil was consequently compressed. Together with the forward movement of the wall, the soil behind the wall tended to settle. Figs. 2.12c&d show the cumulative displacement vector diagrams at 4 years and 7.38 years after excavation. The corresponding deformed shapes are shown in fig. 2.18. The soil behind the wall moved predominantly as a result of the rigid rotation of the wall about the prop position. There was no apparent discontinuity of the soil movement, contrasting with the centrifuge test in which rupture occurred (Powrie, 1986). The wall moved approximately 900mm and 1200mm (prototype scale) respectively near the toe at 4 years and 7.38 years after excavation and the soil in front followed this movement. The soil displacement at these stages would clearly in reality be unacceptable and would cause major concern to surrounding structures. It is also interesting to see from the ground surface movement profiles at various stages (fig. 2.20) that the maximum heave and settlement happened approximately 5m and 15m in front and behind the wall respectively (with the exception at 7.38 years after excavation). This is compatible with the shear strain mechanism suggested by Bolton et al (1989/1990) (fig. 2.21).

In the previous section, it was pointed out that the mobilised shear strains in the short term were already

quite high locally but the isolated regions were not joined together. At just 6 months after excavation (see fig. 2.19), the 10% shear strain envelope extended almost 7m from the wall into the excavation. Near the excavated surface just in front of the wall and around the toe, shear strains of more than 20% were predicted. In four years time, the area of high shear strain (10%) covered almost the complete region in front of the wall and extended into retained soil. In some areas, the shear strain was unrealistically high, reaching values of up to 40%

At 7.38 years after excavation, after which no further results were recorded in the centrifuge test, the zone of high shear strain was more apparent. The line joining the ridges of selected contours is similar to a logarithmic spiral type curve and is almost vertical near the ground surface on the retained side. The pattern is less clear close to ground surfaces because of the shear resulting from the simultaneous swelling. Engineers familiar with the upper bound theorem will recognise that this line resembles the failure mechanism commonly assumed in the analysis of retaining walls of this type.

In practice when a stiff soil undergoes shearing and the stress state reaches the Hvorslev surface (see section 1.4.4), it ruptures in thin layers (Schofield et al, 1968). It is generally acknowledged that the modelling of ruptures using the finite element method is very difficult, and CRISP is no exception. CRISP, in the Schofield soil model, uses a distorted yield surface to model the Hvorslev surface. When a stress state reaches this surface, the soil will continue yielding, resulting in exceptionally high shear strains. It is therefore suggested that the line joining the ridges of the high shear strain contours, which represents the limiting shape of individual contour

as they become longer and thinner, is analogous to the rupture surface (Finno & Nerby, 1989), as observed by Powrie in his test DWC11 (see fig. 2.6).

The distributions of lateral stresses and pore water pressure at 7.38 years after excavation are shown in fig. 2.14. The pore water pressures on both sides were approximately linearly proportional to depth, approaching the condition of linear seepage. The lateral stress distributions were a little irregular, but generally decreased with depth on the retained side and constant on the excavated side. The active and passive effective lateral stresses near the toe were approximately 10 and 400 kPa, giving comparatively high lateral pressure coefficients (calculated based on the actual effective vertical stress). The irregularity in the stress distributions is probably due to the fact that the soil had already reached failure, evidenced by having more than 30% shear strain in some areas near the wall.

The shape of the calculated bending moment at 7.38 years (fig.2.17) after excavation was clearly different from those at earlier times. The previous trend of decreasing in bending moment with time was reversed, and the maximum value increased to approximately 1100 kNm/m, occurring just below the dredge level. A possible explanation of the decrease in bending moment in the medium term is: the diaphragm wall may be regarded as a system resisting some distributions of load w by reactions at two supports R1 and R2 (see fig. 2.21), for which w, R1 and R2 represent the active pressure, prop load and resultant of passive pressure respectively. As time progresses, because of the softening of the soil in front of the wall, R2 decreases. Consequently, the wall rotates about R1 and w decreases (i.e. the soil moves further towards the active condition). By the time 7.38 years after excavation the stress

distributions behind the wall are irregular and the pattern is therefore different from those of earlier time, leading to a lower centroid of the resultant of the active pressures. This in turns results in a higher maximum bending moment at a lower depth. However the predicted prop load decreased further to 220 kN and was compatible with the change in the total horizontal stress as mentioned earlier.

Fig. 2.23 shows the wall deflections as a function of the excavation depth and time after excavation at the dredge level and the toe. During the excavation stage, the deflections were linearly proportional to the depth of excavation and at the end reached almost 300mm at toe. For the time up to 4 years after excavation, the deflections apparently increased linearly with time; but afterwards the rate of increase accelerated and showed no sign of reaching a steady ultimate value. The surface movements against time on the retained side had a similar trend (see fig. 2.24). For soil up to 11m from the wall, the rates of settlement were quite moderate during excavation and in the short term and increased considerably after 4 years' time. These are all indications of soil reaching a state of collapse (Guest 1990).

2.4 STRESS PATH AND MOBILISED SHEAR STRESS AT SOME REPRESENTATIVE LOCATIONS

2.4.1 Stress Path

Stress paths undergone by some representative soil elements during the analysis are shown in fig. 2.27, (for element locations, see fig. 2.25). At some points, there was considerable yielding, making strict comparison irrelevant. Therefore the effective mean normal stress p' and deviatoric stress q were normalised with respect to p'_c, the value at the tip of the Cam-clay yield locus (i.e. $q=0$)

at the current specific volume (see fig.1.9). The convention used here is that if vertical stress is greater than horizontal stress, then q is positive. In the following paragraphs, the term loading is used to indicate that the soil moving further towards the active conditions, and the term unloading towards passive.

Point 1, which was just behind the prop, was very sensitive to the initial stage of increasing gravity level. As mentioned in section 2.3.1, the effective vertical stress and mean normal stress for soil close to the surface would decrease at the end of reconsolidation. Because of its location, the pore water suction developed during the increase of gravity would dissipate fairly quickly. The behaviour was essentially drained unloading and shearing. The subsequent excavation resulted in an increase in both the effective mean normal stress and the deviatoric stress in an approximate ratio of 3/2. Consolidation after excavation eventually brought the stress state to Hvorslev surface. It is interesting to see that the soil was in the passive condition at every stage of the analysis, even though it was located behind the wall: this is probably because of the restraint of the prop.

Points 2 and 3 lay just behind the wall and were near the formation level and the toe respectively. The effect of reconsolidation was less marked. At the time excavation was completed, point 2 was still in an elastic condition, but point 3 was on Hvorslev surface. The ensuing consolidation brought the stress state for both points beyond the Hvorslev surface.

Point 4, which was just below the toe, initially followed a similar path as points 2 and 3, but in negative sense. Even before the completion of excavation, the stress state had already reached the Hvorslev surface. The element

continued yielding strongly along this surface both during and after the remainder of the excavation process. As mentioned earlier, the soil at this location would have ruptured at this stage in practice and the indicated stress path is not really meaningful.

Point 5 was approximately 5m below point 4. From fig. 2.19, it may be seen that the point was located beyond the area of high shear strains. Section 2.3.1 indicated that the vertical effective stress would have increased at the end of the reconsolidation stage and therefore the stress path followed was typical of drained loading. During the subsequent rapid excavation, the element underwent a typical undrained loading, with the stress path went almost vertical. The stress state was little affected by the ensuing consolidation.

Point 6, which was just in front of the wall and below formation level, underwent drained unloading during reconsolidation. The soil then underwent approximately undrained unloading during excavation. In the long term, the soil element moved beyond the Hvorslev surface, similar to point 4.

Point 7 was located close to the analogous rupture plane in the passive region. It has a stress path very similar to point 6; i.e. drained unloading during reconsolidation, followed by undrained unloading up to the end of excavation. The element continued yielding along the Hvorslev surface for the time after excavation instead of going out of bounds as did point 6.

Point 8 lay approximately 10m behind the wall. As with point 1, this point was close to the retained ground surface and therefore behaved similarly in response to the initial stage of increasing gravity. Because the location

was relatively far from the wall, the immediate effect of excavation was less significant. However once the pore water pressures moved towards their long term values, the element was eventually brought to failure at and beyond the Hvorslev surface.

2.4.1 Mobilised Shear Stress

Fig. 2.28 shows the corresponding graphs of deviatoric stress q against shear strain ϵ_s (γ) for the points concerned. It can be seen that at all locations, the maximum deviatoric stress was reached at a shear strain of between about 3% and 5%. There then followed an episode of strain softening with the deviatoric stress decreasing. In practice, the soil would probably have ruptured and the fall in shear strength been more marked.

2.5 Comparison with Experimental Results

When setting up the finite element mesh (fig. 2.3), provision was made such that certain nodes coincided with the instrumentation points in Powrie's test, shown in fig. 2.26. This facilitated direct comparison between the computed and measured values of various quantities. Some of White's results (1987) are also presented.

2.5.1 Soil Movement

Fig. 2.29 shows the surface movements as a function of time for the retained soil. In section 2.3.1, it was suggested that the combined effects of the change in total vertical stress and pore water pressure during the reconsolidation stage should result in surface heave. The finite element analysis predicted a compatible response. In Powrie's test, however, a surface settlement of 120mm (at prototype scale, equivalent to 0.8mm at model scale) was recorded at

LVDT1. This may have been due to errors in data acquisition, for example the LVDTs might not have been in contact with soil prior to the test.

The computed post-excavation movements followed the same trend as those measured, particularly for the soil further from the wall (LVDT5). The LVDTs close to the wall measured very high settlement in the centrifuge test because rupture occurred at approximately 4 years after excavation. Neither the computations by White or by the author were able to replicate this result because of the impossibility of reproducing the rupture behaviour using a continuum model.

The compution by White showed that the ensuing consolidation after excavation had very little effect on the surface movements at all locations. This was probably due to his fixing the pore water pressure hydrostatically at the bottom boundary which resulted generally in less significant changes of pore water pressure.

Fig. 2.30 shows the movements of the soil during the excavation. It can be seen that the measured vertical movements on the excavated side were slightly larger than those calculated from the finite element analysis. This may be due to the time taken for excavation in the centrifuge test - significant heave might have already occured by the end of the excavation process. The post-excavation soil movements (with the displacement scale halved) are shown in fig. 2.31. It is clear that the movements for the soil just in front of the wall were significantly higher and apparently followed the rigid body rotation of the wall in the finite element analysis. In the centrifuge test, the wall rotation was smaller and therefore the soil in front was less affected. In addition, the movement of the soil near the prop was higher

and steeper in the test as a result of the soil rupture (see section 2.3.3). Other than the excavated surface and the small area near the prop location, the computed soil movements in both instances were in good agreement with those observed in the centrifuge test.

2.5.2 Pore Water Pressure

The variations of the pore water pressure with time are shown in fig. 2.32. The computed pore water pressures and the responses to different loading stages are very similar to the measured values, bearing in mind that the physical size of each pore water pressure tranducer was 6mm in diameter which would respond to an area 750mm in diameter at prototype scale. White's results generally displayed larger discrepancies during the stage of increasing gravity: this is probably because of his assumed initial stress state was slightly different.

2.5.3 Bending Moment

Fig. 2.33 compares the computed and measured bending moments variation with time. At all locations, the measured post-excavation bending moments decreased with time. At BMT6, Powrie recorded a positive bending moment of 200kNm/m (at prototype scale) at end of reconsolidation. This implies that contraflexural rotation occurred near the toe which is unlikely in practice for such stiff wall of relatively short length. The discrepancy may be due to the fact that the strain gauges were sensitive to temperature drift, as pointed out by Powrie. The computed bending moments followed a similar trend until approximately 4 years after the completion of excavation. They then tended to increase, possibly because most of the soil had reached failure and the results followed may not be meaningful.

earlier at BMT6 as a consequence of the large toe deflection that brought the soil to local failure in this region shortly after end of excavation.

In all cases the magnitudes of bending moment computed were much larger than those measured, by a factor of up to three in BMT6 immediately after excavation. White obtained a similar over-prediction in his analysis. At first, it was thought that this might be due to the inability of the program to calculate the bending stresses. Separate analyses were carried out on a prismatic beam with simple load (uniformly and triangularly distributed) and boundary conditions (simply supported or encastré). The results were compared with those calculated using engineers' beam theory and it was confirmed that the program is able to handle the bending effect with a reasonable degree of accuracy provided that elements having an aspect ratio of not greater than 2 are used. Furthermore, bending moments calculated from the horizontal stresses acting on the wall (see Appendix A) were generally compatible with those derived from the stresses inside the wall.

The possible reason for the discrepancy between the computed and experimental results is that because in the finite element analysis the wall was rigidly propped prior to excavation, the soil was restrained from forward movement and hence unable to move towards the active condition. As a result, the lateral stresses were high close to the prop position. Consequently, the centroid of the horizontal stresses exerted by the soil behind the wall was also high, leading to increased bending moments and prop loads. However, it is difficult in practice to achieve a perfectly rigid prop, so in the centrifuge model test the bending moments were lower.

CHAPTER 3

ANALYSIS OF WALLS OF DEEPER EMBEDMENT PROPPED AT THE CREST AND THE EFFECTS OF WALL STIFFNESS

CHAPTER 3 - ANALYSIS OF WALLS OF DEEPER EMBEDMENT PROPPED AT THE CREST AND THE EFFECTS OF WALL STIFFNESS

In this chapter, the behaviour of walls propped at the crest of 10m and 15m embedment will be investigated. In discussing the effects of the relative soil:wall flexibility, results from the propped wall of shallower embedment described in chapter 2 will be used. The results from all the walls propped at the crest will be summarised at the end of this chapter.

The present analyses were based primarily on the tests carried out by Powrie (1986). The walls were propped at the crest and of either 10m or 15m embedment. The stiffness was generally the same as that of the wall of 5m embedment ($EI=9.8\times10^6$ kNm² per metre at prototype scale), but the behaviour of a more flexible wall ($EI=1.2\times10^6$ kNm² per metre) of 15m embedment was also investigated. The finite element meshes used were similar to that shown in fig. 2.3, with the appropriate modifications to the total length and thickness of the wall. Although the exact time schedules were slightly different, the sequence of the analysis and the method of simulating the centrifuge model test were essentially unchanged.

In the centrifuge tests, none of the deeper walls collapsed outright and therefore these analyses were concerned with serviceability rather than collapse.

3.1 Results from Finite Element Analyses

3.1.1 Stresses and Pore Water Pressure

Figs. 3.1a-3.3a show horizontal stresses and pore water pressure distributions at the end of reconsolidation. It can be seeen that they were generally similar to that of 5m

embedment wall: close to the K_o=1 condition near the toe but with the effective lateral stress maintaining approximately constant above the dredge level because of the restraint of the rigid prop.

At the end of excavation, as with the wall of 5m embedment, there was a considerable reduction in pore water pressure due to excavation. Nevertheless the zone of suction developed on the excavated side extended to different depths depending on the rigidity and the embedment of the wall, reaching approximately 2.5m, 4m, 5m and 3m respectively for the rigid walls of 5m, 10m, 15m embedment and the 15m flexible wall. This is because the soil in front of the wall will have a higher lateral effective stress if the wall is able to move forward near dredge level, leading to a smaller reduction in pore water pressure, i.e. less suction. The lateral effective stress at this stage is almost unchanged on the retained side. An observation of particular interest is that for the flexible wall the effective stress reached its minimum value at a depth just above formation level where the wall deflection was the greatest. The total horizontal stress on the excavated side dropped considerably as a direct result of excavation. The total horizontal stress near the toe on the retained side also fell significantly, following the trend of decrease in the pore water pressure. By 6 months after excavation, the pore water pressures had almost reached their long term steady seepage conditions for all four walls (see figs. 2.14c, 3.1c-3.3c).

In the long term, for all three walls (10m and 15m embedment), the effective lateral stresses on the retained side fell. However, because of the kinematic restraint imposed by the prop, the reductions were small over the upper half. Near the toe, perhaps because of a tendency for localised rupture (see next paragraph), the decreases

were more significant. In each case, there is a region less influenced by the effects of local rupture and prop restraint where the stress varied linearly with depth (approximately between 10m and 17m). The earth pressure coefficients in this region were calculated (based on the actual effective vertical stress) to be 0.73, 0.85 and 0.70 for the 10m, 15m and 15m flexible walls respectively. The corresponding values near the toe are 0.29, 0.44 and 0.75. For the flexible wall, a lower value of K=0.60 was computed just above the formation level. It can be seen that the reduction in effective horizontal stress is related to the wall movement and hence the wall flexibility.

On the excavated side, the short term reduction in the effective horizontal stress for all the walls is in average of 10 kPa. In the long term, there was a comparatively large reduction in the lateral effective stress for the wall of 10m embedment (approximately 60 kPa near the toe), probably due to the softening of the soil. For the deeper walls, because of a further rise in the pore water pressure towards the steady seepage condition, the lateral effective stresses in general fell slightly.

Figs. 3.4-3.6 show the contours of mobilised shear strain for the three deeper walls at different times. It can be seen that, in all cases at the end of excavation, most of the soil had a shear strain of less than 2% and the largest shear strain occurred near the toe of the wall. In the medium term, the wall of 10m embedment developed relatively larger shear strains (up to 10%) around the toe and at the surface just in front of wall which might lead to the softening of the soil. Although it might be considered that these localised high shear strain regions are indications of incipient rupture on the excavated side, their magnitudes are much smaller than in the case of 5m embedment and outright collapse seems unlikely at this

stage. For the rigid wall of 15m embedment, the shear strain was even smaller, reaching 6% near the toe. For the more flexible wall, the shear strain was also small, but the contours were of a different pattern. In contrast to the rigid walls, the maximum shear strain was near the toe at the back of the wall rather than directly below it, implying a possible contraflexural rotation. Nevertheless both walls of 15m embedment were likely to have been remote from collapse.

3.1.2 Soil Movements

Figs. 3.7a-3.9a show the cumulative displacement vector diagrams at the end of the reconsolidation stage for each of the three walls. In all cases the displacements were essentially vertical and consistent with the assumption of consolidation as discussed in chapter 2.3.1. Because of the deeper embedment of these walls, the horizontal wall movements were less marked and did not in any of the three cases exceed 10mm at prototype scale.

The cumulative displacement vector diagrams immediately after excavation are shown in figs. 3.7b-3.9b. The associated deformed shapes are shown in figs. 3.10a-3.12a. For the rigid walls, movements were predominantly the result of a rigid body rotation of the wall. The rotation was smaller for the wall of deeper embedment, indicating that it was necessary to mobilise a lower degree of shear strength. The movements of the soil close to the wall were generally compatible with the wall movement - horizontal in front, and at approximately 45° downwards behind the wall. Away from the wall the soil movements were comparatively insignificant.

For the more flexible wall, considerable bending deformation was superimposed onto the rigid body rotation. As a result, the movement of the wall was greatest near dredge level. However the toe deflections in both rigid and flexible walls of 15m embedment were of the same order and lay between 100mm and 150mm at prototype scale (see fig. 3.13).

The movements of the soil due to excavation alone in both the finite element analyses and the centrifuge tests (Powrie, 1986) are shown in figs. 3.14-3.16. For the soil close to the wall, the computed movements were approximately horizontal following the incremental rotation of the wall. The soil further away from the wall generally moved at 45° downward behind and at 45° upward in front of the wall. It can be seen that the computed and measured soil movements are generally in good agreement.

In the medium term (4 years after excavation), the soil displacements of the more flexible wall were in general similar to those immediately after excavation, except close to the ground surface. Far behind the wall, as the pore water pressure decreased towards the linear seepage condition, the effective stresses increased and the soil therefore settled. On the excavated side, the soil heaved as the pore water pressures gradually increased to their long-term values. The cumulative displacement vector diagrams and deformed meshes at 4 years after excavation are shown in figs. 3.7c-3.9c and figs. 3.10b-3.12b respectively. There was further settlement behind and heave in front of the wall in the longer term (14 years after excavation) but these changes were minimal.

The long term post-excavation soil movements in the finite element analyses are compared with the results from the centrifuge tests in figs. 3.17-3.19. Behind the wall, the

measured movements were generally large, particularly near the prop location. This was either due to the yielding of the prop or the localised rupture of the soil in the vicinity. The finite element analysis was simulated using a rigid prop and the program is unable to model the rupture behaviour (see section 2.3.3). Consequently, the computed movements of the soil just behind the prop were minimal. For the soil near the excavated surface, the computed movements were generally close to vertical, indicating that the heave due to the increase in pore water pressure is highly significant. This is probably due to the fixing of the pore water pressure boundary at the excavated surface to zero (i.e. acting as a water source) rather than allowing the development of pore water suction at the surface as was the case in the centrifuge tests.

Fig. 3.20 shows the surface movement profiles. The maximum soil settlements behind the wall were generally around 150 to 180mm. The heave in front varied with both the wall embedment and time. In contrast to the 5m embedment wall the soil surface profiles for the deeper walls did not display pronounced peaks. For the 10m embedment wall, the maximum settlement and heave occurred approximately 20m and 10m from the wall respectively. For the deeper walls, the maximum settlement occurred at or beyond 20m from the wall but the maximum heave occurred approximately 13m and 7m in front for the rigid and flexible walls respectively.

The surface movement from finite element analyses for rigid walls (including 5m embedment, see section 2.3.3) are again broadly compatible with the shear strain mechanism proposed by Bolton et al 1989/1990) for walls propped at the crest. For the more flexible wall, the shear strain mechanism might be modified by adding a hinge at an appropriate depth near the toe (see fig. 3.21).

3.1.3 Wall Deflections

Fig. 3.13 shows the deflected shapes for all four walls at various times after excavation. The variation in wall movements at some representative locations as a function of time are plotted in fig. 3.22. For the deeper walls (10 and 15m embedment), the deflections decreased considerably in the short term after excavation. Then the deflection increased steadily for the 10m embedment wall whereas for the 15m embedment walls, it continued to decrease. The more flexible wall attained its eventual deflected position in a shorter time than the rigid wall. This behaviour is best explained by the changes of lateral stresses and pore water pressure during the time after excavation (figs. 3.23 and 3.24). During the post-excavation period, the pore water pressures on both sides of the wall tended to move to their respective long-term values. The magnitude of the pore water pressure changes in front of the wall were significantly higher than those behind - this effect alone (i.e. ignoring the change in lateral effective stress) would reduce the wall deflection. However as the excess pore water pressures dissipated (more significantly in front of the wall), the effective stresses would change in similar magnitudes but in opposite direction (i.e. higher reduction in front). In turn the soil would provide less resistance to the wall movement - this would lead to a higher deflection.

In the short term for all three walls, the pore water pressures behind the wall did not change significantly over the upper one third of the wall and increased by an average of 25 kPa over the lower region. At the same time, there was an average decrease of 10 kPa in the lateral effective stress. This resulted in an overall decrease of lateral total stress above the dredge level and an increase below (see fig. 3.23) but the net resultant change was small. On

the excavated side, the increase in pore water pressures was significantly higher than the decrease in lateral effective stress, leading to an overall increase in the lateral total stress. Hence the wall deflections decreased in all cases in the short term (fig. 3.22).

For the time after the initial post-excavation period, the changes in lateral stresses and pore water pressures behind the wall were small, (as shown in fig. 3.24 for the changes from 6 months to 14 years after excavation). In the mean time, the pore water pressures on the excavated side increased further towards their respective long-term values in all cases. As observed from the contours of shear strain at 4 years after excavation (figs. 3.4b-3.6b), the shear strains for the soil just in front of the wall below the surface were large which would result in the softening of the soil. The consequence will be a significant decrease in the effective stress, as shown in fig. 3.24 for the depth from 10m to approximately 15m. If the embedment depth of the wall is deep, this softening effect will be confined to the area near the surface, as shown in the two walls of 15m embedment. With the increase in the lateral total stress near the toe as a result of the rise in pore water pressure, the overall change in lateral total stress was small. Therefore, the wall deflections for the deepest embedment walls were approximately unchanged in the long term. The reason that the more flexible wall attained the eventual deflected shape in a shorter time is because the pore water suction developed by excavation was in this case smaller and extended to a shallower depth below the formation level (see figs. 3.2b & 3.3b). The time required for the pore water pressures to recover to near their long term values would therefore be reduced.

For the wall of 10m embedment, in addition to the soil softening near the surface, the higher shear strains near

the toe led to a similar effect. As a result, the lateral effective and total stresses both decreased near the surface and the toe. Hence the wall deflection increased steadily in the longer term. It can be seen from fig. 3.22 that the wall deflection was still increasing by the time 14 years after excavation.

For the shallowest embedment wall (5m embedment) described in chapter 2, the shear strains in the short term were already high (fig. 2.19), the soil softening effect would probably dominate the deflection of the wall which therefore did not show any decrease even in the short term (fig. 3.22)

3.1.4 Bending Moments and Prop Loads

Fig. 3.25 shows the computed bending moments and prop loads for walls of different embedment depths and stiffness. The measured bending moments from the centrifuge tests are also plotted in fig. 3.25. It is not surprising that, for walls having the same retained height and flexural rigidity, the magnitudes of the bending moments increased significantly with the depth of embedment. For walls of same total length, the more flexible wall attracted a much smaller bending moment. The overall maximum bending moments computed occurred immediately after excavation in all cases and were equal to 1803, 3543, 5360 and 3060 kNm per metre (prototype scale) for rigid walls of 5m, 10m and 15m embedment and the 15m flexible wall respectively.

In all cases the bending moments decreased with time after excavation. As described in earlier sections, the increase in magnitudes of pore water pressures in front of the wall were higher and mostly occurred within 6 months after excavation, leading to a similar increase in the total lateral pressure. Consequently, most of the drop in the

bending moments occurred in the short term. In the longer term, following the decrease in the prop loads (see next paragraph), there were small decreases in the bending moments for all the walls. Comparing the results from the centrifuge tests, the computed bending moments were generally higher, probably due to the restraint imposed by the prop (see section 2.5).

The corresponding computed prop loads at different times after excavation are displayed for each wall on the same figure. It can be seen that the prop loads decreased after excavation, with most of the drop occurring in the short term, and were consistent with the change in the lateral stresses.

3.2 The Effect of Wall Stiffness

In order to investigate the effect of wall stiffness on the bending moments and prop loads, further analyses based on the same embedment depths as the previous investigations were carried out. For each embedment depth, a different wall stiffness EI was achieved by varying the Young's modulus E. In some cases, the second moment of area I was varied: it was however apparent that the first method will produce acceptable results, with relatively fewer modifications to the input data.

3.2.1 Bending Moments

Rowe (1952) carried out an investigation into the behaviour of flexible retaining structures using model tests in sand with $K_o<1$. Disregarding the self-weight of the soil, he showed that the model and the prototype walls will have similar behaviour if their respective flexibility numbers ($\rho=H^4/EI$) are identical. He concluded that the normalised bending moment (with respect to the cube of the total wall

length) is a function of the flexibility number and there exists a critical flexibility number below which the bending moment will not increase (see fig. 3.26). The results of the present analyses have been analysed on the same basis. However a direct comparison with Rowe's results is difficult because the two sets of results have different ranges of flexibility (see fig. 3.27) and different K_o values. Also shown in fig. 3.27 is the range of flexibility in a separate analysis carried out by Potts and Fourie (1985). Their results were based on a series of finite element analysis of walls in stiff clay having K_o=0.5 or 2.0. Unfortunately they did not consider the effect of pore water pressure, which (it will be shown in the next chapter) is generally critical to practical design, and therefore a comparison with Potts and Fourie's results is not considered to be relevant.

Figs. 3.28 a&b show the normalised bending moment against the logarithm of the flexibility number in the short and the long term respectively. In the short term, it can be seen that the bending moment decreased with increase in the flexibility for the same retained height ratio. Rowe suggested that this behaviour is due to the re-distribution of passive pressures as ρ increases. In the finite element analyses, although the lateral effective stress in front of the wall did not show a distribution similar to that observed by Rowe, the stress was higher near the soil surface for the more flexible wall under otherwise identical situations (see figs. 3.2b and 3.3b). Consequently, the resultant of the passive pressure for the more flexible wall was positioned higher than the rigid walls.

In the long term, the bending moments were lower than their corresponding short term values. Bending moments for the deeper walls (h=0.4H and 0.5H) show a similar trend of

decreasing with the increase in the wall flexibility. The trend for the wall of 5m embedment (h=0.667H) is however anomalous, probably because it had collapsed by this time.

3.2.2 Prop Loads

Using the same approach as Rowe on similarity, the prop loads can be normalised with respect to the square of the total wall length and the results are plotted in fig. 3.29. It can be seen that the variation in prop loads with wall flexibility is very similar to that of the bending moments in both the short term and the long term. The behaviour is consistent with the computed changes in lateral stresses described in section 3.1.1.

3.3 Summary

The finite element program CRISP, has been used to investigate the behaviour of diaphragm walls in clay. It has been demonstrated that the results are in good agreement with the centrifuge model tests provided appropriate soil parameters and boundary conditions are used.

From the analyses, it was found that a wall propped at the crest of 10m retained height and 5m embedment would certainly collapse in the long term. Also if wall deflection and soil movements around the wall are critical, such a shallow embedment wall may not be adequate even in the short term. Walls of 10m or 15m embedment will not collapse but the soil around the wall may rupture locally. The soil movements and bending moments will depend on the relative soil:wall stiffness.

If the walls are rigidly propped prior to excavation, the soil behind the wall near the prop is prevented from moving

forward and towards the active condition: the lateral stress near the prop will therefore be high. As a result, the bending moments and prop loads would be high. For walls of the same flexural stiffness, the maximum bending moments will increase with the total length of the wall. For walls of same retained height ratio, a flexible wall will attract a lower bending moment, but the wall deflection will be higher and greatest near formation level.

CHAPTER 4

LIMIT EQUILIBRIUM-BASED CALCULATIONS AND MOBILISED STRENGTH METHOD

CHAPTER 4 - LIMIT EQUILIBRIUM-BASED CALCULATIONS AND MOBILISED STRENGTH METHOD

4.1 Introduction

The finite element method is undoubtedly a very powerful tool in the analysis of diaphragm walling problems. However, for various reasons - for example a comprehensive anslysis may not be necessary at an early stage of design, the lack of detailed soil parameters and the non-availability of a sophisticated program - simple methods of investigating the behaviour of walls are sometimes more useful.

In assessing wall stability, a limit equilibrium method or a lower bound plasticity approach is often used. However, the results obtained by such methods are not unique and depend on both the definition and the value of factor of safety employed (Bica and Clayton 1989). Although the bending moments under working conditions can be calculated by applying a suitable factor of safety, it is unfortunate that no indication of the soil and wall movements is available.

A method - the mobilised strength method - which relates the mobilised strength to the deformation of the soil for walls propped at the crest is investigated later in this chapter. This method is based on the idealised strain field which was suggested by Bolton and Powrie (1988), in which the increment of soil shear strain $\delta\gamma$ in the zone of soil behind the wall is uniform and equal to twice the incremental wall rotation $\delta\theta$. Using this method the stability of the wall is first calculated in terms of the mobilised shear strength. Then the wall deflection, bending moments and prop load are evaluated.

4.2 Limit Equilibrium-Based Methods for the Calculation of Bending Moments Under Working Conditions

In chapter 3, it was shown that the maximum bending moment of a diaphragm wall is dependent on the wall stiffness (fig. 3.28). In Rowe's paper (1952), he plotted the results from his tests as a percentage of the maximum bending moment measured for a stiff wall having $\log_{10}\varrho < -3.5$. He showed that the bending moments in sheet-pile walls would not exceed the values calculated using limit equilibrium method and their magnitudes are mainly a function of pile flexibility and soil relative density. In another study, Potts & Fourie (1985) also characterised their computed maximum bending moments in the finite element analyses with reference to the values calculated by a limit equilibrium method. They concluded that for soil having high K_o values, the bending moments and prop loads can be higher than those calculated by limit equilibrium method.

However, the calculated bending moments under working conditions using limit equilibrium method depend on both the value and definition of the factor of safety employed and are therefore not unique. Potts & Fourie's calculations were based on the so-called bearing capacity analogy suggested by Burland et al (1981). Adopting the same definition and assuming that the wall is smooth, the limit equilibrium values of the factor of safety, bending moment and prop load for the walls analysed by the finite element method in chapters 2 and 3 can be calculated and are shown in table 4.1.

Embedment depth,m	Smooth Interface 5	10	15	Rough Interface 5	10	15
Factor of safety, F	0.12	0.54	1.09	0.22	0.97	1.95
Prop load P, kN/m	--	--	586	--	406	553
Max. bending moment M, kNm/m	--	--	3954	--	2431	3761

Table 4.1 Calculated factors of safety, bending moments and prop loads using the Burland-Potts approach limit equilibrium method

It can be seen that the two shallower walls (5 and 10m embedment) would be unable to stand in the long term. As already shown in chapter 2, the wall of 5m embedment did collapse at the end of both the centrifuge test and the finite element analysis. The 10m embedment did not collapse outright (see chapter 3.1.3), but the deflection was still increasing at the end of the analysis, and it would perhaps have failed at a later time. Also shown in table 4.1 are the values calculated if the wall is assumed to be rough ($\delta=\phi'$). The factor of safety for the 10m embedment wall is now improved to 0.97 and the wall is therefore still marginally below safety. The bending moment and prop load are shown but may not be strictly meaningful.

Potts and Fourie (1984) demonstrated that a diaphragm wall of total length of 20m will be on the verge of stability with a retained height of 15.26m for a dry soil with ϕ' = 25° (i.e. the effects of pore water pressure are ignored). At an excavation depth of 9.26m, the factor of safety would be 6.1. Taking into account the pore water pressure at steady seepage condition for an identical wall, the long

term factor of safety if the retained height and embedment depth are equal to 10m will be 0.97 even if the wall surface is rough. The effect of the pore water pressures has greatly reduced the margin of safety and thus is important in the analysis of diaphragm walls.

4.2.1 Factored Limit Equilibrium Approach

As mentioned earlier, the factors of safety calculated for the diaphragm walls using the limit equilibrium method will be different using various definitions. However it is commonly accepted that for normally consolidated soils, the full active pressure will be developed for a small movement in the soil whereas the full passive pressure will require a comparatively larger movement. Using this assumption, many different approaches based on limit equilibrium calculations have been developed (Bica and Clayton, 1989).

However, if a soil is initially over-consolidated (i.e. $K_o>1$) and close to the passive condition, the soil deformation required to mobilise the full passive pressure would be reduced whereas the movement required to mobilise the full active pressure may be increased (Padfield & Mair, 1984). Also, for walls rigidly propped at the crest, the kinematic restraint imposed by the prop would prevent the development of full active conditions, as already shown in the finite element analyses. Consequently, the assumption of full active pressure behind the wall in the limit equilibrium calculations may be inappropriate in these cases.

Therefore it is justifiable to assume, in contrast to traditional convention, that the lateral pressure behind the wall will stay in the insitu conditions for shallow depths of excavation where movement is negligible and the lateral pressure coefficient in the retained soil (K_r) is

equal to K_o. In front of the wall, the lateral pressure and the earth pressure coefficient in the excavated soil (K_e) will increase as excavation proceeds, until a depth is reached such that the full passive pressure is mobilised. Thereafter the pressure behind the wall will decrease until a depth of excavation at which the full active pressure is mobilised. Further excavation will, in theory, bring the wall to collapse. At every stage before collapse, $K_o \geq K_r > K_a$ and $K_o < K_e \leq K_p$. For the wall analysed by Potts and Fourie (1985) of total length H of 20m and in a soil of $\phi' = 25°$, $w = 20kN/m^3$, $\delta = \phi' = 25°$, the mobilised lateral pressure coefficients as a function of excavation depth for various K_o conditions were calculated using the above assumptions and are shown in figs. 4.1a-d. The equivalent earth pressure coefficients by the load factor method (CP2, 1951), which does not take into account the in-situ soil conditions, are shown in fig. 4.1e.

It may be useful to define the soil strength factors for the soil adjacent to the wall, such that:

factor for soil on retained side $F_r = K_r/K_a$

factor for soil on excavated side $F_e = K_p/K_e$

Higher values for these factors imply that a smaller soil strength is mobilised. These factors are strictly not the factors of safety but are indications of serviceability of the wall.

Also shown on figs. 4.1a&c are the lateral pressure coefficients at different depths of excavation from finite element analyses (Potts and Fourie, 1984). These coefficients are calculated using the average effective lateral stresses presented in the published paper and the nominal effective vertical stresses. It can be seen that

the values are in good agreement for both K_o=0.5 and K_o=2.0, justifying the argument that full active pressure is not developed.

Figs. 4.2 and 4.3 show the calculated bending moments and prop loads by the factored limit equilibrium approach as a function of excavation depth for various K_o conditions. The results based on the Burland-Potts approach are also shown. Under working conditions, the calculated bending moments and prop loads by the factored limit equilibrium method are substantially higher than those calculated by the latter method, especially for high K_o values. In reality, the lateral pressure on the retained side may fall, even for shallow excavation, and hence the factored limit equilibrium method may be inappropriate. However since this method and the load factor method are two extreme cases of assuming zero and full mobilisation of soil strength initially on the retained side, the results calculated will form respectively the upper and lower bounds of the limiting bending moments and prop loads under working conditions for soil having K_o>1 condition. The results from Potts and Fourie's (1984) finite element analyses are also plotted on the figs. 4.2 and 4.3 and it can be seen that they fall between these bounds for K_o=2.0 and excavation depths up to approximately 12m.

4.2.2 Bending Moment Reduction

Following the factored limit equilibrium approach and assuming the steady seepage pore water pressure, the limit equilibrium values of the bending moments, prop loads and the load factors for the walls considered in the finite element analyses in chapters 2 and 3 were calculated. It can be seen from table 4.2 that the values for the rough interface are higher than those of smooth interface. It is

Embedment depth,m	Smooth Interface 5	10	15	Rough Interface 5	10	15
Max. bending moment M_{max}, kNm/m	--	4296	8604	1705	5716	8763
Prop load P, kN/m	--	720	1267	341	958	1288
Pressure coefficient:						
excavated side K_e	--	2.56	2.56	3.86	3.65	2.59
retained side K_r	--	0.66	0.99	0.42	1.00	1.00
Soil strength factor:						
excavated side F_e	--	1.00	1.00	1.00	1.06	1.49
retained side F_r	--	1.69	2.53	1.27	3.07	3.07

Table 4.2 Calculated bending moments, prop loads and factors on soil strength using the factored limit equilibrium approach

because at the same retained height ratio, a wall having a rough surface will provide a higher K_p value. This in turn will lead to higher values of K_r, bending moments and prop loads for a given excavation depth prior to collapse.

Fig. 4.4 shows the computed long term maximum bending moments from the finite element analyses as a percentage of the maximum bending moments calculated using the limit equilibrium-based methods. The computed maximum bending moments are higher than those calculated using the Burland-Potts approach (1981) for walls having $\log_{10}\varrho$ less than approximately -1. On the other hand, the maximum bending moments are less than those calculated using the factored limit equilibrium approach. These results do not show clear cut-off of critical flexibility number as suggested by Rowe. However if the curves derived from the factored limit equilibrium approach are extrapolated to the limit of

the common practical design range of $\log_{10}\varrho > -3.5$, the maximum bending moment is unlikely to exceed 80% of the value calculated for a soil having condition of $K_o=1$.

4.3 Mobilised Strength Method

The limit equilibrium-based methods considered in section 4.2 have crudely assumed either full active pressure behind or full passive pressure in front of the wall under working conditions. In reality, the mobilised strength on both sides of the wall will depend on the soil deformation as well as on the initial stress state of the soil. A method based on the mobilised strength of the soil will be discussed in this section. The version introduced in this dissertation assumes the soil behaves approximately elastically. This restriction is not necessary in the approach presented by Bolton et al (1989/1990) but its introduction here will become clear in next section.

4.3.1 Assumptions and Calculations

Bolton (1979) suggested that the soil adjacent to a structural component often deforms only slightly in response to loading and the concepts of elasticity are then useful to investigate the stress distribution. If a diaphragm wall is rigidly propped at the crest, the wall will move forward below the prop as a result of excavation. The magnitude and the shape of the wall deflection are dependent on both the retained height:total wall length ratio and the relative soil:wall stiffness, as discussed in chapters 2 and 3. However if the wall is rigid, the deflection will occur mostly as a result of rigid body rotation about the prop position and the local bending is negligible (see fig. 4.5). Furthermore, if an appropriate safe margin is provided, the magnitude of the rotation under working conditions would be small. In such a case,

the soil movements will follow the rigid body rotation of the wall and because deformation is small, it is reasonable to assume that the behaviour of the soil is approximately elastic.

Assume that the soil is initially in the condition K_o=1. At a depth z, the vertical and horizontal total stresses are wz, where w is the bulk unit weight of soil (w is used here to distinguish it from the shear strain γ). After excavation the horizontal stress for soil behind the wall is reduced by $\delta\sigma_{act}$ and the vertical stress remains essentially unchanged. The Mohr's circle representation of the stresses is shown in fig. 4.6a. Therefore,

vertical stress $\sigma_v = wz$ ....(4.1)

horizontal stress $\sigma_h = \sigma_v - \delta\sigma_{act} = wz - \delta\sigma_{act}$ ...(4.2)

incremental shear stress $\delta\tau = \frac{1}{2}\,\delta\sigma_{act}$ ....(4.3)

characteristic incremental shear strain $\delta\gamma = 2\delta\theta$ ....(4.4)

and from the theory of elasticity,

$$\delta\tau = G\,\delta\gamma = 2G\,\delta\theta \qquad ....(4.5)$$

where G = shear modulus

combining equations 4.3 and 4.5,

$$\delta\sigma_{act} = 4G\,\delta\theta \qquad ....(4.6)$$

Generally, the shear modulus of a soil is not a constant but depends on the shear strain relative to an appropriate datum and the current stress state. It is often assumed that G is proportional to depth (Gibson, 1967). Hence, if $G^* = G/z$, equation 4.6 becomes:

$$\delta\sigma_{act} = 4G^*z\,\delta\theta \qquad ...(4.6a)$$

Substituting equ. 4.6a into equ. 4.2, the lateral stress behind the wall is:

$$\sigma_h = wz - 4G^* z\ \delta\theta \qquad \ldots.(4.7)$$

Similarly, the horizontal stress in front of the wall will be increased by $\delta\sigma_{pass}$, and the total vertical stress below formation level would be reduced by an amount equal to the self-weight of the excavated soil. The stresses are shown in fig. 4.6b. Therefore,

$$\sigma_v = w(z-h) \qquad \ldots.(4.8)$$

$$\sigma_h = wz + \delta\sigma_{pass} \qquad \ldots.(4.9)$$

$$\delta\tau = \tfrac{1}{2}(wh + \delta\sigma_{pass}) \qquad \ldots(4.10)$$

and the characteristic incremental shear strain in front of the wall is now:

$$\delta\gamma = 2(1+h/d)\ \delta\theta \qquad \ldots(4.11)$$

Using the elastic relationship, the incremental shear stress will be:

$$\delta\tau = 2G(1+h/d)\ \delta\theta \qquad \ldots(4.12)$$

Combining equations 4.10 and 4.12, the change in horizontal stress becomes:

$$\delta\sigma_{pass} = 4G^* z\ (1+h/d)\ \delta\theta - wh \qquad \ldots(4.13)$$

Substituting equ. 4.13 into equ. 4.9 will give the lateral stress in front of the wall.

$$\sigma_h = w(z-h) + 4G^* z\ (1+h/d)\ \delta\theta \qquad \ldots(4.14)$$

The horizontal stress distribution is plotted in fig. 4.7.

Then considering the moment equilibrium about the prop position, the wall rotation $\delta\theta$ required to maintain stability can be calculated in terms of the retained height ratio m (which is defined as the ratio of the retained height to the total length of the wall) and the soil constants,

$$\delta\theta = \frac{w \quad m(3-m^2)}{G^* \; 8(m^2+m+2)} \qquad \ldots(4.15)$$

where m = retained height ratio

$$= \frac{\text{retained height, h}}{\text{total wall length, H}}$$

If the shear force at the toe is neglected, the prop force may be calculated for a given wall rotation from the assumed stress distributions and the condition of horizontal equilibrium. The normalised prop load is then:

$$\frac{\delta F}{wH^2} = \frac{m(m^3-4m^2+3m-2)}{4(m^2+m+2)} \qquad \ldots(4.16)$$

and the normalised bending moment along the wall at a depth z is:

$$\frac{\delta M}{wH^3} = A(z/H) + B(z/H)^3 + C[z/H-m]^2 + D[z/H-m]^3 \quad ..(4.17)$$

where A,B,C and D are constants depending on the retained height ratio m,

$$A = \frac{m(-m^3+4m^2-3m+2)}{4(m^2+m+2)}$$

$$B = \frac{-m^3-2m^2+m-4}{12(m^2+m+2)}$$

$$C = \frac{m^2(3-m^2)}{4(m^2+m+2)(1-m)}$$

$$D = \frac{-3m^3+m+4}{12(m^2+m+2)(1-m)}$$

and $[z/H - m] = 0$ if $z/H < m$

Having established the bending moment distribution, it is now possible to evaluate the wall deflection δ by means of the differential equation:

$$\frac{d^2\delta}{dz^2} = \frac{-M}{EI} \qquad \ldots (4.18)$$

where EI = diaphragm wall flexural rigidity

Integrating equation 4.18 twice and putting in the boundary condition that at z=0, δ=0, then the wall deflection in non-dimensionalised form is:

$$-(\delta/H) \times (EI/wH^4) = A(z/H)^3/6 + B(z/H)^5/20 + C[z/H-m]^4/12 + D[z/H-m]^5/20 + J(z/H) \qquad \ldots (4.19)$$

where J = integration constant.

From equation 4.19, it can be seen that the wall deflection is not unique and an additional boundary condition is required in order to determine the integration constant J. It is possible to find this extra condition if the wall deflection at a particular depth can be determined from other sources, such as finite element analysis or experimentally.

Alternatively, if this simple method is to be applicable generally, it is desirable that no other information should be necessary. It was therefore decided to assume that the average rotation θ_{av} (defined as the ratio of toe deflection to the total length of the wall) is equal to the rotation required to maintain wall stability (fig. 4.8), i.e.

$$\frac{\delta_{toe}}{H} = \theta_{av} = \frac{w}{G^*} \frac{m(3-m^2)}{8(m^2+m+2)} \qquad \ldots (4.20)$$

Then substitution of the boundary condition at z=H, $\delta=\delta_{toe}$ enables the integration constant be determined:

$$J = -(A/6 + B/20 + C(1-m)^4/12 + D(1-m)^5/20) - \theta_{av}(EI/wH^4)$$

and equ. 4.19 becomes:

$$\delta/H=-(wH^4/EI)x\{ A(z/H)^3/6 + B(z/H)^5/20 + C[z/H-m]^4/12 + D[z/H-m]^5/20\}$$
$$+(wH^4/EI)x\{ A/6+B/20 + C(1-m)^4/12 + D(1-m)^5/20\} + \theta_{av}(z/H) \quad ..(4.21)$$

To simplify the expression, equation 4.21 can be written as:

$$\delta/H = (wH^4/EI) \times f(m,z/H) + (w/G^*) \times f(m,z/H) \quad ...(4.21a)$$

where f(m,z/H) denotes a function of m and z/H.

The first part of equation 4.21a is the local bending of the wall, which is dependent on wall flexibility (wH^4/EI). The second part relates to the rigid body rotation and by definition is proportional to the soil weight strength ratio w/G^*.

As a brief summary, the inter-dependence of the various quantities is summarised in the table below:

Variables to be evaluated		Variables dependent on soil properties and wall geometry			
		$\frac{wH^4}{EI}$	$\frac{w}{G^*}$	$\frac{h}{H}$	$\frac{z}{H}$
Average rotation	θ_{av}	No	Yes	Yes	No
Prop load	$\frac{F}{wH^2}$	No	No	Yes	No
Bending Moment	$\frac{M}{wH^3}$	No	No	Yes	Yes
Deflection	$\frac{\delta}{H}$	Yes	Yes	Yes	Yes

Table 4.3 Inter-dependence of various quantities in mobilised strength method

4.3.2 Average Wall Rotation

Fig. 4.9 plots the average wall rotation θ_{av} against retained height ratio (equation 4.15) for a homogeneous soil of unit weight w and increase in shear modulus with depth G^*. It can be seen that the average rotation required to maintain moment equilibrium about the crest is initially proportional to the depth of excavation, indicating that higher degree of soil strength is necessary as a result of the loss of lateral support on the wall as excavation proceeds. The soil at this stage is essentially elastic. Then the curve becomes flatten and reaches a peak value at approximately h=0.7H, implying that less rotation (i.e. strength) is required for deeper excavation. The result is perhaps surprising but it is purely theoretical since equation 4.12 indicates that the passive resistance

on the excavated side is approximately inversely proportional to the embedment depth. Therefore if the retained height ratio is high, an exceptionally large shear strength will be mobilised for the soil in front of the wall which in reality would exceed the maximum strength available. Consequently, there will be limits for the possible maximum excavation if different limiting shear strain conditions are imposed (fig. 4.9). Such a limit serves both to safeguard against the collapse of the wall and to maintain the applicability of the elastic analysis, and in general should be rather less than 10%. For weaker soils, i.e. with lower G^*, the value of θ_{av} required to maintain equilibrium increases. This is because a higher rotation (i.e. shear strain) is needed in order to mobilise the same amount of shear strength as a stiffer soil.

4.3.3 Bending Moment and Prop Load

Disregarding the limitation on soil elasticity, the normalised prop load and maximum bending moment are again approximately proportional to the excavation depth, at least initially, (see figs. 4.10 and 4.11). As excavation proceeds, the resultant of the passive pressure provided by the remaining soil decreases. It is therefore reasonable that the normalised prop load will increase. Due to the increase in prop load and the simultaneous lowering of the centroid of the resultant force of the passive pressure, the normalised bending moment also increases. Therefore if the retained height is constant, the mangitudes of both the bending moment and prop load increase with embedment depth as the total wall length also increases.

Since the wall is assumed to be rigid and the toe deflection is set equal to the length of the wall muitiplied by the average rotation, the wall flexibility is not involved in the equations of the wall rotation, bending moment and prop load. This is to some respect analogous to the limit equilibrium calculation. However, the normalised bending moment is related to the ratio of retained height to the total wall length (fig. 4.12).

4.4 Bending Factor

4.4.1 Definition of Bending Factor

Consider now the deflections of walls having different flexibility (wH^4/EI) under otherwise identical conditions. It can be seen from fig. 4.13 that there is relatively larger local bending for the more flexible wall but the deflection for stiff wall is close to pure rigid body rotation. For the approximate solution to be applicable, the deflection due to local bending must be "small" compared with the rotation. It is therefore necessary to define the size of the acceptable error.

Fig. 4.14 shows the deflection of a typical wall of finite stiffness. Let δ_B and δ_R be the actual wall deflection and the wall movement due to the rigid body rotation respectively. The difference between δ_B and δ_R would be the wall movement due to the local bending alone and varies over the length of the wall, with the maximum value occurring near the mid-height. From equations 4.21a and the assumption that the toe deflection is equal to the average rotation multiplied by the total wall length,

$$(\delta_B-\delta_R)/H=-(wH^4/EI)x\{A(z/H)^3/6+B(z/H)^5/20+C[z/H-m]^4/12+D[z/H-m]^5/20\}$$
$$+(wH^4/EI)x\{A/6+B/20+C(1-m)^4/12+D(1-m)^5/20\} \quad .... \quad (4.22)$$

According to equation 4.22, $(\delta_B-\delta_R)_{max}$ will increase as the wall flexibility (wH^4/EI) increases. Now define a bending factor β, which is equal to the ratio of maximum difference between the actual deflection and the deflection of the assumed rigid body rotation to the deflection due to rotation, i.e.

$$\beta = \left(\frac{\delta_B - \delta_R}{\delta_R}\right) \times 100\% \qquad \ldots(4.23)$$

If a wall is rigid, the deflection would be due mainly to rigid body rotation; the local bending would be insignificant and equation 4.23 indicates that the bending factor would be small. Conversely, the bending factor will be large for flexible walls.

From equations 4.20 and 4.23,

$$\beta = \frac{(wH^4/EI) \times f(m,z/H)}{(w/G^*) \times f(m,z/H)}$$
$$= (G^*H^4/EI) \times f(m,z/H)$$

Hence β is a function of the product of the flexibility number ρ (Rowe, 1952) and the increase shear modulus with depth G^*. This variable will be called the flexibility ratio P in the following sections.

4.4.2 Results and Discussions

In this section, some typical results of the application of the mobilised strength approach to diaphragm walls will be presented. Fig. 4.15a shows the idealised Young's modulus profiles of the five different soils under consideration. The description adopted for the soil is relative and does not relate to the real strength of the soil. Generally it

is reasonable to assume that the soil stiffness increases with depth (Gibson, 1967). Assume that the soil has a Poisson's ratio ν' of 0.33, then the corresponding values of G^* can be calculated and are tabulated below:

Soil type	1	2	3	4	5
Relative stiffness	Very stiff	Stiff	Medium	Soft	Very soft
G^*	2000	500	200	145	80

Singly-propped reinforced concrete diaphragm walls in practice commonly have a total wall length of between 5m and 25m and a thickness between 0.4m and 2.0m. Taking the Young's modulus of concrete as 28×10^6 kN/m^2, the range of Rowe's flexibility number ρ is shown in table 4.4 and the range of flexibility ratio will vary from 0 to 300.

Wall thickness,m	Total length of diaphragm wall, m				
	5	10	15	20	25
0.4	4.19	66.97			
0.6	1.24	19.84	100.45		
0.8	0.52	8.37	42.37	133.92	
1.0	0.27	4.29	21.69	83.33	167.48
1.5			6.43	20.32	49.60
2.0				8.57	20.93

$\frac{H^4}{EI}$ (in units of 10^{-3} m^3/kN)

Table 4.4 Table of flexibility number in common practical design

Having established the range of flexibility ratios, it is now possible to plot the bending factor β as a function of flexibility ratio P (fig. 4.16). In each case, four curves representing retained height ratios of 0.4, 0.5, 0.6 and 0.7 are shown. It can be seen that, the bending factor β increases as the wall becomes more flexible - i.e. the local bending effect will be more significant for more flexible walls. The bending factor decreases as the retained height ratio m increases, because the deflection due to rigid body rotation (δ_R) increases with m (for m up to 0.7). For design purposes, diaphragm walls could be separated into two broad categories. If the wall is thick and short, the wall deflection due to bending will be small and the wall would be categorised as rigid. In addition, the retained height ratio in this category should be small so that the shear strain mobilised is small and therefore the soil stress state lies within the elastic region. On the other hand, a slender wall having a high retained height ratio would be categorised as flexible. The implications of two different categories are shown in fig. 4.17.

4.4.3 Threshold Flexibility Ratio

Obviously the mobilised strength method will be best applied to a rigid wall. However it was pointed out earlier that if the wall deflection due to local bending is small, this method will produce an acceptable approximate solution. A threshold flexibility ratio P_T, must therefore be defined such that walls having smaller values than P_T will be called rigid walls and the mobilised strength

method is applicable. The definition of such a threshold flexibility ratio can be easily obtained by limiting the bending factor β to a certain amount in the graph of β vs P (fig. 4.16), for example 20%. Then for each retained height ratio, a value of P_T can be found which corresponds to β=20%.

4.5 Applicability of the Mobilised Strength Method

4.5.1 Examples

As an example, for a medium strong soil with G^*=200 kN/m² with retained height ratio m=0.5, from fig. 4.16,

$$P_T = 4.3$$

For the mobilised strength method to be applicable, a wall of total length H=20m made of concrete (E_{con} = 28x10⁶kN/m²),

$$I = \frac{G^* H^4}{E P_T} = \frac{200 \times 20^4}{28 \times 10^6 \times 4.3} = 0.2658 \text{ m}^4/\text{m}$$

and therefore the wall should be thicker than 1.5m. Alternatively, if the wall is 1.0m thick, i.e.

$$I = 0.0833 \text{ m}^4/\text{m}$$

$$H^4 = \frac{E I P_T}{G^*} = 55998 \text{ m}^4$$

Hence the wall should not be longer than 15m.

Even if a more rigorous limit is imposed on the approximation, say bending factor β not exceeding 10% (in such case P_T=2.1), the wall thickness and length would be 1.9m and 12.5m respectively. In general, most diaphragm wall designs are close to this range and therefore this approximate method should be applicable.

For a wall of h=10m, H=20m, t=1.5m, E_{con}=28x10^6 kNm^2 constructed in soil with w=20 kN/m^3 and G^*=200 kN/m^2 per metre depth, the previous example has shown that the method should be applicable. Subsequently, the soil and wall deformation may be calculated,

$$m = h/H = 0.5$$
$$w/G^* = 0.1$$

equ. 4.15 indicates θ_{av} = 0.0625 rad

and δ_{toe} = 0.00625x20 = 125 mm

so that the approximate deflection near dredge level

= 125 x 1.2 x 10 ÷ 20 = 75 mm

Using the shear strain mechanism (see fig. 2.21), the settlement behind and heave in front of the wall will both be 125mm.

4.5.2 Comparison with Finite Element Analyses

In this section, results from finite element analyses (summarised in table 4.5) in chapters 2 and 3 will be compared with the calculations using the mobilised strength method.

The increase in shear strength with depth G^* in the finite element analysis can be estimated from fig. 2.6. Between the depth of 5 and 30m, G^*=98 kN/m³. The unit weight of the soil in the analyses is 17.34 kN/m³, and leads to a (w/G^*) = 0.177.

Fig. 4.18 shows the average wall rotations calculated from the finite element analyses as a function of retained height ratio. For the shallow embedment wall (R250), the rotation is higher than the value calculated using the simple method. This is not surprising, since the soil in front of the wall would have a shear strain of more than 10% and thus exceeds the elastic limit which was discussed in chapter 2. Also the soil and wall movements will be large even in the short term for a wall of such shallow embedment. For the other walls, the computed rotations are of the same order of the calculated values.

The normalised prop loads and maximum bending moments from the finite element analyses are shown in figs. 4.19 and 4.20. It can be seen that, both the computed and calculated values are in a reasonable agreement with the finite element results being generally higher. It has already been mentioned in chapter 3 that the computed bending moments and prop loads in the finite element analysis may have been over-predicted because of the restraint of the rigid prop.

Limiting the bending factor β to 20%, the threshold flexibility ratios P_T can be determined from fig.4.16 and are equal to 3.33, 4.17 and 7.10 for m=0.4, 0.5 and 0.667 respectively. As it can be seen from table 4.5, the most flexible wall (R271) is considerably more flexible than P_T and therefore the mobilised strength is not quite

Analysis	R250	R260	R270	R271
Embedment depth, m	5	10	15	15
Retained height ratio	0.667	0.5	0.4	0.4
Flexural rigidity EI, $x10^6$ kN/m²	9.8	9.8	9.8	1.2
Flexibility ratio P	0.439	1.387	3.386	27.658
Toe deflection δ, mm (fig. 3.13)	273	203	144	108
Average wall rotation θ, rad	0.0182	0.0102	0.0058	0.0043
Bending factor β, %	2	11	38	185
$\frac{F}{wH^2}$	0.119	0.101	0.083	0.052
$\frac{M_{max}}{wH^3}$	0.031	0.026	0.020	0.010

Table 4.5 Summarised results of the finite element analyses

appropriate. However, even with a relatively large bending factor (=185%, analysis R271), the shear strain behind the wall (fig. 3.6) was still small and reasonably uniform. For the other walls, the shear strains behind the wall varied generally from 2% to 6%, except the region of localised rupture near the toe. From the plots of the mobilised shear stress against the shear strain (fig. 2.28), the assumption made in section 4.3 of this dissertation that the mobilised shear stresses are proportional to the shear strain is reasonably justified. Therefore the mobilised strength method should be useful to assess the behaviour of diaphragm walls generally.

4.5.3 Further Improvements

It has been shown that the mobilised strength is useful to estimate the behaviour of the diaphragm walls generally. However there is still scope for refinement if appropriate data are available.

Firstly, in deriving the equations, it has been assumed that the soil is in the initial condition K=1. The method could, however, be modified to tackle the situation of different in-situ earth pressure coefficients. Secondly, the mobilised shear stress in the idealised method presented in this dissertation was taken to be proportional to the rotation of the wall (i.e. the shear strain). In reality, the stress-strain relationship for most soils is rather complex, especially when the shear strain is small (Jardine et al 1986). In addition since the shear strains on either side of the wall are different it may be necessary to use different stress-strain relationships (Corson, 1987) to characterise the incremental shear

stress. Therefore this method can be improved if the simple relationship between the stress and strain is replaced by a more appropriate function. However this would inevitably lead to more complex calculations, requiring the aid of a microcomputer routine.

CHAPTER 5

ANALYSIS OF WALLS PROPPED AT DREDGE LEVEL

CHAPTER 5 - ANALYSIS OF WALLS PROPPED AT DREDGE LEVEL

5.1 Introduction

The behaviour of diaphragm walls rigidly propped at the crest has been discussed in previous chapters. It has been shown that the maximum bending moments in these walls normally occur near dredge level and their magnitudes (for a given retained height) depend on both the wall stiffness and the total wall length. Also, the movements for stiff walls will result mainly from rigid body rotation about the prop at the crest, and there would be further deflection due to local bending for the more flexible walls. Consequently, the wall deflection is largest near or below dredge level, which may be undesirable in practice. In addition, for operational reasons, it is not always possible to construct a permanent prop near the crest. Therefore, in order to reduce the wall deflection near the final formation level and overcome the restriction on prop position, engineers are often required to design diaphragm walls propped nearer dredge level.

In this chapter, the stability of diaphragm walls propped at dredge level is first assessed by the limit equilibrium method. In order to investigate the behaviour of the wall as excess pore water pressures dissipate, a series of finite element analyses is carried out on walls of different flexural stiffness and embedment depths which are propped at dredge level prior to excavation.

5.2 Limit Equilibrium Analysis

The assessment of walls propped at dredge level using the limit equilibrium method is not straightforward. For walls propped at the crest, it is clear that movement into the cutting will occur as a result of excavation and thus the

soil behind the wall will tend to move towards the active conditions whereas passive conditions will tend to be developed in front. However, if the prop is near dredge level, the direction of movement of the wall is less clear and the choice of a design stress distribution is therefore difficult. Following the approach of Powrie (1986) on a simple analysis, the stress conditions for the soil close to the wall after excavation can be characterised into three zones, as shown in fig. 5.1. As a result of excavation, the vertical stress in zone 3 would decrease and the soil is likely to move towards the passive conditions (i.e. the earth pressure coefficient increases: the magnitude of the total lateral stress is likely, however, to decrease). If the wall is rigidly propped at dredge level, its top will tend to rotate into the retained soil due to such a reduction in the horizontal stress in front of the wall. On the other hand, the top of the wall will tend to rotate into the excavation due to the loss of support on the wall caused by the removal of the soil above dredge level, and the stress state of the soil in zone 1 will move towards active conditions. The sense of wall rotation as a result of the combined effects of the loss of lateral support above and below the prop is not immediately apparent.

For a rigid wall of shallow embedment, it is only possible for the wall to rotate clockwise (from the point of moment equilibrium about the prop) and the stress distributions associated with such a rotation are shown in fig. 5.2. For rigid walls of deep embedment, a prop at dredge level will resemble a prop at the crest if looking from the toe of the wall. The soil in zone 1 can then be regarded as a surcharge and the situation can be assessed as a bearing capacity problem (fig. 5.3). In this case, the wall is likely to rotate anti-clockwise and the corresponding stress distributions are shown in fig. 5.4. For a flexible

wall, the overall movement may be influenced by some local bending about the prop, resulting in the crest and the toe both moving forward into excavation. The stress conditions will be complicated in this circumstance.

Consider now a diaphragm wall rigidly propped at dredge level with a retained height of 10m, and assume that the water tables are at the soil surface level on both sides of the wall and the pore water pressures correspond to the steady state seepage conditions (Burland et al, 1981). For shallow embedment depths, as explained earlier, the stress conditions would be active in zones 1 and 3 and passive in zone 2. Assume that the mobilised angles of soil friction on either side of the wall are identical and the wall is rough ($\delta=\phi'_m$). Then for a soil having bulk unit weight of 17.34kN/m^3, the angle of soil friction required for rotational equilibrium about the prop as a function of embedment depth is shown in fig. 5.5. It can be seen that the angle of shearing required decreases as the embedment depth is increased. This is reasonable, and compatible with the mobilised strength method discussed for walls propped at the crest in chapter 4. Apparently, at an embedment depth of approximately 5.8m, no soil strength is needed to resist rotational failure. However, based on a lower bound analysis, a mobilised friction of more than 25° is required, irrespective of wall friction, to prevent bearing failure at toe level of the wall (fig. 5.6). In addition, for walls of shallow embedment, the hydraulic gradient in front of the wall is likely to be severe and must be given separate consideration.

If the embedment depth is extended beyond 5.8m, the effect due to unloading on the excavated side dominates and hence there is a reversal in the calculated direction of wall rotation. From fig. 5.5, the angle of soil friction

required for rotational failure increases as the depth of embedment is increased (at least initially) implying that the wall is made less safe by increasing the embedment. This seems unrealistic and is probably the result of the idealised stress distribution assumed - i.e. stress discontinuities at prop level and vertically below the toe - and the constant mobilised soil strength. In reality, the change in stress would be smoother and different soil and wall friction might be mobilised along the wall, particularly when the wall movement is small. Therefore, a simple stress distribution might be difficult to justify for certain embedment depths where the wall rotation is on the verge of reversal, in this case around 5.8m.

For deep embedments, the angle of soil friction required to prevent rotational failure decreases as the depth is increased, and is consistent with the suggestion that a wall of deep embedment propped at dredge level resembles a wall propped at the crest. The angles of shearing required in both situations would be expected to be equal if the embedment depth is extended to infinity as shown in fig. 5.7.

Fig. 5.8 shows the maximum bending moments and the prop loads calculated as a function of embedment depth using the suggested idealised stress distributions. For walls propped at dredge level, it is obvious that the maximum bending moments would occur at the dredge line. Consequently the magnitudes of the maximum bending moments would be determined exclusively by the total horizontal stress behind the wall above dredge level. For shallow embedment depths (less than 10m), the maximum bending moment increases steadily as the embedment depth is increased and the stress state behind the wall above dredge level changes from active to passive conditions. For deeper embedments, the wall is remote from collapse and

therefore the variations in the mobilised soil friction and the horizontal stress behind the wall with the embedment depth are very small, resulting in an approximately constant maximum bending moment.

The bending moment diagrams and the corresponding prop loads for walls of 5m, 10m and 15m embedment are shown in fig. 5.9. For the deep embedment walls (10 and 15m), the bending moments drop nearly to zero at depths above the toe, indicating that the shear forces in the wall section below these depths were nearly zero (shear force = rate of change of bending moment with depth, S=dM/dz). This implies that the total lateral stresses on either side of the wall were approximately equal and might suggest that walls deeper than the depth of near-zero bending moment (in this case, a total length of approximately 20m) might not necessarily improve the wall stability.

It is also interesting to see from fig. 5.8 that the calculated prop loads are comparatively insensitive to the depth of embedment, being in the range 1600 to 2200kN.

5.3 Finite Element Analyses

It was shown in the previous section that a wall of shallow embedment propped at dredge level would probably rotate in a direction with the crest moving into excavation. For rigid walls of deep embedment, rotation would be in the opposite sense. Around the transition, the wall movement and the stress distribution are not immediately obvious. In this section, a series of finite element analyses was carried out to investigate the behaviour of walls propped at dredge level.

The present analyses are again based on the centrifuge tests performed by Powrie (1986). The walls were propped at dredge level - by preventing horizontal movement at the appropriate node in the finite element modelling - prior to excavation. The finite element meshes and the parameters used were similar to those of the walls propped the crest (fig. 2.3 and table 2.1). In total, six analyses representing different embedment depths and wall flexural stiffness were carried out (see table 5.1).

Author's Analysis Reference	Powrie's Test Reference	Wall Embedment (m)	Prop Location	Wall Stiffness EI ($x10^6 kNm^2/m$)
R350	DWC12	5	Dredge level	9.8
R360	DWC13	10	Dredge level	9.8
R370	---	15	Dredge level	9.8
R351	DWC17	5	Dredge level	1.2
R361	---	10	Dredge level	1.2
R371	---	15	Dredge level	1.2

All finite element analyses and centrifuge model tests were for a retained height of 10m at prototype scale.

Table 5.1 Summary of finite element analyses for walls propped at dredge level

According to the limit equilibrium analysis, the required angles of soil friction to resist rotational failure for these walls would be below the strength available (ϕ'=21.6°) for kaolin (see fig. 5.5) and therefore collapse is not expected. Although the soil strength required for the bearing failure of the shallowest wall exceeds 21.6°, there was no evidence of such a failure mechanism in the centrifuge tests, perhaps because a higher soil strength was available; or because the pore water pressure in the test was different from the steady state value assumed; or because the lower bound analysis is unduly conservative.

5.3.1 Stresses and Pore Water Pressures

Figs. 5.10-5.15 show the lateral stresses and pore water pressure distributions at different instants for each analysis. Also shown on the figures are the corresponding lateral earth pressure coefficients (calculated based on the actual vertical effective stress) from the the finite element analysis.

At the end of reconsolidation, the pore water pressures in all cases had recovered to the hydrostatic equilibrium condition, but the lateral stresses distributions were slightly different in each case, particularly near the crest because of the tendency of the soil near the ground surface in the centrifuge test (and the finite element modelling) to swell. For the walls of 5m embedment, because the cantilevered sections above the prop were abler to move forward, allowing lateral stress relief near the crest, the lateral stress behind the wall increased approximately linearly with depth. However, for the deep embedment walls, there were more resistance to forward movement of the crest - since the prop was rigidly in place at the beginning of the analysis, forward movement of the crest would require movement of the toe back into the retained soil. As a result, walls of deeper embedment were unable to develop linear stress distributions. However such non-linearities were smaller for the more flexible walls, and less marked than those of the walls propped at the crest. In general the stresses were close to the K=1 condition at this stage. The lateral stress distributions in front of the wall were also close to K=1 condition with earth pressure coefficients falling generally below unity near the toe. The lateral stresses near the excavated surface (pre-determined) were higher than K=1 in all cases, probably due to the swelling of the soil. The deviation

from the idealisation for the walls of 5m embedment was even larger because of their higher wall rotations at the same stage.

At the end of excavation, there was a small increase in pore water pressure, lateral effective and total stresses above dredge level on the retained side in all cases because of the wall movement into the retained soil (which will be discussed in more detail in the next section). However, the reductions in pore water pressures both on the retained side near the toe and generally on the excavated side of the wall were considerably larger. The pore water suction developed in front of the wall extended to depths of 3.5m, 5m and 5.5m below the excavated surface for walls of 5m, 10m and 15m embedment respectively. Since there was no lateral movement of the wall at dredge level because of the prop, the depths of pore water suction for both rigid and flexible walls of the same embedment were identical.

By the end of excavation, the lateral stresses behind the wall had developed distinctive distributions for different walls. For the 5m embedment walls, the lateral effective stress below the dredge line increased (by nearly 100kPa near the toe), and the overall lateral total stress also increased although there was some reduction in pore water pressure. It can be seen from the lateral pressure coefficient diagrams (fig. 5.10-5.11) that the soil here was moving towards a more passive condition. In contrast, the lateral effective stress (and total stress) at this location for the deep embedment walls decreased and the stresses were generally moving towards a more active condition near the toe. In addition, in the case of the walls of 10m and 15m embedment, the lateral effective stresses behind the more flexible walls increased with depth over the upper half, reached maximum values near dredge level and remained constant or decreased slightly

over the lower half. On the other hand, the lateral effective stresses for the rigid walls were approximately constant over the upper half and increased steadily over the lower half (apart from near the toe). The different behaviour of the effective stresses on the retained side for walls having different flexural stiffness was to a large extent due to the nature of the wall deflection - rigid body rotation for stiff walls but large local bending for flexible walls.

The lateral stresses in front of the wall were more straightforward. The lateral total stresses decreased, following the large reduction in vertical total stress due to excavation, but the development of pore water suctions ensured that the immediate changes in effective stresses were small, as would be expected.

In the long term (by 4 years or more after excavation), the suction developed in front of the wall due to excavation had mostly dissipated and resulted in a large increase in pore water pressures with respect to the end of excavation. Behind the wall, the pore water pressure decreased and moved closer to the steady seepage condition, but its effect on the lateral effective stress was small becasuse of its magnitude being small, as shown in the figures of post-excavation changes in the lateral stresses (figs. 5.16-5.18) and the lateral earth pressure coefficients diagrams (figs. 5.10-5.15). The variations in lateral total stress followed a similar trend of the pore water pressure and decreased generally.

On the excavated side, the lateral effective stress for the walls of 5m embedment increased whereas the stresses for the walls of deeper embedment decreased. These changes in lateral effective stresses are consistent with the directions of wall movement suggested by the limit

equilibrium analysis. Overall, the lateral total stresses increased in all cases, mainly due to the recovery of pore water pressures.

Fig. 5.19 compares the lateral effective stress distributions from the finite element analyses with those calculated from the limit equilibrium method (section 5.2). Near the retained soil surface and on the excavated side generally, the results from the finite element analysis were higher, probably because of the tendency of the soil to swell. The lateral effective stresses on the retained side above the dredge line for the 5m embedment walls were very close to what would be expected from the limit equilibrium calculation, but the stresses for the walls of deeper embedment were smaller than the passive values assumed. Below the dredge line, the lateral effective stresses tended to move to the distributions assumed in the limit equilibrium calculation, particularly near the toe - i.e. passive for the 5m embedment wall and active for walls of 10m and 15m embedment. There were larger discrepancies between the two methods of calculations near the dredge line. This may be due to the stress discontinuities assumed in the limit equilibrium analysis which would not exist in reality and therefore the abrupt change in stress distribution near the dredge line would be expected to be smoother, as shown in the results from the finite element analysis. Generally, apart from regions near the soil surfaces and at dredge level, the limit equilibrium method gave a reasonable prediction of lateral effective stress.

Comparing these results with those for walls propped at the crest, the lateral effective stresses in present analyses were generally higher behind the wall and lower in front if they had the same embedment ratio.

5.3.2 Soil and Wall Movements

Fig. 5.20 shows the displacement vector diagram for the rigid wall of 10m embedment at the end of reconsolidation. In the vicinity of the wall, the movements of the soil followed a rigid body rotation of the wall about the prop with the crest moving into the excavation, but the magnitude of the rotation at this stage was rather small. Away from the wall, the movements were close to vertical, due mainly to the effect of consolidation. The soil movements for other walls at this stage were very similar, with larger rotations for the shallower embedment walls and more significant bending effects for the more flexible walls.

The variations in the crest and toe deflections as a function of depth of excavation and time after excavation are shown in fig. 5.21. It is interesting to see that although the overall shapes of wall deflection were different (which will be discussed in the following paragraphs), the toe deflections were substantially independent of the wall stiffness if the embedment depths were identical. Furthermore the toe deflections for the deeper walls (of 10m and 15m embedment) were approximately equal, suggesting that there might be a critical depth of wall embedment below which there is no change in the deflection at the toe. However, because of the different embedment depths, the average wall rotation ($\theta=L/\delta$) and the degree of strength mobilised were higher for the wall of 10m embedment than the deeper wall.

During excavation, the over-burden pressure at formation level is gradually reduced, so the soil in front of the wall would provide less resistance to the wall movement and the toe would be expected to move forward. On the other hand, the removal of the soil (and therefore support) in

front of the wall would result in the crest tending to move forward. If a wall is rigid, the overall wall deflection would depend on the relative magnitudes of these two effects. It can be seen from fig. 5.21 that the effect due to removal of the over-burden seemed to dominate the behaviour of walls of deeper embedment depths - the toe deflections were approximately proportional to the excavation depth. In contrast the loss of lateral support in front of the wall was apparently more important for the walls of 5m embedment, resulting in the outward movement of the crest and the toe moving into the retained soil (at least during initial excavation). However if the wall is more flexible, bending effects may enable both the crest and the toe to move forward at the same time during the first stage of excavation, as shown in fig. 5.21 (R351, R361 and R371).

After excavation, the toe deflection decreased (i.e. the toe moved into the retained side) because of the increase in lateral total stress in front of the wall due to the dissipation of pore water suction as explained in section 5.3.1. In most cases this occured mainly within 12 months of excavation. Above the prop, the movement of the wall was consistent with that of the toe with the crest moving in the opposite direction, but the magnitudes of the deflections were dependent on the wall stiffness, being smaller for the more flexible wall.

Fig. 5.22 shows the deflected shapes for all the walls immediately and at 4 years after excavation. For the rigid walls, it is clear that the deflections were primarily due to rigid body rotation about the prop. For the flexible walls, local bending was also significant, mostly within the region extending to about 3m above and below the prop position. For the flexible walls of 15m embedment, further

small bending in the opposite direction occurred beyond approximately 7m below the excavated soil surface.

The incremental (with respect to the end of reconsolidation) displacement vector diagrams for all the walls, at two different instants are shown in figs. 5.23-5.28. Immediately after excavation, for the rigid walls, the soil movements near the wall followed the rigid body rotation of the wall about the position of the prop. Slightly further from the wall, in addition to the effect of wall rotation, the response to vertical unloading became more significant, resulting in the soil in front moving upward at an approximately 45°. Behind the wall, the soil moved predominantly vertically downward. The soil movements for the more flexible walls were generally similar, with the backward horizontal movement just below the retained surface being much smaller, causing the soil to move in a more vertical direction

In the long term, the swelling of the soil in front of the wall dominated the behaviour and the movements were almost vertical in all cases. On the retained side, the soil still moved principally in response to the rigid body rotation of the wall but in an more vertical direction due to the superimposed effects of consolidation.

Fig. 5.29 shows the measured soil movements from the centrifuge test for the flexible wall of 5m embedment, DWC17 (Powrie, 1986). During excavation, the movements occurred mainly in a region close to the wall with the maximum value apparently near the prop location. In the long term, the soil on the excavated side moved approximately vertically upward, suggesting that swelling

was highly significant, and the maximum movement again occurred near the prop position. Comparing fig. 5.29 with fig. 5.24 and noting that the scales for displacement are different in each case, the most obvious discrepancy is behind the wall above the dredge level. This may be due to the props not being properly in contact with the wall at the beginning of the centrifuge test whereas in the finite element analysis the horizontal movement at that position was always prevented. Furthermore, the soil around the bottom left region in the centrifuge test moved approximately horizontally towards the left in the long term. The reason for such movement was unclear but might be an indication that something unusual had happened, or of an error in the measurement of the reference marker positions in the centrifuge model test.

5.3.3 Bending Moments and Prop Loads

For a wall propped at dredge level, it is obvious that the maximum moment would occur at the level of the prop and that its magnitude will be determined by the stresses and pore water pressures on the section of the wall above dredge level. In section 5.3.1, it was shown that the changes in the lateral stresses and pore water pressures above dredge level due to excavation and subsequent excess pore water pressure dissipation were quite small in all cases and were substantially unaffected by the wall stiffness and the embedment depths. It is therefore not surprising that the bending moments above dredge level were broadly similar for all the walls irrespective of the wall stiffness and the embedment depth, as shown in fig. 5.30 and table 5.2. Below dredge level, the bending moments for the walls of 5m embedment decreased steadily to zero at the toe. For the deeper embedment walls, the bending moments

Wall Embedment & Stiffness		Max. Bending Moment, kNm/m		Prop Load, kN/m	
		Short term	Long term	Short term	Long term
5	rigid	2770	1850	2049	1468
10	rigid	3050	2200	2161	1553
15	rigid	2750	2110	2203	1576
5	flexible	2820	1990	1996	1454
10	flexible	3100	2180	2034	1458
15	flexible	2850	2110	2136	1550

Table 5.2 Calculated maximum bending moments and prop loads

dropped to zero at depths between 13.5m and 16.0m and became positive thereafter, implying that the walls underwent contraflexural rotations at these locations. In each case, the bending moments decreased with time in a manner compatible with the changes in lateral total stress.

Also shown on the same figure are some results of the bending moments and prop loads measured from the centrifuge tests (Powrie, 1986). In general, the calculated values from the finite element analyses were higher, probably due to the higher stresses resulting from the props being truly rigidly in place prior to the beginning of the analysis.

Fig. 5.31 shows the prop loads from finite element analyses as a function of the excavation depth and time after excavation. It can be seen that the prop loads were approximately proportional to the depth of excavation and then decreased considerably during the initial period after excavation, due mostly to the strong pore water pressure recovery in front of the wall. Thereafter, the prop loads remained almost unchanged. It is interesting to see that the prop loads were similar in all the cases irrespective

of the stiffness and the total length of the wall, and were in broad agreement with the result from the limit equilibrium calculation shown in fig. 5.8.

5.4 Summary

Based on a limit equilibrium analysis, it has been shown that walls propped rigidly at dredge level with a retained height of 10m could rotate in either direction on excavation, depending on the depth of embedment. For walls of very deep embedment, the analysis may be analogous to that of the walls propped at the crest. The results of finite element analyses have shown that if the wall is rigidly propped at dredge level, the wall deflection would occur primarily as rigid body rotation, again with the possibility that the crest moves into the retained soil.

For walls propped at dredge level, the maximum bending moment will occur at the position of the prop and therefore its magnitude will be determined by the lateral effective stresses and pore water pressure on the cantilevered section above this level. Where the crest rotated into the retained soil, the finite element analyses indicated that the wall flexural stiffness and embedment depth have little effect on the lateral stresses above the dredge level over the range of flexibility considered and hence the maximum bending moment would not be much affected. The finite element analysis also indicated that the toe deflection will remain approximately unchanged and the bending moment will reverse in sign below a certain depth of embedment. These results may suggest that there will be a critical depth of embedment, extending the wall deeper than which will not improve stability. In addition, both the finite element analyses and the limit equilibrium calculations have shown that the prop load is in general comparatively insensitive to the stiffness and total length of the wall.

In comparison with the walls propped at the crest of the same overall length, the lateral stresses for walls propped at dredge level were generally higher; the degree of soil strength mobilised was smaller; and the prop loads were considerably higher. In addition, the wall deflections and the soil movements around the wall were in general smaller. However, the bending moments for the two cases are diffcult to compare because the bending moments for walls propped at the crest will be affected by the overall length whereas the values for walls propped at dredge level are to be determined only by the cantilevered section.

The limitations of the present finite element analyses are that they were based on the assumption that the prop was rigidly in place prior to excavation, which might be difficult or impossible to achieve in practice. Therefore the results presented in this chapter may not truly represent the behaviour which would be expected in reality. More commonly, a diaphragm wall with permanent props at dredge level will be constructed either unpropped until the dredge level is reached or with one or more rows of temporary props nearer the crest. The first option will require a considerable depth of embedment to satisfy the stability criterion even in the short term, and the behaviour of the walls in the second case incorporating a single temporary prop near the crest will be similar to that discussed in chapters 2 and 3, for which the soil movements and bending moments near dredge level will be large and need to be considered.

CHAPTER 6

ANALYSIS OF THE RETAINING WALLS FOR THE A1058 CRADLEWELL BYPASS

CHAPTER 6 - ANALYSIS OF THE RETAINING WALLS FOR THE A1058 CRADLEWELL BYPASS

6.1 Introduction

In previous chapters, the results of investigations into the behaviour of diaphragm walls propped rigidly either at the crest or at dredge level were presented. These investigations were based primarily on the centrifuge model tests which involved some idealisation - in particular, the prop was modelled as rigid and was constructed prior to excavation of the soil in front of the wall - and therefore some of the results may differ slightly from those which might be expected from a field structure. In this chapter, the results of a series of finite element analyses carried out to investigate the effects of some of the factors affecting the practical design and the construction of a wall propped at formation level are presented.

6.2 The Cradlewell Bypass Retaining Walls

As part of the A1058 Cradlewell Bypass in Newcastle-upon-Tyne, a cutting is required near the Holy Trinity Church, approximately 2.5km north-east of the mainline railway station, as shown in fig. 6.1. As with many developments in urban areas, the restricted space available for construction has necessitated the specification of diaphragm type retaining walls.

At the time that the present analyses were carried out, the detailed design of the retaining walls had not been finalised, but a preliminary design study had indicated that the retaining walls would be formed by secant piles of 1.8m diameter. At the deepest section, the final formation level would be approximately 9m below the original ground level. It was suggested that the final carriageway

pavement slab, 1m in thickness, be reinforced and utilised as a permanent prop. No special connection was envisaged between the slab and the wall - i.e. a butt joint - so that the transfer of bending moment across this joint would be dependent on the cross-section remaining in compression. The provisional total length of the piles at the deepest section was 18m. In order both to avoid short term failure and to reduce soil and wall movements during construction, a temporary prop was to be placed at 4m below ground level. A typical cross-section through the cutting at its deepest point is shown in fig. 6.2.

According to the available site investigation reports (1966, 1972, 1985 & 1989), the soil at the site consists generally of stiff over-consolidated boulder clay to depth of approximately 30m. This stratum is underlain by coal measures rocks, which may be regarded as effectively rigid in comparison with the boulder clay.

It is intended to monitor the performance of the structure during and after installation of the walls. The analyses described in this chapter were carried out in order to identify the factors which would be most likely to influence its behaviour.

6.3 Finite Element Modelling

6.3.1 Soil Parameters

It is generally accepted that the behaviour of soil will depend on its current stress state and its stress history. A dense or heavily over-consolidated soil will normally behave quasi-elastically and fail by forming thin rupture planes or in some cases tensile fractures.

Although a linear elastic-perfectly plastic model (with modulus increasing with depth and a Mohr-Coulomb failure criterion) might be argued to be appropriate for the stiff, heavily over-consolidated boulder clay, the Schofield model in CRISP was again taken as the constitutive soil model in the present analysis. It was chosen in preference to the first model because in the Schofield model, the soil stiffness in each element is calculated in the program CRISP according to its stress history and the current stress state. It was anticipated that the changes in stress in the soil behind the wall would be considerable. In addition, after the removal of the temporary prop, there will be a tendency for the wall to separate from the soil, and it was important that the constitutive model was able to accommodate such a situation. Furthermore, it has been demonstrated in previous chapters that this soil model can be used to represent reasonably closely the behaviour of a heavily over-consolidated soil.

The results from the drained triaxial tests in the 1966 site investigation report (table 6.1) indicated that the soil friction angle ϕ' was in the range of 21° to 30°, with an average of about 26°. It was decided to adopt ϕ'=26° and the slope for the critical state line M was calculated accordingly to be 1.03. The results from the laboratory tests in the 1989 site investigation report (table 6.2) showed that the permeability of the boulder clay is generally in the range of 0.4-3.7 x 10^{-10}m/sec. Although results from some shallower depths revealed a slightly higher permeability, it was believed that these were less representative of the soil generally. A permeability of 10^{-10}m/sec was adopted for the finite element analysis. The bulk unit weight of the soil was taken as 22 kN/m^3.

Borehole	Depth	Natural Moisture Content (%)	Bulk Density (lb/cu.ft)	Liquid Limit (%)	Plastic Limit (%)	Plasticity Index	Classification	Cohesion Intercept (lb/sq.ft)	Angle of Shearing Resistance
3	4'6 - 5'0	11.2	125.3	30	13	17	CL	163	27° 48'
5	5'0 - 6'6	15.3	115.7	31	15	16	CL	212	27° 48'
31	5'0 - 6'6	17.4	105.7	35	20	15	CI	587	21° 21'
51	15'0 - 16'6	10.5	127.5	30	13	17	CL	477	25° 7'
71	4'6 - 6'0	12.6	123.0	31	14	17	CL	161	26° 26'
72	9'0 - 10'6	8.1	117.3	24	13	11	CL	293	30° 38'

Table 6.1 Index classification and results of drained triaxial compression tests (from table D, 1966 S.I.)

BOREHOLE/ SAMPLE NO.	DEPTH (m)	EFFECTIVE CELL PRESSURE/ PRESSURE RANGE (kN/m^2)	COEFFICIENT OF PERMEABILITY (m/s)
902/11	7.30	200 - 400	1.0×10^{-10}
902/14	9.40	200 - 400	2.1×10^{-10}
902/17	11.30	200 - 400	2.2×10^{-10}
904/5	1.95	50 - 100	1.0×10^{-9}
904/7	2.55	50 - 100	3.7×10^{-10}
905/3	1.30	48 - 96	1.4×10^{-9}
905/10	8.50	100 - 200	1.2×10^{-9}
913A/9	5.15	55	1.2×10^{-10}
914/10	6.00	85	4.7×10^{-11}
914/16	10.30	130	2.6×10^{-10}
914/19	12.00	150	3.9×10^{-11}
914/28	18.00	205	5.5×10^{-11}
914/31	20.00	225	1.1×10^{-11}
915/33	17.20	195	1.4×10^{-10}

Table 6.2 Summary of permeability values from laboratory tests (from table 4, 1989 S.I.)

The Cam-clay parameters λ, κ and Γ (for their definitions, see section 1.4.2) were estimated from the oedometer test results for the Tyneside Metro site investigation (1972), as shown in fig. 6.3. Although the values of the Cam-clay parameters should strictly be related to isotropic compression and swelling, it is believed that the error introduced by these data from one-dimensional tests is insignificant in comparison with the other uncertainties involved. From fig. 6.3, it is difficult to determine the maximum pre-consolidation pressure p_c' and the value of λ. However since the soil was heavily over-consolidated and the wall was unlikely to subject to severe loading, the values of p_c' and λ are not considered of prime importance.

For the purpose of estimating the parameters, the soil was assumed to have been subjected previously to an effective overburden pressure of 2500 kPa. The insitu earth pressure coefficients prior to installation of the walls were then calculated using the equation suggested by Mayne & Kulhawy (1982):

$$K_o = \sigma_h'/\sigma_v' = (1-\sin\phi')\ OCR^{\sin\phi'} \qquad .....(6.1)$$

The maximum value of K_o allowed was taken as the Rankine's passive coefficient K_p (=2.56 for ϕ'=26°). The earth pressure coefficients and the lateral effective stresses calculated on these bases are shown in fig. 6.4.

The soil parameters finally adopted for analysis are shown in table 6.3.

Soil parameters:
(Schofield model)

κ = 0.016		γ_w= 9.81	kN/m³
λ = 0.155		γ_b= 22.0	kN/m³
Γ = 2.41	(e_o=1.41)	k_v= 1 x 10^{-10}	m/sec
M = 1.03		k_h= 1 x 10^{-10}	m/sec
ν = 0.2			
ϕ_H'= 15.5°		k_x= 1 x 10^{-6}	m/sec
s = 2.0		k_y= 1 x 10^{-6}	m/sec

Table 6.3 Parameters used in the finite element analysis of the Cradlewell Bypass retaining walls

Taking Poisson's ratio ν'=0.2 (Stroud & Butler, 1975), the insitu stiffness of the soil assumed in the Schofield model can be calculated using equations 2.1 and 2.2, and the resulting profile is shown in fig. 6.5 (profile 5). For comparison, soil stiffness profiles estimated using other methods are also shown in fig. 6.5, namely:

1. E' = (18.0 + 0.45 z) MPa, based on the 1985 Cradlewell site investigation SPT blow counts (fig. 6.6) with E'=450N (Stroud & Butler, 1975).

2. E' = (6.4 + 1.45 z) MPa, based on the 1989 Cradlewell supplementary site investigation SPT blow counts (fig. 6.6) with E'=450N.

3. E' = (3.4 + 1.25 z) MPa, based on the 1966 drained triaxial test results (secant moduli at 1% shear strain).

4. E' = (32.5 + 0.50 z) MPa, idealised stiffness profile based on the 1989 elastmeter test results. The actual values measured, listed in table 6.4, are also shown. It is understood that these were secant moduli at 0.01% cavity strain after a stress reversal.

Borehole No.	Depth (m)	Test No.	Initial Tangent		Re-load Loop				Cavity Strain Range %	Adjusted Strain	Cavity Range (0.01%)	Limit Pressure P_L (MN/m^2)	Undrained Cohesion C_u (MN/m^2)	
					Tangent		Secant							
			G (MN/m^2)	E (MN/m^2)	G (MN/m^2)	E (MN/m^2)	G (MN/m^2)	E (MN/m^2)		G (MN/m^2)	E (MN/m^2)			
913	5.00	1	3.51	8.43	5.31	12.74	3.71	8.90	0.052	16.81	40.33	2.07	1.05	
	10.00	2	4.16	10.00	7.99	19.18	12.11	29.06	0.049	28.72	68.93	3.16	1.24	Notes:
	15.00	3	5.03	12.06	8.00	19.20	13.70	32.88	0.037	23.11	55.45	3.59	1.36	Poisson's Ratio assumed to be 0.2 for determination of drained elastic modulus.
914	5.00	1	0.17	0.41	0.96	2.30	1.84	4.42	0.017	3.24	7.78	0.65	0.27	
	10.00	2	6.16	14.80	12.61	30.26	26.56	63.74	0.013	22.67	54.50	1.99	0.63	
	15.00	3	3.38	8.12	6.62	15.89	31.50	75.60	0.009	31.50	81.91	1.90	0.70	
	20.00	4	3.01	7.22	4.44	10.66	6.58	15.79	0.075	24.38	58.50	2.65	1.24	

Table 6.4 Summary of elastmeter test results in glacial clay (from table 3, 1989 S.I.)

It may be seen from fig. 6.5 that the Cam-clay stiffness profile based on κ=0.016 is apprarently on the high side in comparison with the other idealised profiles, particularly below the depth of 20m. However the actual results from the elastmeter tests (table 6.4) displayed considerable scatter. The results from the standard penetration tests (fig. 6.6) indicated an equally scatter of data points. Also secant modulus at 1% strain from triaxial compression tests would be expected to be on the low side and therefore the chosen profile does not seem unreasonable. In a later analysis (section 6.5.3), a higher value of κ=0.032 was used to investigate the effect on the behaviour of the walls of a lower soil stiffness.

6.3.2 Other Parameters and Boundary Conditions

Because the walls are to be formed by a series of secant piles of 1.8m diameter, the thickness of the walls will vary along their length. However it is believed that the overall behaviour will be similar to a plane strain condition and a complex 3-dimensional analysis was not considered to be justified. Consequently, the uniform wall thickness equivalent to a diaphragm wall for the secant piles was calculated according to the equations shown in fig. 6.7. The walls were modelled as linear elastic with Young's modulus E=17x10^{6}kPa. This value of stiffness was adopted to take account the possibility of long term cracking and the uncertainty in the evenness in the wall thickness. The shear modulus G was calculated to be 7.4x10^{6}kPa for ν=0.15.

The interface between the wall and soil was modelled using slip elements as described in section 2.2.1 with ϕ'=26°, c'=0, t=0.001m, G=7500kPa and E'=20000kPa. The temporary prop was initially modelled as rigid (EA/L = 1x10^{10}kN/m).

For a full strength rigid connection between the wall and the carriageway slab, rotation in either member will undoubtedly induce a differential compressive/tensile force on the other through the connecting nodes (see fig. 6.8). It was, however, decided not to rely on the transfer of bending moment between the wall stem and the permanent carriageway slab. Therefore a triangular element was used to represent the part of the slab adjacent to the wall so that the two members were connected by a single node. The results in later sections will show that the bending moments transferred were negligible. In reality, a butt joint would still permit the transfer of bending moment provided that the cross-section remained in compression. Therefore the bending moments of the wall and the slab presented in section 6.4 are likely to be over-estimated due to the connection effect alone. The elastic properties (i.e. E, G and ν) of the permanent prop slab were identical to those of the wall.

The finite element mesh used for the analysis is shown in fig. 6.9. This represents one half of the cross-section through the cutting. The boulder clay in general extends to a depth of 30m near the vicinity but the base boundary was set conservatively at about 40m below ground level. The soil was assumed free to move along the vertical boundary whereas nodes at the base were restrained from any movement - i.e. pinned.

The record of the water tables in the standpipe piezometers (table 6.5) shows that the water level is in general more than 3m below ground level. Throughout the analysis, the water table behind the wall was maintained pessimistically at 1m below ground level. At the far vertical boundary, the pore water pressure was maintained in hydrostatic

Borehole No.	Depth to water, m.b.g.l.					
	16/4/89	17/4/89	18/4/89	19/4/89	20/4/89	21/4/89
912	-	3.59	3.42	3.05	2.77	-
914	Dry	Dry	Dry	Dry	Dry	Dry
915	-	-	-	-	-	-

Table 6.5 Record of water level readings in standpipe piezometers (from table 2, 1989 S.I.)

1	2	3	4	5	6	7
40.4	0.0	0.0	0.0	2.56	1.0	0.0
39.4	1.0	0.0	22.0	2.56	1.0	22.0
38.4	2.0	9.8	34.2	2.56	1.0	34.2
36.4	4.0	29.4	58.6	2.56	1.0	58.6
31.4	9.0	78.4	119.6	2.17	1.0	119.6
26.4	14.0	127.4	180.6	1.83	1.0	180.6
22.4	18.0	166.6	229.4	1.66	1.0	229.4
21.5	18.9	175.4	240.4	1.63	1.63	392.5
15.4	25.0	235.2	314.8	1.46	1.46	461.0
8.4	32.0	303.8	400.2	1.34	1.34	537.3
0.0	40.4	386.1	502.7	1.23	1.23	619.3

Column
1 Level, m.A.O.D.
2 Depth below original ground surface, m
3 Pore water pressure, kPa
4 Vertical effective stress, kPa
5 Insitu lateral earth pressure coefficient prior to installation of the walls (equation 6.1)
6 Pre-excavation lateral earth pressure coefficient
7 Pre-excavation lateral effective stress, kPa

Table 6.6 Calculated insitu lateral effective stresses

equilibrium with this groundwater level. The base boundary and the centreline of the cutting were modelled as impermeable. The water table in front of the wall was kept at the excavated surface during excavation, and 1m below final formation level (beneath the slab) after excavation.

As with previous chapters, the present analysis modelled only the behaviour of the wall after the piles were installed and therefore the insitu stress conditions mentioned in section 6.3.1 have to be modified. At Bell Common, the lateral earth pressure coefficients in the heavily over-consolidated London clay decreased from their insitu values of approximately 1.6 to values very close to unity (Tedd et al, 1984) during the construction of the secant piles. It was assumed that the insitu stresses above the toe level of the piles in the present retaining walls would move similarly towards the condition K=1 during pile construction. The lateral stresses corresponding to these assumed conditions were calculated (listed in table 6.6) and input as the initial stresses in the program. However, since the soil stiffness used in CRISP is formulated corresponding to the current mean normal stress (see equations 2.1 & 2.2), the pre-excavation stiffness profile was different from the insitu profile, as shown in fig. 6.5 (profile 5a).

6.3.3 Sequence of Analysis

The construction process envisaged in practice was simulated as closely as possible in the analysis using the following load increments (starting with the wall already in place):-

1. Excavation to 4m below ground level (b.g.l.) by the removal of the top 4 layers of elements over a period of 16 days (stage 1).

2. Construction of the temporary prop by adding a bar element in 1 day.

3. Further excavation to 10m b.g.l. by the removal of the next 5 layers of elements over another 28 days (stage 2).

4. 7 days' excess pore water pressure dissipation (stage 3a).

5. Construction of the carriageway slab by adding the concrete elements in 7 days (stage 3b).

6. 7 days' excess pore water pressure dissipation (Stage 3c).

7. Dismantling the temporary prop by the removal of the bar element in 1/2 day (stage 3d).

8. 120 years' excess pore water pressure dissipation, modelling the long term behaviour of the wall (stage 4).

6.4 Results and Discussions

6.4.1 Soil and Wall Movements

Figs. 6.10 and 6.11 show the cumulative displacement vector diagrams and wall deflections respectively at four different instants, namely immediately after excavation to 4m below ground level (stage 1), immediately after excavation to 10m below ground level (stage 2), immediately after placement of the permanent prop and removal of the temporary prop (stage 3) and 120 years after completion of the retaining walls (stage 4 + 120 years). At stage 1 the wall deflection was mainly a result of rotation about the toe, which itself moved forwards by approximately 3mm (fig. 6.11). The soil in front of the wall moved predominantly vertically due to unloading, whereas behind the wall, the soil followed the wall deflection and moved mainly

horizontally into the cutting. At stage 2, the soil movements were similar to before but generally larger in magnitude. It is interesting to see that the analysis predicted an upward movement for the soil immediately behind the wall. Such a phenomenon is quite common in finite element analysis but rarely occurs in practice (Hubbard et al, 1984). This may be because the soil stiffness used in the finite element analysis is unable to reflect the stiffer response in reality when the change in stress (and strain) is small (Jardine et al, 1986). As a result of the temporary prop, the mode of wall deflection at this stage was quite different from before - the toe continued to move forward but the crest moved backwards into the retained soil because of rotation about the prop. Bending effects at this stage are rather more significant.

Immediately after the removal of the temporary prop (stage 3), the wall rotated about the permanent prop position, resulting in a very large incremental deflection over the upper half of the wall (from 15mm to 46 mm at the crest) as shown in fig. 6.12. The soil movements followed closely the wall deflection, being almost horizontal into the cutting near the crest, with much smaller movements elsewhere. In the long term, the soil swelling due to the dissipation of the excess pore water pressures dominated the behaviour, with the post-construction soil movements being almost vertical. There was some further wall rotation into the excavation about a pivot slightly below the permanent prop position (rather than exactly at the connection because of the simultaneous compression of the prop), but most of this movement occurred within 2 years of construction as shown in fig. 6.12.

Figs. 6.13 and 6.14 show the post-construction soil surface movements (incremental) on both sides of the wall. As explained earlier, the comparatively large upward movement

immediately behind the wall was unlikely to occur in practice. The soil in front of the wall swelled approximately uniformly due to the reduction in effective vertical stress as the negative excess pore water pressures dissipated. It can be seen from fig. 6.14 that there were differential vertical movements between the soil and the wall, indicating that slip was taking place.

In contrast to the results presented in chapter 5, the walls in the present analysis did not rotate into the retained soil about the position of the permanent prop. This may be partly because the permanent prop (concrete slab) used in this analysis was of finite stiffness and would compress according to the axial load acting upon it. A small translational movement of the wall could affect both the stresses behind the wall and the sense of wall rotation. Perhaps more significantly, placing a carriageway slab on the excavated surface imposes a restraint on the soil heave and thus the effect of the removal of overburden (which causes the toe to move into the excavated side) was less significant than in the cases presented in chapter 5. Therefore it is not surprising that the wall rotated in a direction with the crest moving into the cutting.

6.4.2 Stresses and Pore Water Pressures

The lateral stresses and pore water pressure distributions at different stages are shown in fig. 6.15. At the end of excavation (stage 2), the pore water pressures on both sides of the wall dropped considerably as a result of the removal of the soil but the changes in the average effective stress were insignificant, as would be expected for undrained behaviour. Just below the excavated surface, the lateral stresses were unrealistically high, probably due to numerical difficulties.

Immediately after removal of the temporary prop (stage 3), the sudden change in the wall deflection led to the development of pore water suctions near the retained surface and resulted in a decrease in the total lateral stress. The pore water pressure on the excavated side increased slightly, probably due to the loading by the placement of the slab. Apart from the zone near the crest, the changes in lateral total and effective stresses were small.

In the long term, the pore water pressures decreased behind and increased in front of the wall, moving in both cases to values very near to those given by the linear approximation to steady seepage. The lateral effective and total stresses in general increased slightly in the excavated soil. There was a marked drop in lateral effective stress in the retained soil above the formation level as a result of pore water pressure recovery but the change in lateral total stress was rather insignificant. It is interesting to see that both the lateral effective and total stresses were nearly zero for a depth of up to 3m below the retained surface. In practice, if the wall moved as predicted when the temporary prop was removed, a tension crack might have developed between the wall and soil, resulting in the soil standing unsupported in the short term. In the long term, as the pore water suction dissipated, the soil would perhaps fail and slump to fill the crack. Since the Schofield model is able to reduce the soil stiffness when the mean normal stress decreases, it is able to simulate this effect more realistically, and the results of near-zero stresses might imply that the soil had failed as may occur in practice.

Depth,m	Lateral pressure coefficients on retained side				Lateral pressure coefficients on excavated side			
	Stage1	Stage2	Stage3	Stage4+ 120years	Stage1	Stage2	Stage3	Stage4+ 120years
0.11	0.69	0.73	0.86	0.14				
0.50	0.73	0.80	0.73	0.11				
0.89	0.72	0.83	0.52	0.05				
1.11	0.69	0.84	0.44	0.02				
1.50	0.68	0.86	0.43	0.03				
1.89	0.65	0.86	0.38	0.02				
2.11	0.68	0.87	0.40	0.04				
2.50	0.75	0.90	0.52	0.13				
2.89	0.81	0.92	0.64	0.21				
3.11	0.83	0.92	0.68	0.25				
3.50	0.86	0.94	0.72	0.32				
3.89	0.88	0.95	0.75	0.38				
4.11	0.89	0.96	0.77	0.41	3.44			
4.50	0.90	0.96	0.80	0.45	1.96			
4.89	0.92	0.96	0.83	0.49	1.18			
5.11	0.92	0.96	0.84	0.51	1.16			
5.50	0.93	0.95	0.86	0.55	1.11			
5.89	0.94	0.95	0.87	0.58	1.08			
6.17	0.94	0.95	0.88	0.60	1.09			
6.75	0.95	0.94	0.90	0.65	1.07			
7.33	0.96	0.94	0.93	0.69	1.06			
7.67	0.96	0.93	0.94	0.71	1.05			
8.25	0.97	0.93	0.96	0.75	1.05			
8.83	0.98	0.93	0.98	0.79	1.04			
9.11	0.98	0.93	0.99	0.81	1.04			
9.50	0.98	0.93	1.00	0.83	1.04			
9.89	0.99	0.94	1.01	0.85	1.04			
10.17	0.99	0.94	1.01	0.86	1.04	3.52	2.02	3.21
10.75	0.99	0.95	1.03	0.89	1.03	1.91	1.59	2.02
11.33	1.00	0.95	1.04	0.91	1.03	1.16	1.19	1.32
11.75	1.00	0.96	1.03	0.92	1.03	1.16	1.12	1.24
12.60	1.01	0.98	1.04	0.94	1.03	1.13	1.08	1.17
13.45	1.01	0.99	1.04	0.96	1.03	1.14	1.09	1.15
13.96	1.01	1.00	1.04	0.97	1.03	1.15	1.11	1.13
14.85	1.03	1.03	1.06	1.02	1.03	1.14	1.12	1.10
15.74	1.06	1.05	1.07	1.08	1.03	1.14	1.13	1.08
16.23	1.06	1.07	1.08	1.11	1.04	1.13	1.11	1.07
17.00	1.07	1.06	1.12	1.18	1.05	1.27	1.19	1.14
17.77	1.09	1.03	1.16	1.29	1.07	1.46	1.29	1.23

Table 6.7 Lateral pressure coefficients at different stages

Table 6.7 tabulates the lateral earth pressure coefficients ($K=\sigma_h'/\sigma_v'$) at different stages on both retained and excavated sides. These values were calculated using the actual effective lateral and vertical stresses from the finite element analysis. At stage 1, with the unpropped wall excavated to 4m below ground level, K moved from the pre-excavation value of 1.0 to approximately 0.7 behind the wall above the excavated surface, due to the crest moving forward. The incremental changes below the formation level were comparatively small on both sides of the wall (except just below the excavated surface), implying that the wall was stable and remote from collapse. After installing the temporary prop, further excavation did not significantly affect the stress condition behind the wall, but the relatively larger forward wall movement near the toe (fig. 6.11) caused the soil on the excavated side to move more towards the passive condition. The excess pore water pressure dissipation ensuing after completion of the retaining walls, and perhaps the development of the tension crack near the retained surface, had a significant effect on the effective stresses behind the wall. At 120 years after construction, the lateral pressure coefficients behind the wall dropped almost to zero in top 2.5m; these values are unrealistically low, even if the earlier suggestion of the failure of the soil in this region is correct. The lateral pressure coefficients below the top 2.5m increased gradually with depth, becoming greater than unity near the toe.

6.4.3 Wall Bending Moments

The predicted bending moments along the wall are shown in fig. 6.16. The shapes of the bending moment diagrams at different stages were generally compatible with those calculated from the limit equilibrium methods described in chapter 5. With the temporary prop in place, the wall

rotated predominantly about the prop position, with the largest deflection occurring near the excavated surface. At this stage, the predicted maximum bending moment was near the formation level and equal to approximately 1260kNm/m (tension on excavated side). After the temporary prop was removed, the wall rotated about the new position at the permanent prop and the bending moments reversed direction with tensile stress now generally on the retained side. The maximum bending moment at this stage was approximately 1150kNm/m. There were only small post-construction changes in bending moment in the long term, which were compatible with the small increase in the total lateral stress over the same period of time.

The analysis predicted some negative bending moments near the retained soil surface (with a maximum of approximately 70kNm/m) in the post-construction period, implying that the longitudinal stress in the wall was tensile on the excavated side. This may be either due to the shear stress acting downwards at the back of the wall (Hubbard et al, 1984) or the small residual tensile force within the interface element. Therefore the predicted bending moments may err on the low side. Assuming that the negative moment was caused by a uniformly distributed tension from the interface element and pessimistically that such a tension will be distributed along the whole length of the wall, the maximum error in the long term maximum bending moment would be approximately 200kNm/m.

6.4.4 Prop Loads

It can be seen from fig. 6.17 that the load on the temporary prop was approximately proportional to the depth of excavation, reaching a maximum value of 602kN/m at the

end of stage 2. When the temporary prop was removed, the load was almost instaneously taken up by the permanent prop*. The prop load decreased thereafter, in a manner consistent with the change in stresses discussed in section 6.4.2.

Comparing the present results with those in chapter 5 and the experiments (Powrie, 1986), the prop loads predicted were considerably smaller (approximately 40% of the finite element analyses and 60% of the actual centrifuge tests). This is reasonable, because the stresses in the retained soil in the present analysis would be expected to be lower due to the movement of the wall prior to the construction of the permanent prop. Consequently, both the prop loads and bending moments are expected to be lower than the centrifuge tests and the finite element analyses thereof.

6.4.5 Carriageway Slab

The carriageway slab in this analysis had two effects; both acting as a permanent prop to the wall and restricting heave of the excavated soil surface. As might be expected, bending moments were developed in the slab as the excess pore water pressures induced on excavation dissipated with time and the soil in front of the wall tended to swell. The slab bending moments shown in fig. 6.18 were deduced, similarly to the wall bending moments, from the stresses inside the slab element. In the analysis, when the slab elements were added to the mesh, the self-weight and the

---

* The permanant prop load was deduced from the axial stress at the centre of the concrete slab element nearest to the wall multiplied by the cross-sectional area.

pre-assigned stiffness of the elements induced a sagging bending moment. In reality, the concrete would have insufficient strength during this time (stage 3b) to sustain the bending moments. Accordingly, the bending moments presented in fig. 6.18 are incremental values with respect to the end of stage 3. Fig. 6.18 shows that the bending moments increased with time with a maximum value at the centreline and rather small values close to the wall.

6.5 Some Factors Affecting The Behaviour of the Retaining Walls

Case	Variation	Pre-excavation K_o value above toe level	Slope of swelling line κ	Wall thickness T_w, m	Slab thickness T_s, m	Temp. prop stiffnes EA/L, kN/m
1	Standard	1.0	0.016	1.50	1.0	$1x10^{10}$
2	Increased K_o	2.0	n/c	n/c	n/c	n/c
3	Reduced soil stiffness	n/c	0.032	n/c	n/c	n/c
4	Reduced wall thickness	n/c	n/c	1.25	n/c	n/c
5	Reduced slab thickness	n/c	n/c	n/c	0.5	n/c
6	Reduced temp. prop stiffness	n/c	n/c	n/c	n/c	$2.8x10^{5}$

Table 6.8 Summary of analyses for the Cradlewell Bypass retaining walls

6.5.1 Introduction

At the time when this study was carried out, the design of the walls had not been finalised. In addition, although the information adopted for analysis in section 6.4 was

thought to be reasonably representative of the actual conditions, some of the parameters used were based on incomplete tests, empirical formulae or data from previous investigations at other nearby sites. Also some analyses were carried out before the results from the 1989 site investigation became available. Therefore the factors most likely to affect the analysis were investigated and the results compared with those presented in section 6.4. Except where otherwise specified, the parameters for the analyses in this section were the same as before, known as the standard case. These analyses are summarised in table 6.8.

6.5.2 Case 2 - Increased Pre-excavation Lateral Earth Pressure Coefficient K_o

Although the analysis modelled the events after the walls were already in place, the effect of stress relief during wall installation is important to the post-excavation behaviour of the retaining wall. A pre-excavation lateral pressure coefficient of unity was assumed above the toe level in the initial analysis (case 1), the effect of a less severe stress relief (K_o=2.0 maximum) will be discussed in this section.

It can been seen from the lateral stress and pore water pressure distribution diagrams (fig. 6.19) that the most obvious difference between the standard and the present analyses was that the lateral effective stresses were higher (nearly double) at all stages. The lateral total stresses increased accordingly. Consequently, the predicted bending moments and prop loads were substantially higher, especially in the long term, as shown in fig. 6.20 and table 6.9. However since the soil stiffness in CRISP

Stage	Case 1: Standard			Case 2: Increased K_o			Case 3: Reduced soil stiffness			Case 4: Reduced wall thickness			Case 5: Reduced slab thickness			Case 6: Reduced temp. prop stiff.		
	2	3	4+ 120 years	2	3	4+ 120 years	2	3	4+ 120 years	2	3	4+ 120 years	2	3	4+ 120 years	2	3	4+ 120 years
Outward deflection at crest of wall, mm	14.9	46.4	54.6	10.3	51.3	60.5	31.3	76.9	90.2	13.9	52.6	62.8	15.7	42.1	48.9	17.6	47.7	55.9
Outward deflection at toe of wall, mm	19.6	14.6	10.4	16.7	11.6	8.5	39.4	27.8	19.3	18.9	14.6	10.6	18.4	14.6	10.7	19.5	14.6	10.6
Outward deflection at temp. prop position, mm	19.5	38.0	43.0	15.6	39.9	45.2	37.3	64.1	72.3	20.1	42.5	48.6	19.5	34.7	38.9	21.5	39.1	44.0
Outward deflection at formation level, mm	24.1	25.1	25.6	20.8	22.4	22.8	43.7	44.9	45.7	25.9	26.7	27.2	23.1	24.4	24.7	24.9	25.9	26.3
Approximate maximum wall bending moment, kNm/m	-1260	1151	1245	-1558	1998	2370	-1445	1421	1345	-1075	963	1113	-1102	1027	1114	-1208	1100	1213
Load in temporary prop, kN/m	582	----	----	953	----	----	651	----	----	555	----	----	545	----	----	553	----	----
Load in permanent prop (carriageway slab), kN/m	----	716	558	----	1075	1087	----	707	548	----	534	471	----	709	564	----	676	538
Max. hogging bending moment in permant prop, kNm/m	----	----	309	----	----	146	----	----	531	----	----	280	----	----	59	----	----	301
Post-construction heave at centre of carriageway slab, mm	----	----	20.6	----	----	14.2	----	----	38.3	----	----	19.8	----	----	23.9	----	----	20.3
Post-construction heave at edge of carriageway slab, mm	----	----	13.6	----	----	10.8	----	----	26.4	----	----	13.2	----	----	12.2	----	----	13.4

Table 6.9 Summary of results for the analyses of the Cradlewell Bypass retaining walls

is formulated according to the current effective mean normal stress, the soil stiffness was also increased (profile 3 in fig. 6.21). As a result, the difference in wall deflection was small (fig. 6.22). Also because of the higher soil stiffness, the post-construction heave in the carriageway slab was smaller, resulting in a smaller hogging bending moment as detailed in table 6.9.

6.5.3 Case 3 - Reduced Soil Stiffness

The results shown in fig. 6.3 for the oedometer tests were rather scattered, making it difficult to determine a unique κ value. In addition, the value of κ is normally not a constant but depends on the stress level and the over-consolidation ratio (Al-Tabbaa, 1987). It was therefore decided to analyse the wall with a higher κ value. It can be seen from fig. 6.3 that the choice of a value of κ=0.032 would not be unreasonable. With this change, the soil stiffness was reduced by a factor of approximately 2 (profile 4 in fig. 6.21).

As would be expected, the predicted wall deflections for a soil of lower stiffness were considerably higher than those for the standard case, rising from 46mm to 77mm immediately after excavation (stage 3) and from 55mm to 90mm in the long term at the crest. The changes in the associated toe deflection were similar, as shown in fig. 6.22 and table 6.9. In the meantime, the predicted wall bending moments at different stages were slightly higher than before, implying that the lateral stresses behind the wall were also higher. The predicted temporary prop loads showed a similar increase but the magnitudes of the permanent prop loads were slightly lower. As a result of the lower soil stiffness, there was a tendency for higher post-excavation heave at the excavated surface, leading to higher hogging bending moments in the permament prop slab.

6.5.4 Case 4 - Reduced Wall Thickness

In order to investigate the possibility of a more economical design, a wall of thickness 1.25m, equivalent approximately to secant piles of 1.5m diameter, was analysed. Keeping the Young's modulus of the wall unchanged, the reduction in wall thickness from 1.5m to 1.25m effectively reduces the flexural stiffness by approximately 40%.

It can be seen from fig. 6.22 that the major difference in the deflection profile at stage 2 was near the excavated surface, where the maximum movement occurred, but this difference was only about 8%. In the long term, there was no noticeable difference in deflection below the formation level whereas the crest deflection increased from 55mm to 63mm. There was also a decrease in wall bending moments at stage 2: this was consistent with the results for walls propped at (or near) the crest in chapter 3 for which the bending moment decreased as the wall became more flexible. The change in the bending moment, in comparison with the standard case, at 120 years after construction was smaller and was in agreement with the suggestion in chapter 5 that bending moments for walls of high stiffness are not much dependent on the exact value of the wall flexibility. The effects on the permanent prop slab heave and moment due to the change in wall thickness were rather insignificant as shown in table 6.9.

6.5.5 Case 5 - Reduced Slab Thickness

The major consequences of reducing the slab thickness to 0.5m were to reduce the permanent prop stiffness and to provide less restraint to the excavated surface heave. It is also important that less excavation was required (to

9.5m rather than 10m as the standard case) and therefore the results presented for this case at stage 2 are not strictly comparable with other cases.

As detailed in table 6.9, the long term hogging bending moment at the centre of the cutting in the slab was very small. This is reasonable because the slab flexural stiffness had been reduced to only 13% of the standard case. The maximum heave was approximately 24mm. Though higher than the standard case, it is still much less than that due to a lower soil stiffness. The variations in wall bending moments between case 5 and case 1 were understandably small as shown in fig. 6.20. However the predicted crest deflection decreased from 55mm to 49mm. This is probably due to the walls rotating about the bottom of the prop slab at a slightly higher position.

6.5.6 Case 6 - Reduced Temporary Prop Stiffness

The chosen temporary prop stiffness ($P/\delta=EA/L$) of 2.8×10^{-5} kN/m represented circular hollow section beams of 600mm diameter, 12.5mm thick, at 2m intervals and spanning across the cutting. With a predicted temporary prop load of 600kN/m at stage 2 in the standard case, this prop stiffness would result in the wall moving forward by approximately 2.1mm at the prop position. It was first thought that with higher wall deflection during excavation, the stress reduction behind the wall would be significant, resulting in a lower wall bending moments in the long term.

It can be seen from fig. 6.22 that the wall deflection was slightly greater, as would be expected, and the predicted temporary prop load decreased correspondingly. By 120 years after construction, though the deflection above the formation level was still higher than the standard case,

the overall influence was less significant. The predicted bending moments shown in fig. 6.20 showed that there was some reduction, but perhaps not as much as was at first expected. Understandably, a lower temporary prop stiffness did not significantly affect the long term post-construction behaviour of the wall and the variations in slab moment, permanent prop load, and slab heave were quite small.

6.5.7 Other Considerations

A supplementary analysis was carried out to investigate the effect of a more rigid connection, which could be beneficial, since a rigidly connected slab will act like a relieving platform in reverse: upward stresses on a platform in front of the wall have the same effect as downward stresses on a platform behind in relieving bending moments in the stem of the wall (Bolton, 1979). In such an analysis, a 8-node quadrilateral element was used instead of a 6-node triangular element in the part of the carriageway slab nearest the wall. An interface element was placed between the two members, allowing separation of the slab from the wall and effectively simulating a butt joint in practice. However, since there was considerable forward movement in the wall at all stages, these members were constantly in contact and the joint was in compression. The results were:

1) to induce a sagging bending moment in the slab at the connection (due to higher compression in the upper fibre of the slab) of 171kNm/m at 120 years after excavation (stage 4+);

2) to reduce the magnitudes of the hogging bending moment and heave in the slab near the centre line - 212kNm/m and 17.3mm respectively at stage 4+ (c.f. 309kNm/m and 20.6mm respectively for the standard case); and

3) to reduce the wall bending moments to a maximum of 930kNm/m at stage 4+ (c.f. 1245kNm/m for case 1).

It has been suggested that in walls of this type a hinge connection might be incorporated at the centre of the carriageway slab to relieve the slab bending moment (Webb, 1989). However, it can be seen from table 6.9 that the maximum hogging bending moments were in all cases less than 531kNm/m. Although this value would be sensitive to the time lag between the completion of excavation and the construction of the slab and also to the permeability of the soil, a higher hogging bending moment could be easily catered for by specifying a thicker depth at the centre of a non-uniform thickness slab rather than allowing undesirably large movements of the carriageway.

The behaviour of a wall of this nature will inevitably be sensitive to the soil permeability and the sequence of construction in practice. An over-estimate of permeability might lead to a quicker dissipation of the excess pore water pressures induced on excavation, and consequently might under-predict the eventual upthrust on the slab. In addition, since the retaining walls are to be formed by secant piles, the possibility of water leaking through them would result in an increase in the pore water pressure in the soil in front of the wall below carriageway level. An increased swelling in the soil would bring further upward loadings on the slab. Unfortunately, there were insufficient data to warrant further investigation of these points, but it may be useful to study these aspects in future if more detailed data are forthcoming.

6.6 Summary

It has been shown in the analysis of the retaining walls for the Cradlewell Bypass that if the wall was allowed to move or rotate prior to the construction of the prop at formation level, considerable reduction in the lateral stresses would result. Consequently, the predicted wall bending moments and prop loads would be substantially lower than those for rigidly propped walls. For walls permanently propped at dredge level, a temporary prop near the crest would reduce wall movements and improve stability during excavation. Modelling a permanent prop of finite stiffness, in contrast to results of a rigid prop, has demonstrated that the incremental wall deflection would be by rotation outward with the crest moving into the cutting. Also, incorporating the carriageway slab as permanent prop will not only improve the wall stability, but also help to prevent excessive heave of the soil in front of the wall.

Amongst the factors likely to affect the behaviour of a diaphragm wall which were considered, an increased lateral earth pressure coefficient perhaps had the most significant effect. The lateral stresses at all stages were related to their assumed pre-excavation values. The resulting bending moments and prop loads were expectedly large but the influence on wall deflection and on the behaviour of the permanent slab was comparatively small because of a simultaneous increase in the soil stiffness. If the soil stiffness were to reduce, the wall deflection would increase proportionally. The lateral stresses were also slightly higher, resulting in a small increase in wall bending moments and prop loads. In addition, there was more long term swelling on the excavated surface, leading to a larger upward loading on the permanent slab. The

effects of reducing the temporary prop stiffness, the wall thickness and the slab thickness were generally small.

It was mentioned earlier that it is intended to monitor the performance of the retaining walls during and after their installation. Undoubtedly, this will bring in more useful information and enable comparisons with the present analyses. In the event of any significant changes in either the wall geometry or the soil parameters, it would be useful to carry out further analyses with the new data.

CHAPTER 7

CONCLUSION

CHAPTER 7 - CONCLUSION

In this chapter, the main points arising from this dissertation will be recapitulated. The first section will concentrate on the behaviour and the applicability of some simple analyses to walls propped at the crest. The second section will cover walls propped at dredge level. In the third section, the behaviour of diaphragm walls will be discussed with reference to the Cradlewell Bypass retaining walls. Finally, suggestions for further research will be made.

7.1 Walls Propped at The Crest

From the finite element analyses in chapters 2 and 3, it has beeen shown that the stability and the serviceability of the walls propped at the crest of 10m retained height would be very much influenced by the embedment depth. A wall of 5m embedment is unlikely to be acceptable in practice because of the comparatively large soil and wall movements during excavation and almost certain collapse as the negative excess pore water pressures induced by excavation dissipated. Walls of 15m embedment would be remote from collapse, evidenced by the generally small shear strain being mobilised around the wall, but local rupture would occur near the toe. Based on a limit equilibrium analysis with water levels at the respective soil surface on either side of the wall, the long term factor of safety for a wall of 10m embedment would be less than unity, even if full wall friction was assumed. The finite element analysis also indicated that the post-excavation toe deflection increased with time. Hence a wall of 10m embedment would be stable in the short and medium term, but might collapse in the longer time.

For walls rigidly propped at the crest, because of the kinematic restraint imposed by the prop, the lateral stresses near the retained soil surface were high (in the finite element analysis), resulting in higher bending moments and prop loads than those measured in the centrifuge tests and calculated using the limit equilibrium methods. The analyses also revealed that the magnitudes of the bending moments and prop loads increased with the total wall length and their values (normalised with respect to H^3 and H^2 respectively) would decrease with the wall flexibility (H^4/EI).

Generally, the deflections of the rigid walls would be due to rigid body rotation about the prop. The settlement of the soil behind the wall and the heave in front could be estimated by using an assumed admissible strain field. For the more flexible wall, there was substantial local bending, particularly near dredge level. The vertical surface movements for such a wall might be estimated using the same principle by incorporating a hinge nearer the toe, but this possibility was not investigated further.

The bending moments and the soil and wall movements calculated by the mobilised strength method were found to be in reasonable agreement with the results from the finite element analyses for the rigid walls. By limiting the acceptable level of local bending for the more flexible walls, the mobilised strength method is believed to be useful in analysing the behaviour of walls propped at the crest in the range of flexibility commonly used in practice.

The confusion in the current design methods based on limit equilibrium analysis was highlighted in chapter 4. An alternative method based on mobilising full passive stress in front of the wall was considered perhaps appropriate in

the analysis of walls in over-consolidated soils, or where the development of active conditions is inhibited by a rigid prop near the crest. The maximum bending moments from the finite element analyses were in all cases smaller than those calculated on the basis of full passive stresses in front of the wall, suggesting a possible bending moment reduction curve for walls in over-consolidated soils if this method is used.

7.2 Walls Propped at Dredge Level

In comparison with the walls propped at the crest, the lateral stresses for the walls propped at dredge level were generally higher, but the wall deflections and the soil movements around the wall were smaller. The degree of soil strength being mobilised in all cases was small and therefore none of the walls considered was expected to fail.

The limit equilibrium analysis showed that the stress conditions around a wall are not straightforward if it is propped near dredge level. Depending on the relative retained height to embedment ratio, the sense of wall rotation could be in either direction, resulting in two contrasting stress fields. The lateral effective stress distributions obtained from the finite element analyses on walls rigidly propped at dredge level prior to excavation, apart from near the soil surface and at dredge level as explained in section 5.3.1, were generally compatible with those from the limit equilibrium analyses.

The overall deflection of the wall during excavation will depend on the relative significance of two different effects - the loss of lateral support on wall above the prop and the reduction in over-burden pressure on the excavated surface. The finite element analysis indicated that the crest would rotate outward for walls of shallow

embedment (at least initially) and in opposite sense for deep walls. However, movement of the crest into the retained soil is rarely observed in practice, probably because of the effects of the sequence of prop installation and the wall flexibilty.

The maximum bending moments for walls propped at dredge level will be determined by the lateral total stress acting on the wall above the prop. Results from both finite element analysis and limit equilibrium method indicated that these values were generally not much affected by the total length and the flexibility of the retaining wall in most cases over the range considered. The prop loads were generally insensitive to the wall length and flexibility, but their magnitudes were much higher than those computed for the walls propped at the crest.

7.3 The Cradlewell Bypass Retaining Walls

If a wall was allowed to move at the formation level, as in the Cradlewell Bypass retaining walls, considerable reduction in lateral stresses would result, leading to substantially lower bending moments and prop loads than in rigidly propped walls. It has also been demonstrated that incorporating the carriageway slab as a permanent prop would be an economical method of both improving the wall stability and reducing the soil heave in front of the wall in the post-excavation period.

Amongst all the uncertainties, an increase in pre-excavation lateral earth pressure coefficient would probably have the most sigificant effect on the behaviour of the wall. The lateral stresses at all stages were related to their pre-excavation values and therefore resulted in higher bending moments and prop loads. The wall deflection and soil movements were less significantly

affected by this because of the simultaneous increase in soil stiffness which results from the use of the Schofield soil model.

If the soil stiffness were to reduce, the wall deflection would increase proportionately, but its influence on the wall bending moments and prop loads was rather small. Also there would be a higher upward loading on the slab as a result of an increased tendency to heave in the soil in front of the wall.

The effects due to the changes in temporary prop stiffness, wall and slab thickness were generally small. However, if the carriageway was to be rigidly connected to the wall, the bending moments in the the wall and near the centreline of the slab would be reduced, but a sagging moment would result in the slab near the connection. The permeability of the soil might be another crucial factor in the interaction between the soil and the wall, particularly in the long term, but this was not investigated herein.

7.4 Further Research

The finite element method has been used extensively in this dissertation in the analysis of walls propped at the crest or at dredge level. During this research, many problems were encountered and subsequently solved. However, due to the expense and time required, it was not possible to consider every problem and sometimes a compromise had to be made. Therefore there is scope for improvement in our understanding of the behaviour of diaphragm type retaining walls and further research is necessary.

1. Regarding the finite element program CRISP, a model which can represent the rupture behaviour of the soil is needed in order to investigate collapse mechanisms for walls in heavily over-consolidated soils. Also a soil

model which can reflect the higher soil stiffness due to small incremental changes in strain or a reversal of stress will possibly help to reduce the unrealistic soil heave predicted just behind the wall. In addition, to simulate more realistically the effects of slipping and separation of the wall from the soil, the present slip interface element could be improved.

2. Further work is required on the changes in stress and soil movements which occur during the installation of walls in over-consolidated soils. Although measurements from field structures and analytical calculations show that the earth pressure coefficient would generally move towards unity, a higher pre-excavation K_o value would affect significantly the bending moments and the prop loads under working conditions. A better understanding of this effect is of paramount importance.

3. More centrifuge model tests on walls propped at dredge level could be carried out, particularly if the formation level prop could be installed after the excavation is completed. The yielding of the prop will certainly have an important influence on the bending moments and prop loads but this has yet to be investigated quantitatively.

4. Further research could be carried out on the effects of surcharge loading. It was pointed out by many researchers that retaining wall failures are often caused by excessive and unexpected surcharges on the structures they support. This effects is likely to assume an increasing importance with the impending harmonization throughout Europe of new loading standards for highway structures as heavier lorries are introduced on to British roads.

FIGURES

List of Figures

Chapter 5

Chapter 6

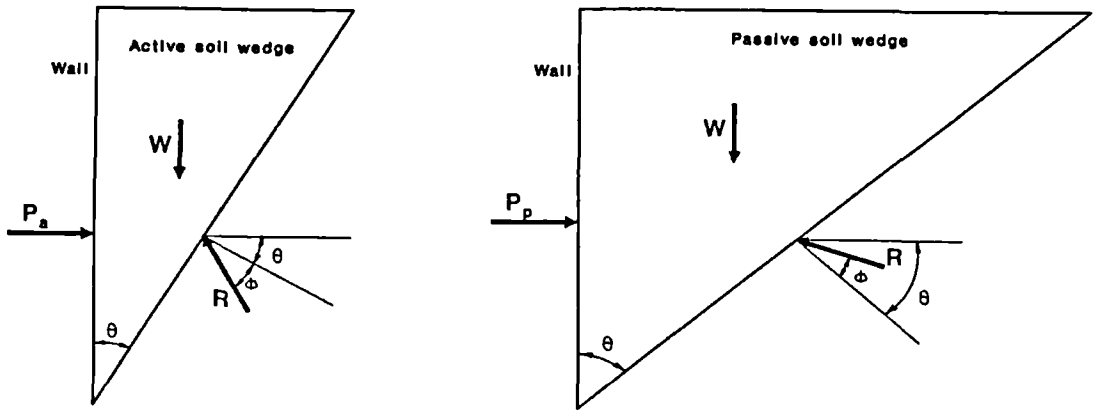

Fig. 1.1 Soil wedge and forces assumed in Coulomb's method

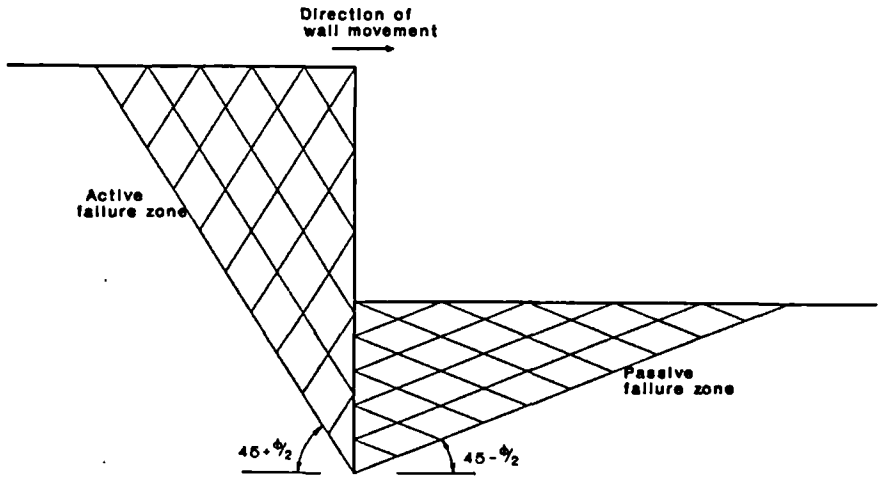

Fig. 1.2 Rankine's stress field

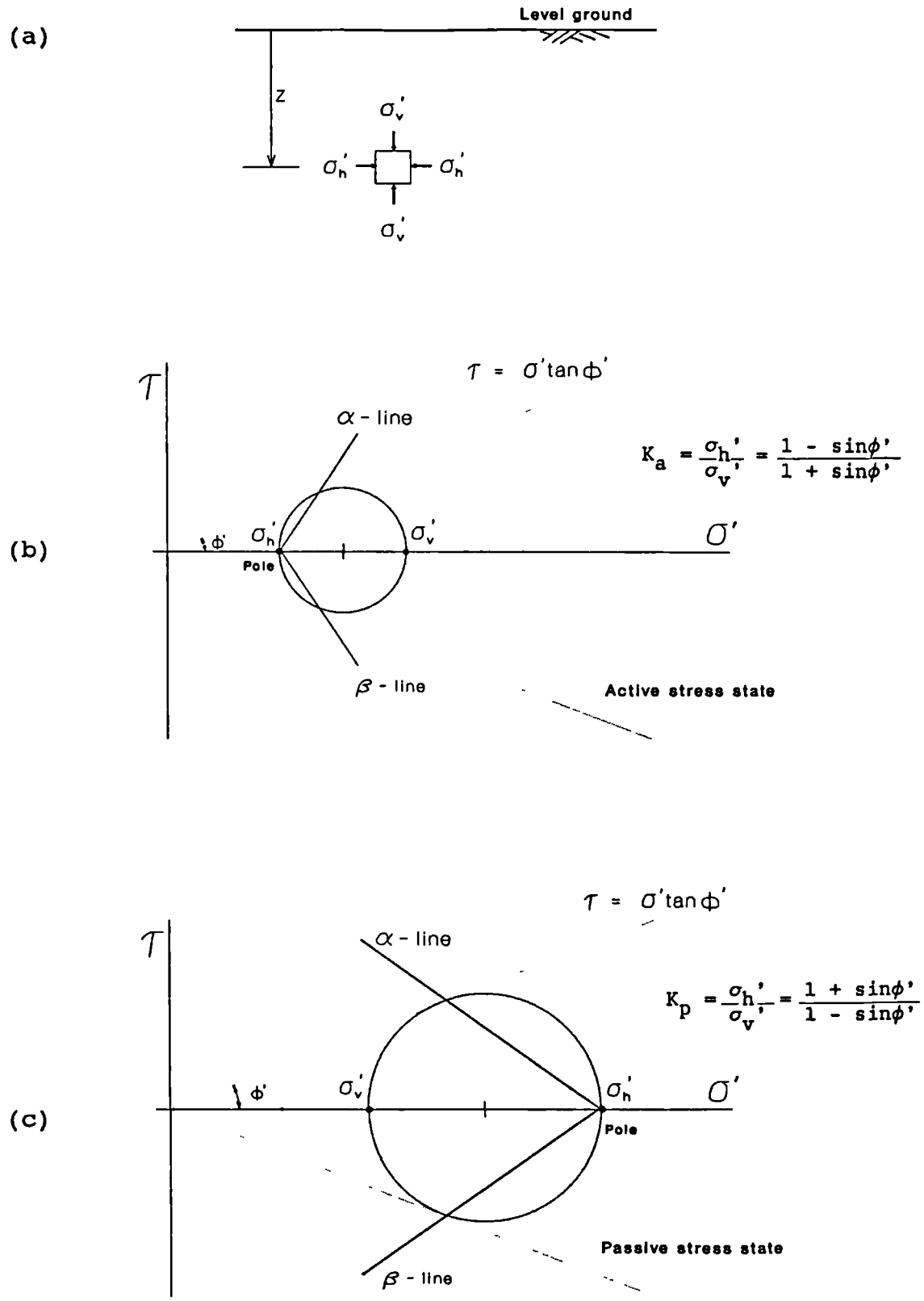

Fig. 1.3 (a) Stress state of a soil element at failure in a semi-infinite soil mass, (b) & (c) the Mohr's circle representation

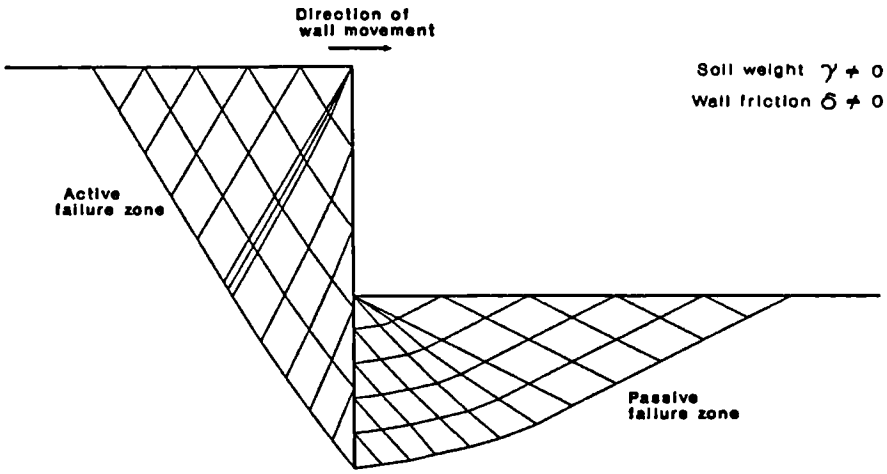

Fig. 1.4 Stress field above toe level for rough wall

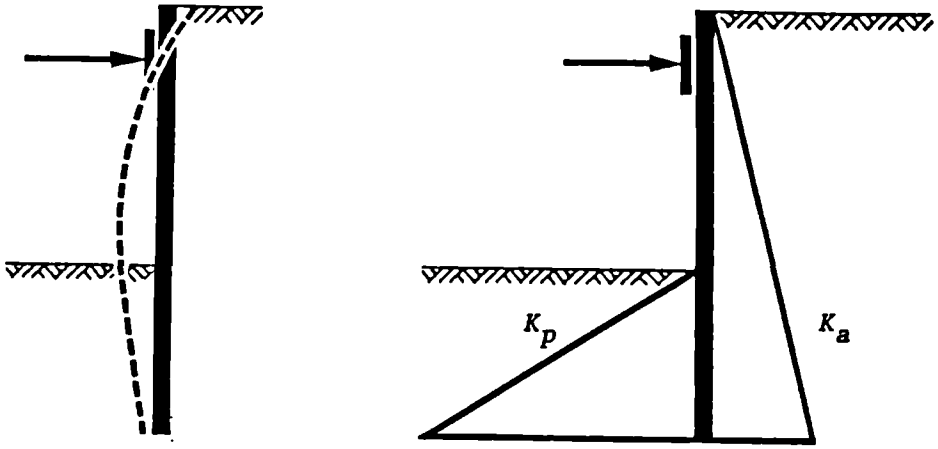

a. Wall deflection b. Idealised stress distribution

Fig. 1.5 Free earth support method for propped wall (from Padfield & Mair, 1984)

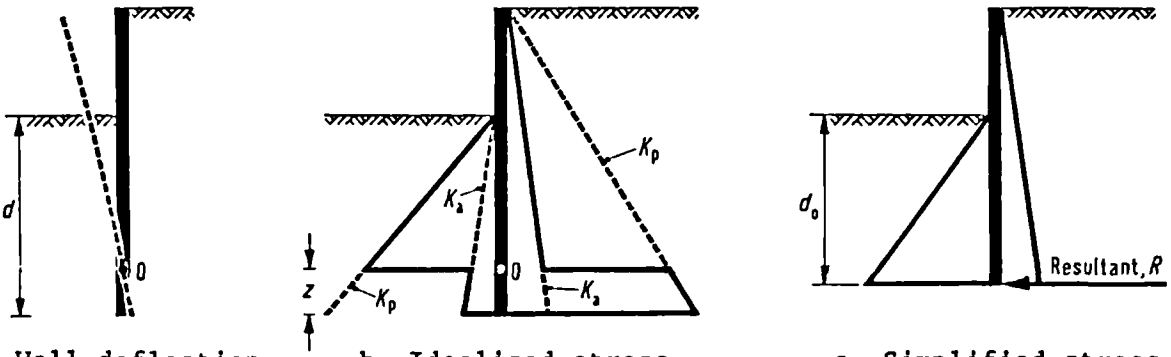

a. Wall deflection b. Idealised stress distribution c. Simplified stress distribution

Fig. 1.6 Fixed earth support method for cantilever wall (from Padfield & Mair, 1984)

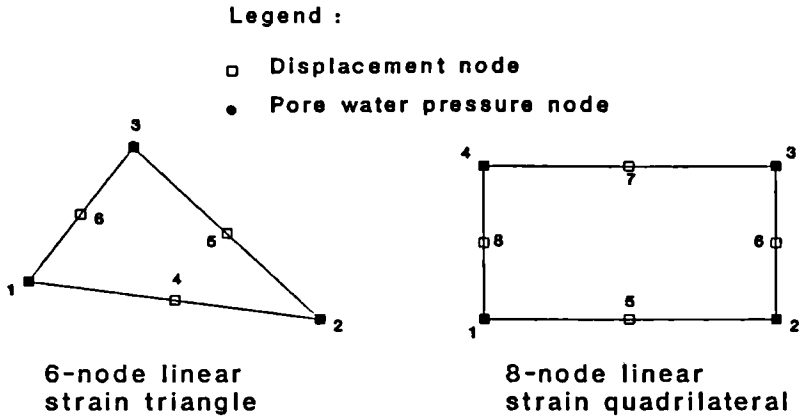

Fig. 1.7 Elements used in CRISP

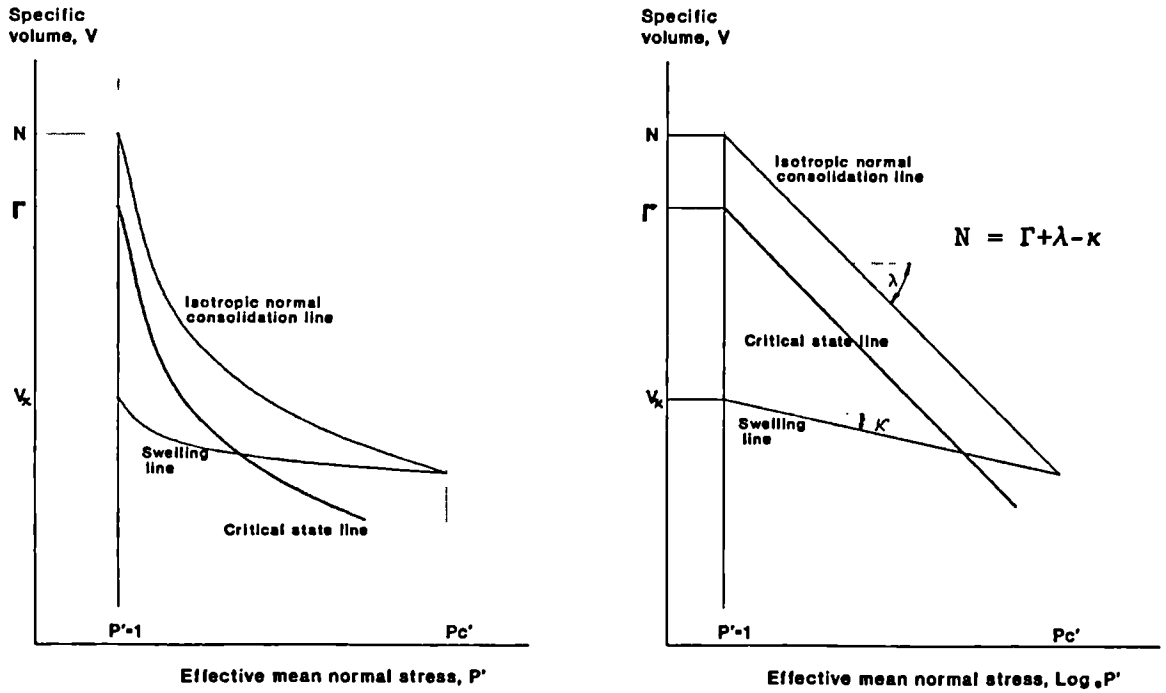

Fig. 1.8 Specific volume against effective mean normal stress

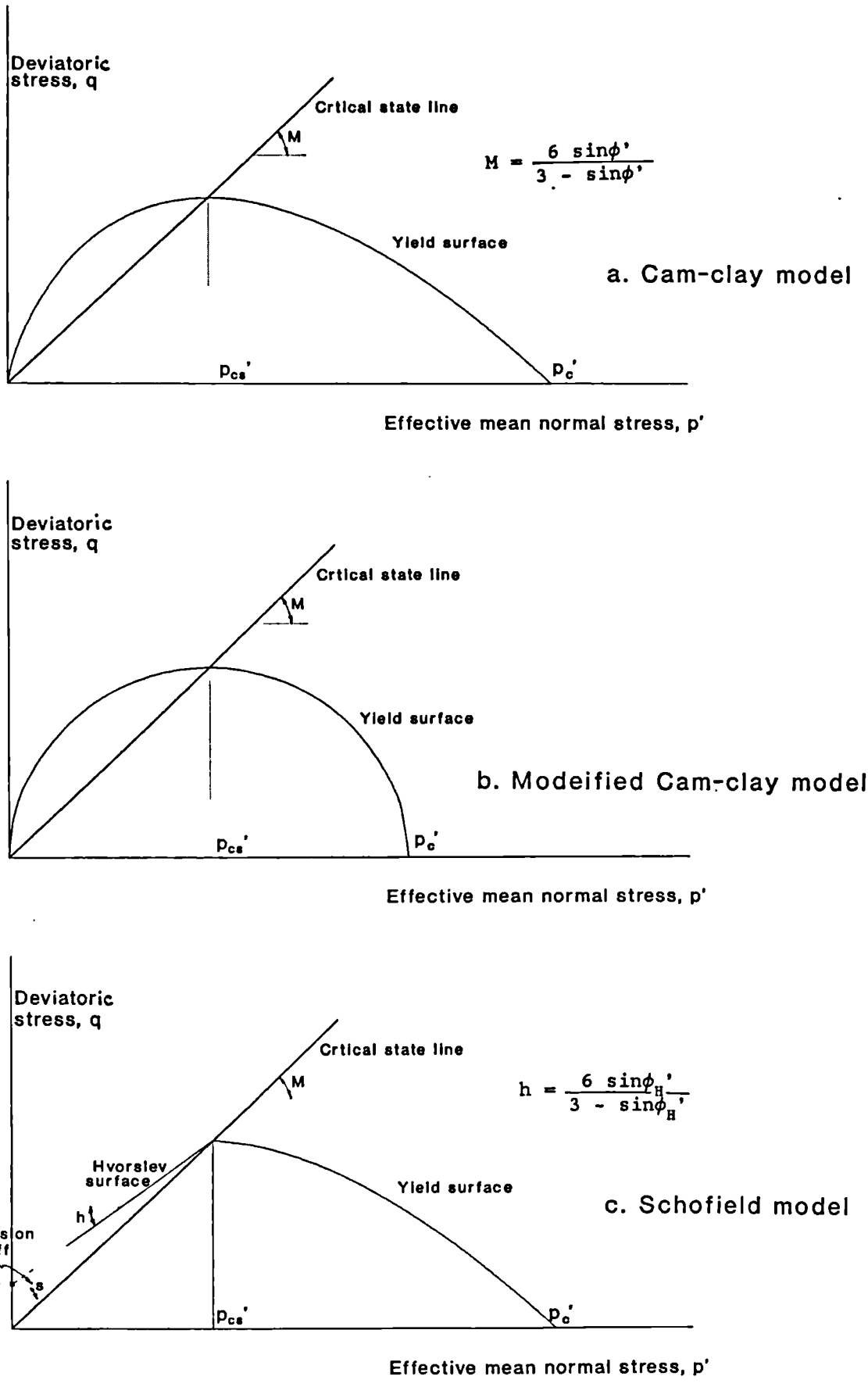

Fig. 1.9 · Yield surfaces for various Cam-clay models

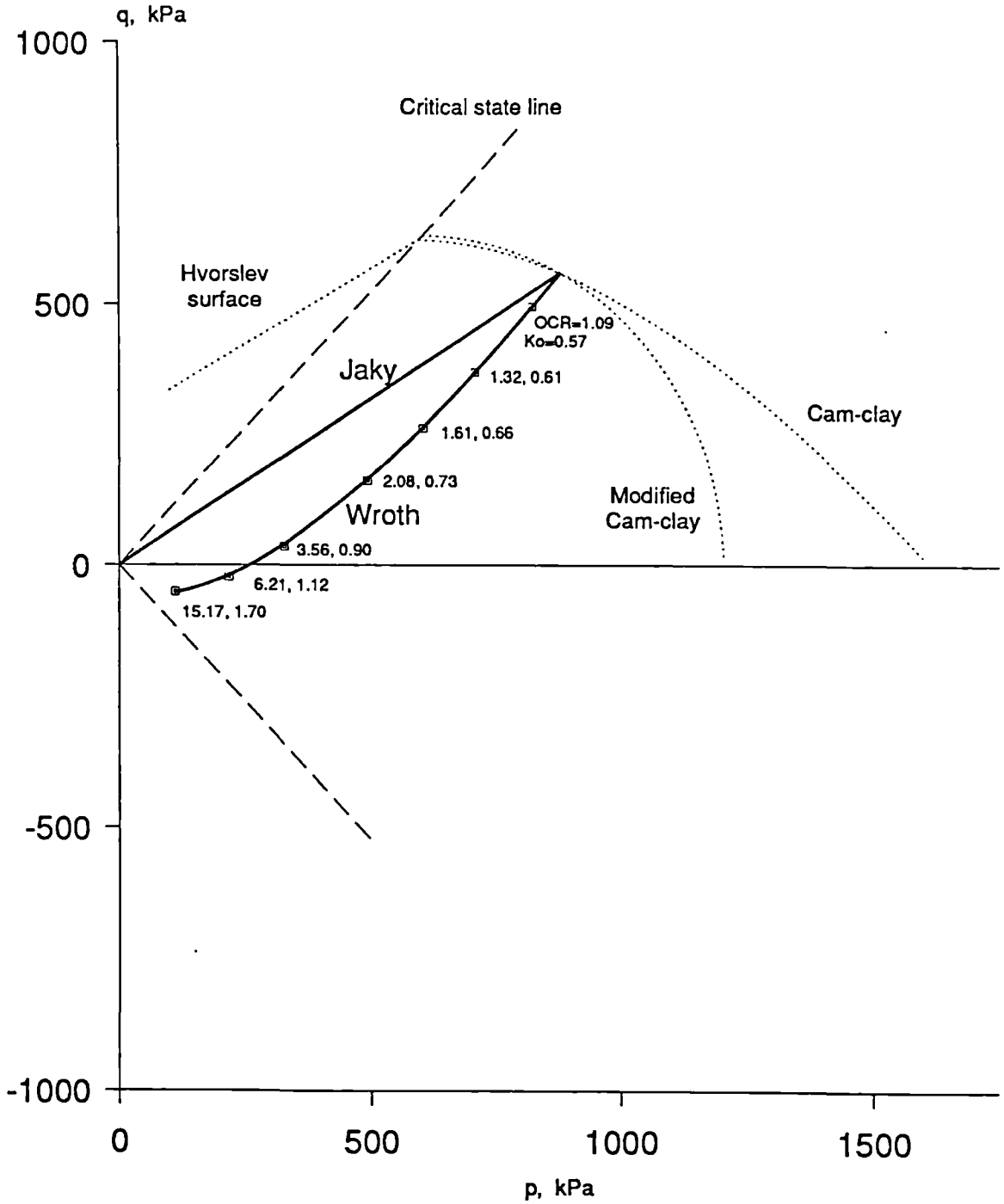

Fig. 2.1 Estimated stress path in soil sample preparation

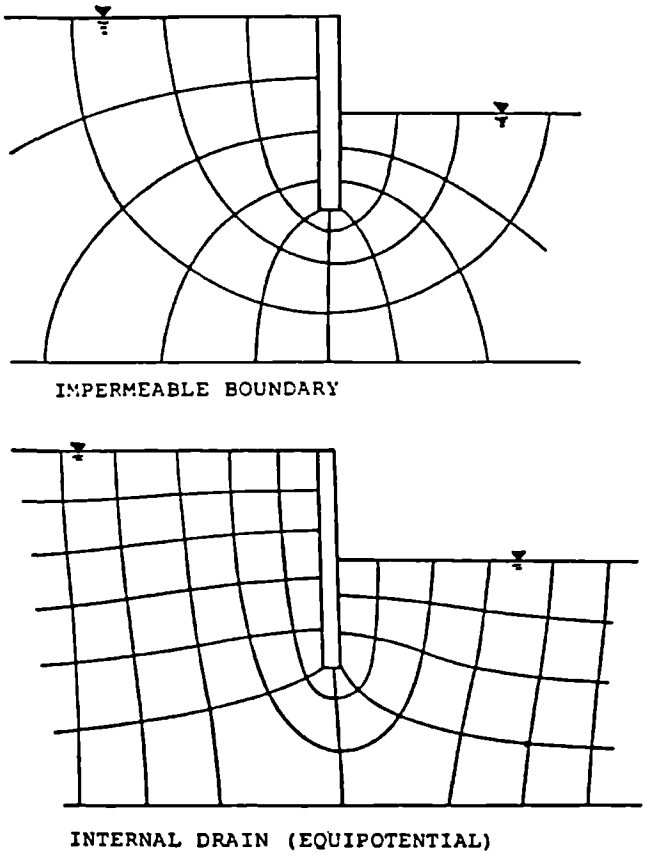

Fig. 2.2 Flownets for different base boundary conditions (from Powrie, 1986)

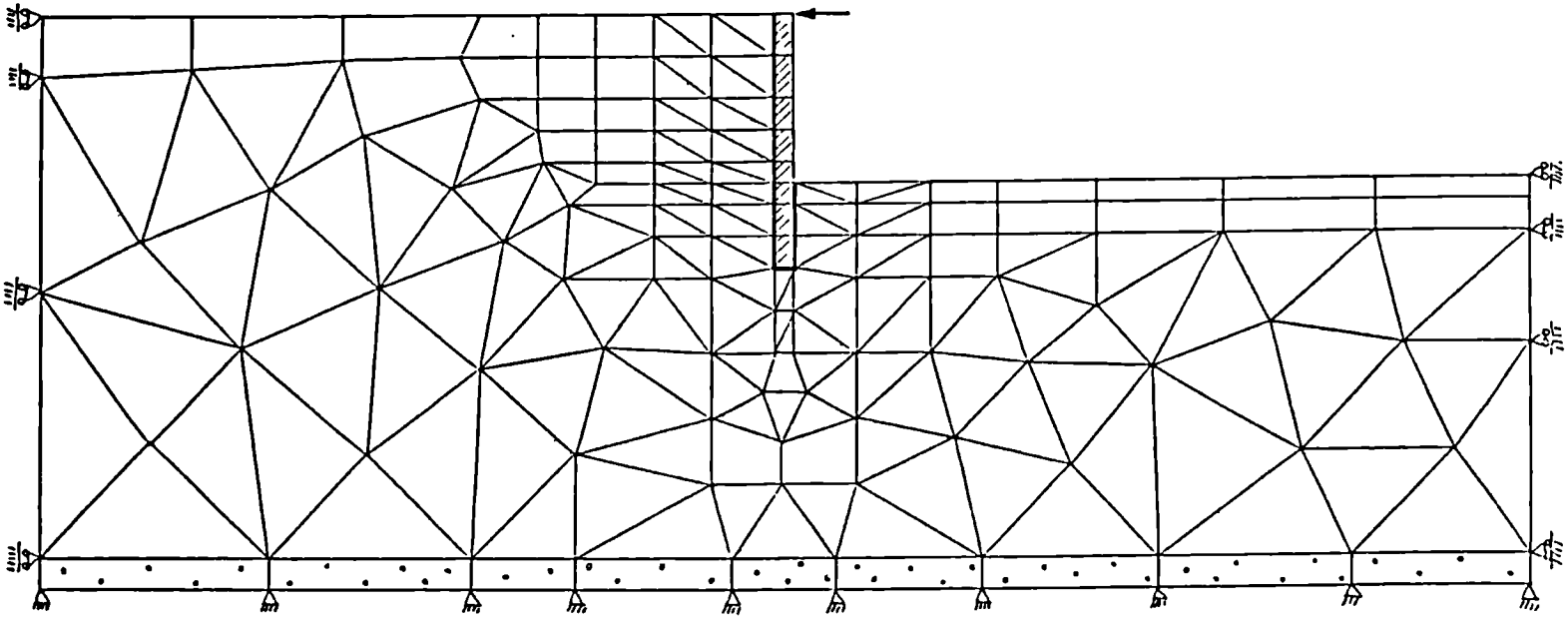

Fig. 2.3 Finite element mesh and boundary conditions for wall of 5m embedment

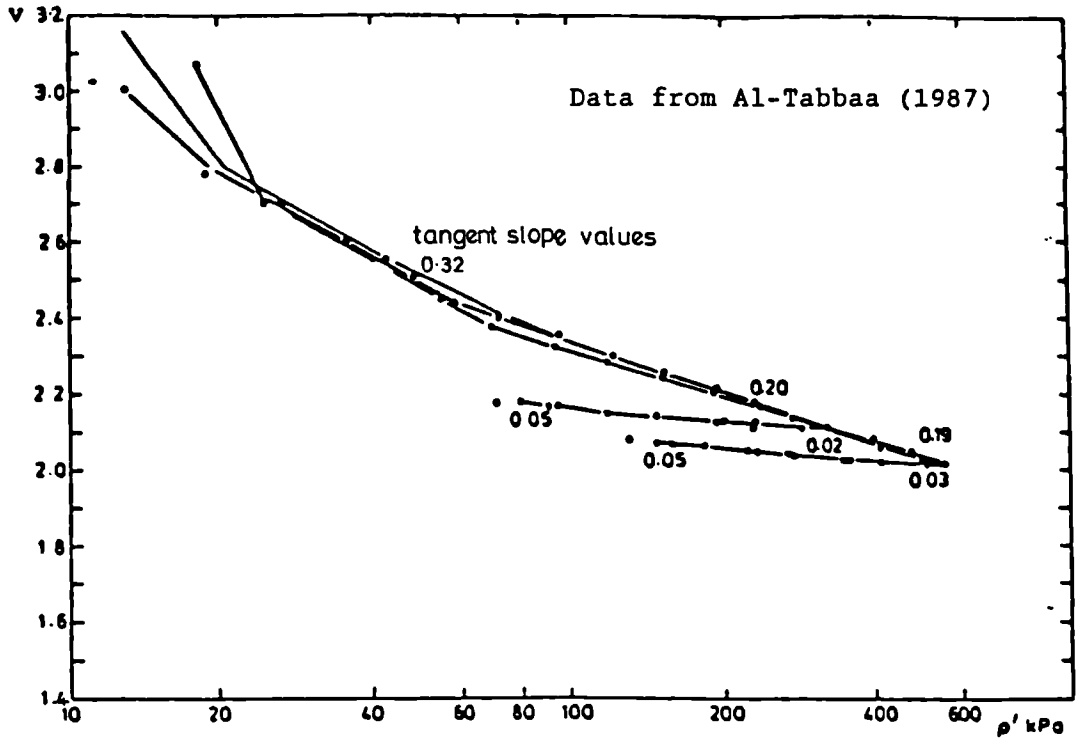

Fig. 2.4 Specific volume vs $\log_e p'$ for oedometer tests, showing the slopes of the normal compression and swelling line (from Powrie, 1986)

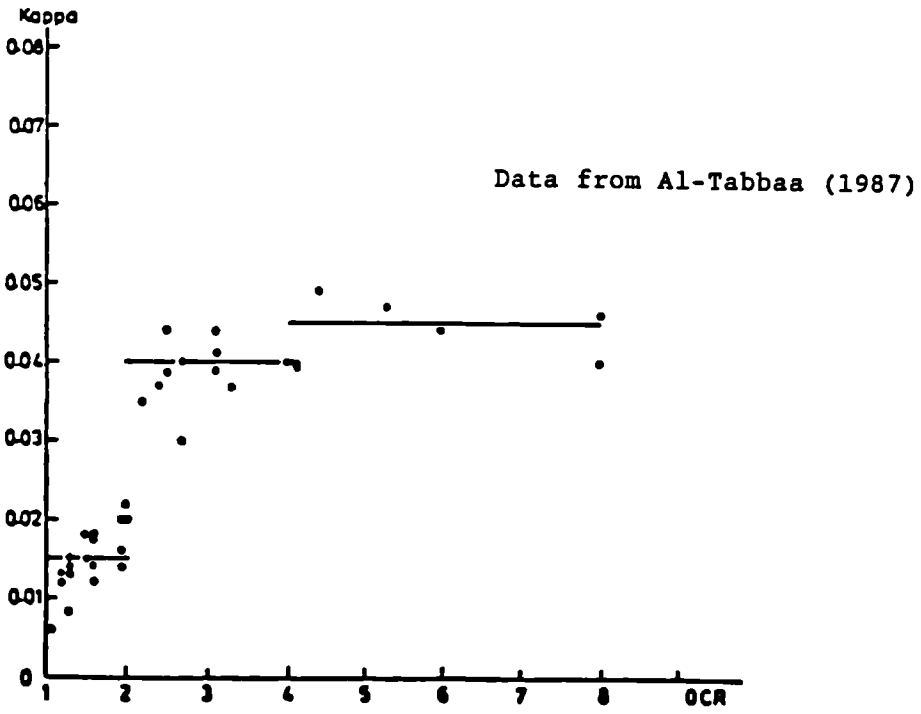

Fig. 2.5 Slope of swelling line vs over-consolidation ratio (from Powrie, 1986)

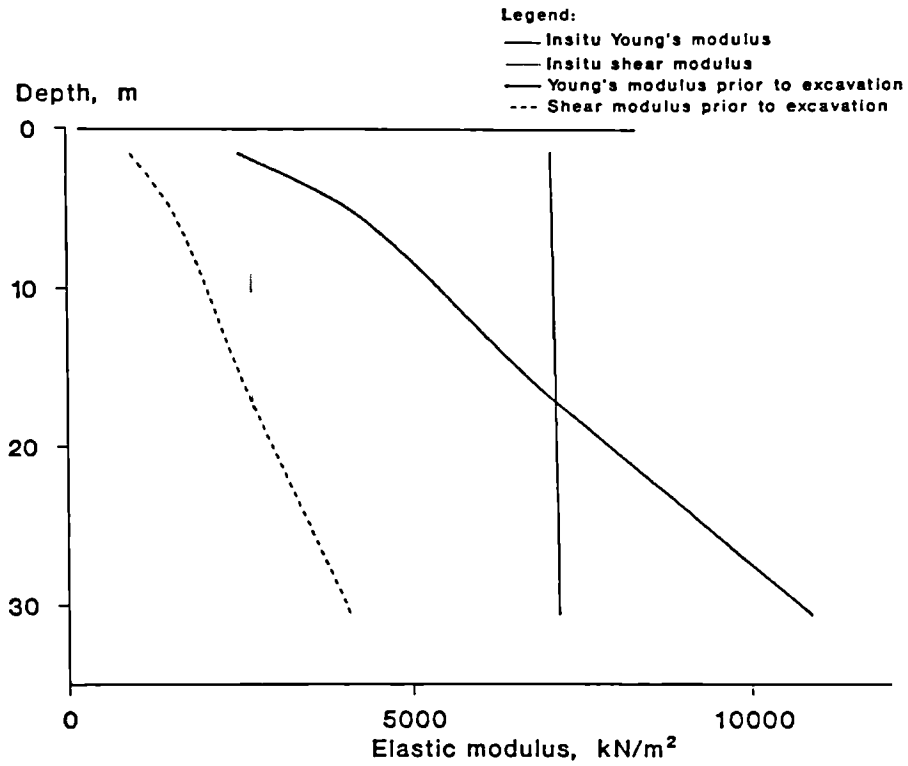

Fig. 2.6 Calculated stiffness profiles for the soil in the finite element analysis

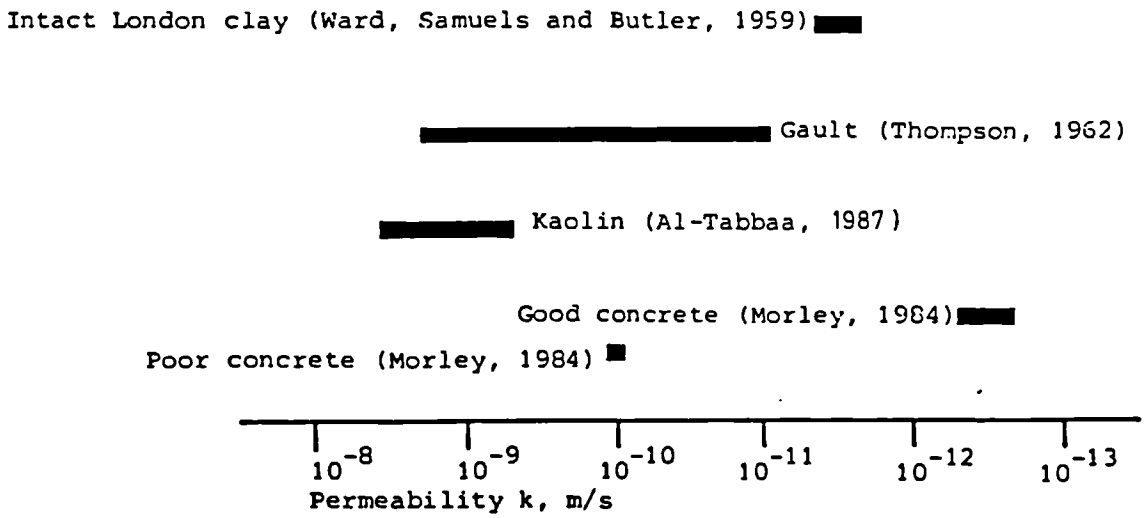

Fig. 2.7 Permeability of clay and concrete (from Powrie, 1986)

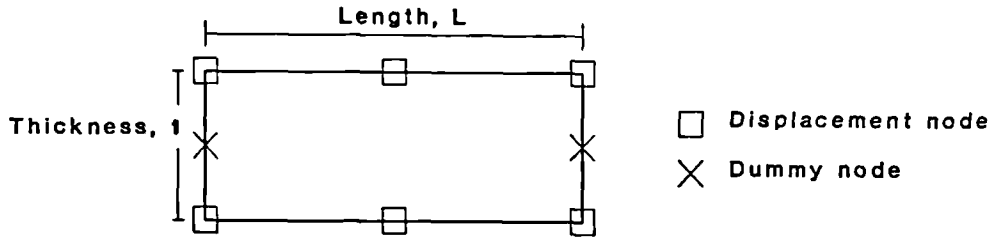

Limiting shear stress:

$$\tau_{lim} = c + \sigma_n' \times \tan \phi$$

Modulus in normal direction:

$$k_n = \frac{E\,(1-\nu)}{(1+\nu)(1-2\nu)}$$

c = Cohesion
ϕ = Friction angle
E = Young's modulus
ν = Poisson's ratio

Shear modulus:

if $\tau < \tau_{lim}$, $k_s = \frac{E}{2(1+\nu)}$

if $\tau \geq \tau_{lim}$, $k_s = k_{res}$, residual shear modulus

Fig. 2.8 Parameters used in slip interface element

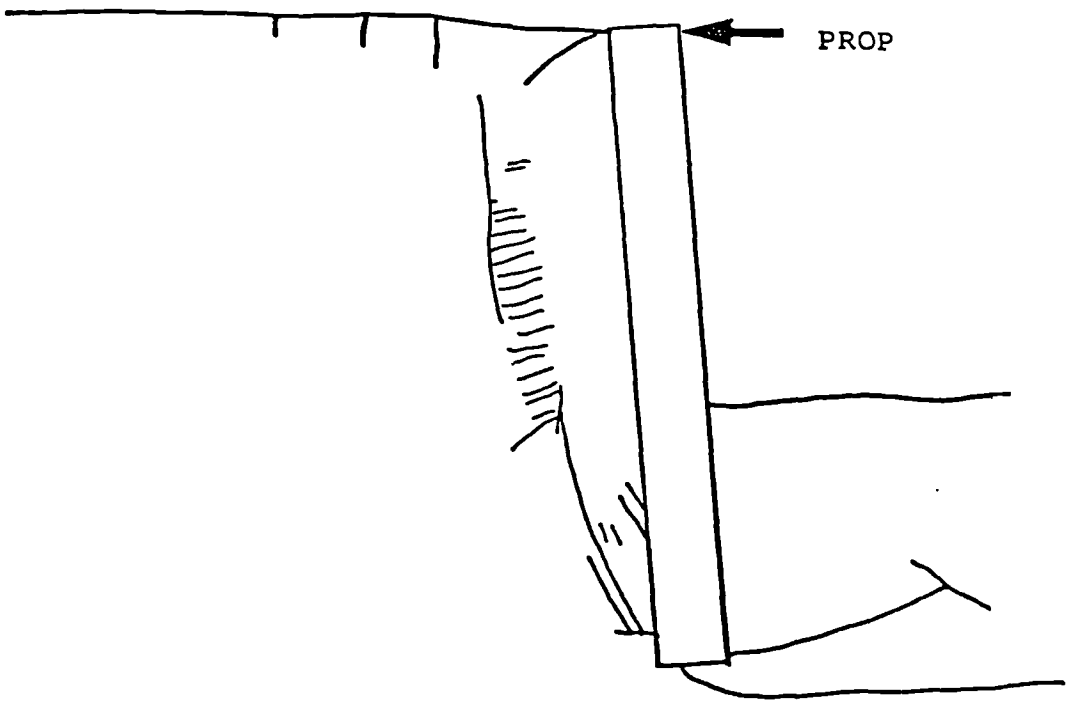

Fig. 2.9 Rupture pattern observed in centrifuge test, DWC11 (from Powrie, 1986)

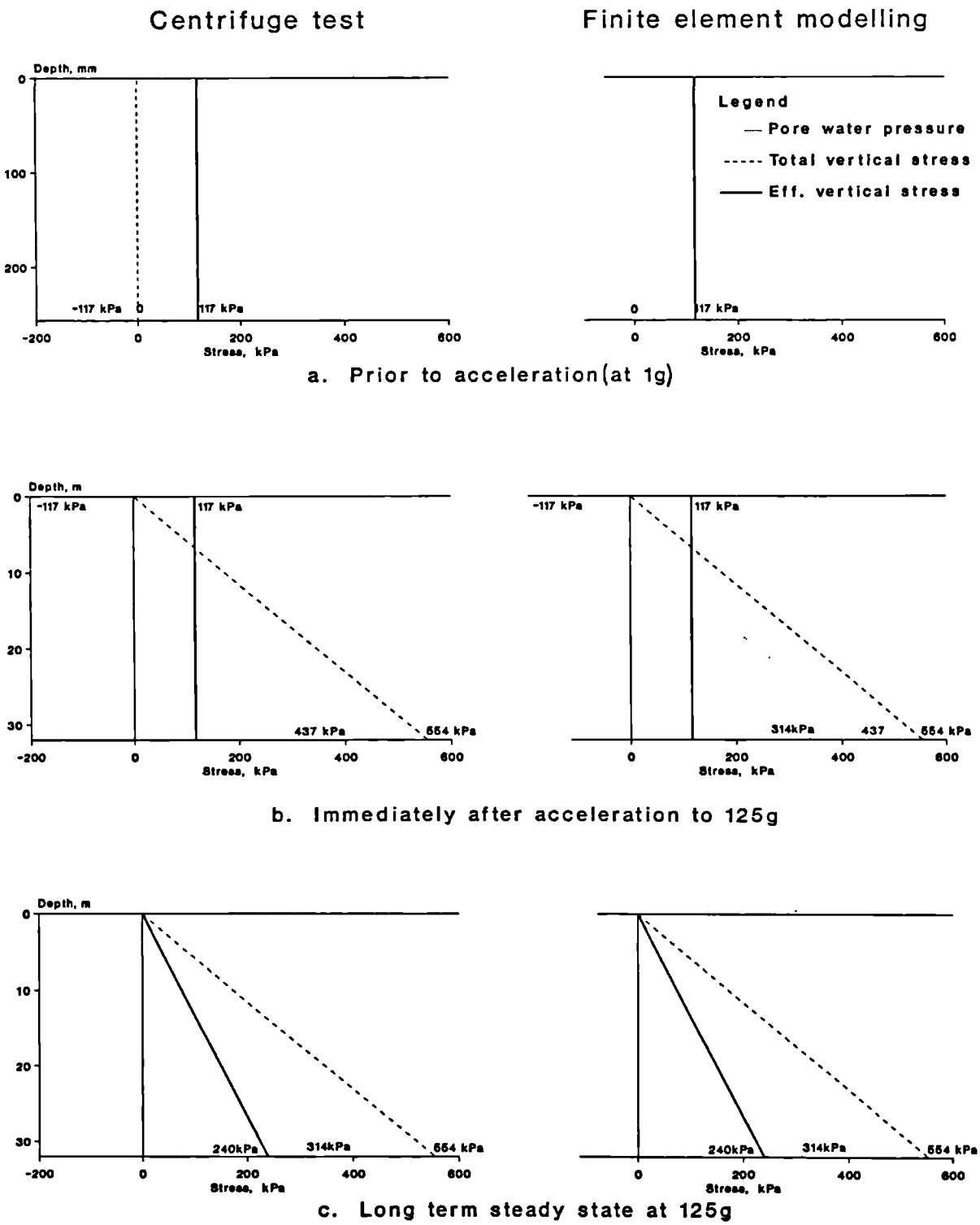

Fig. 2.10 Idealised vertical stress and pore water pressure distributions in centrifuge test and finite element analysis

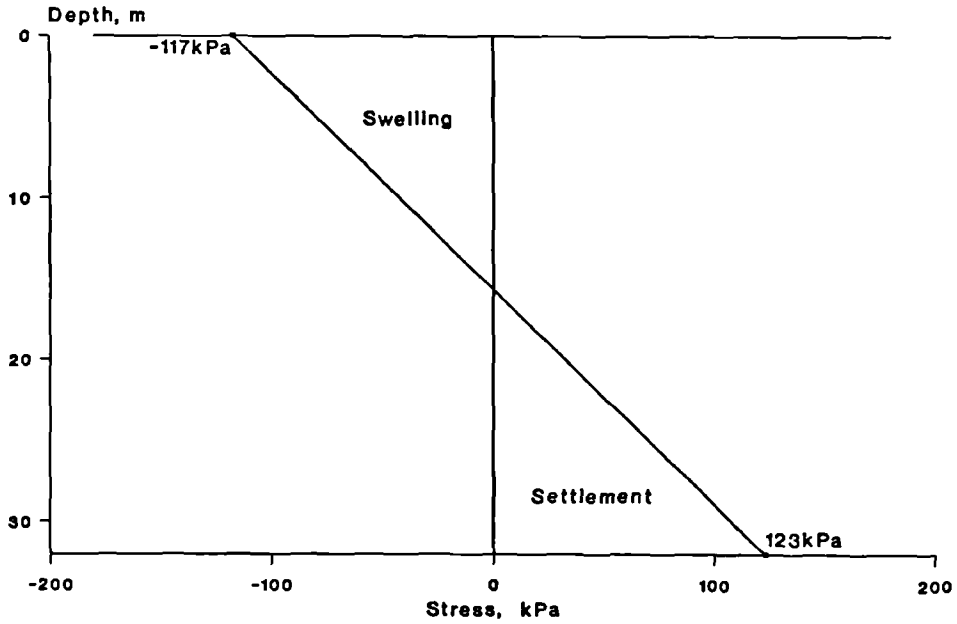

Fig. 2.11 Change in vertical effective stress during reconsolidation

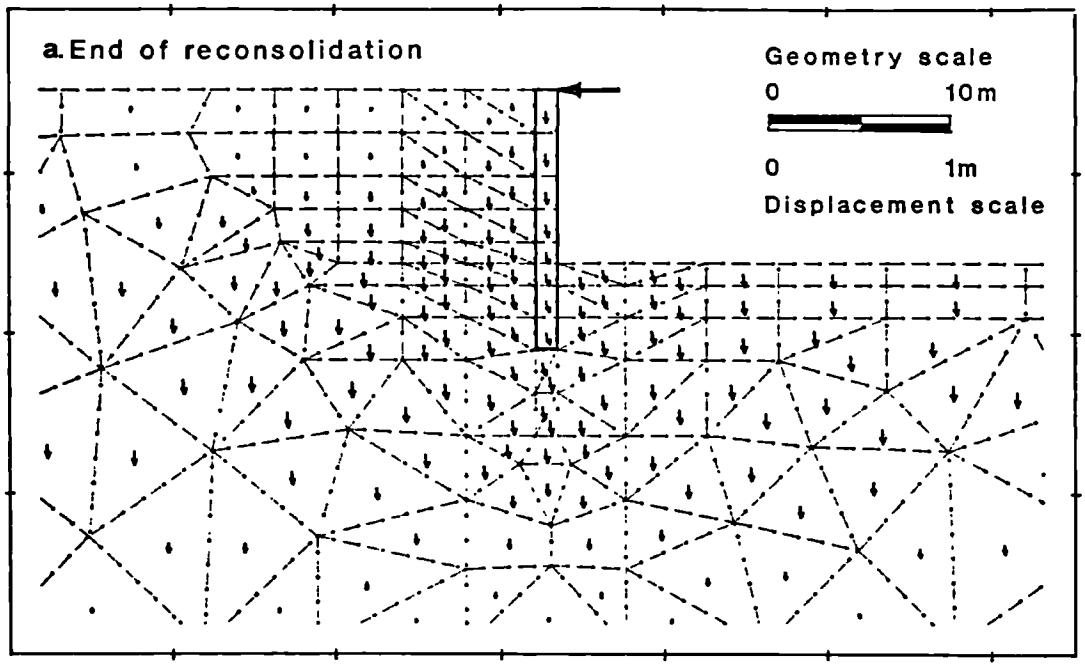

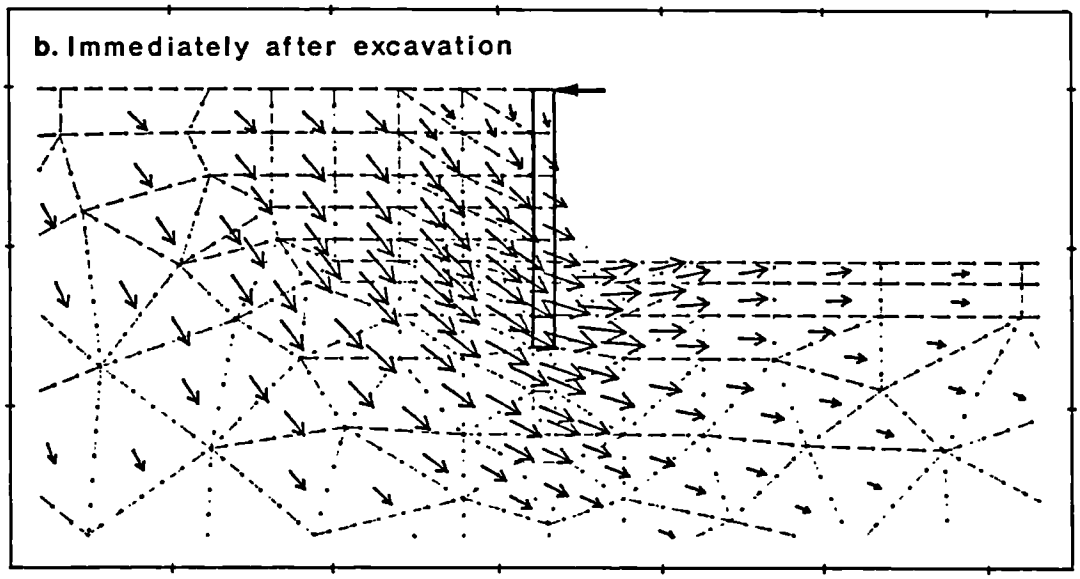

Fig. 2.12 Cumulative displacement vector diagrams

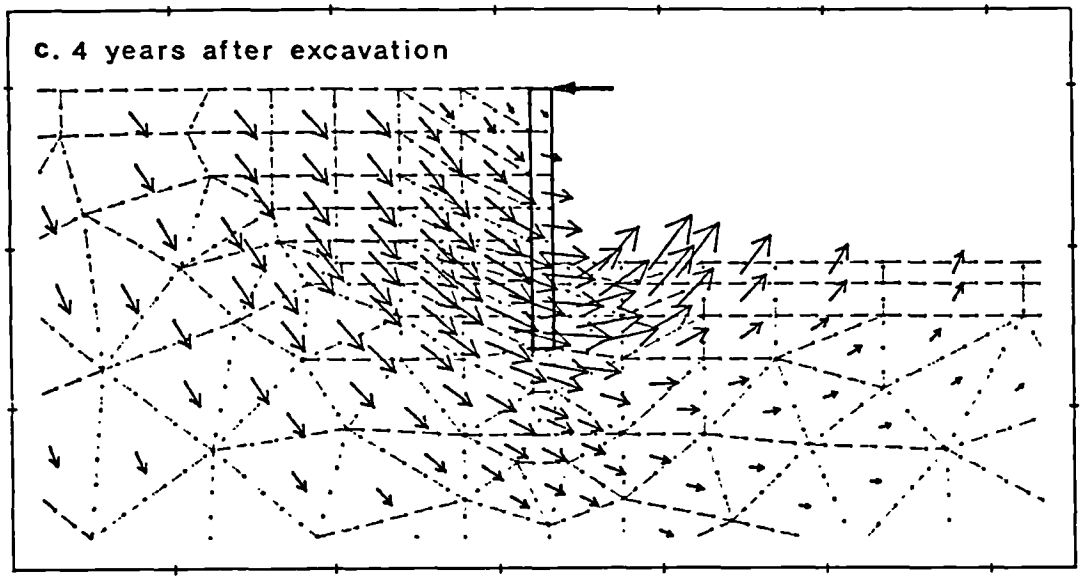

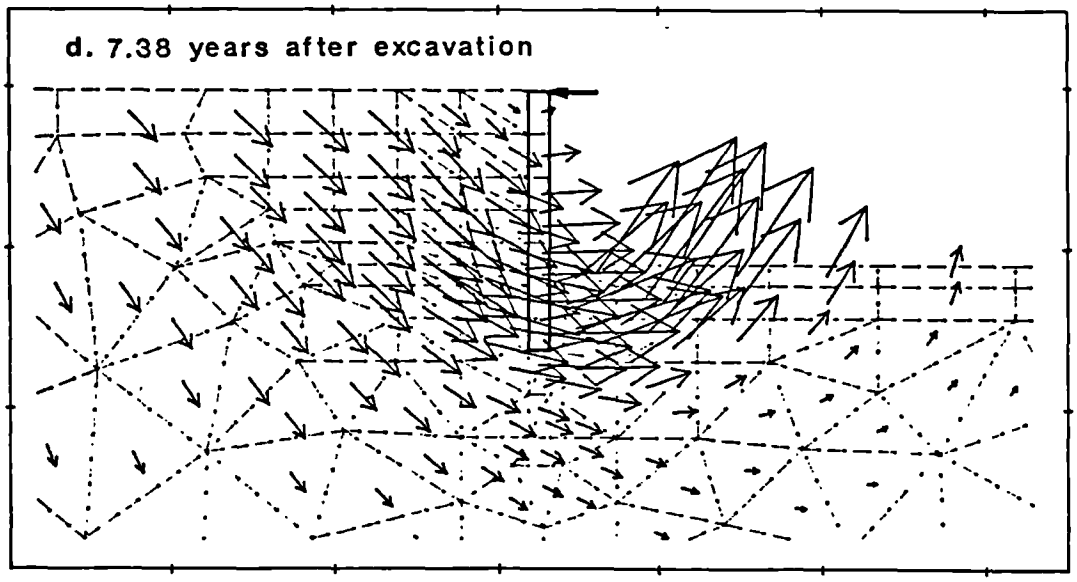

Fig. 2.12 Cumulative displacement vector diagrams

The displacements shown on the contours are at model scale

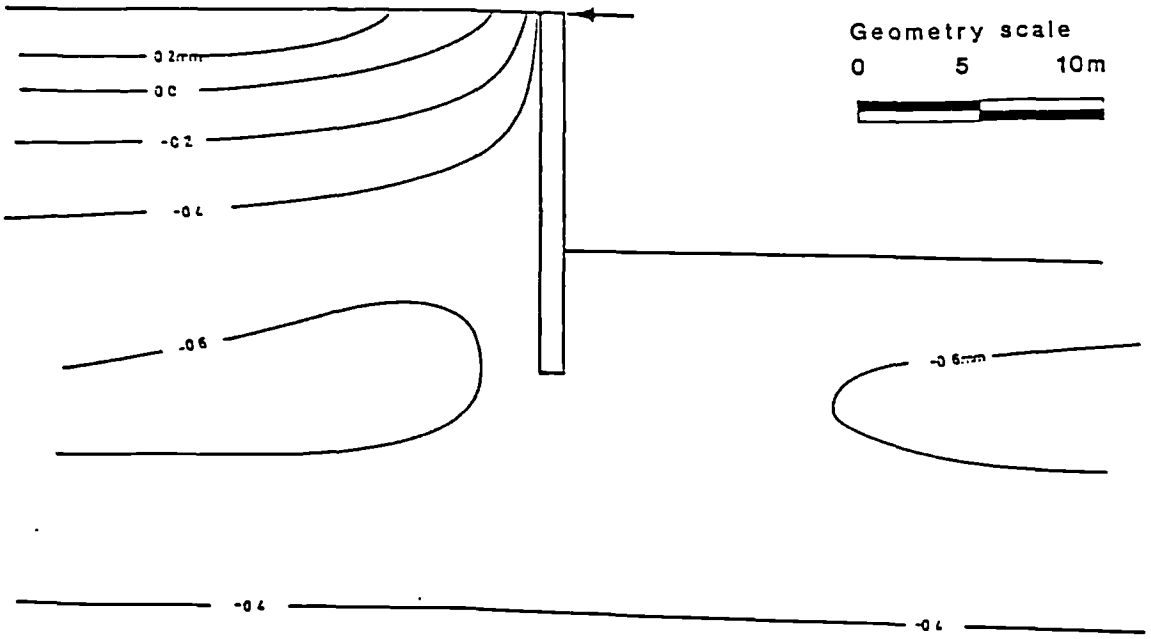

a. Vertical displacement

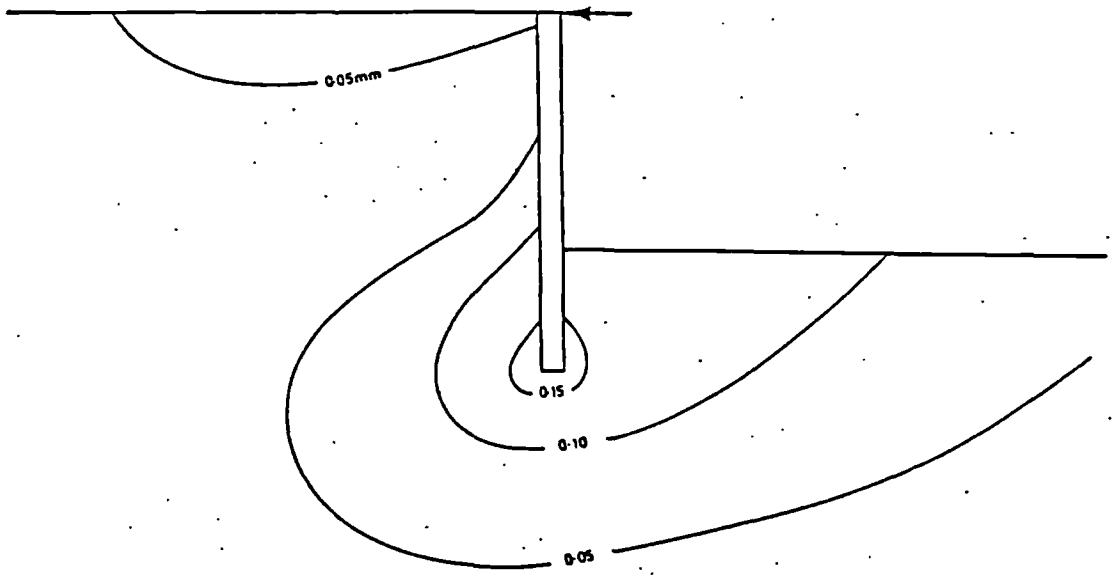

b. Horizontal displacement

Fig. 2.13 Contours of cumulative displacement at the end of reconsolidation

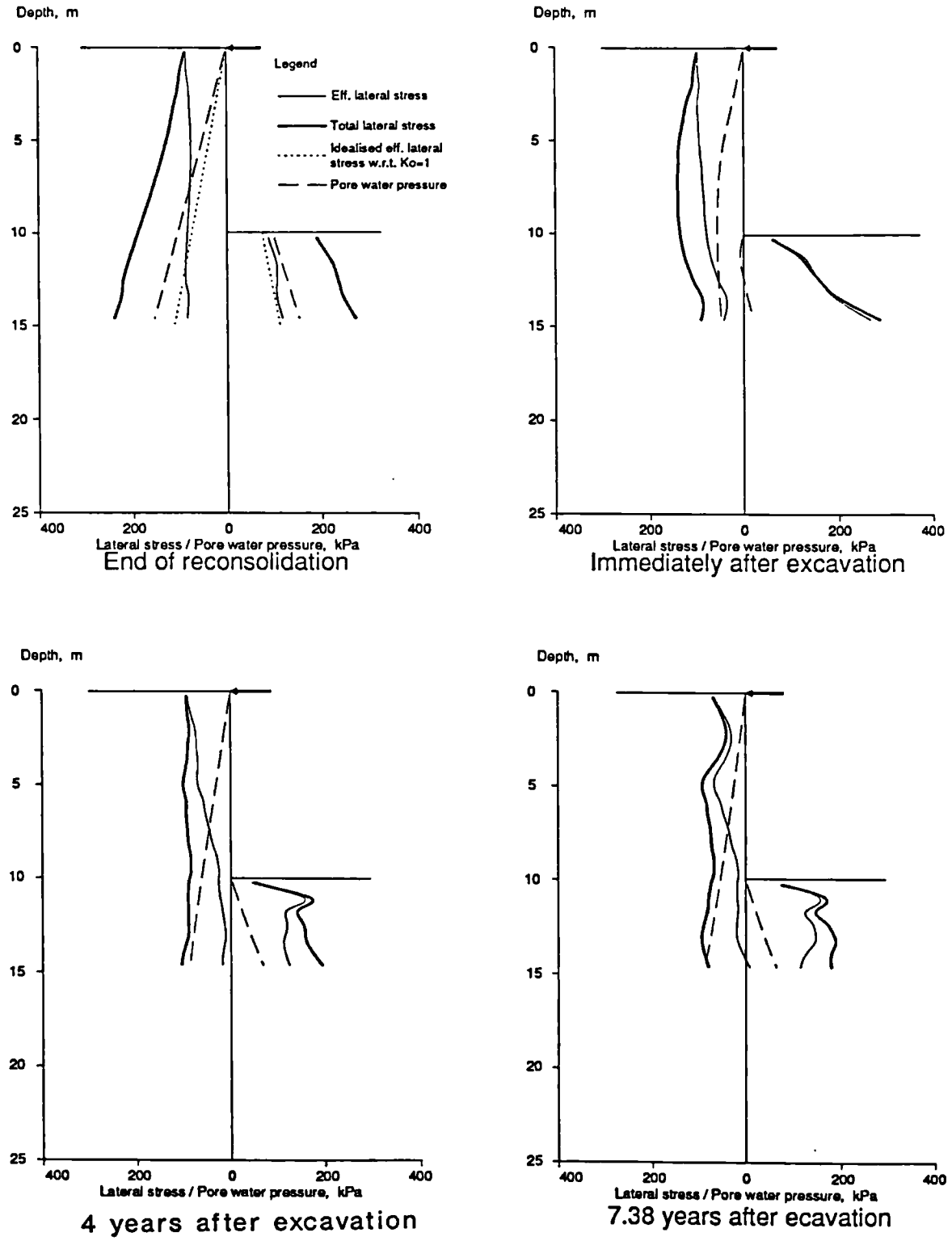

Fig. 2.14 Lateral stresses and pore water pressure distributions

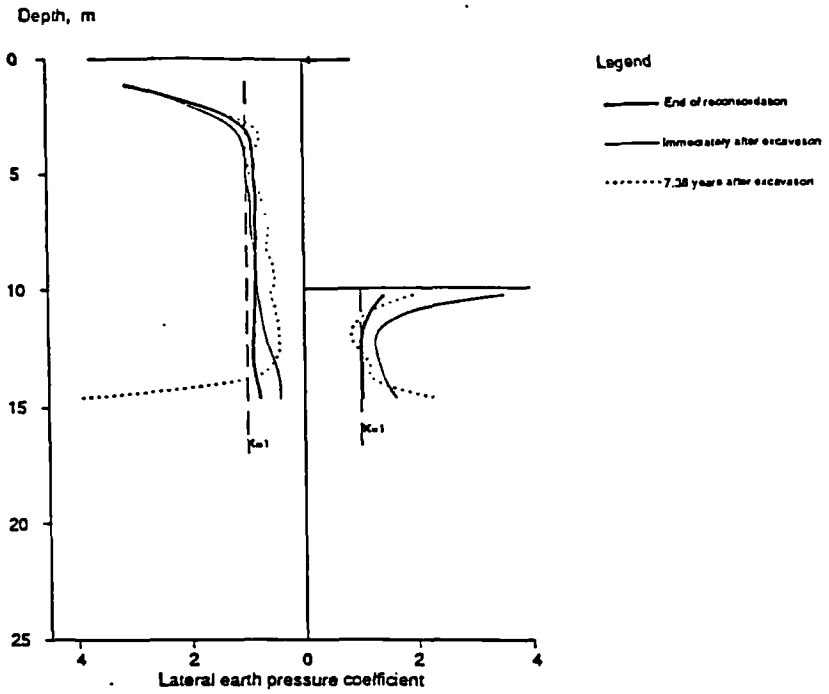

Fig. 2.15 Lateral earth pressure coefficient distributions

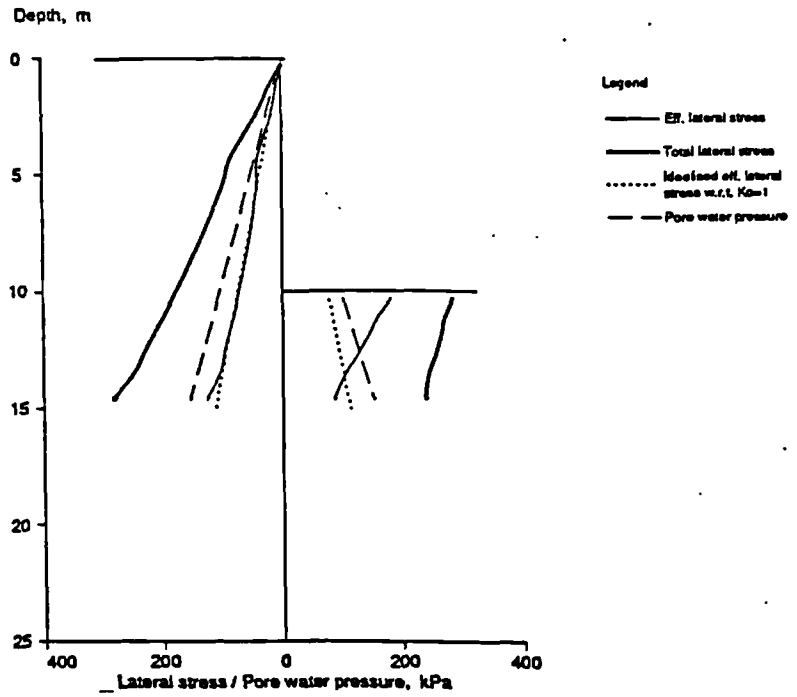

Fig. 2.16 Lateral stresses and pore water pressure distributions for unpropped wall of 5m embedment at the end of reconsolidation

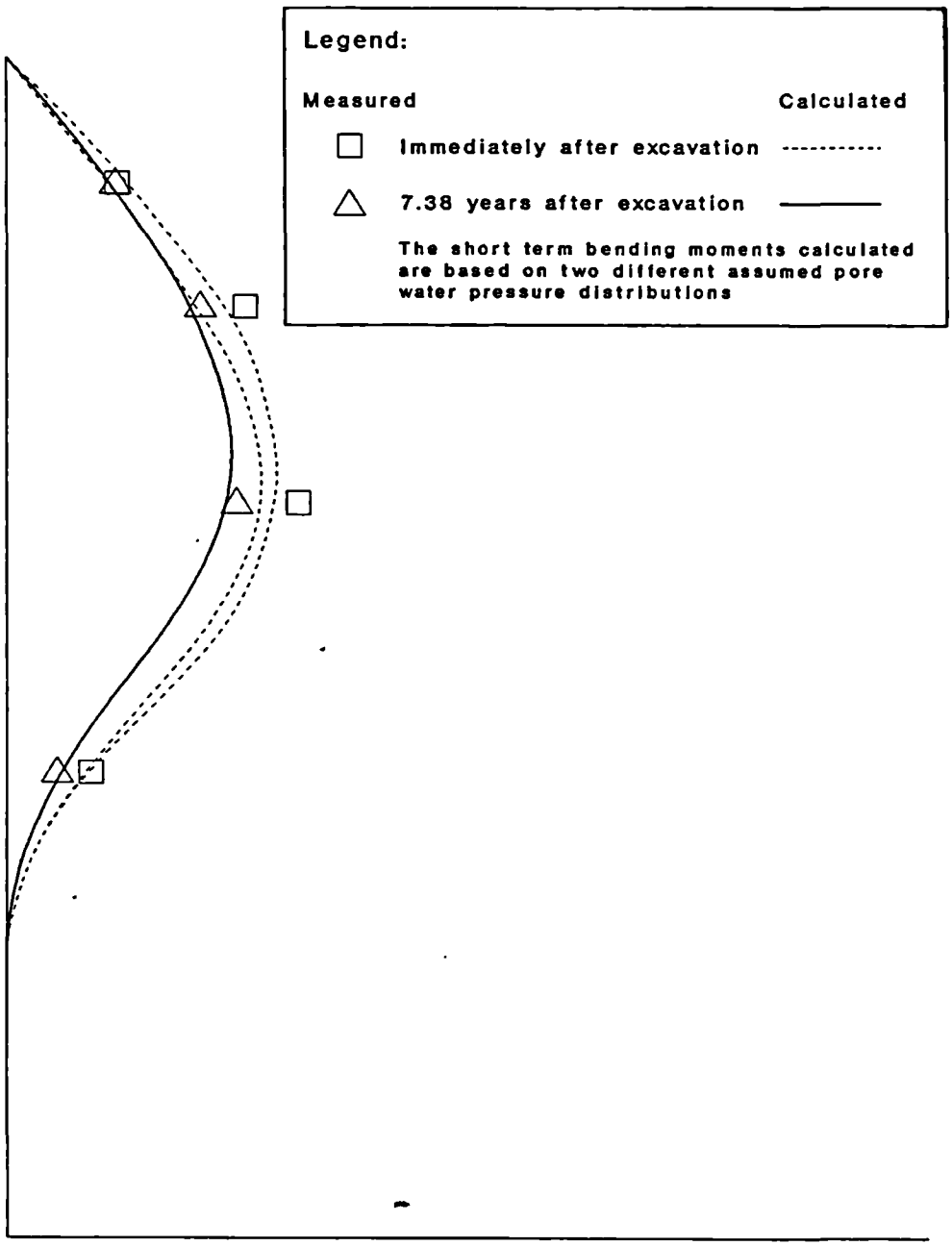
Legend:
Measured
Calculated
Immediately after excavation
7.38 years after excavation
The short term bending moments calculated are based on two different assumed pore water pressure distributions

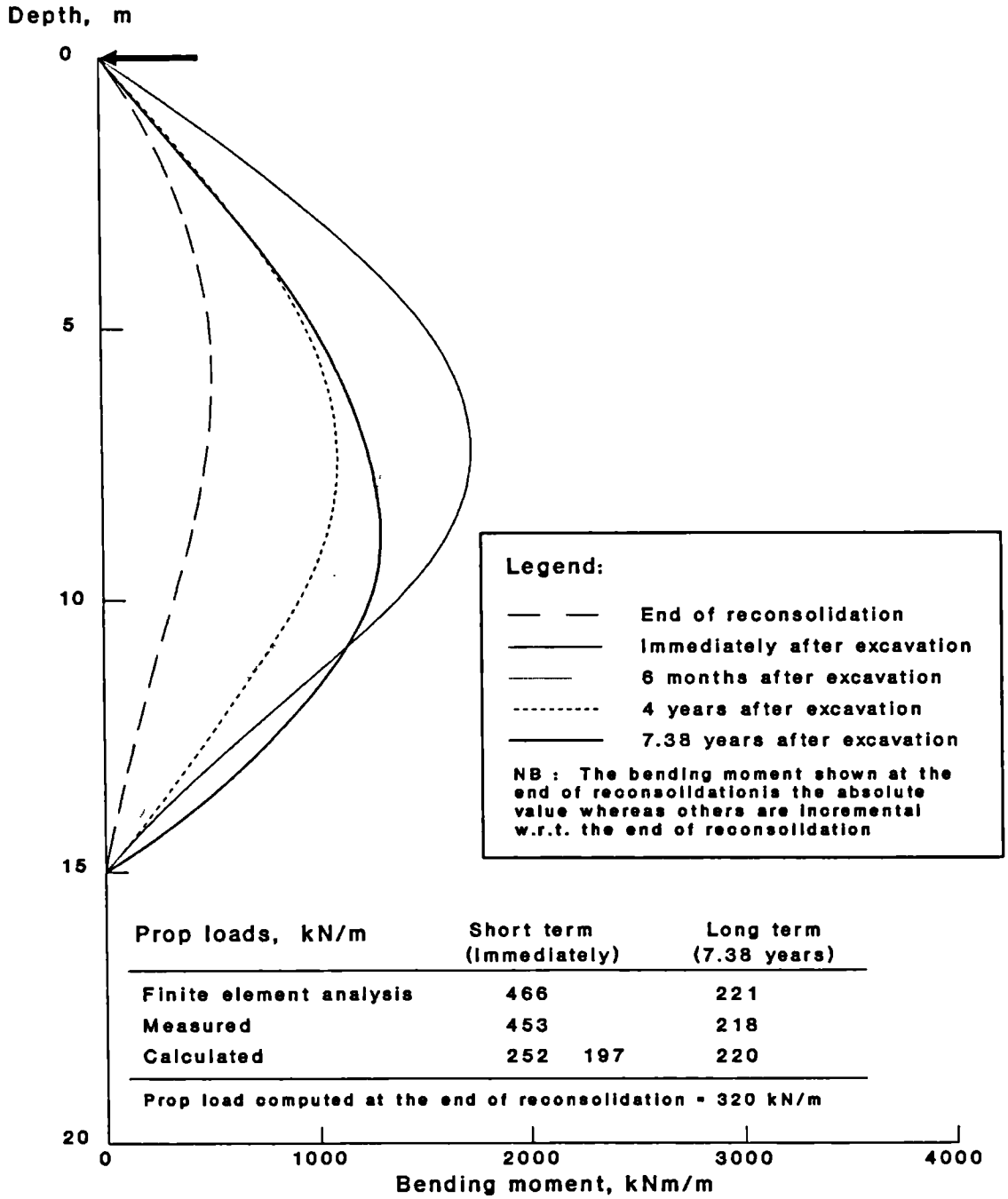

Fig. 2.17 Computed bending moment diagrams and prop loads (with the measured and calculated values from centrifuge test superimposed, from Powrie, 1986)

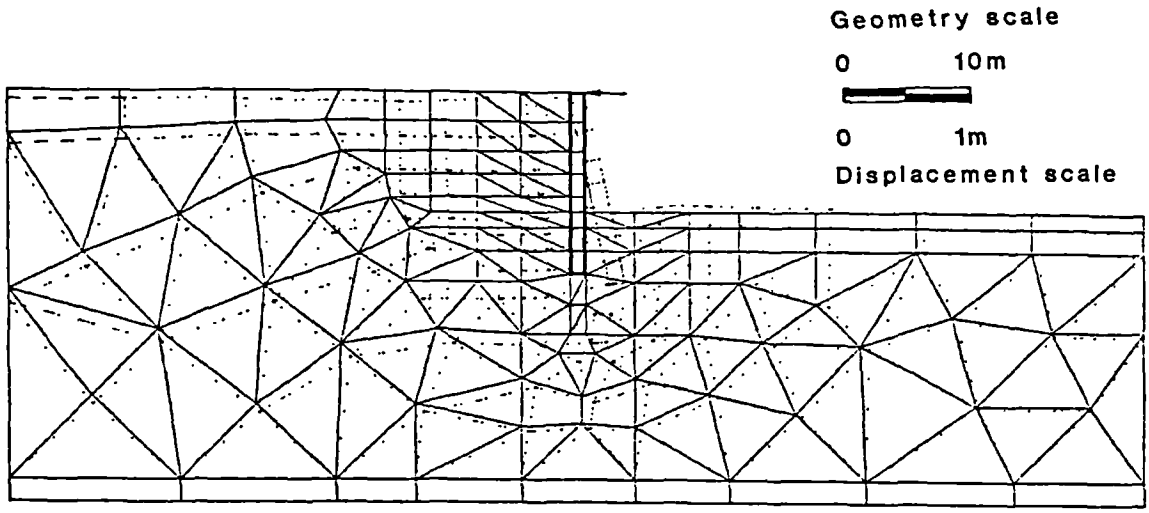

a. Immediately after excavation

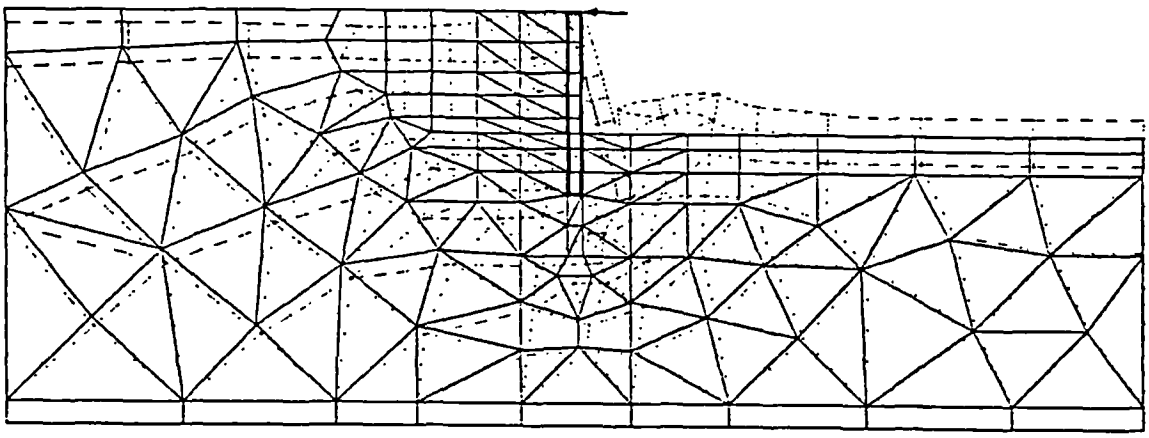

b. 4 years after excavation

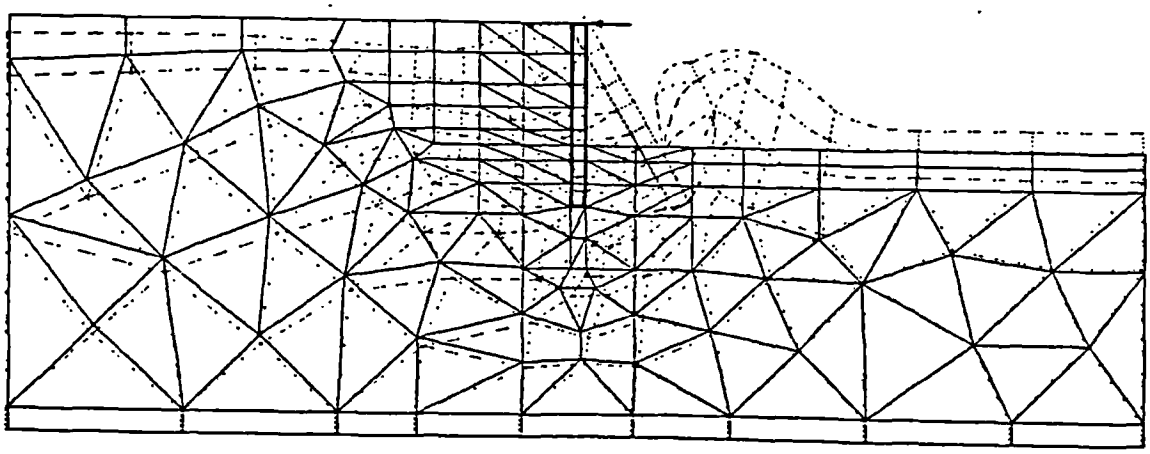

c. 7.38 years after excavation

Fig. 2.18 Cumulative soil and wall movements

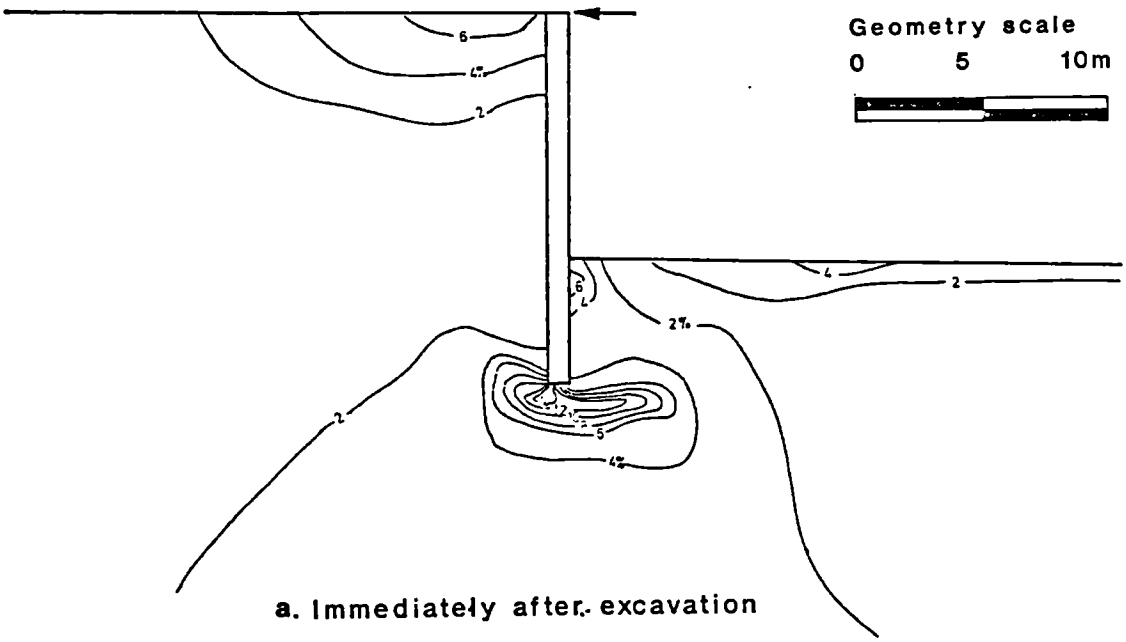

a. Immediately after excavation

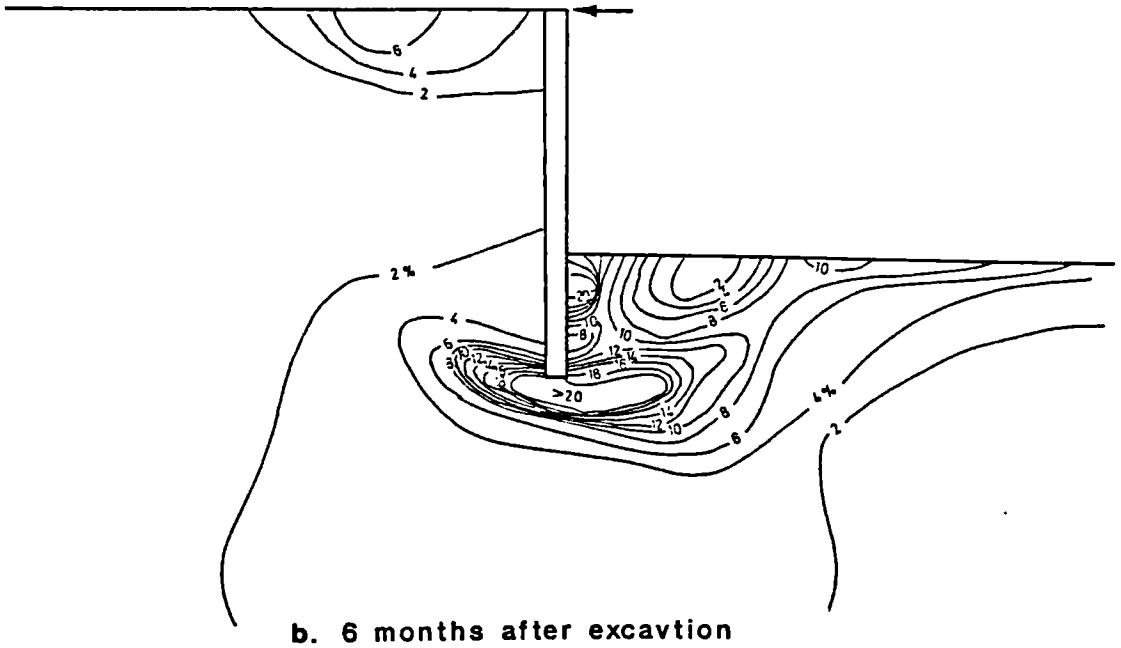

b. 6 months after excavtion

Fig. 2.19 Contours of mobilised shear strain

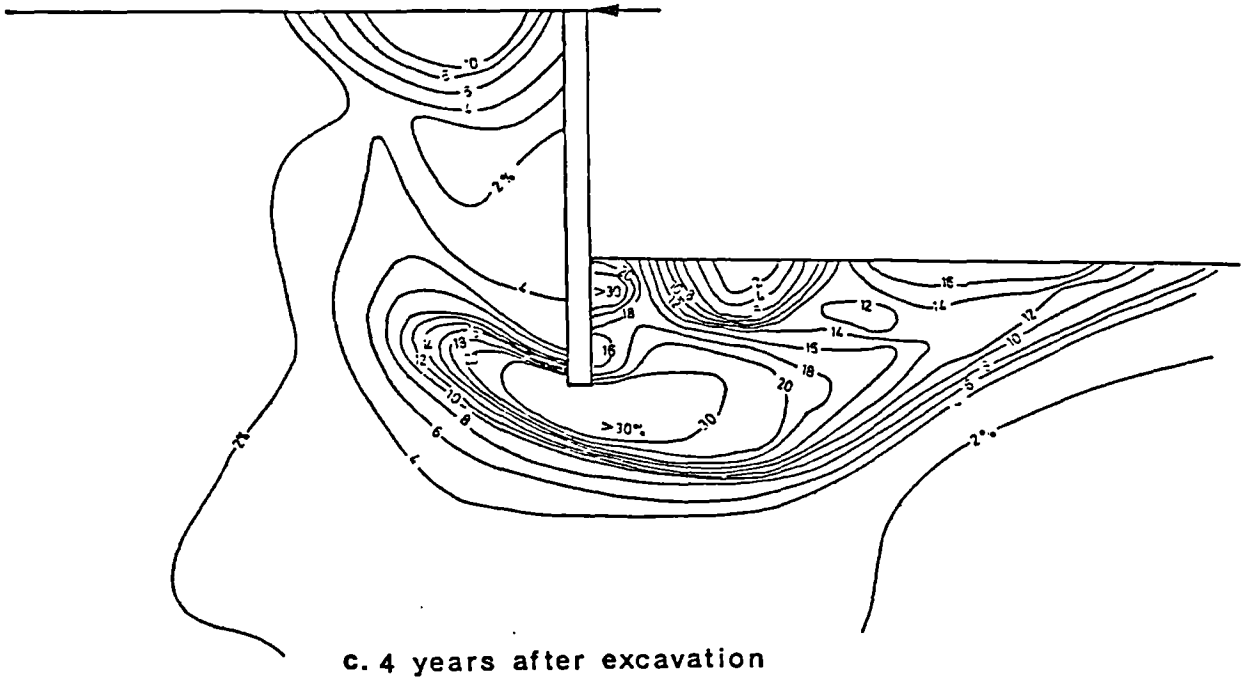

c. 4 years after excavation

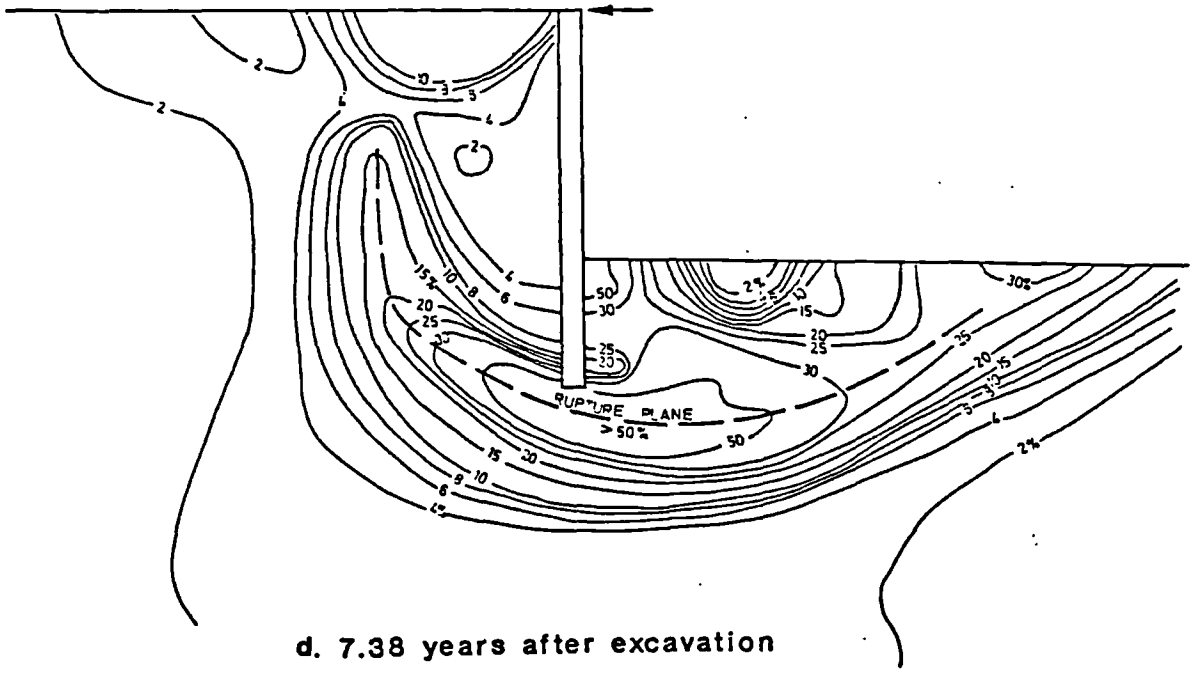

d. 7.38 years after excavation

Fig. 2.19 Contours of mobilised shear strain

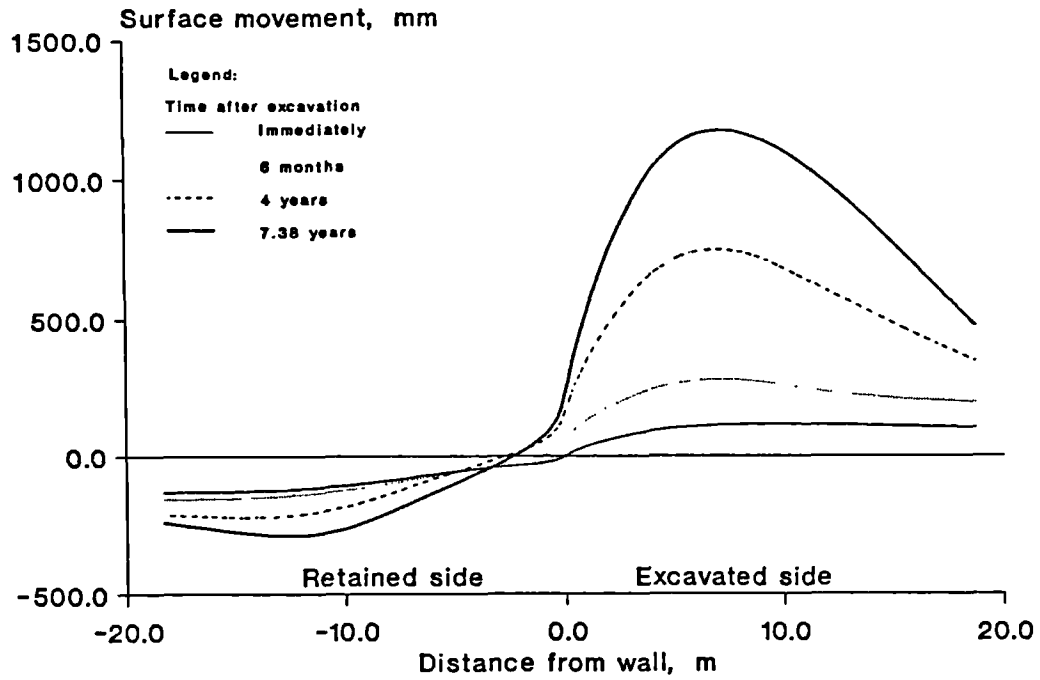

Fig. 2.20 Vertical movement profiles at ground surface for propped wall of 5m embedment

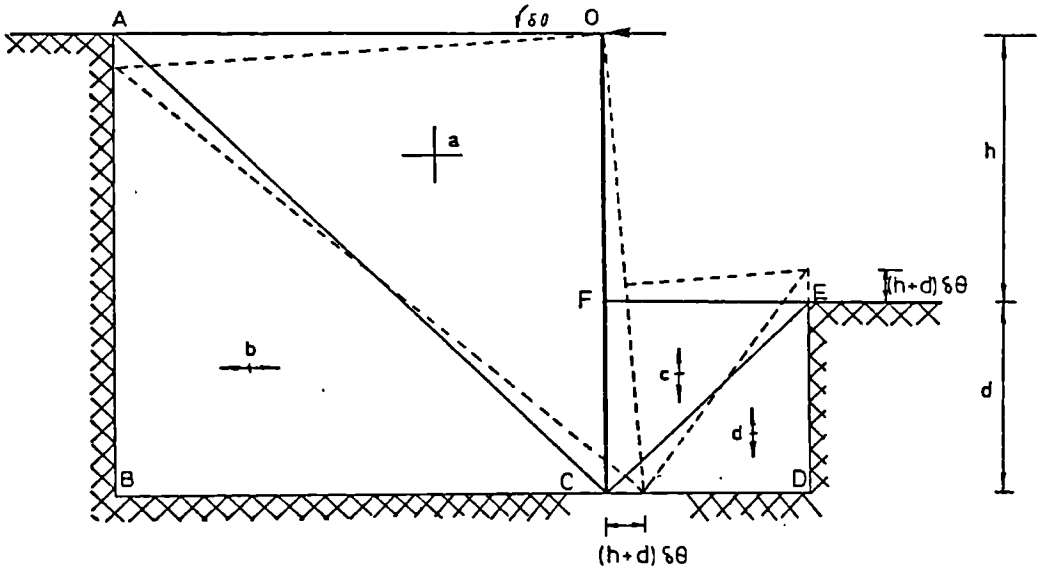

Fig. 2.21 Admissible strain field for rigid wall propped at the crest (from Bolton et al, 1989)

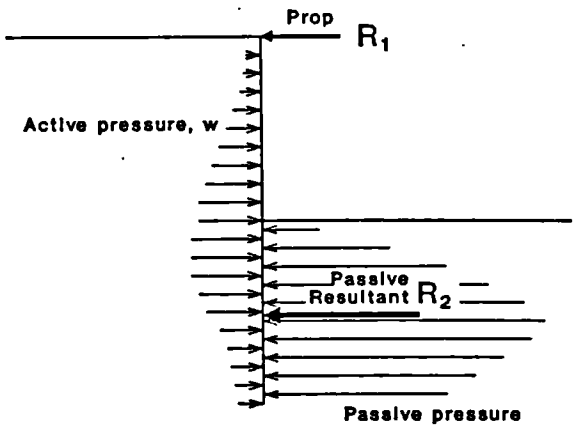

Fig. 2.22 Systematic representation of lateral stresses and forces

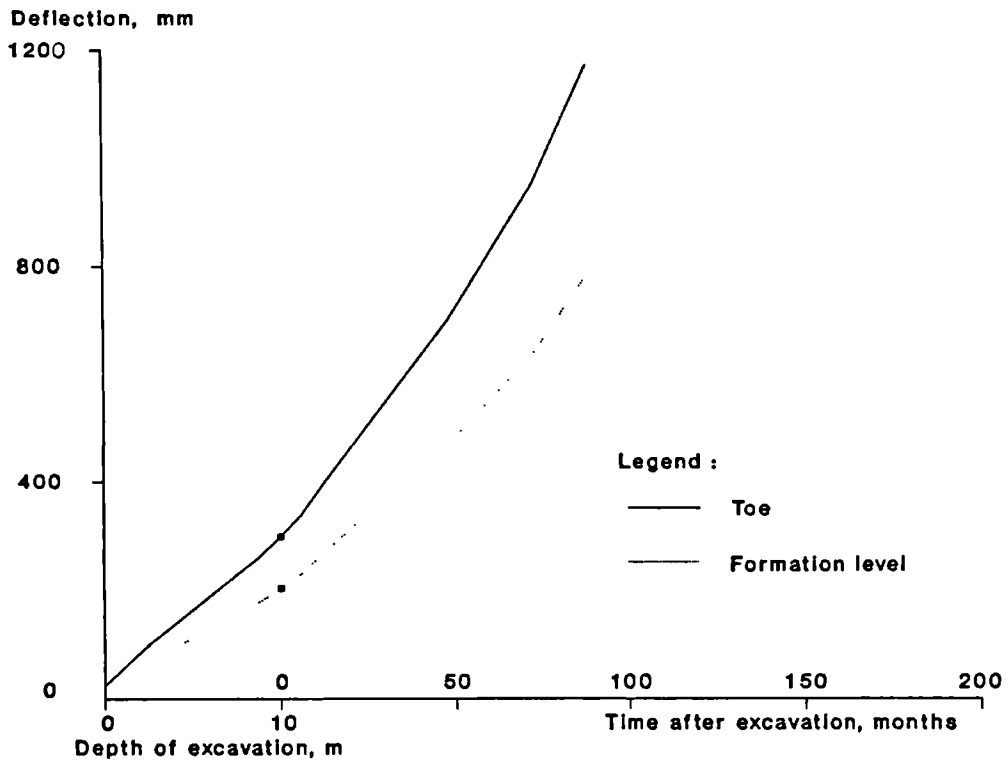

Fig. 2.23 Wall movements against excavation and time

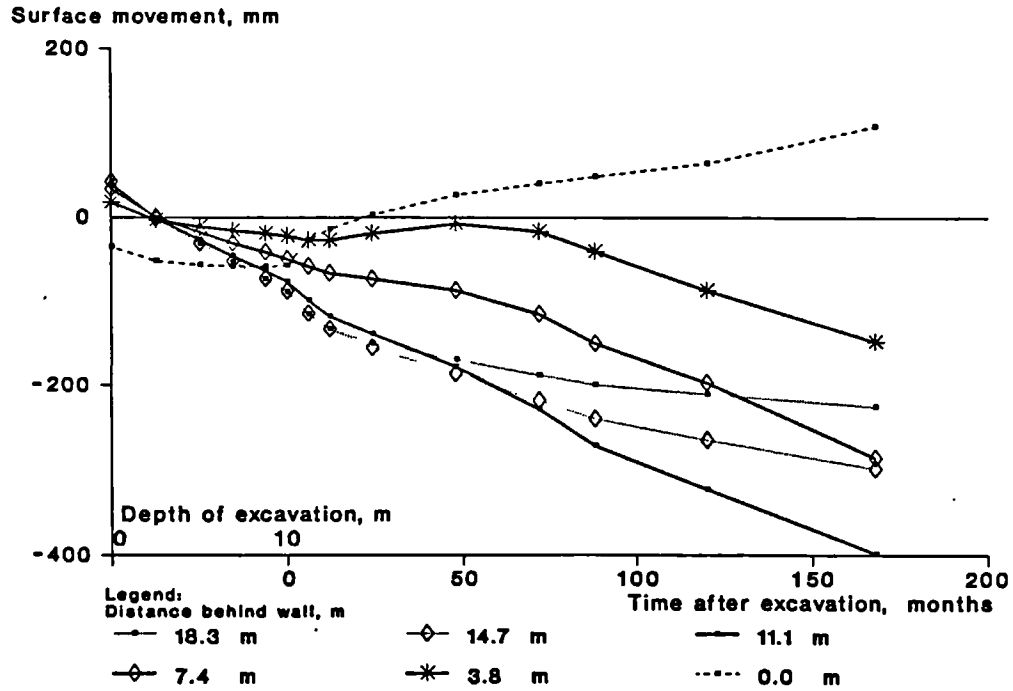

Fig. 2.24 Surface movements of retained soil against excavation and time

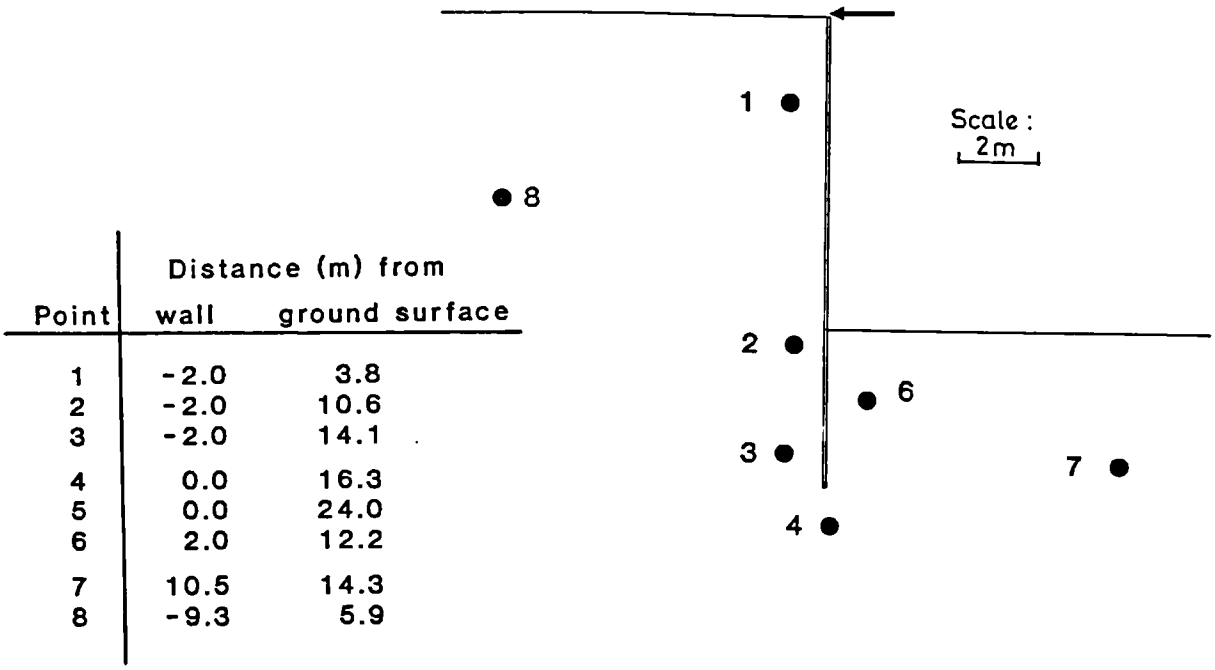

Point	Distance (m) from wall	Distance (m) from ground surface
1	-2.0	3.8
2	-2.0	10.6
3	-2.0	14.1
4	0.0	16.3
5	0.0	24.0
6	2.0	12.2
7	10.5	14.3
8	-9.3	5.9

Fig. 2.25 Location of points for stress path

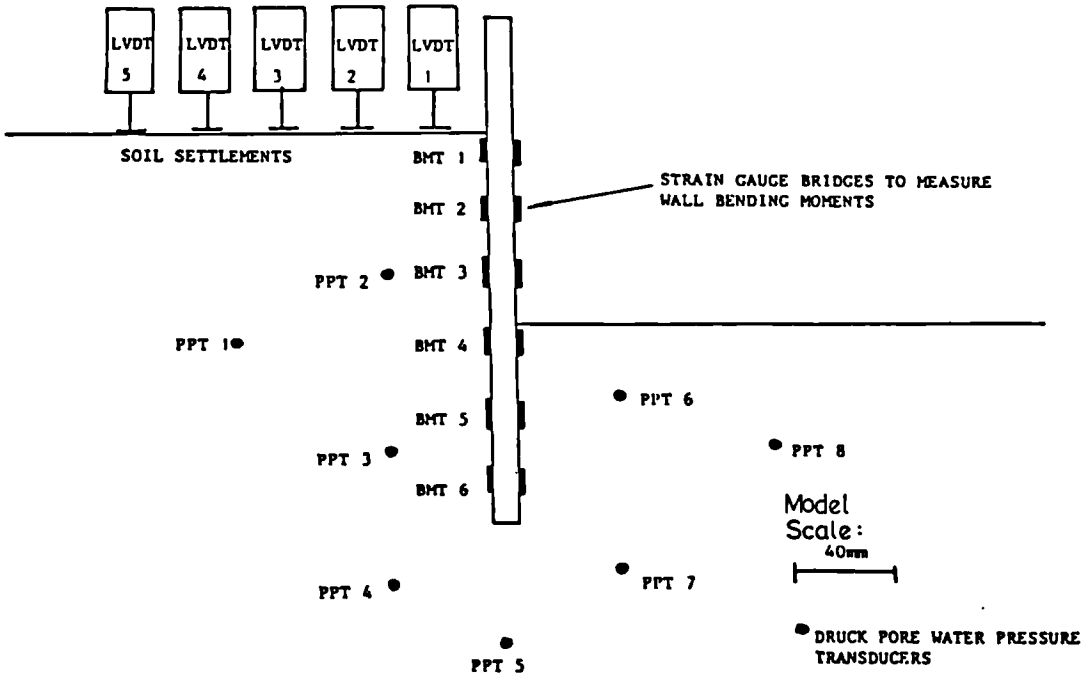

Fig. 2.26 Layout of instrumentation in centrifuge model test, DWC11 (from Powrie, 1986)

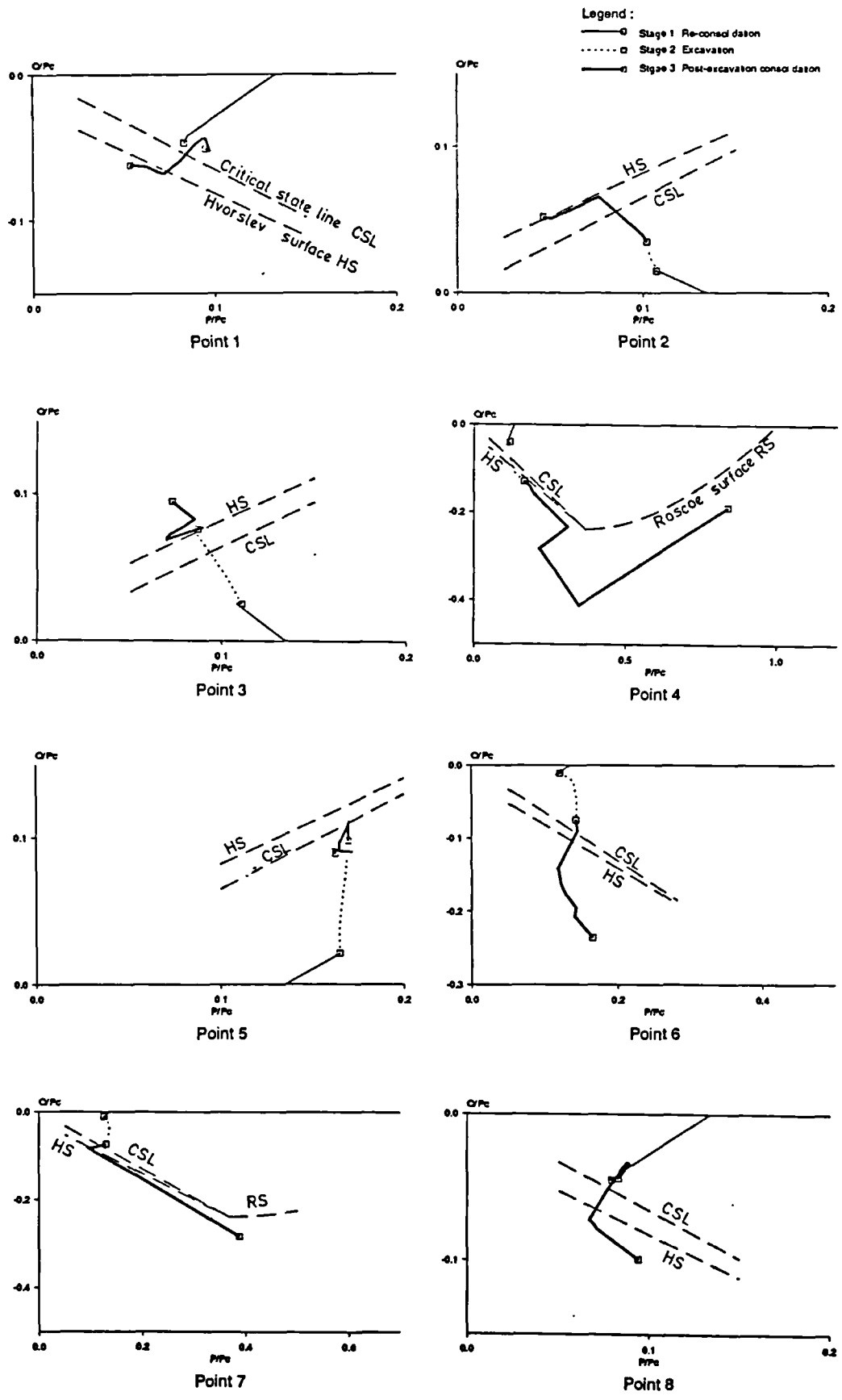

Fig. 2.27 Normalised stress paths of selected soil elements (see fig. 2.25 for location)

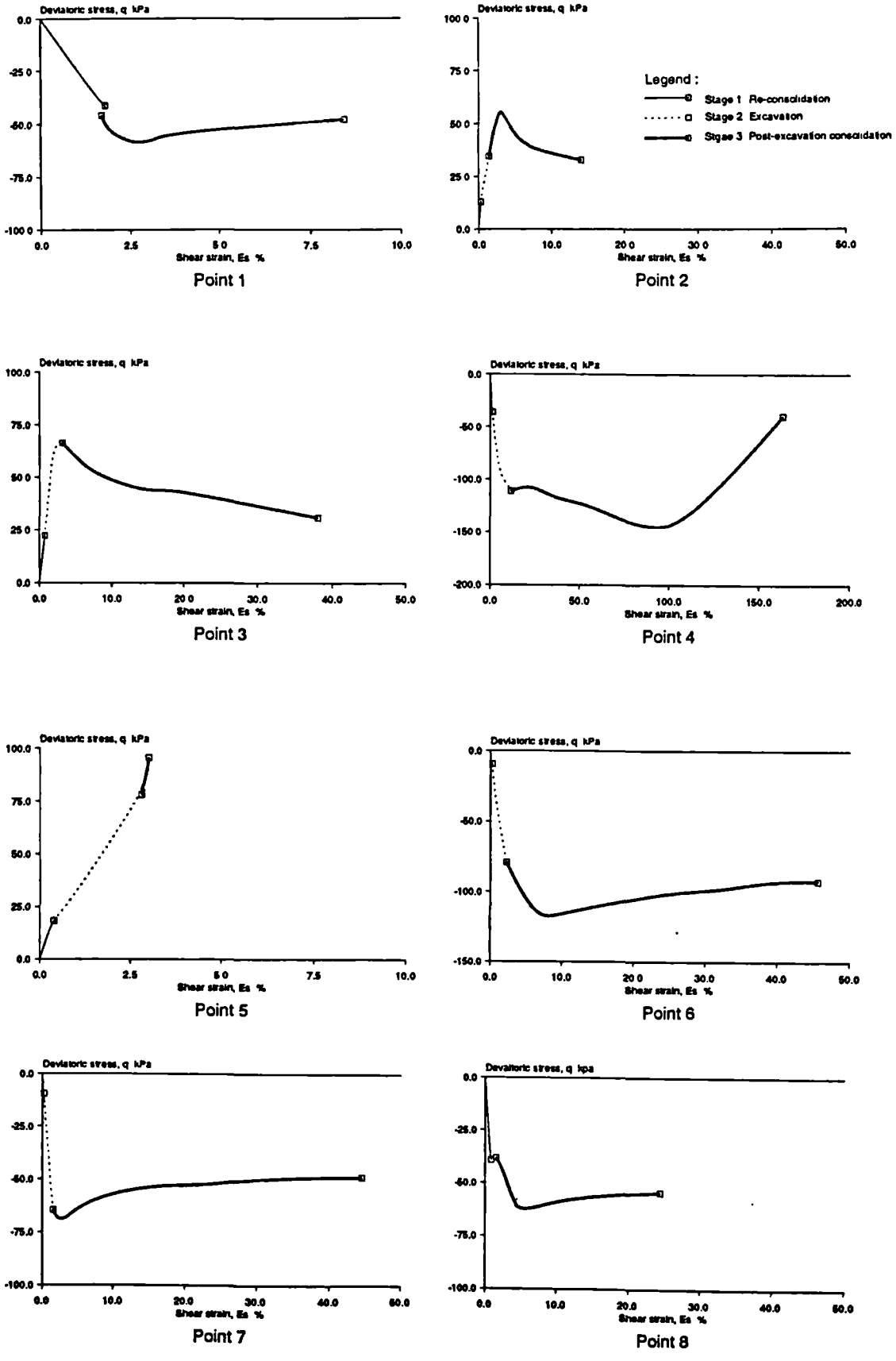

Fig. 2.28 Mobilised shear stress vs shear strain

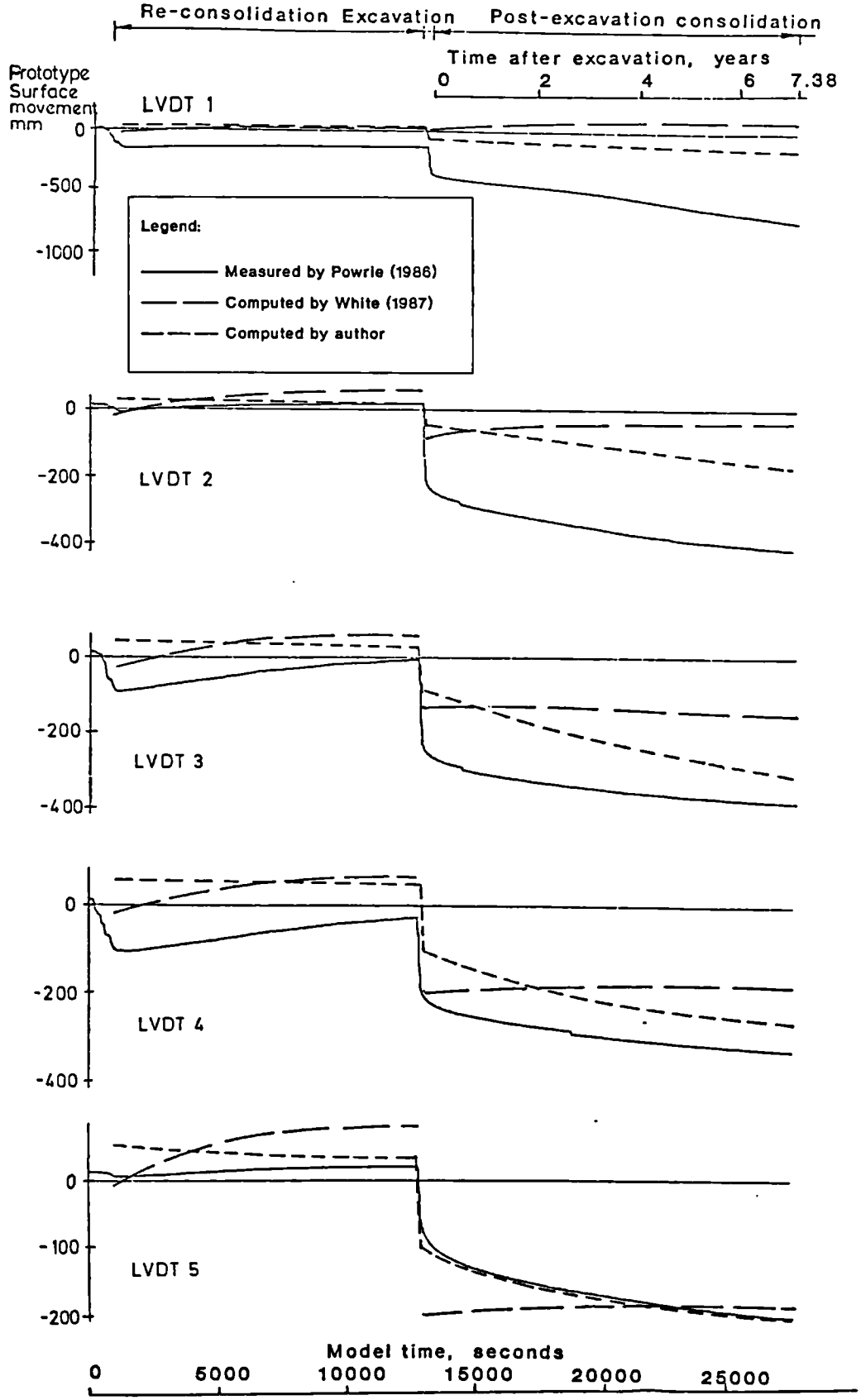

Fig. 2.29 Comparison of computed and measured surface movements on retained side against time

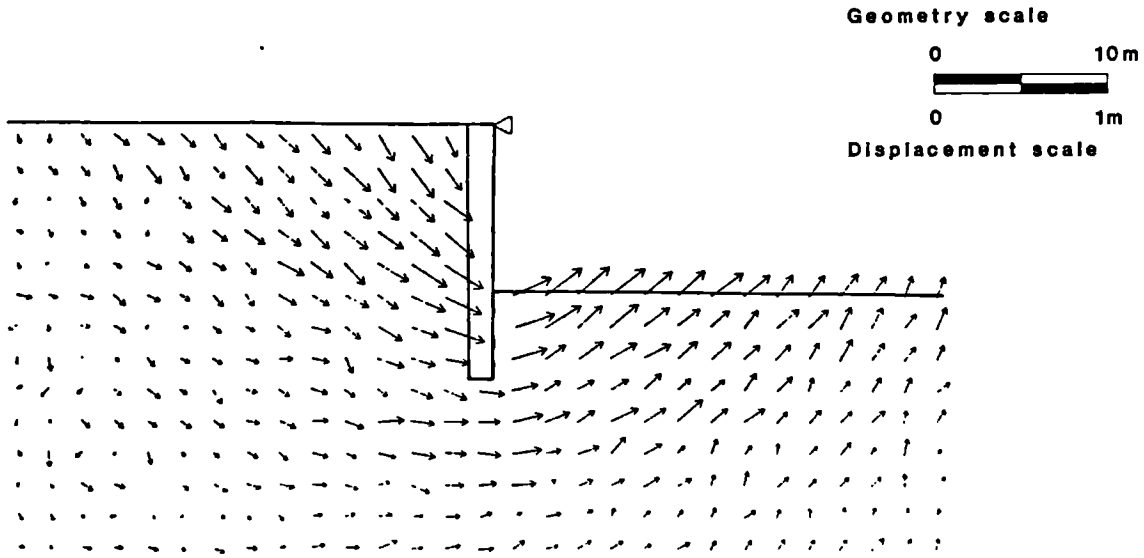

a. Centrifuge test

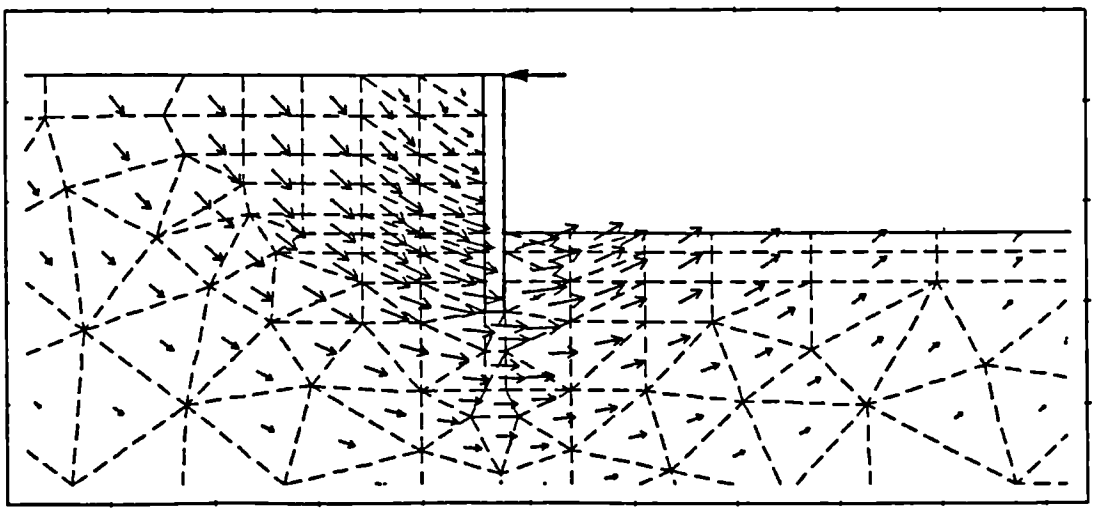

b. Finite element analysis

Fig. 2.30 Comparison of soil movements during excavation

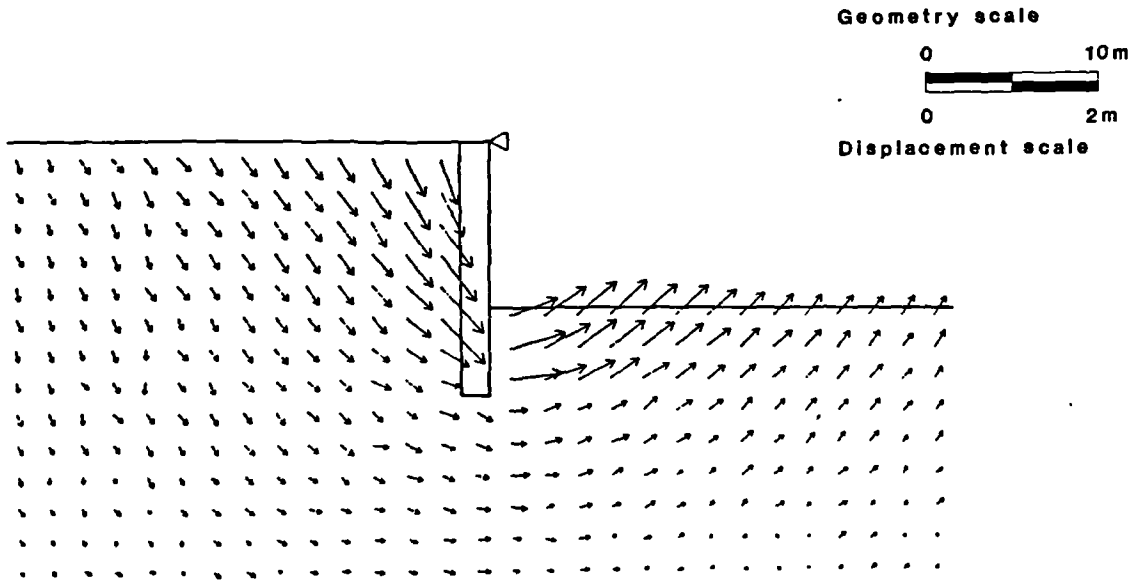

a. Centrifuge test

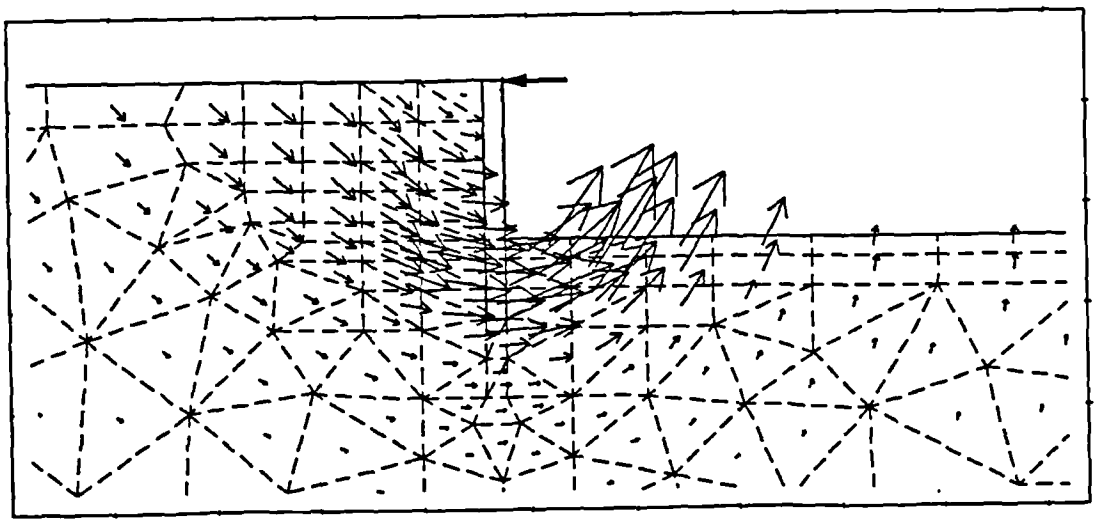

b. Finite element analysis

Fig. 2.31 Comparison of post-excavation soil movements

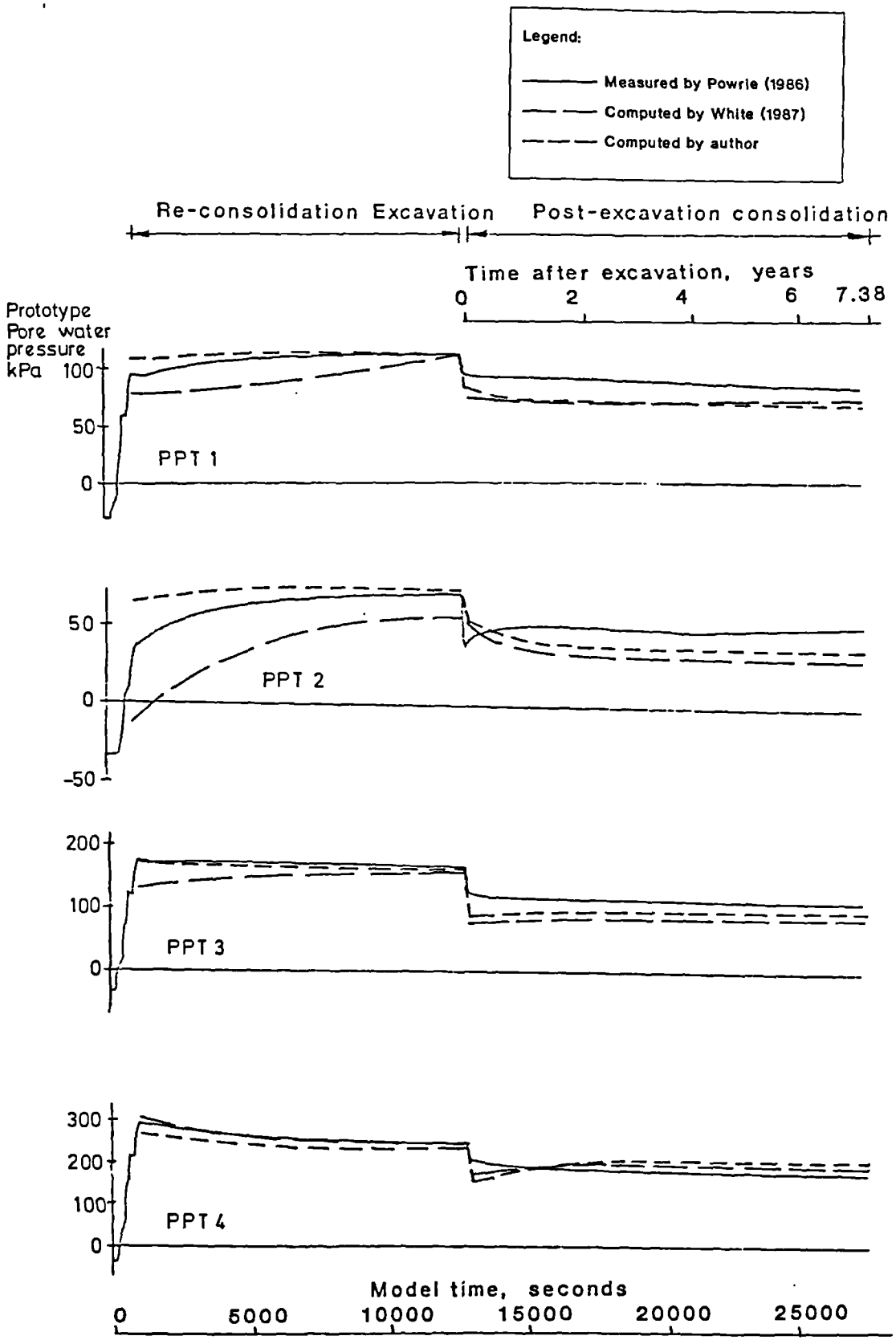

Fig. 2.32 Comparison of computed and measured pore water pressures against time (PPT1-4)

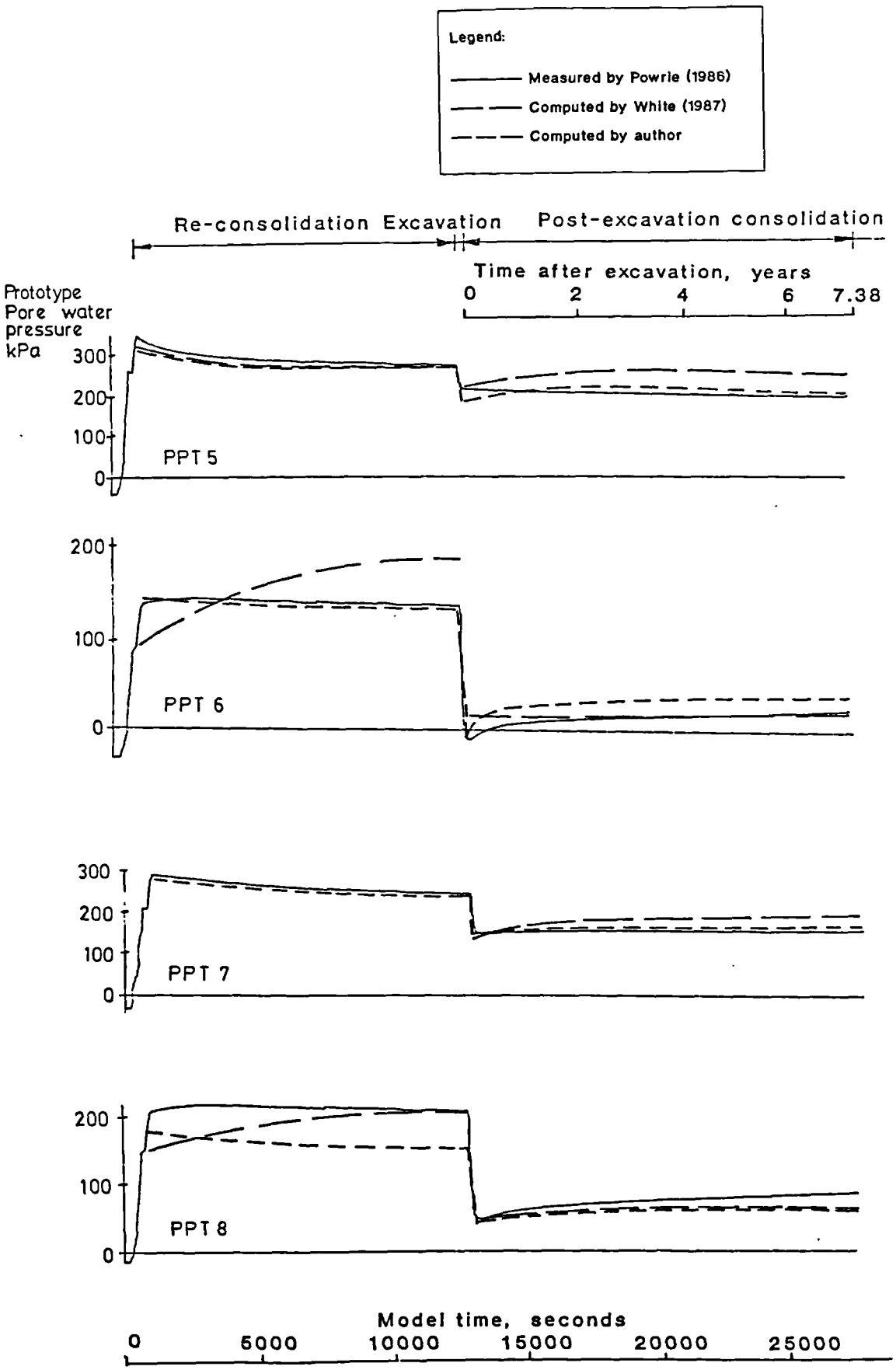

Fig. 2.32 Comparison of computed and measured pore water pressures against time (PPT5-8)

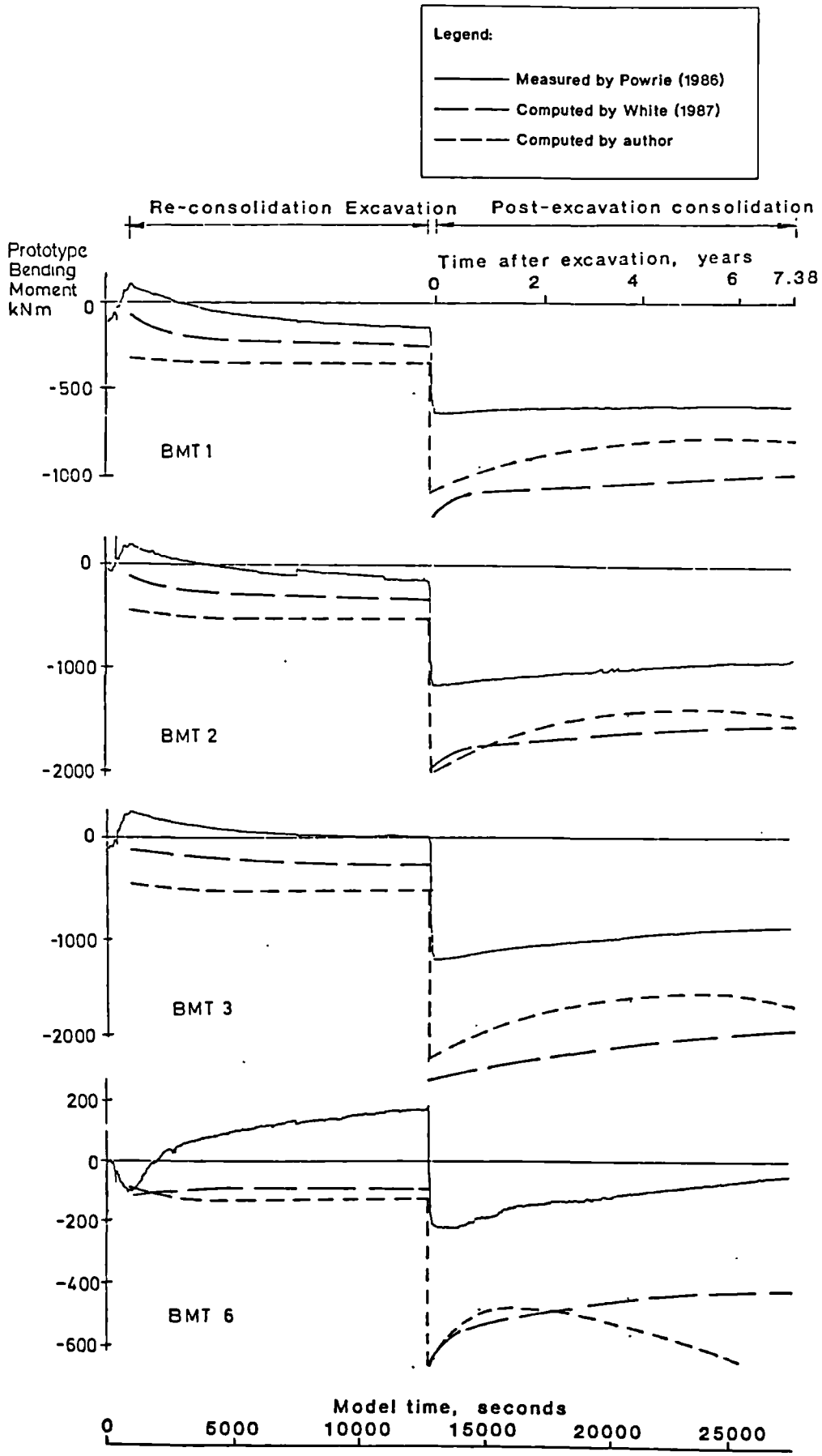

Fig. 2.33 Comparison of computed and measured bending moments against time

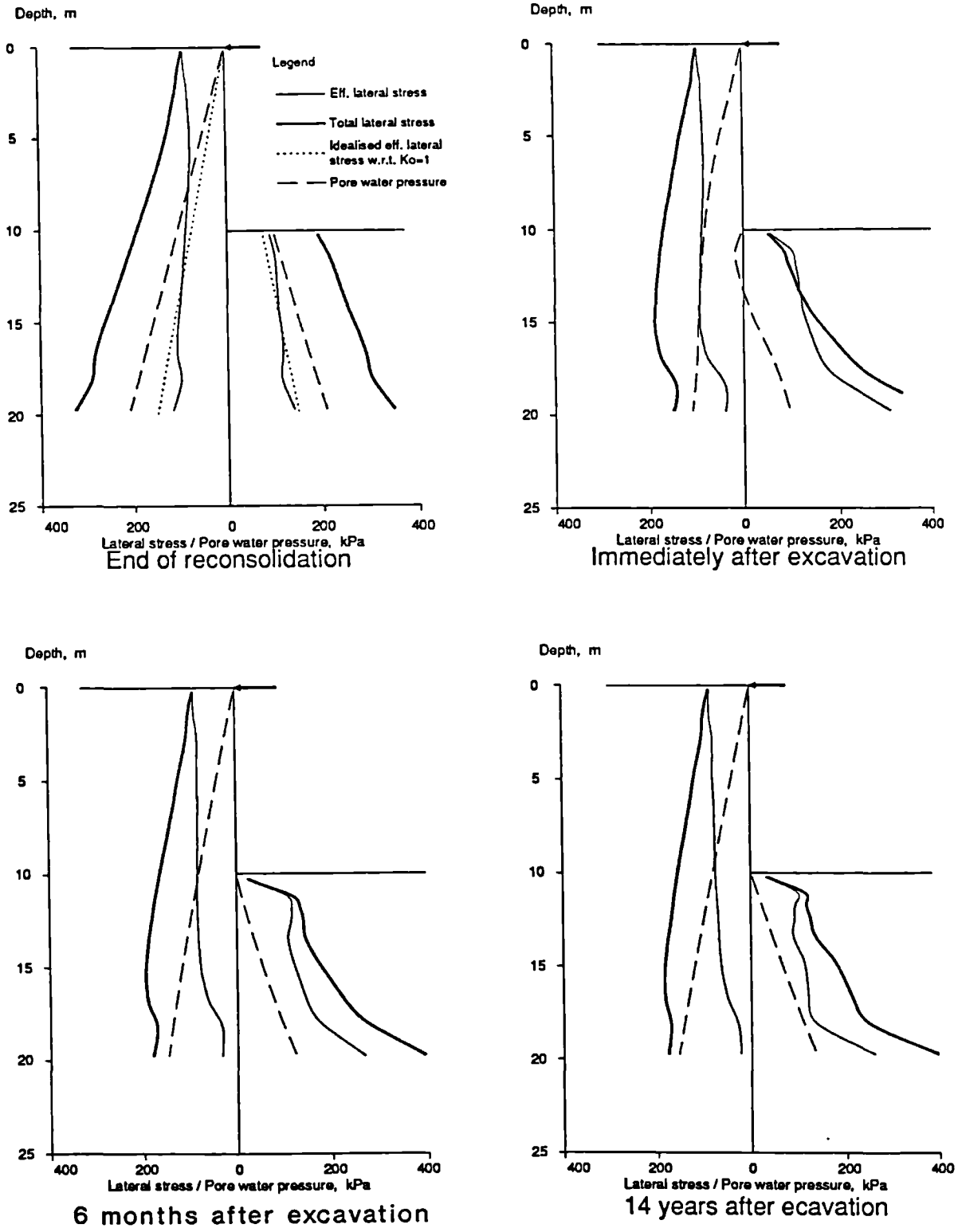

Fig. 3.1 Lateral stresses and pore water pressure distributions for wall of 10m embedment

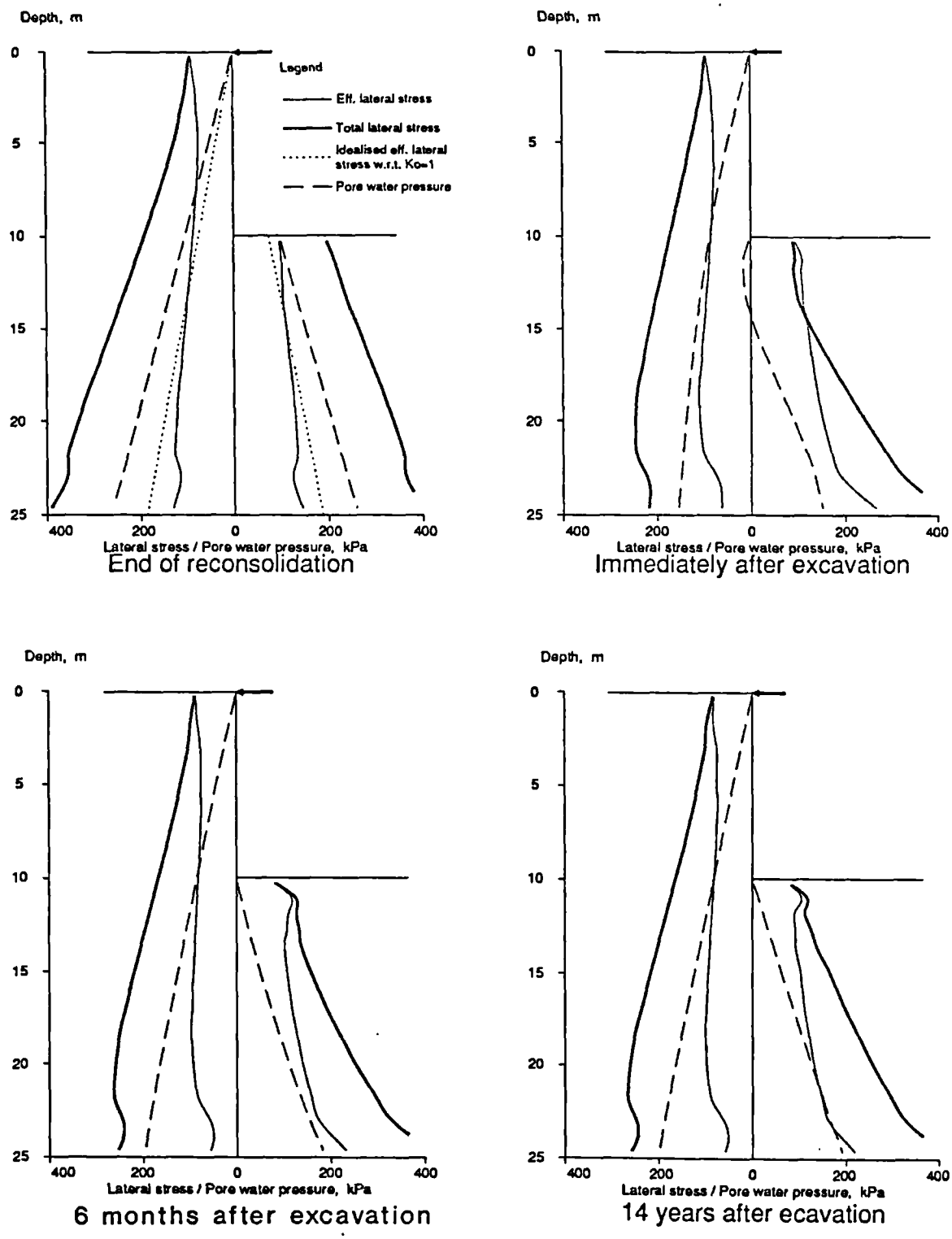

Fig. 3.2 Lateral stresses and pore water pressure distributions for wall of 15m embedment

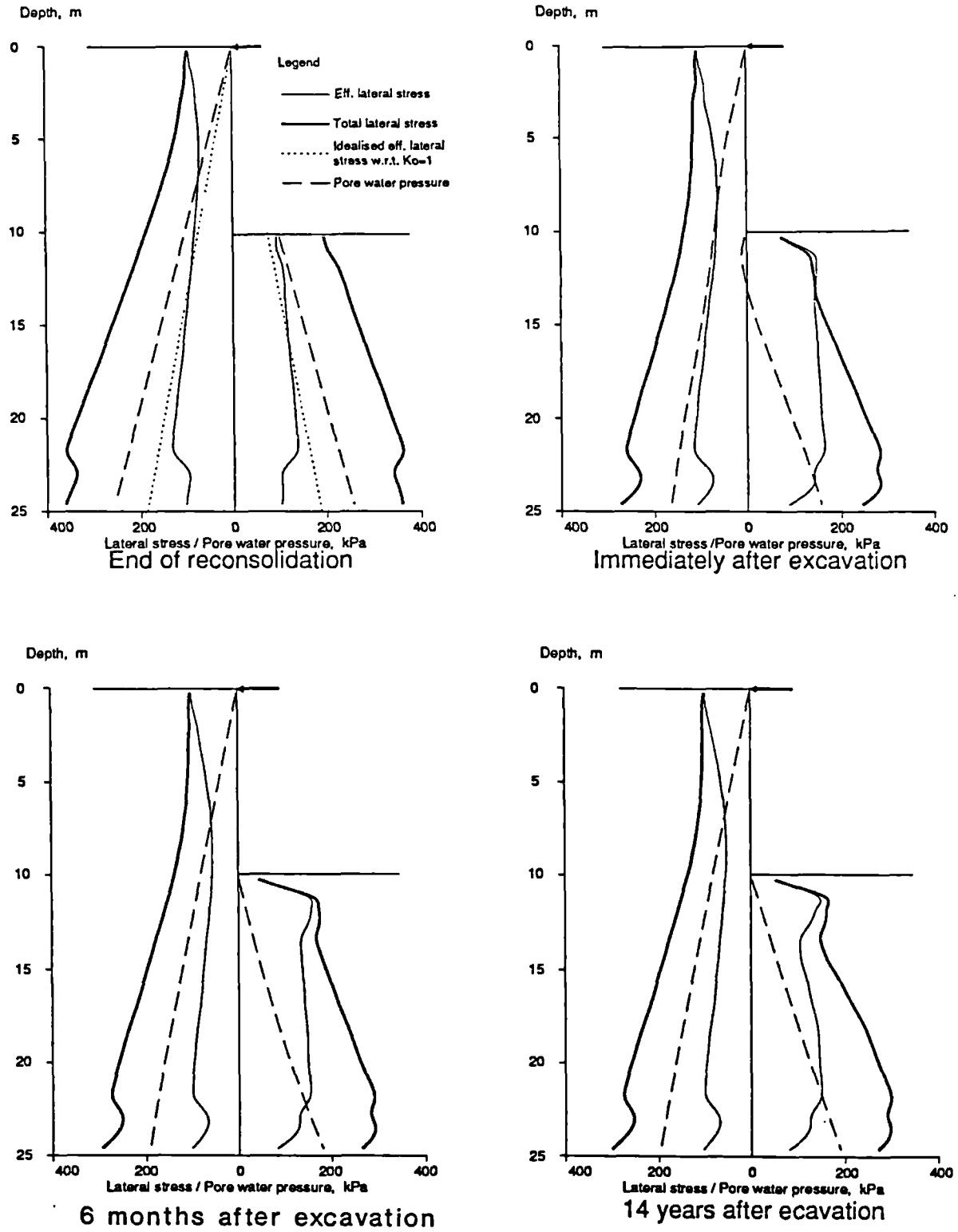

Fig. 3.3 Lateral stresses and pore water pressure distributions for more flexible wall of 15m embedment

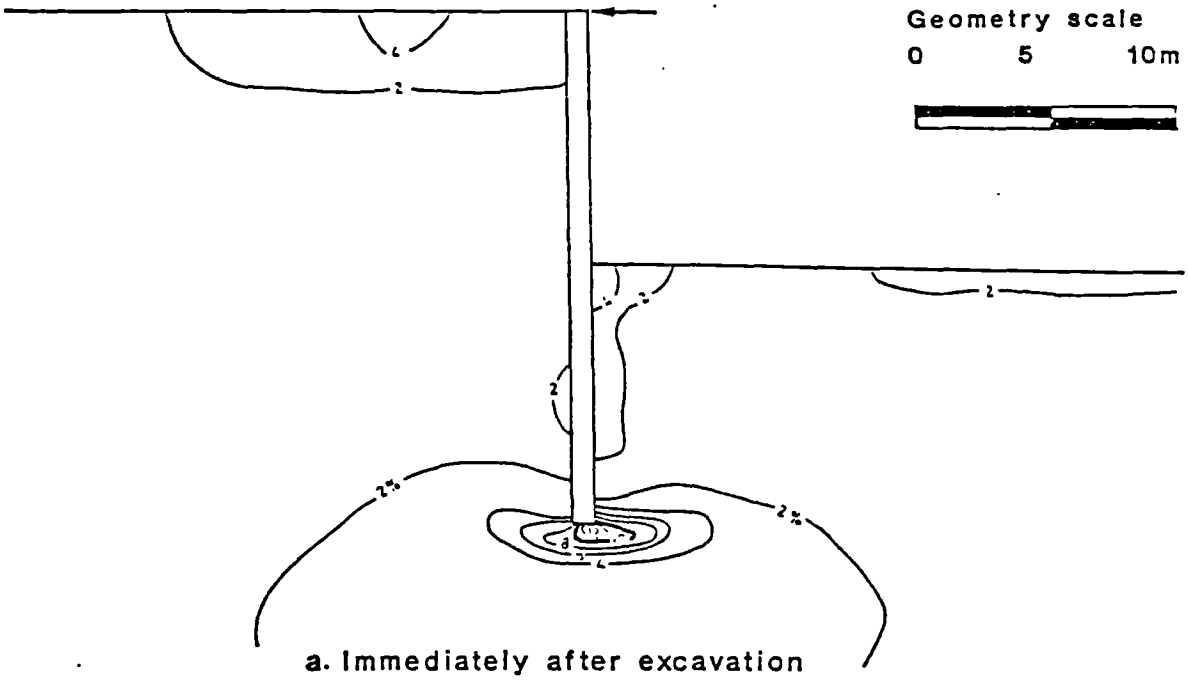

a. Immediately after excavation

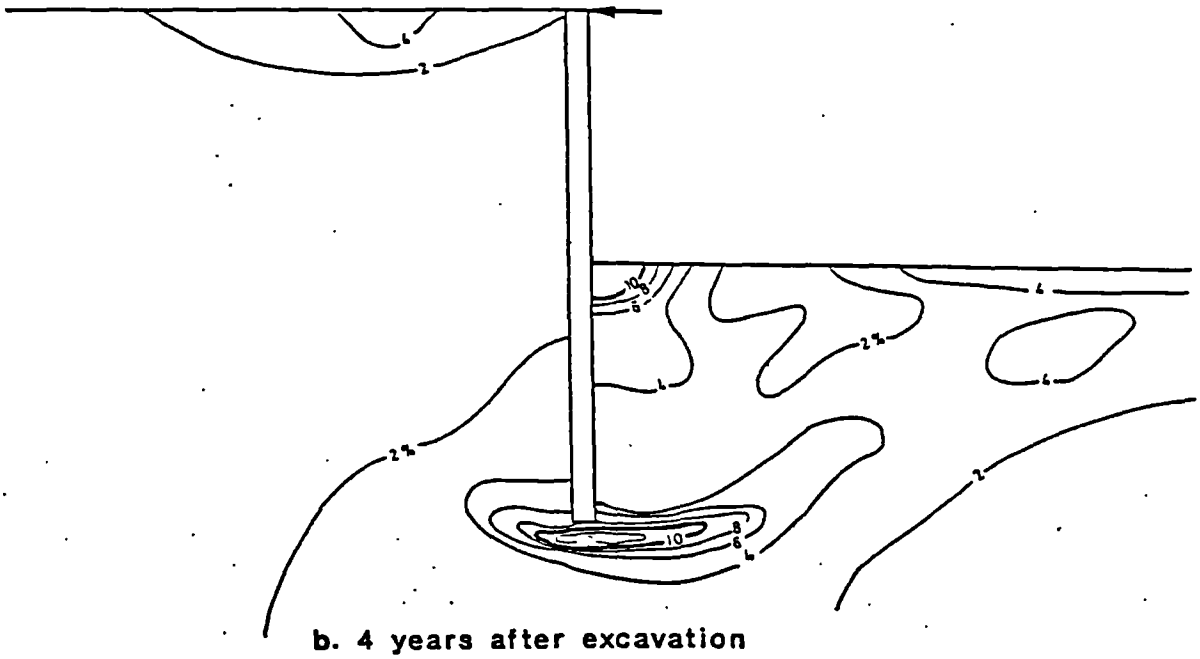

b. 4 years after excavation

Fig. 3.4 Contours of mobilised shear strain for wall of 10m embedment

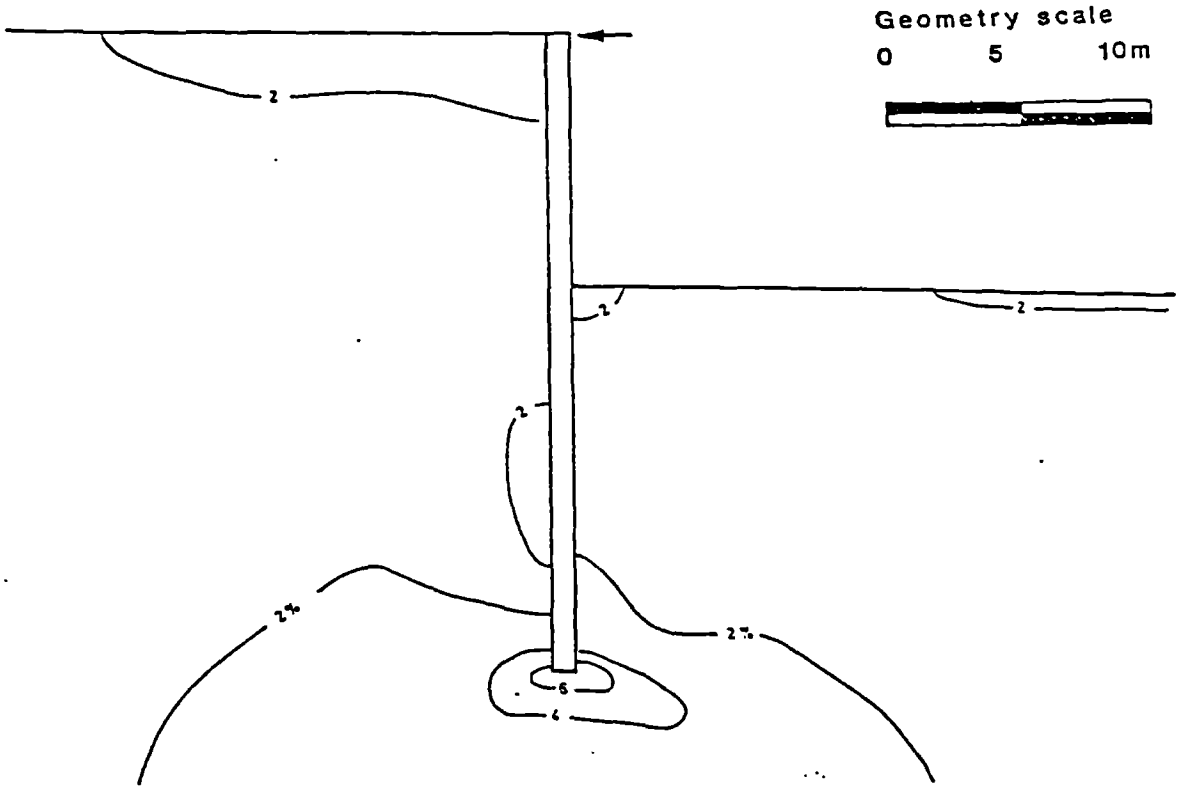

a. Immediately after excavation

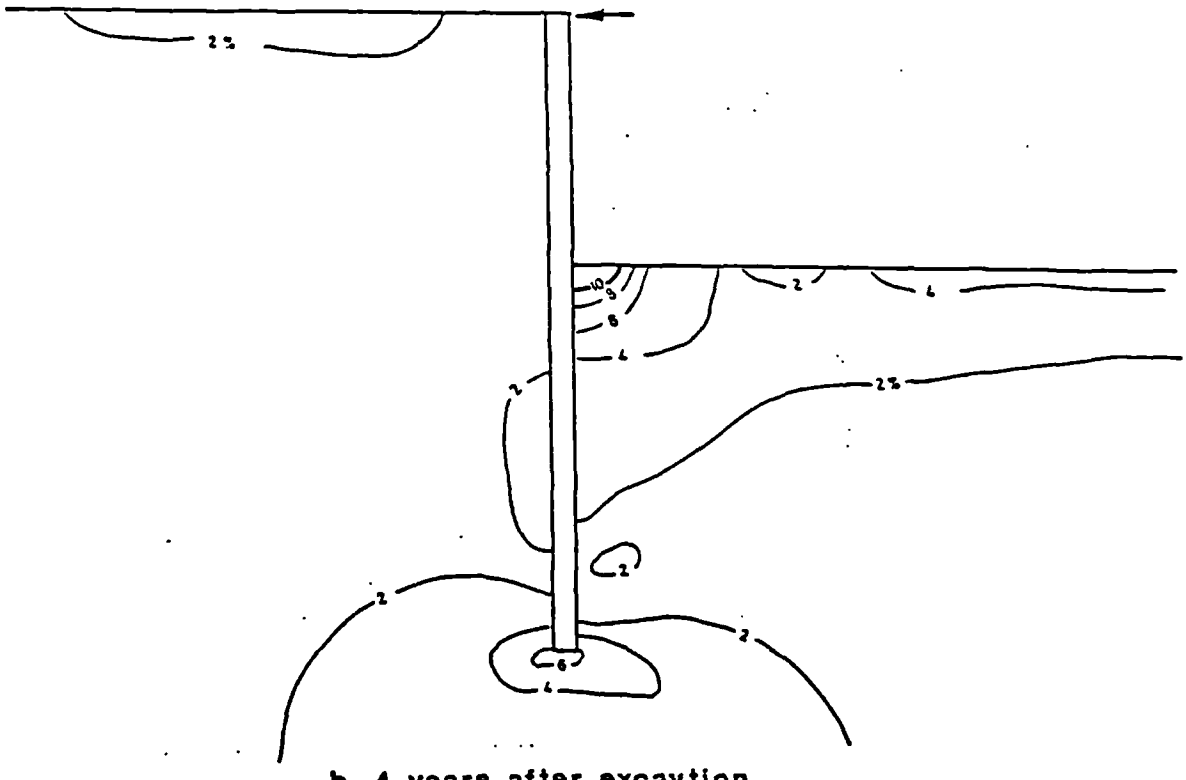

b. 4 years after excavtion

Fig. 3.5 Contours of mobilised shear strain for wall of 15m embedment

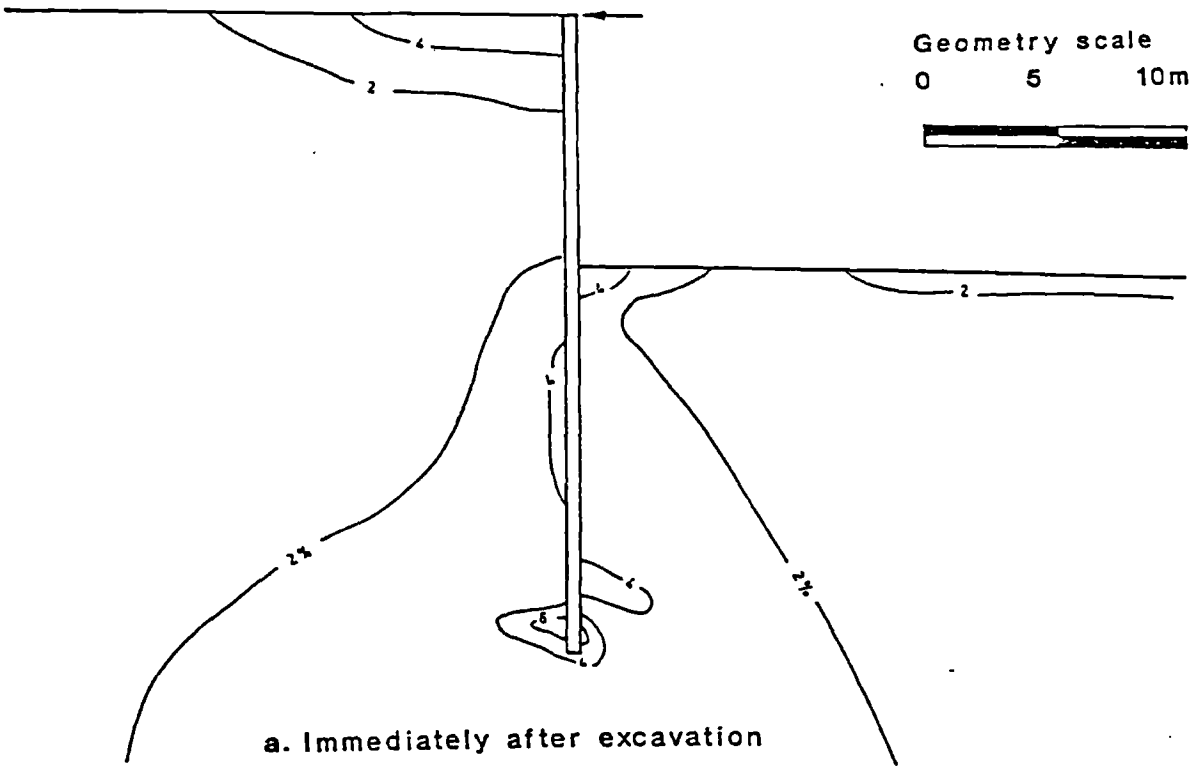

a. Immediately after excavation

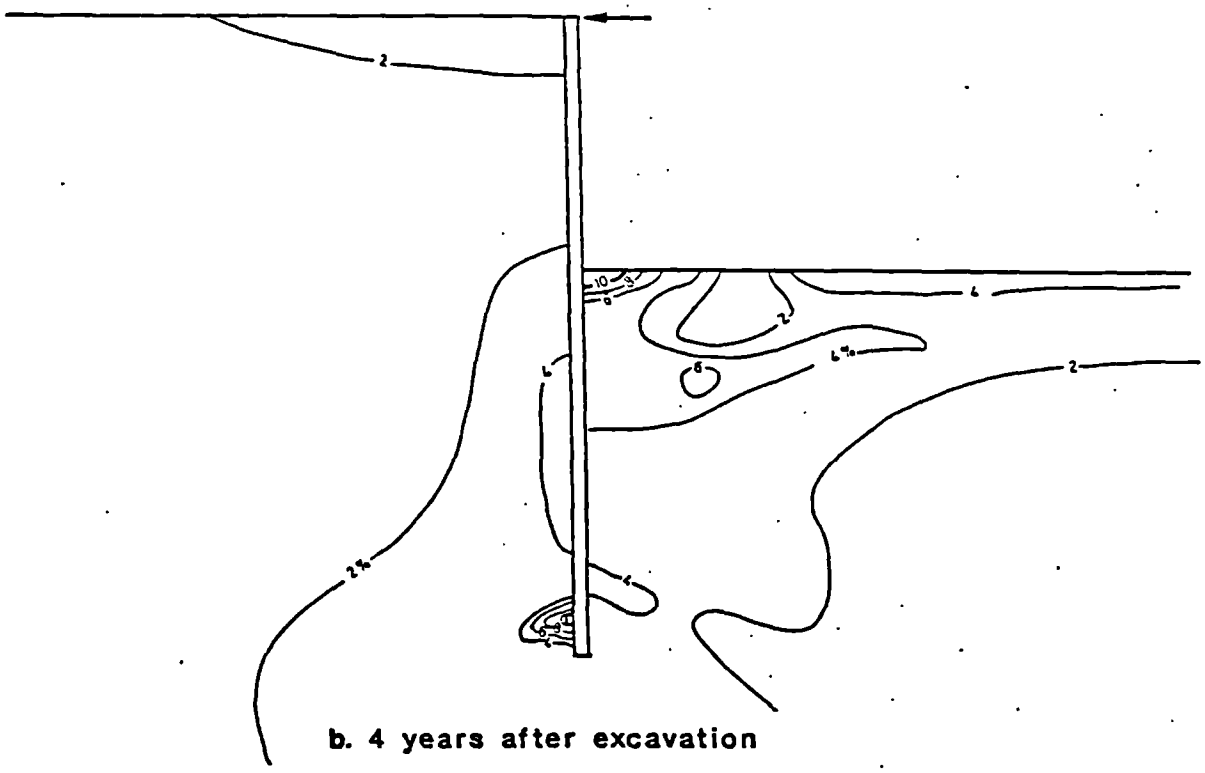

b. 4 years after excavation

Fig. 3.6 Contours of mobilised shear strain for more flexible wall of 15m embedment

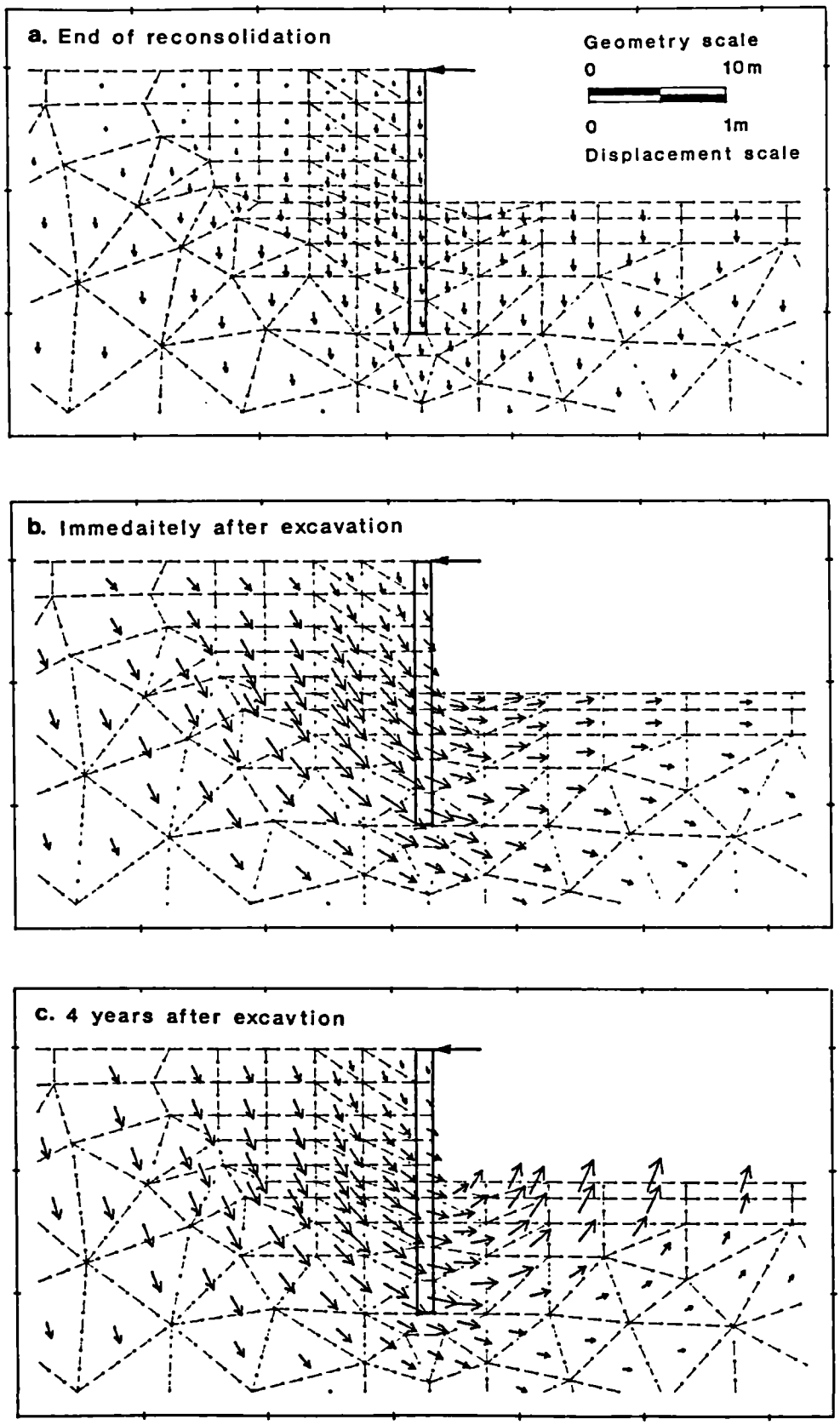

Fig. 3.7 Cumulative displacement vector diagrams for wall of 10m embedment

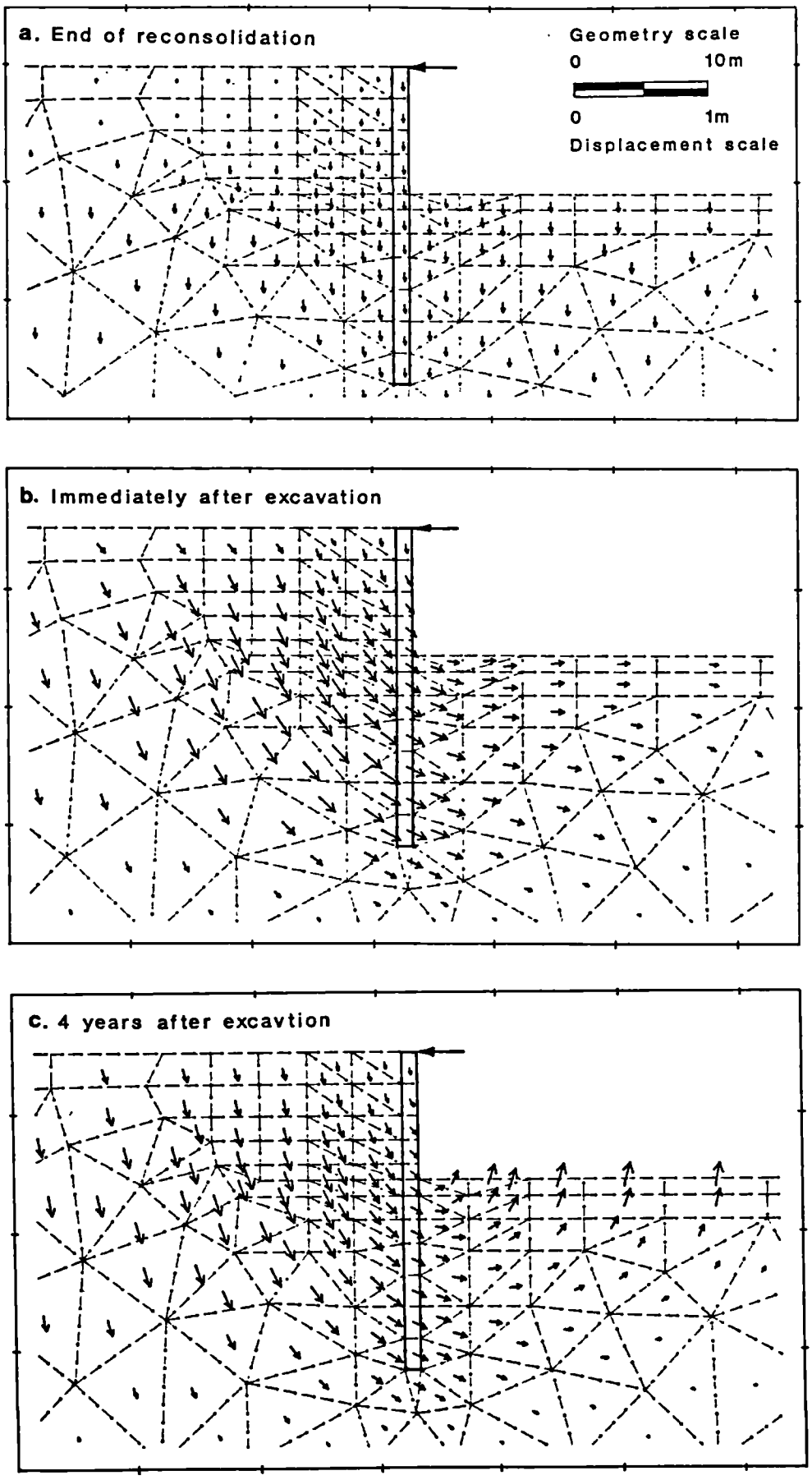

Fig. 3.8 Cumulative displacement vector diagrams for wall of 15m embedment

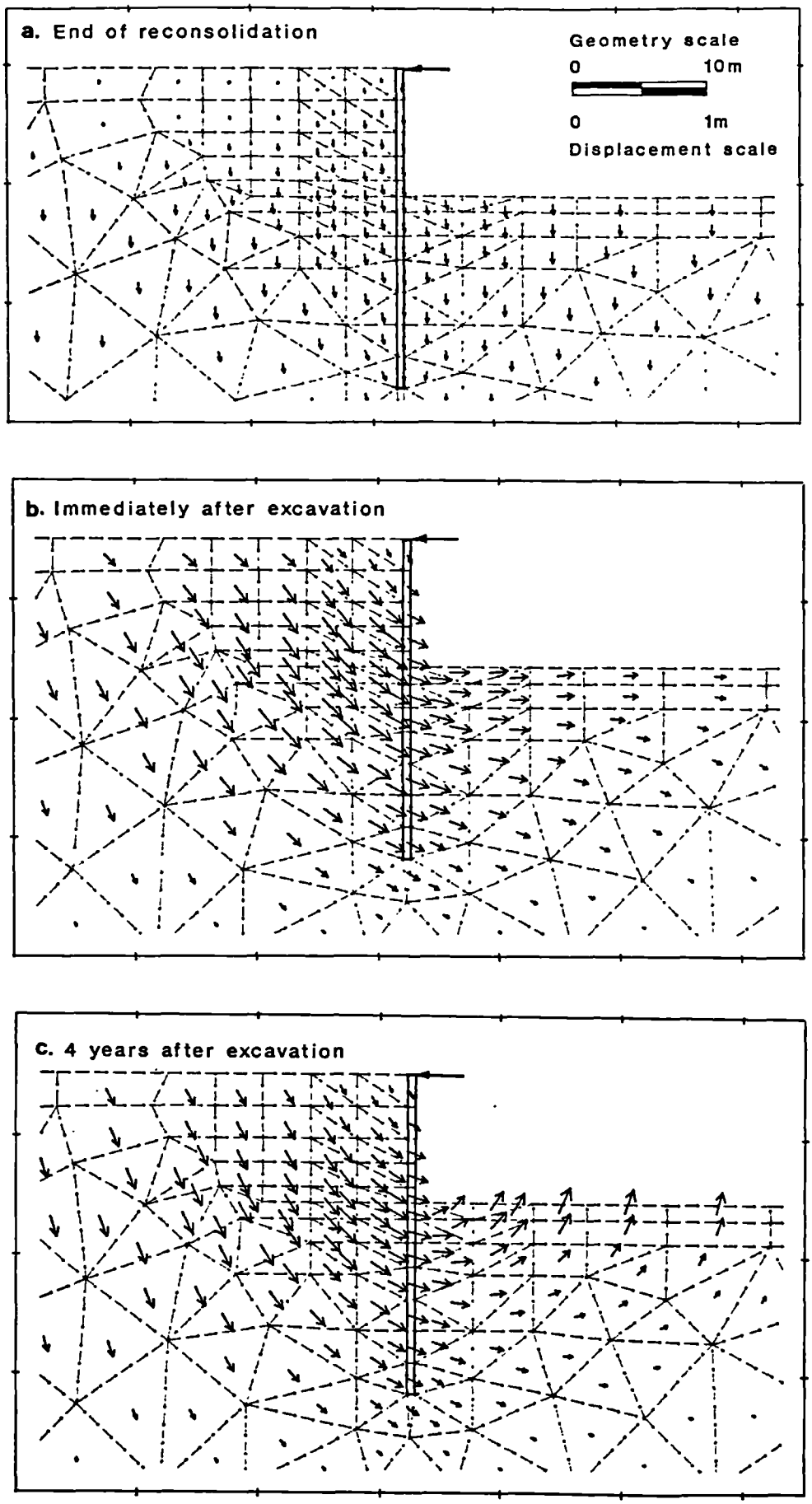

Fig. 3.9 Cumulative displacement vector diagrams for more flexible wall of 15m embedment

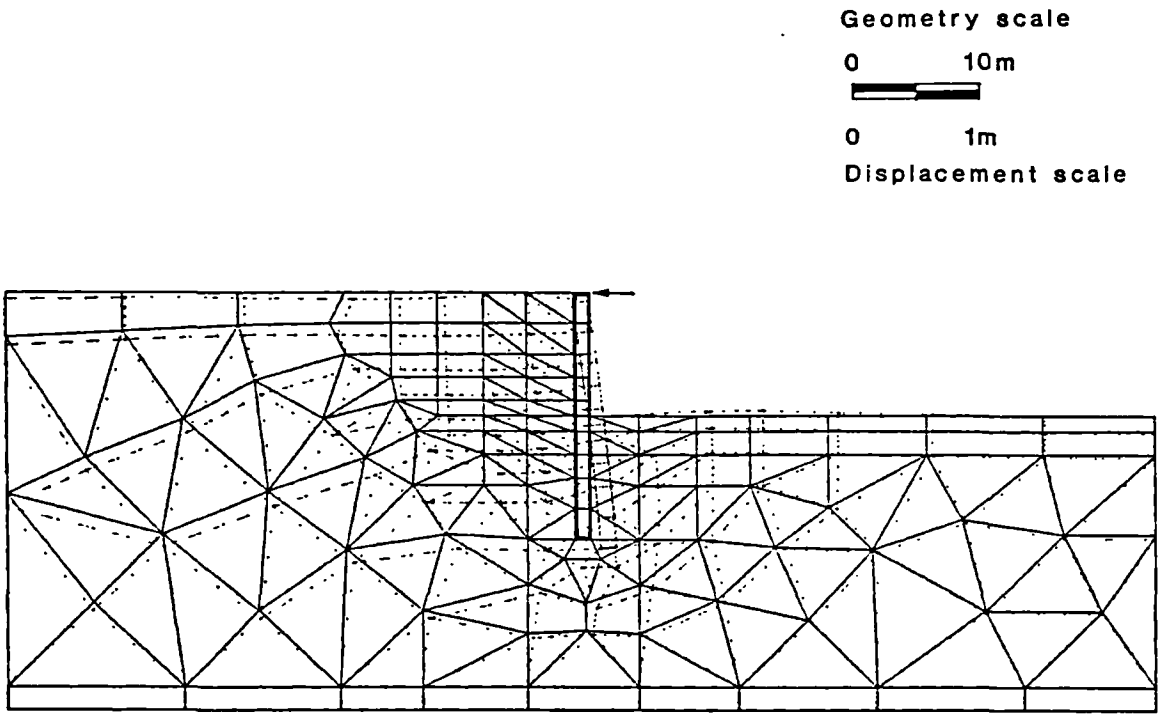

a. Immediately after excavation

b. 4 years after excavation

Fig. 3.10 Cumulative soil and wall movements for wall of 10m embedment

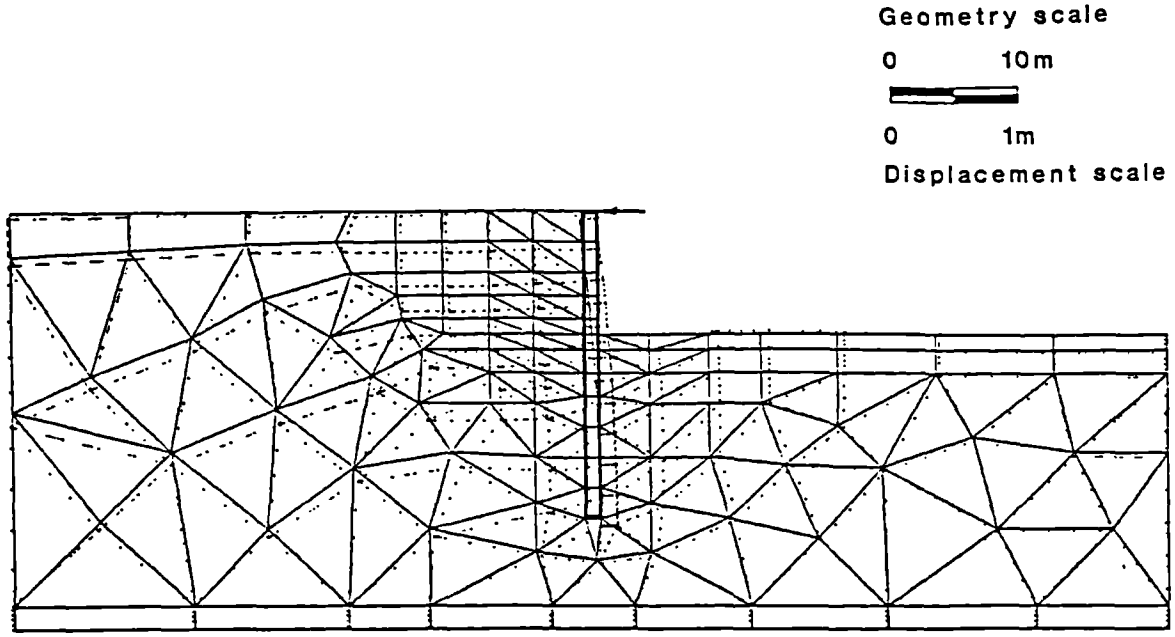

a. Immediately after excavation

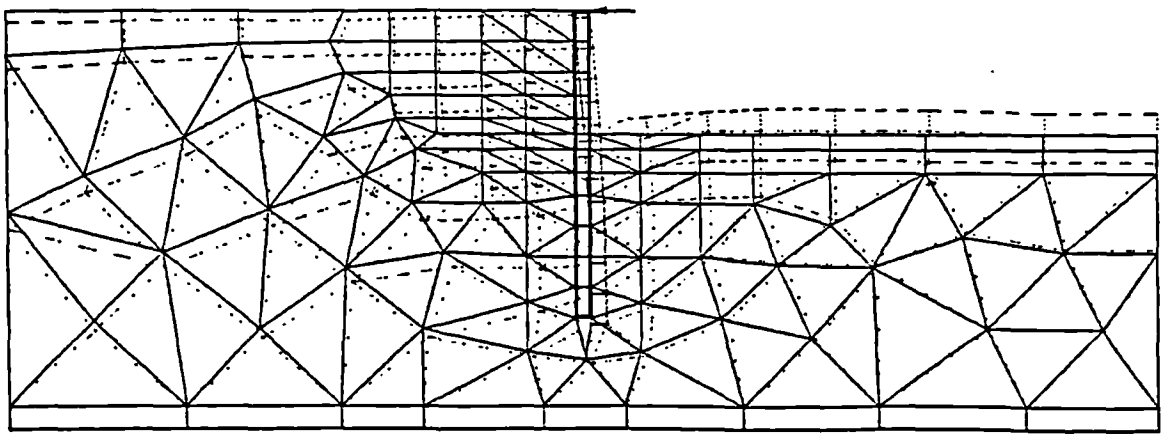

b. 4 years after excavation

Fig. 3.11 Cumulative soil and wall movements for wall of 15m embedment

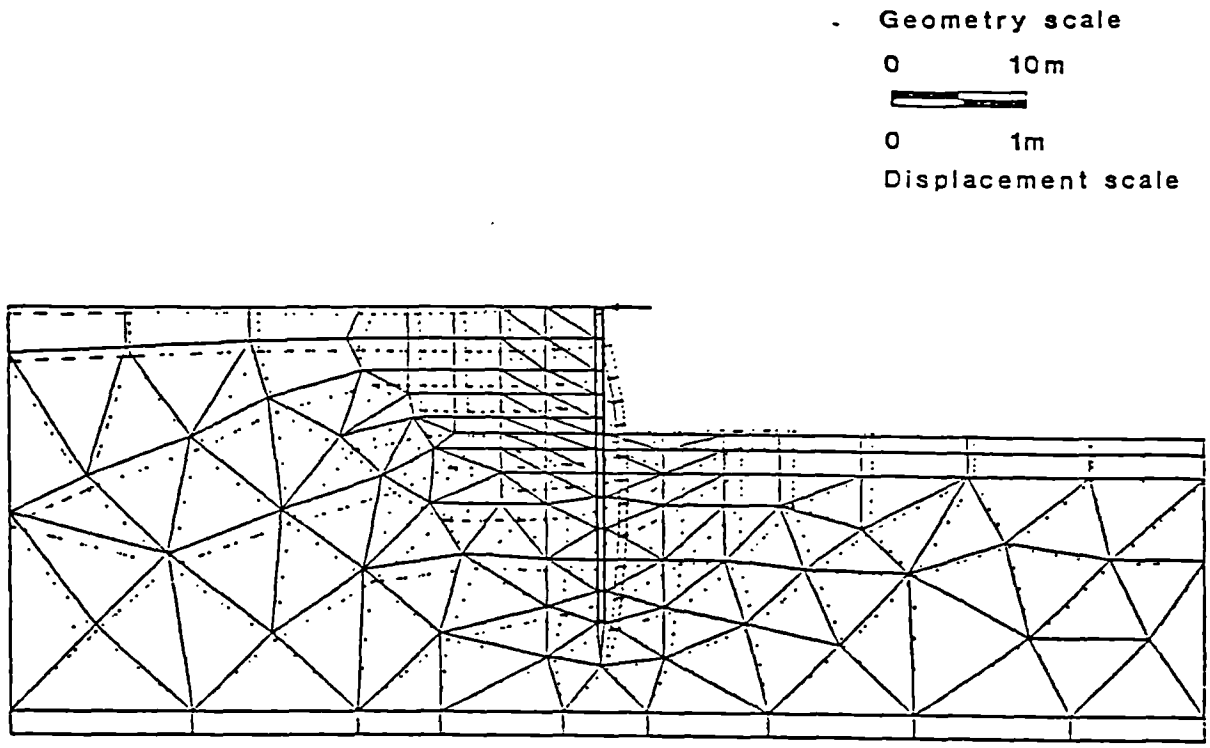

a. Immediately after excavation

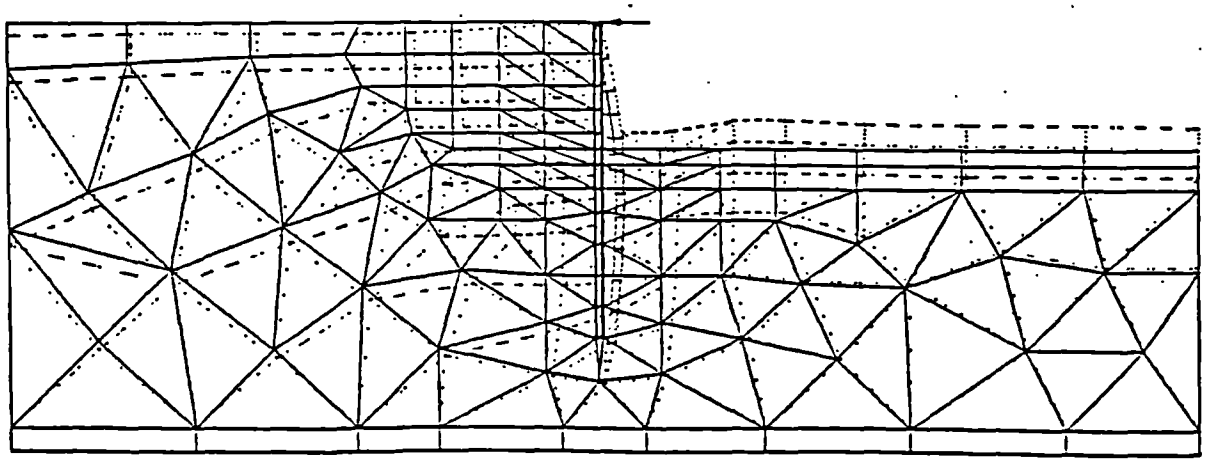

b. 4 years after excavtion

Fig. 3.12 Cumulative soil and wall movements for more flexible wall of 15m embedment

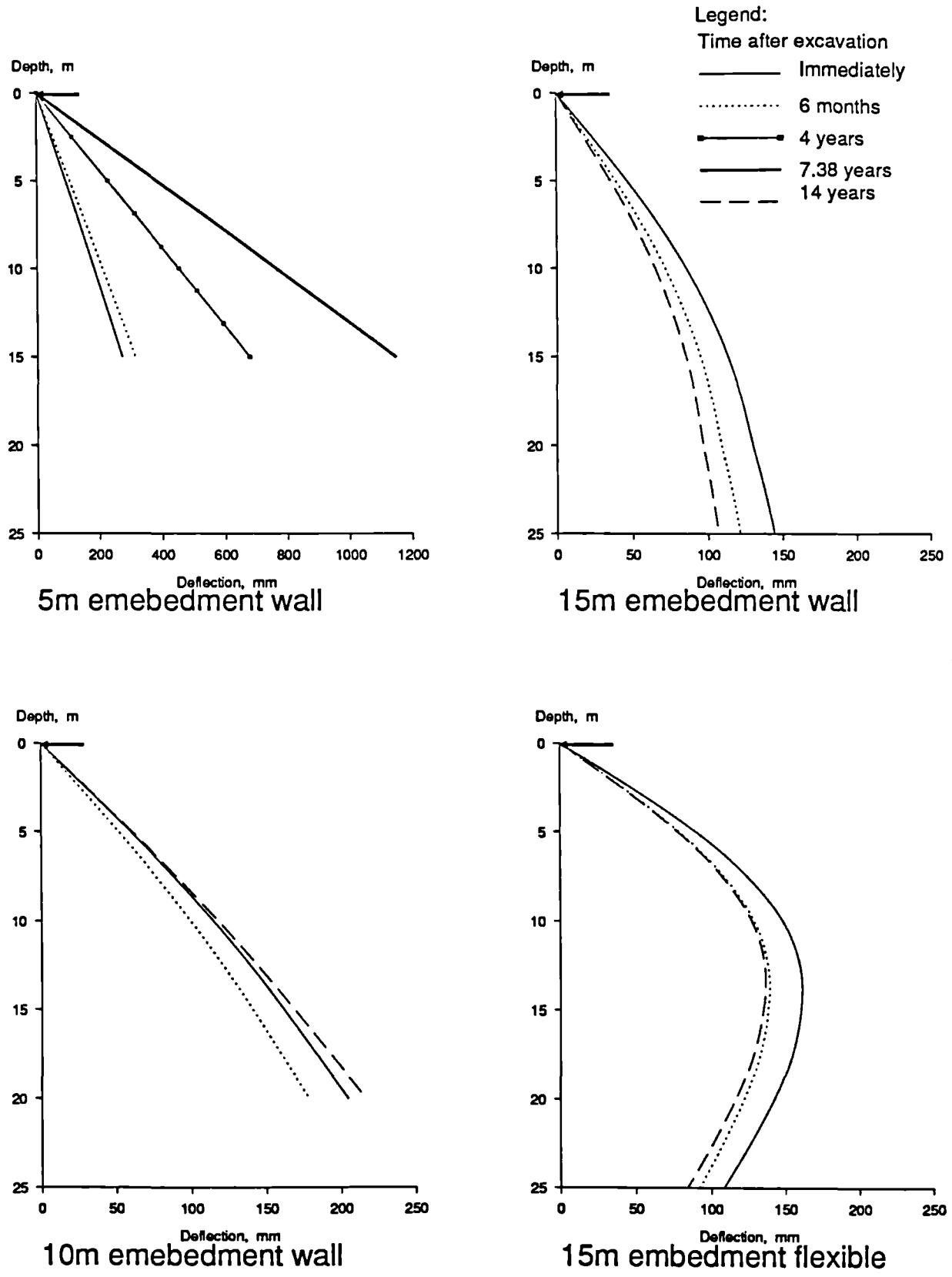

Fig. 3.13 Wall deflections for walls propped at the crest

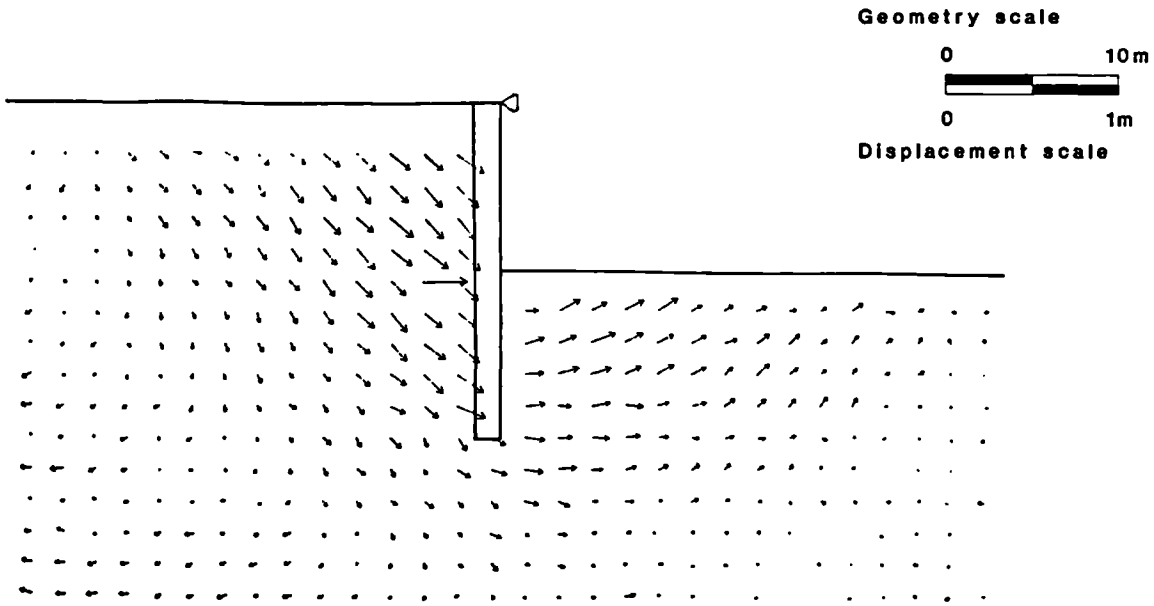

a. Centrifuge test

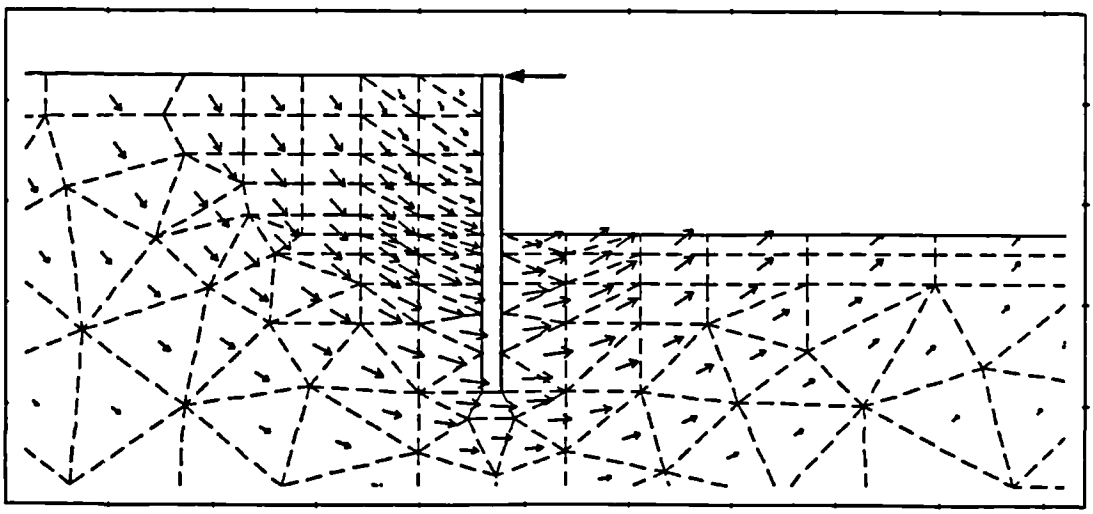

b. Finite element analysis

Fig. 3.14 Comparison of soil movements during excavation for wall of 10m embedment

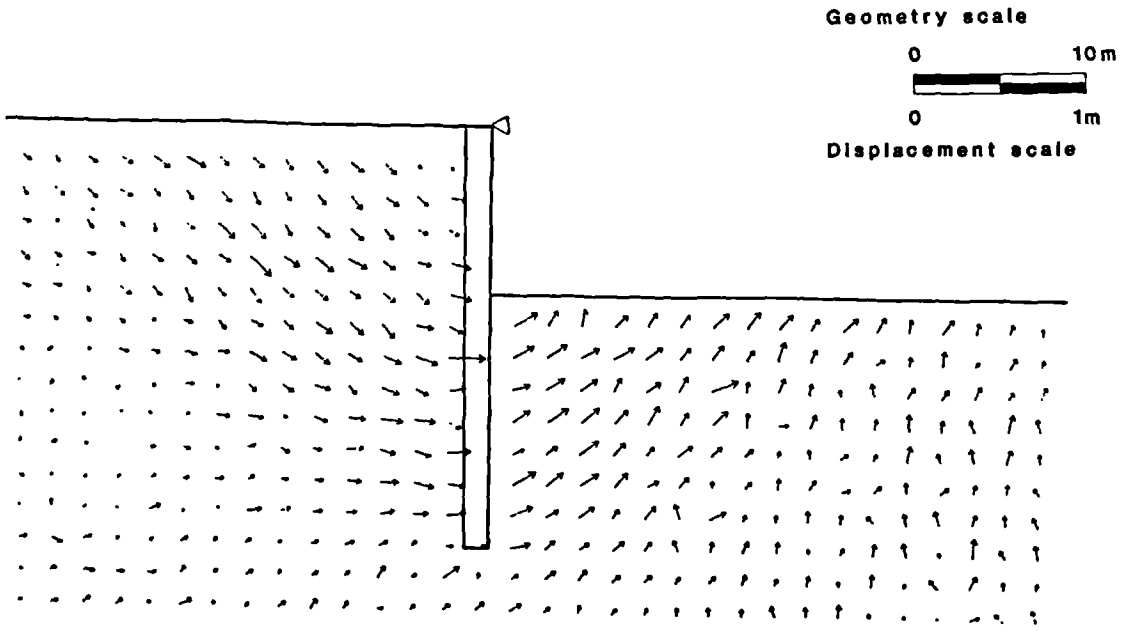

a. Centrifuge test

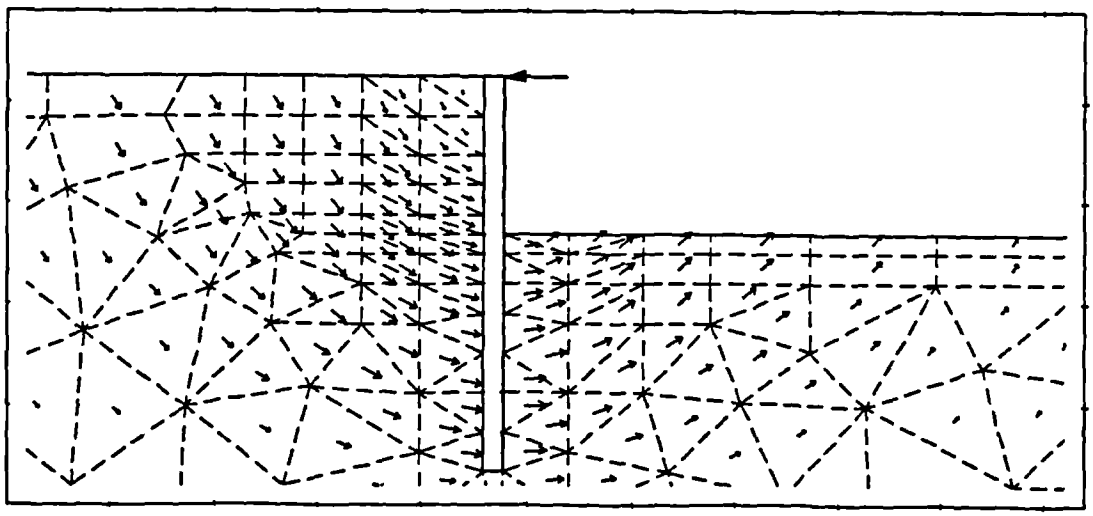

b. Finite element analysis

Fig. 3.15 Comparison of soil movements during excavation for wall of 15m embedment

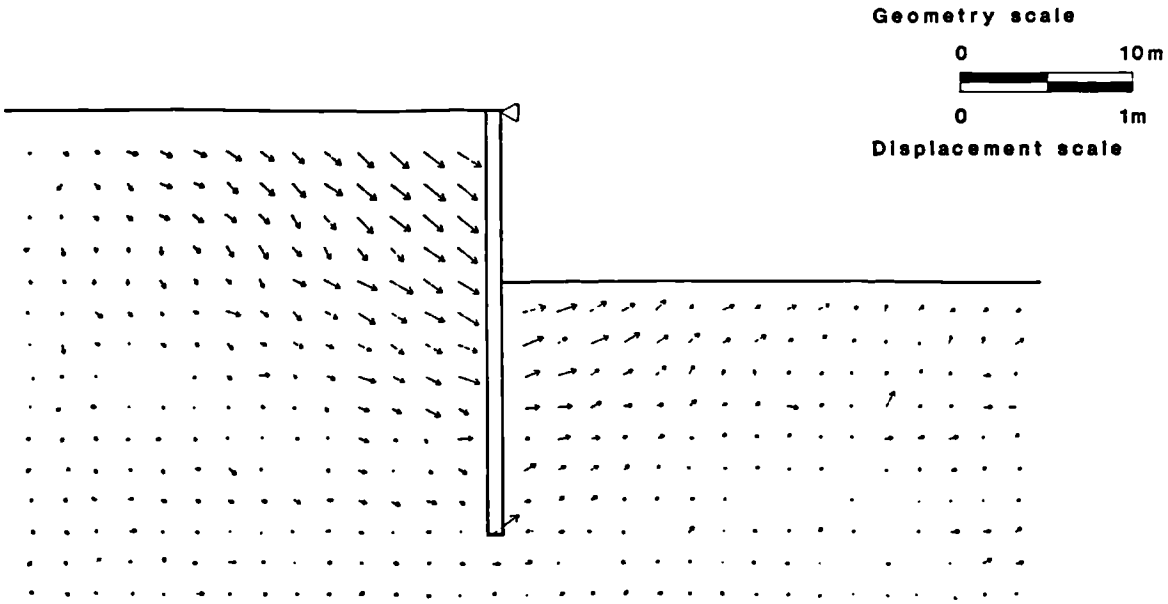

a. Centrifuge test

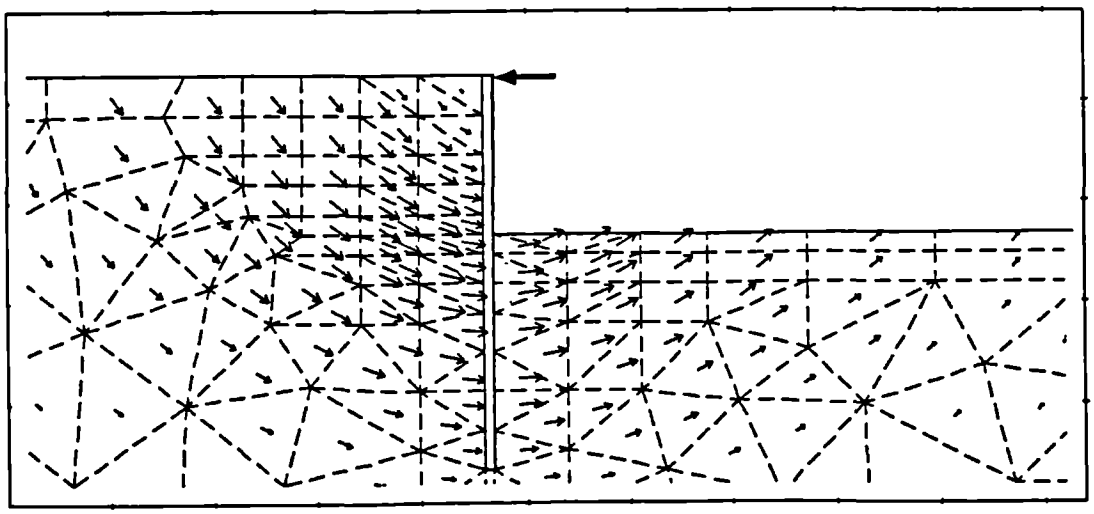

b. Finite element analysis

Fig. 3.16 Comparison of soil movements during excavation for more flexible wall of 15m embedment

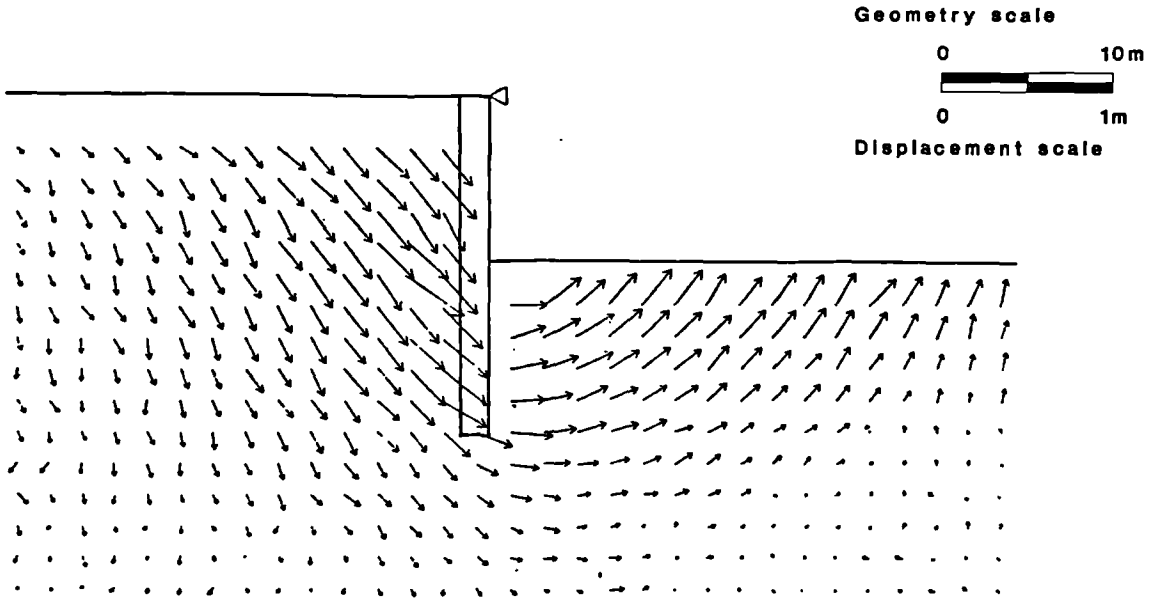

a. Centrifuge test

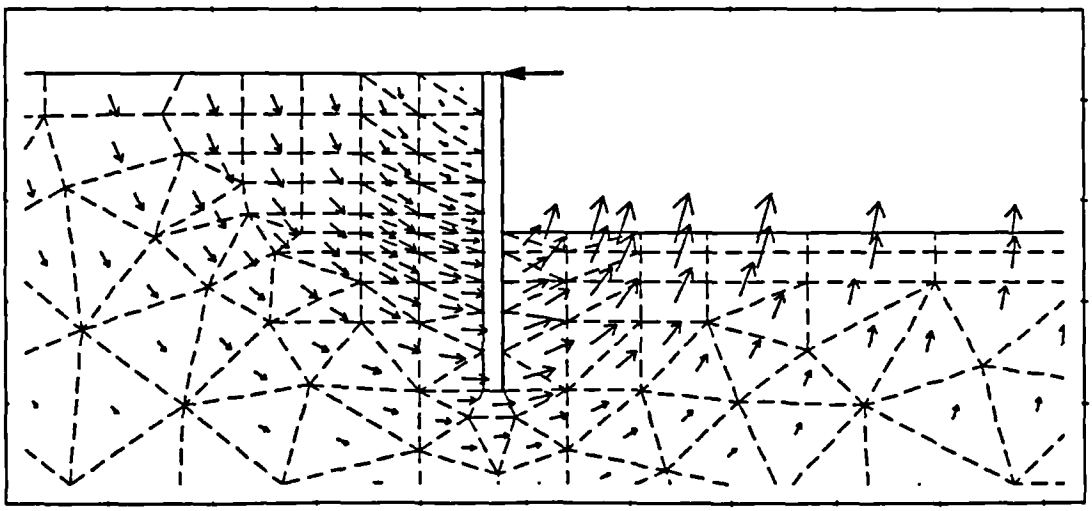

b. Finite element analysis

Fig. 3.17 Comparison of post-excavation soil movements for wall of 10m embedment

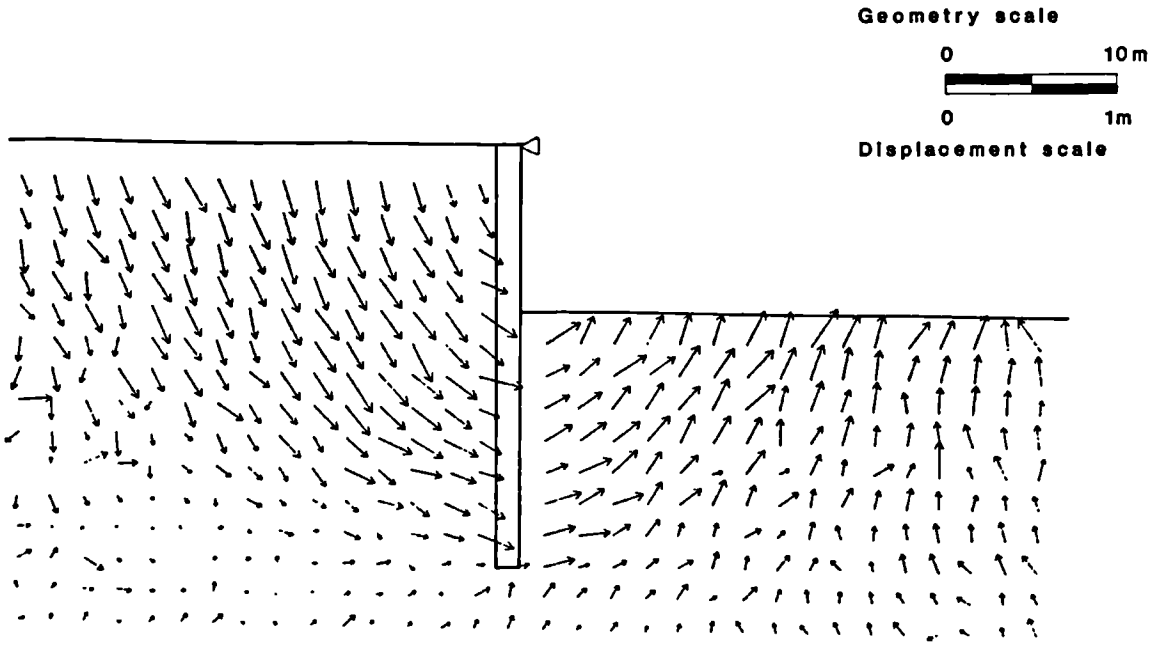

a. Centrifuge test

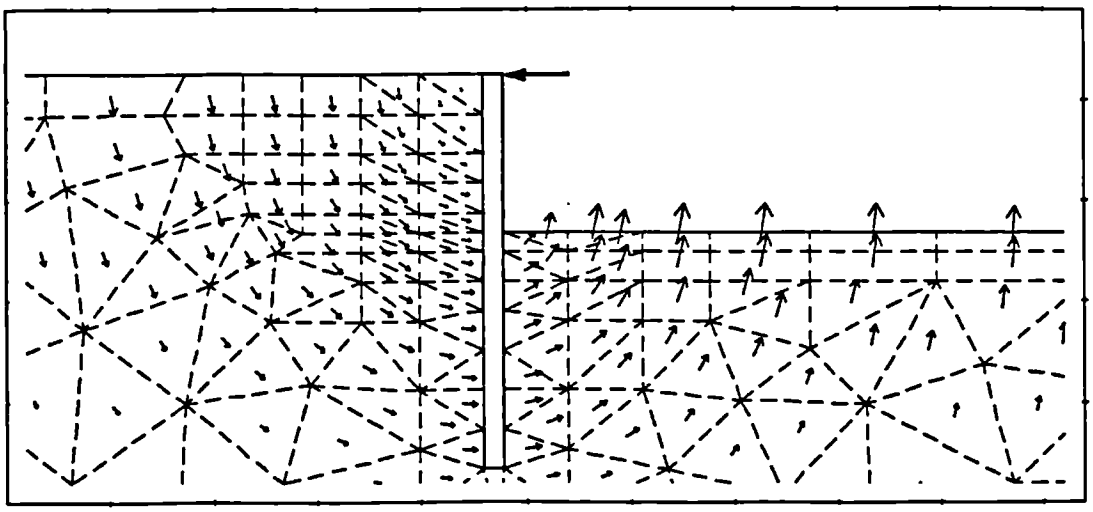

b. Finite element analysis

Fig. 3.18 Comparison of post-excavation soil movements for wall of 15m embedment

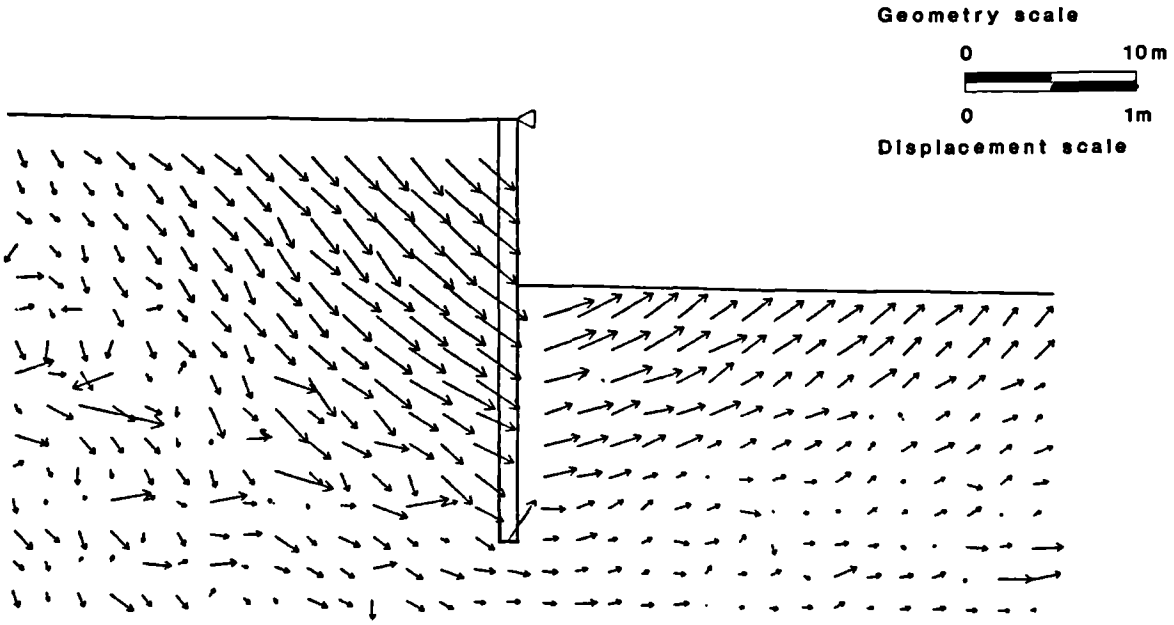

a. Centrifuge test

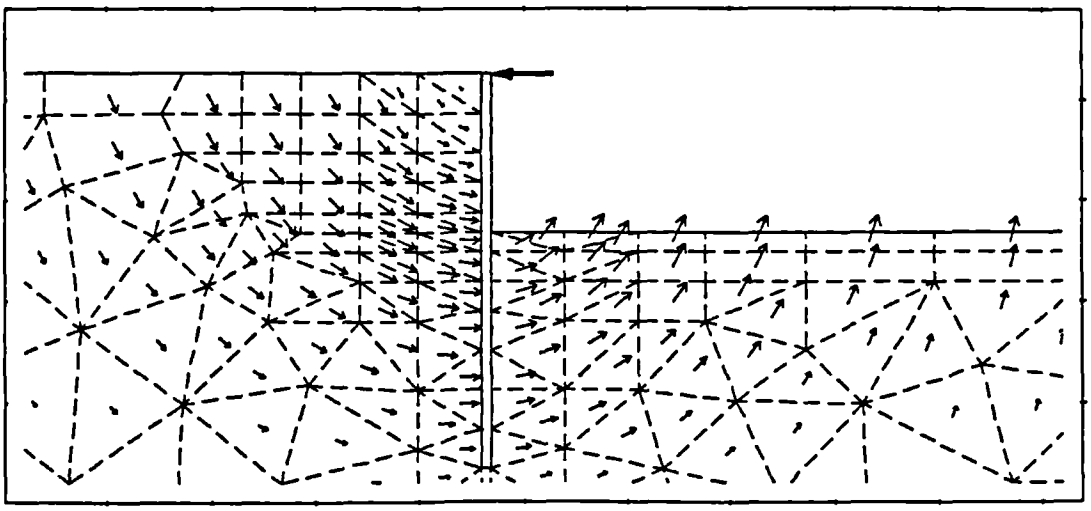

b. Finite element analysis

Fig. 3.19 Comparison of post-excavation soil movements for more flexible wall of 15m embedment

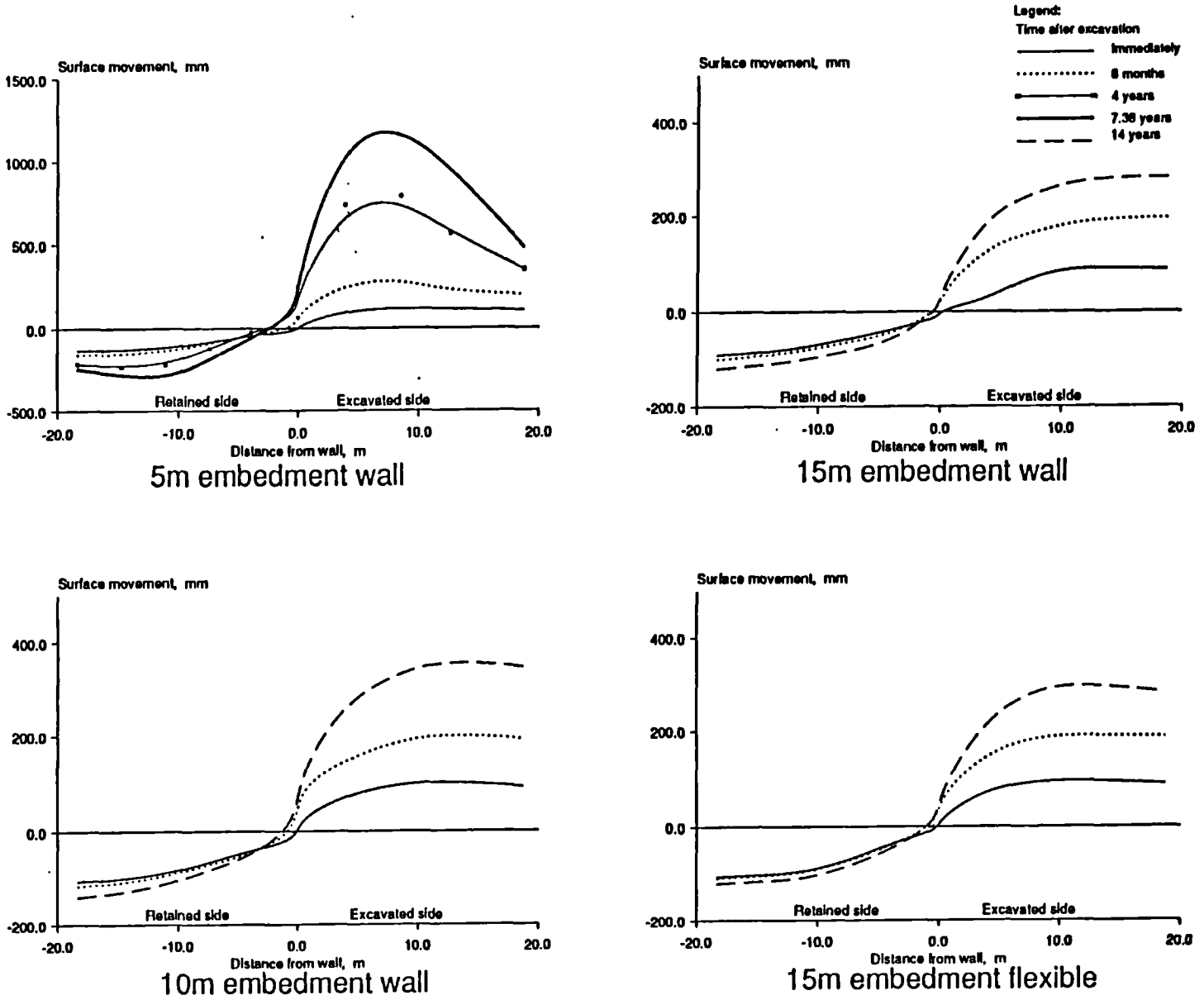

Fig. 3.20 Vertical movement profiles at ground surface for walls propped at the crest

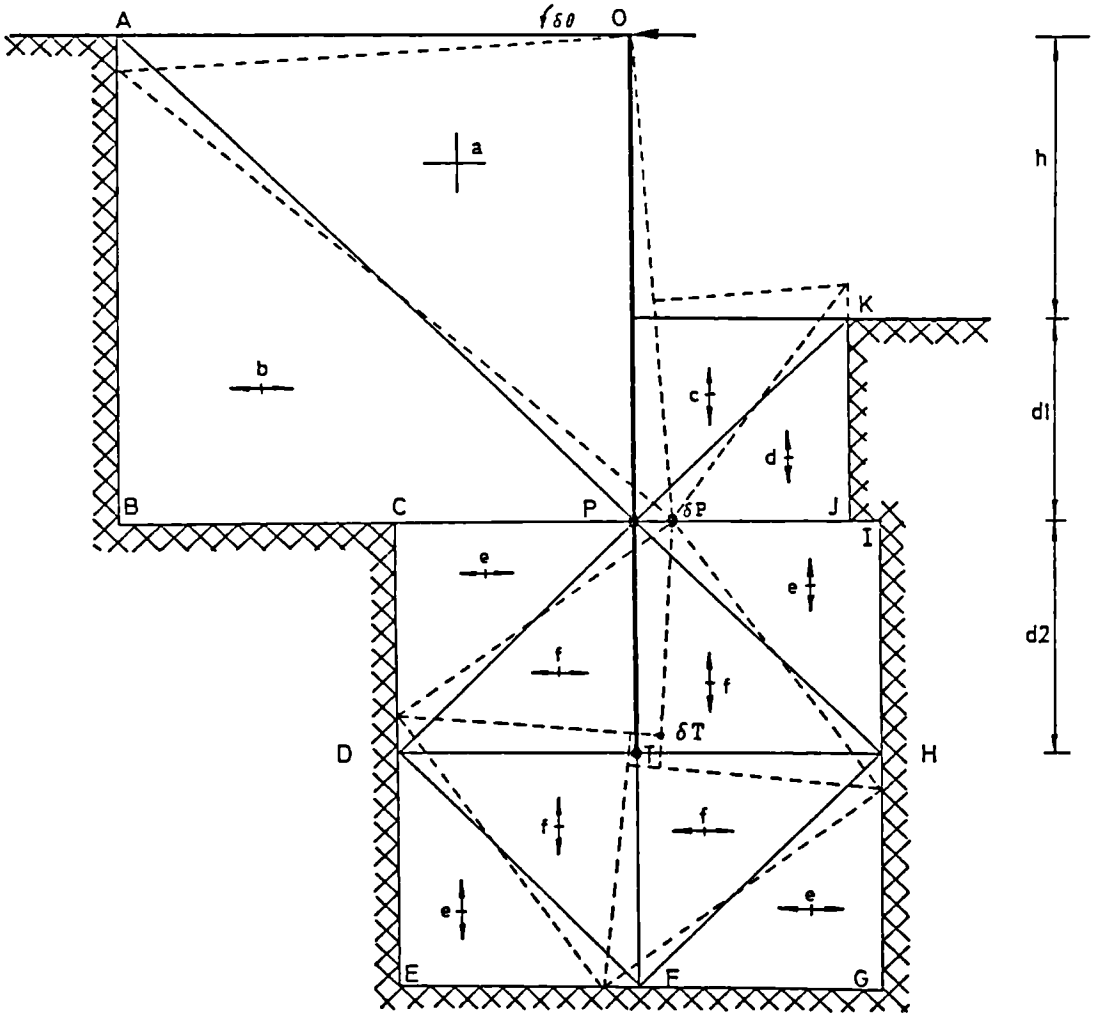

δT = deflection at toe, T
δP = deflection at hinge, P

a = 0
b = $\delta\theta$
c = h $\delta\theta$ / d1
d = (h+d1) $\delta\theta$ / d1
e = (h+d1) $\delta\theta$ / d2
f = (2(h+d1) $\delta\theta$ − δT) / d2

Convention:
Compressive
Tensile

Fig. 3.21 Admissible strain field for flexible wall propped at the crest

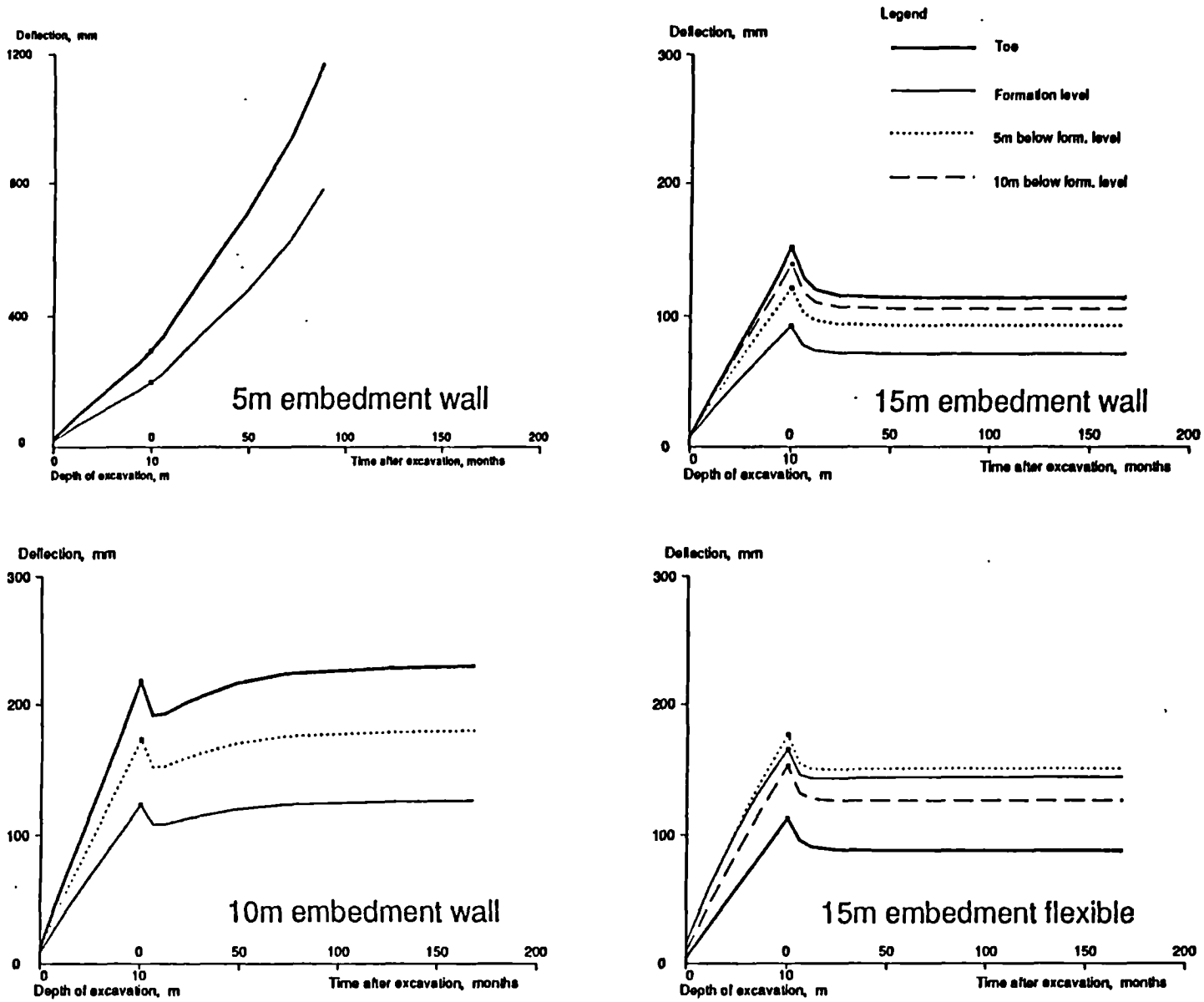

Fig. 3.22 Wall movements against excavation and time for walls propped at the crest

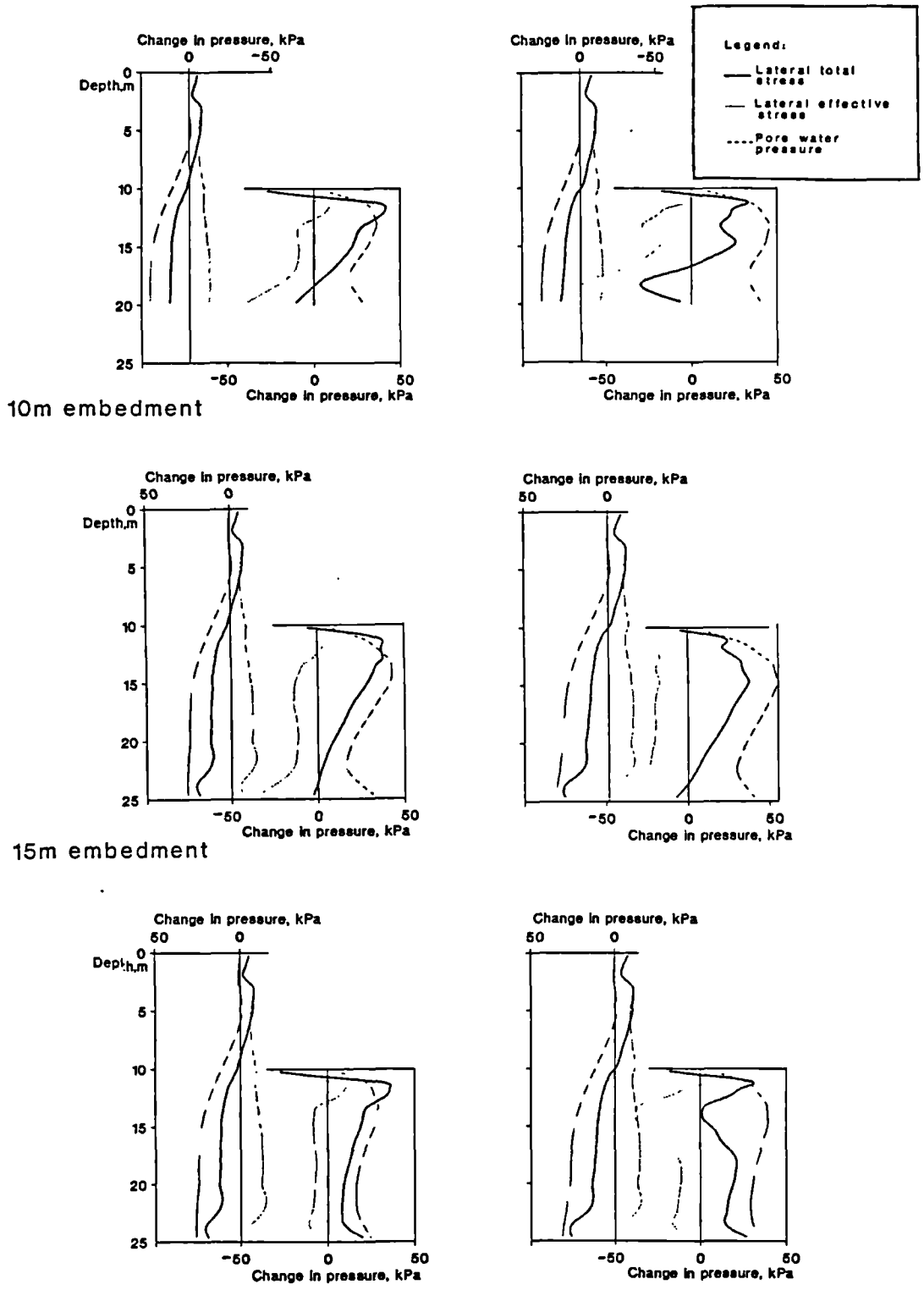

Fig. 3.23 Post-excavation changes in lateral stresses and pore water pressures

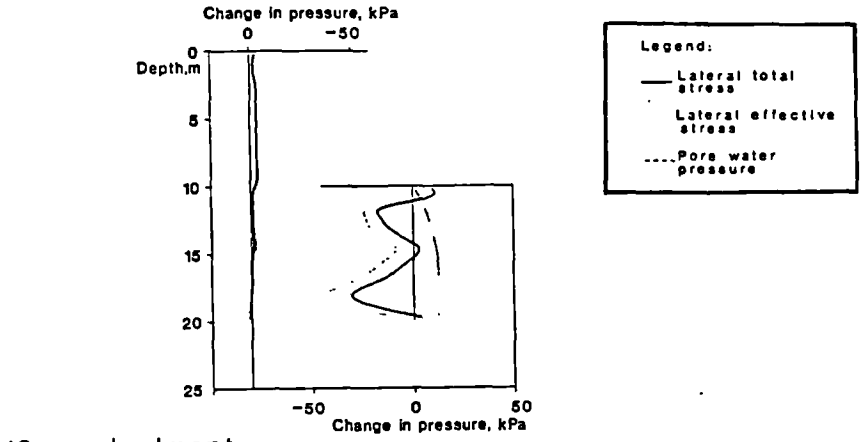

10m embedment

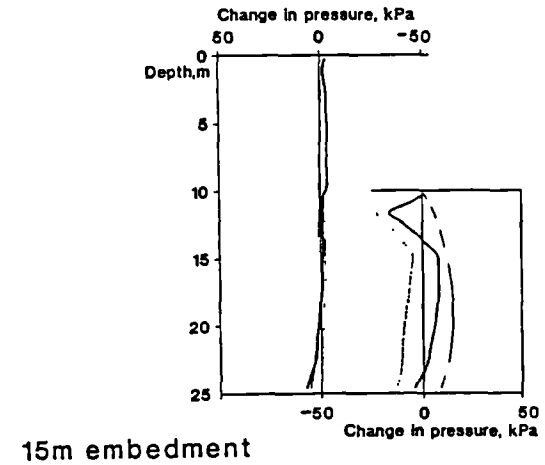

15m embedment

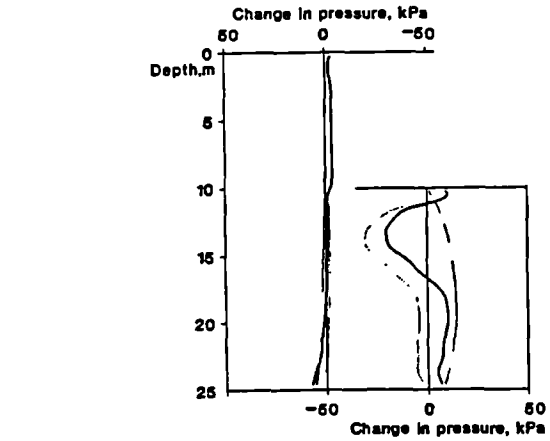

15m embedment flexible

Fig. 3.24 Changes in lateral stresses and pore water pressures from 6 months to 14 years after excavation

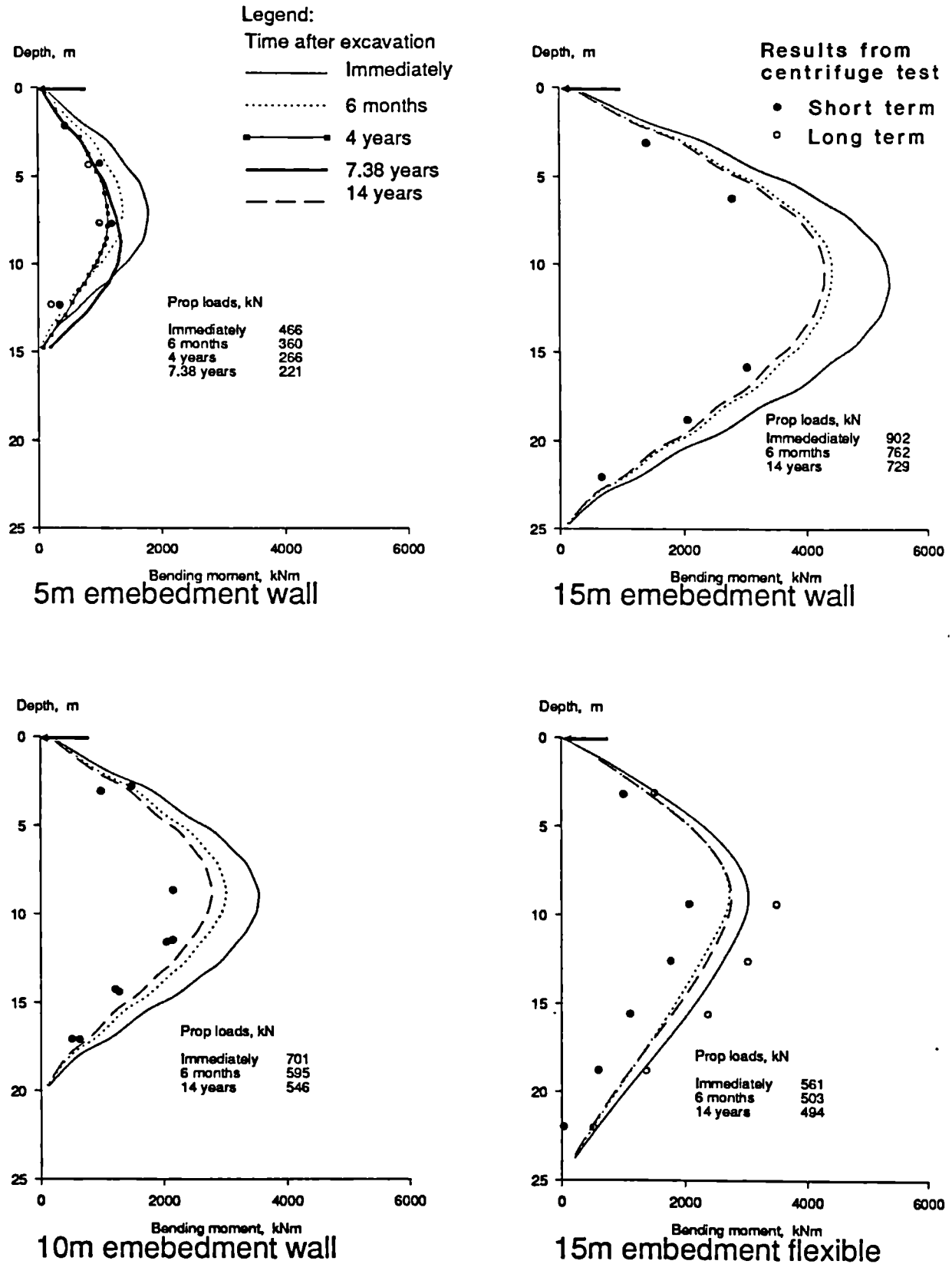

Fig. 3.25 Bending moments and prop loads for walls propped at the crest

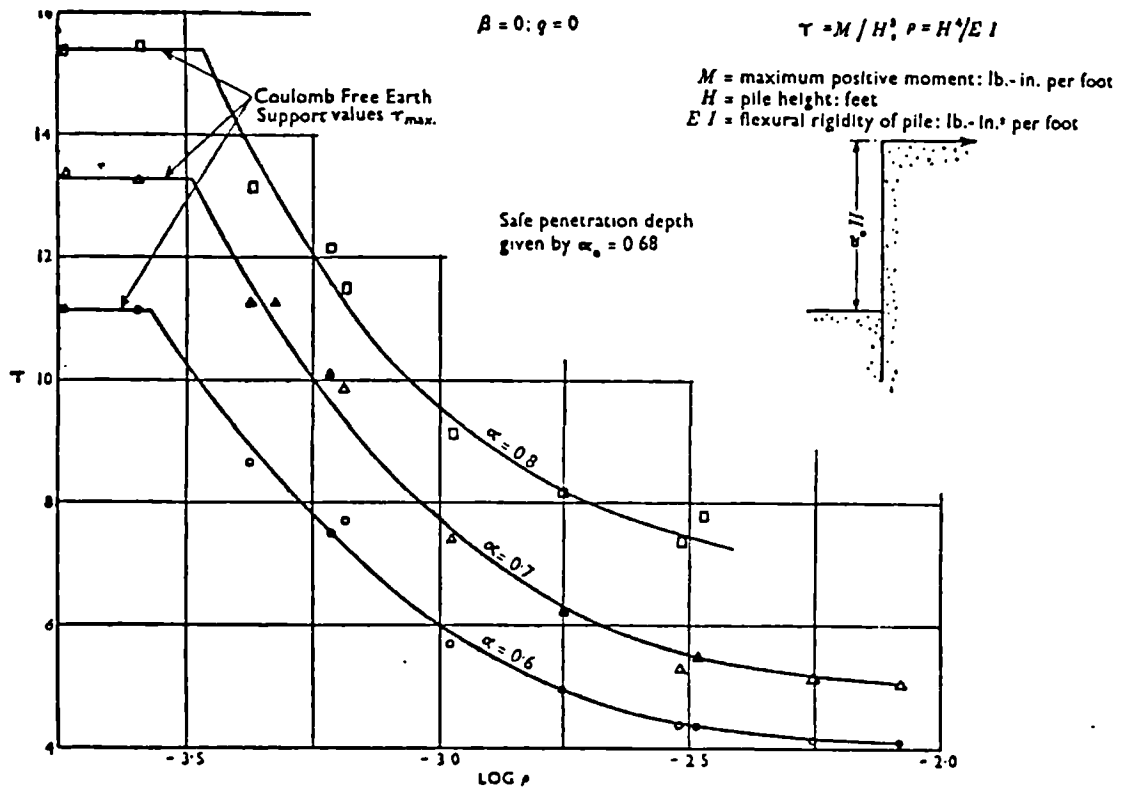

Fig. 3.26 Variation in normalised maximum bending moments against flexibility number (from Rowe, 1952)

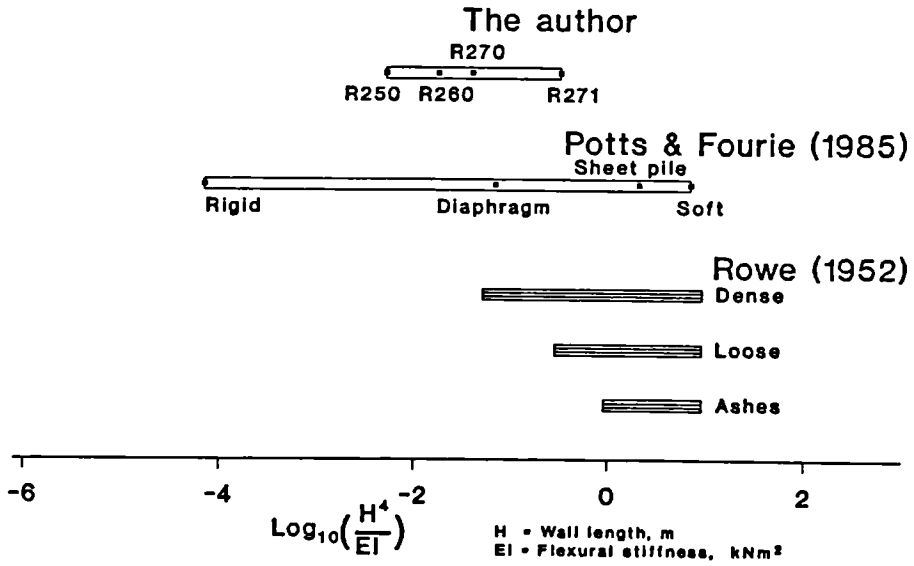

Fig. 3.27 Ranges of flexibility number in various studies

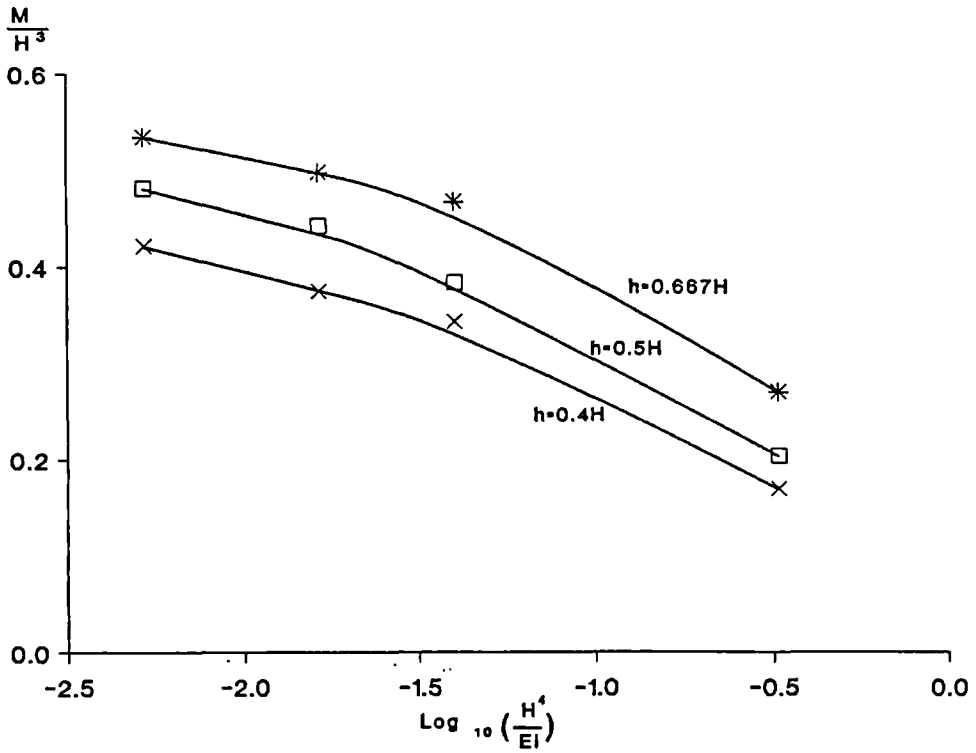

a. Short term

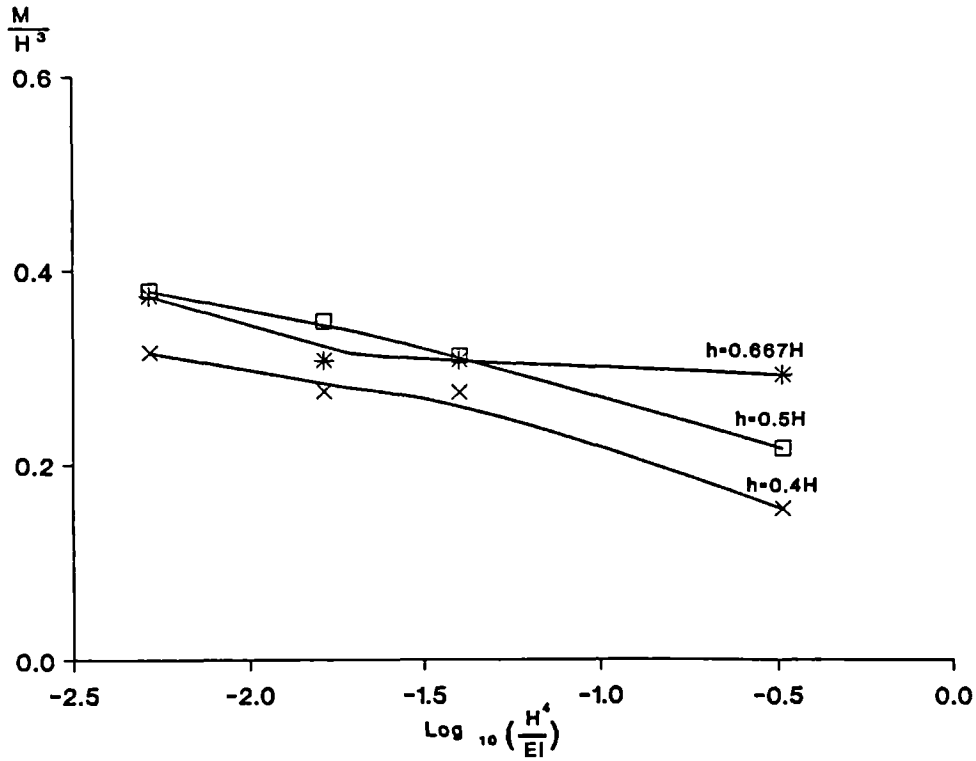

b. Long term

Fig. 3.28 Variation in normalised maximum bending moments against flexibility number from finite element analyses

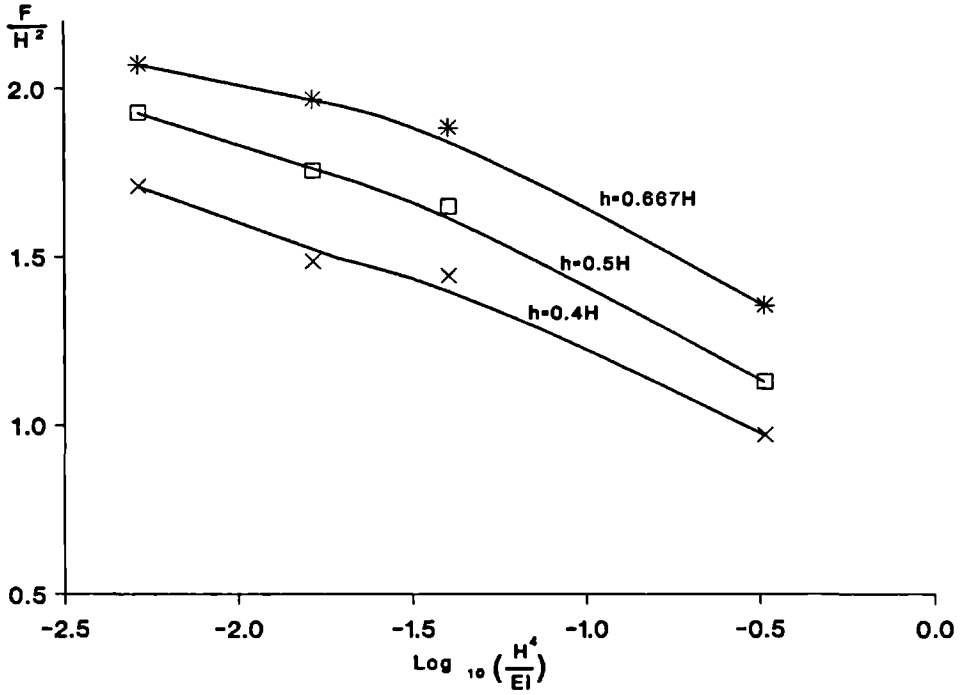

a. Short term

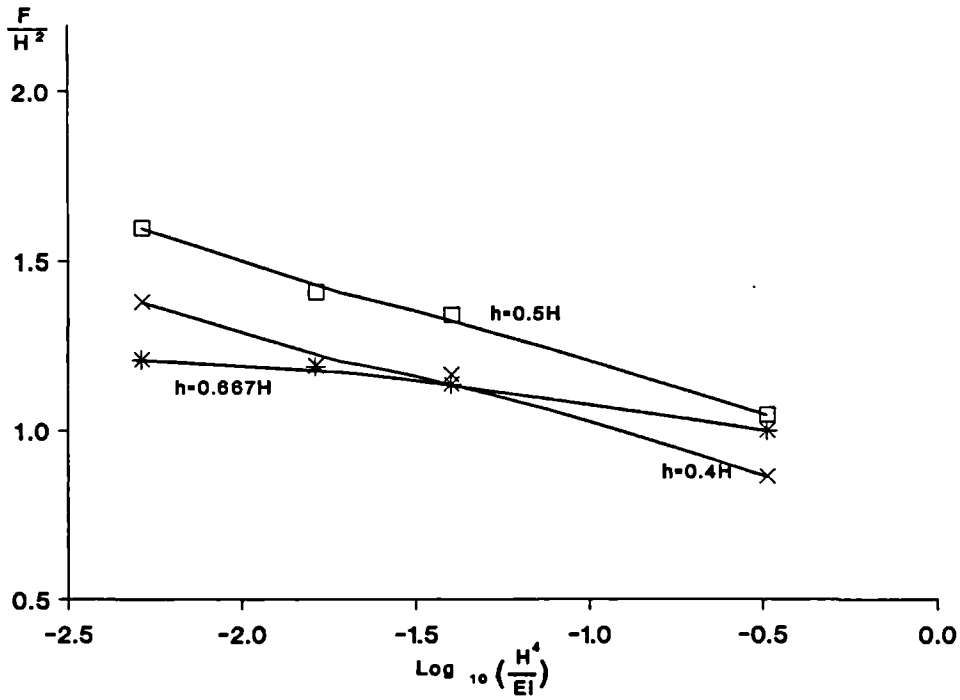

b. Long term

Fig. 3.29 Variation in normalised prop loads against flexibility number from finite element analyses

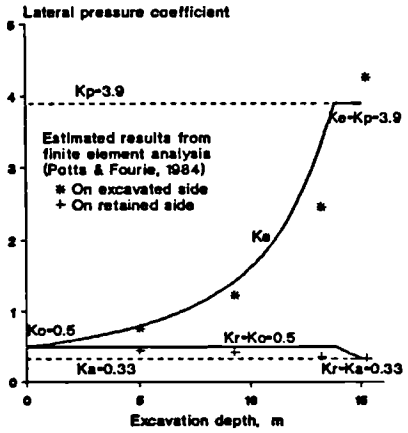

a. Ko=0.5

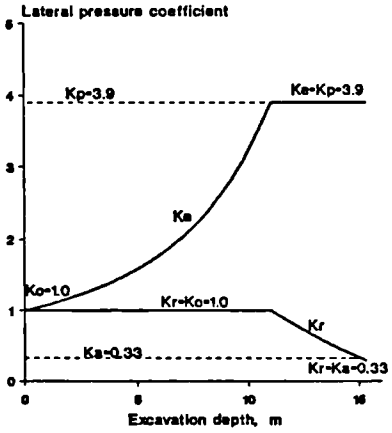

b. Ko=1.0

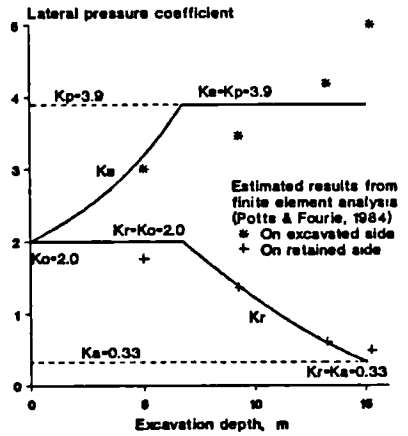

c. Ko=2.0

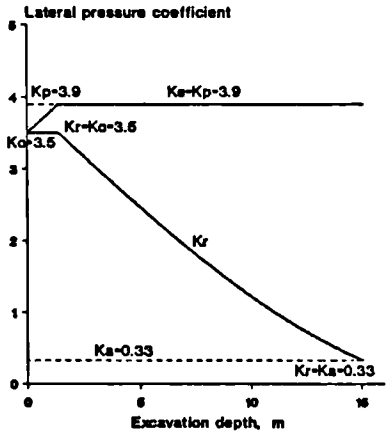

d. Ko=3.5

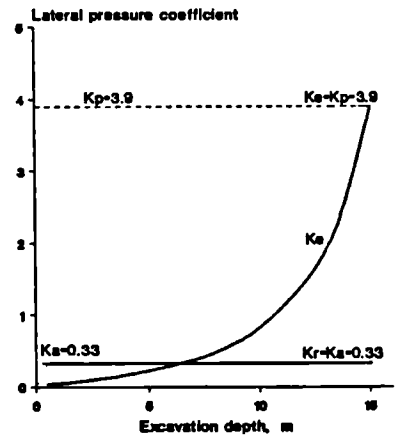

e. Load factor method

Legend:
Lateral pressure coefficients

active	= Ka
passive	= Kp
on retained side	= Kr
on excavated side	= Ke

Fig. 4.1 Mobilised lateral earth pressure coefficients against depth of excavation

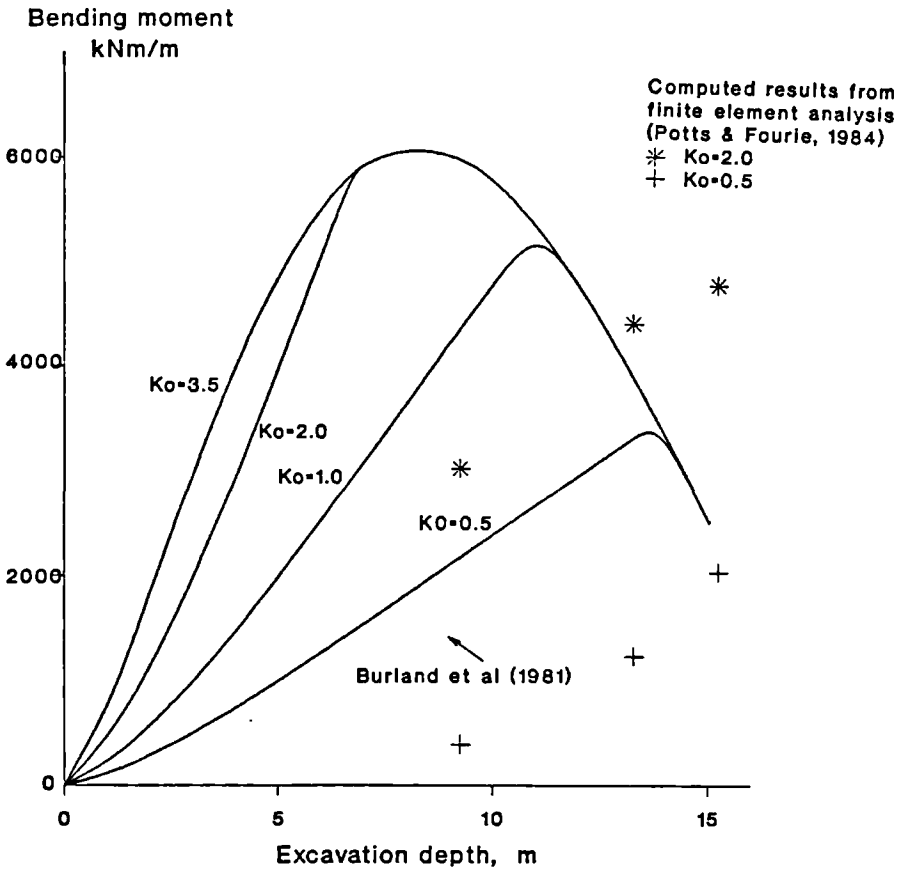

Fig. 4.2 Calculated maximum bending moments using factored limit equilibrium approach

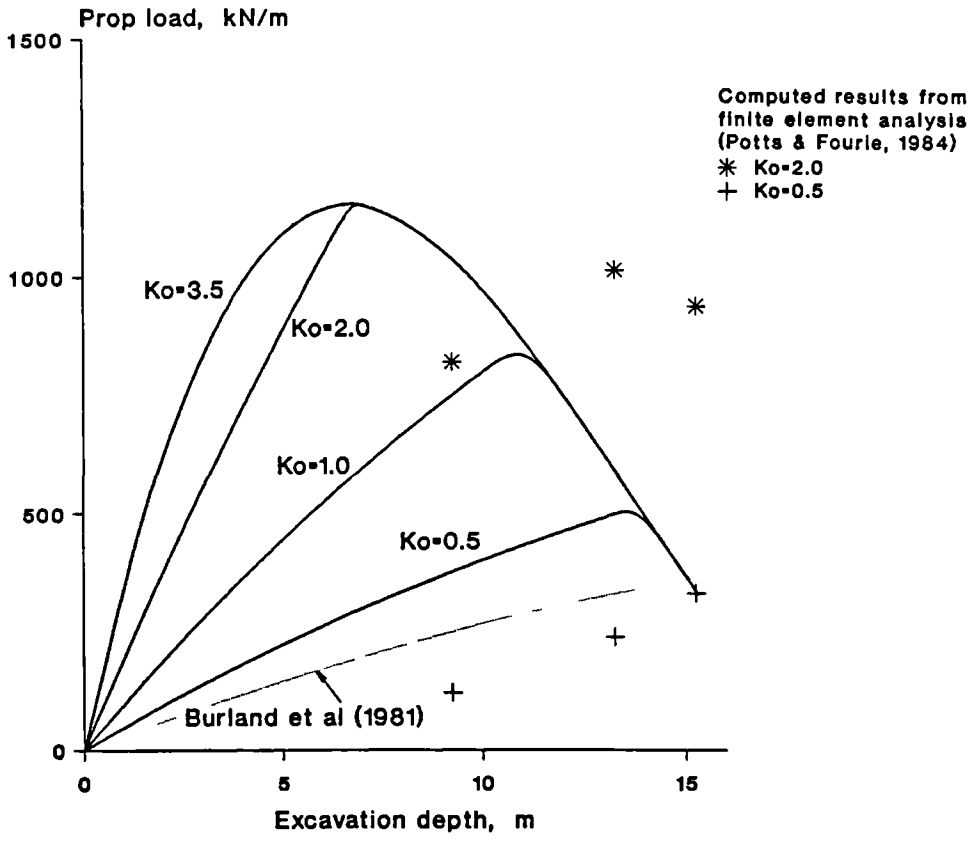

Fig. 4.3 Calculated prop loads using factored limit equilibrium approach

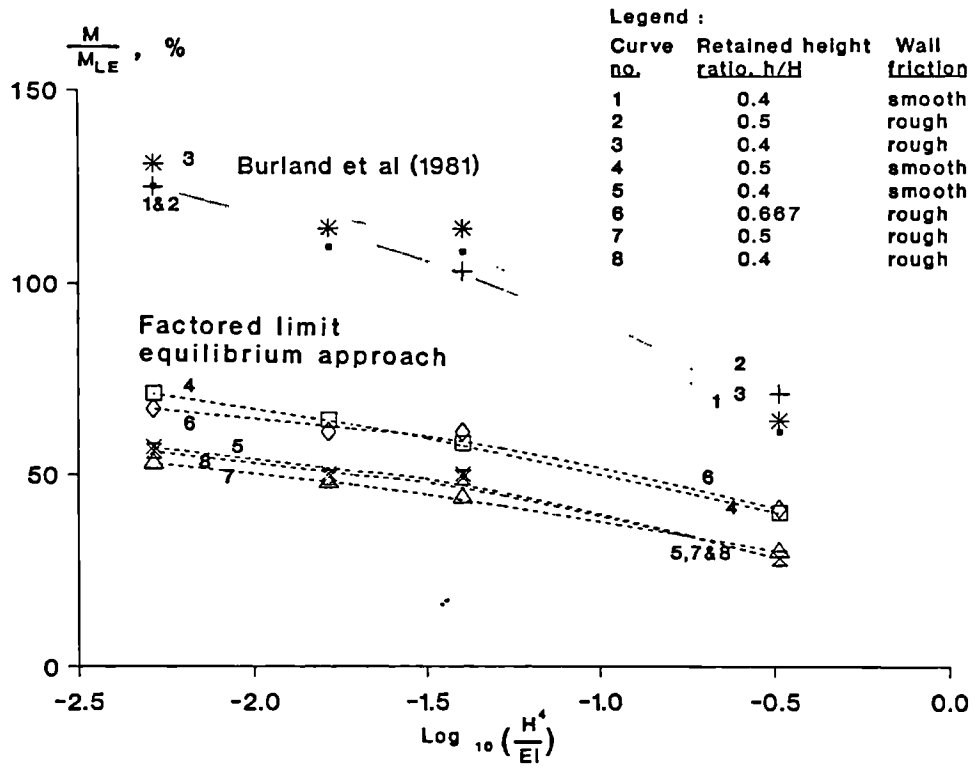

Fig. 4.4 Variation in computed maximum bending moments as a percentage of the values calculated from limit equilibrium-based methods

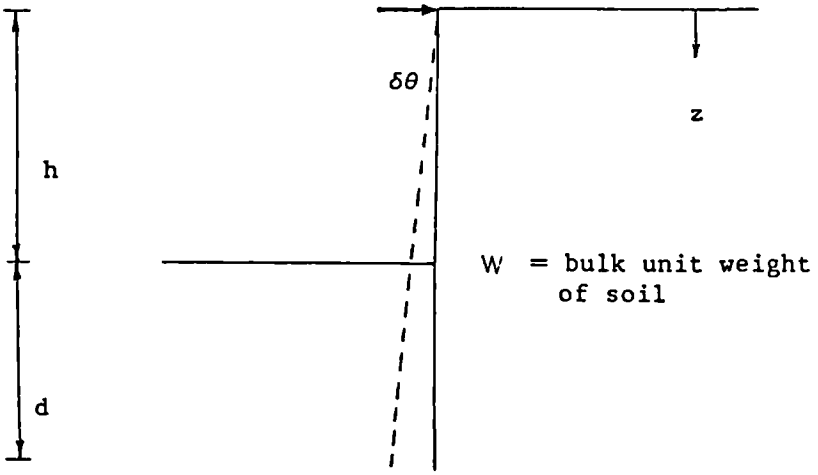

Fig. 4.5 Idealised wall movement during excavation

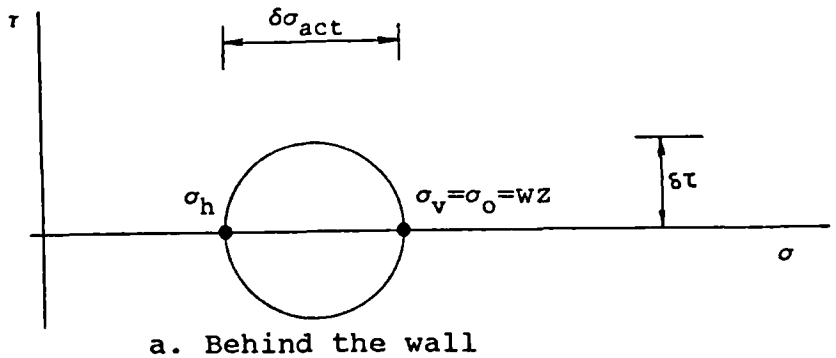

a. Behind the wall

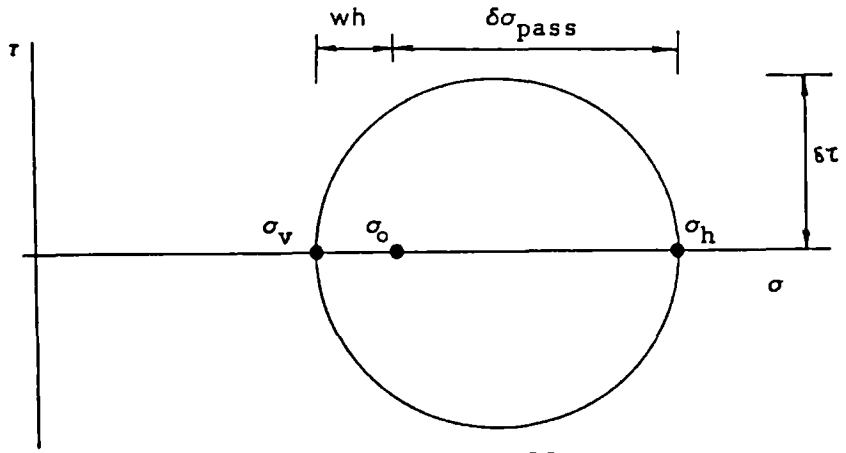

b. In front of the wall

Fig. 4.6 Mohr's circle representation of stresses

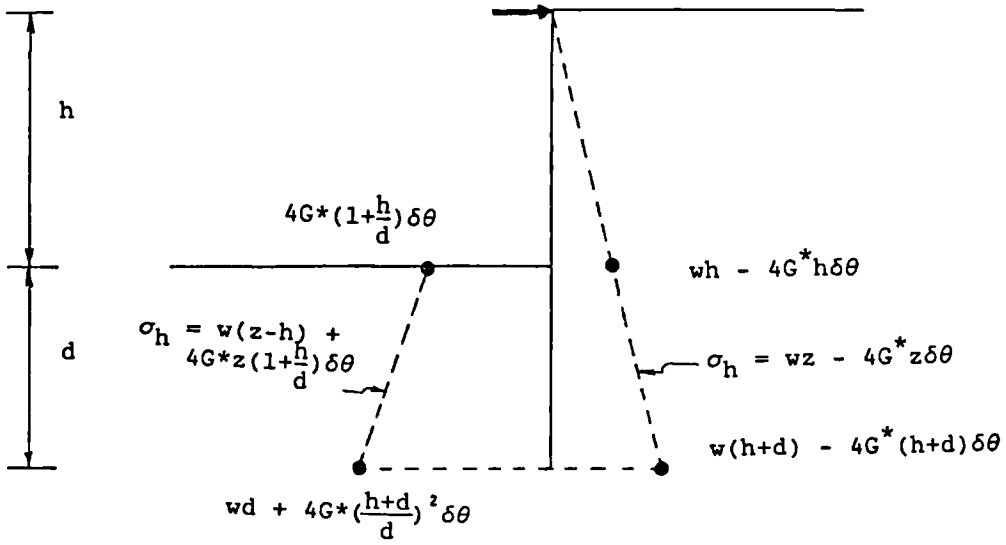

Fig. 4.7 Lateral stress distribution

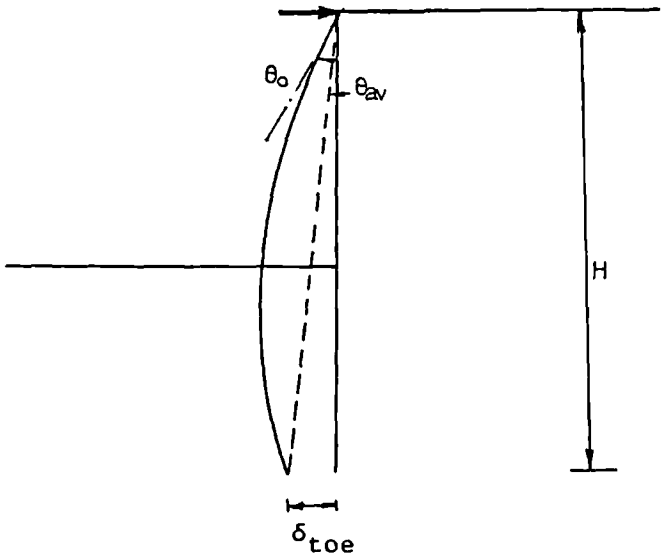

Fig. 4.8 Definition of average rotation in mobilised strength method

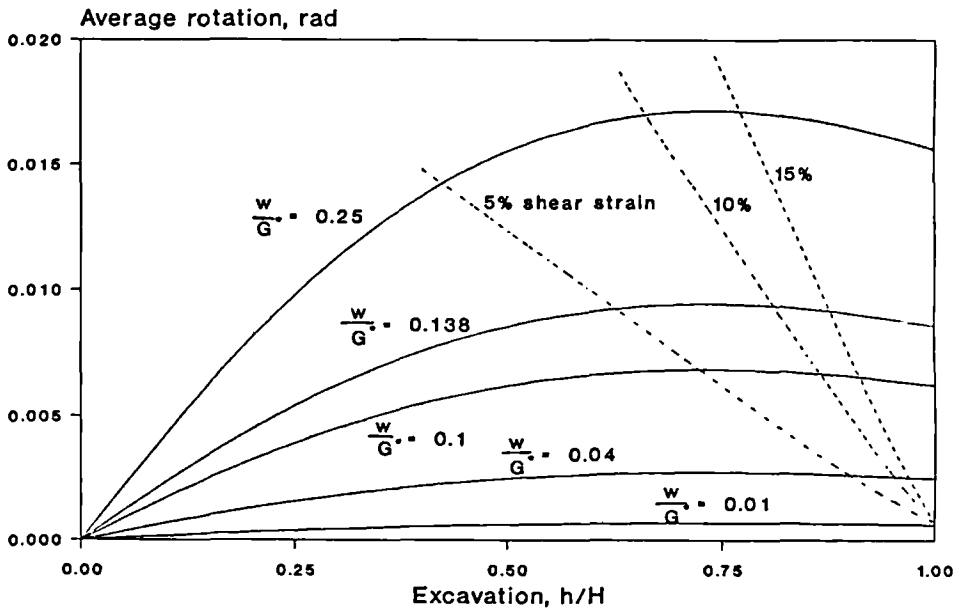

Fig. 4.9 Average wall rotation against excavation

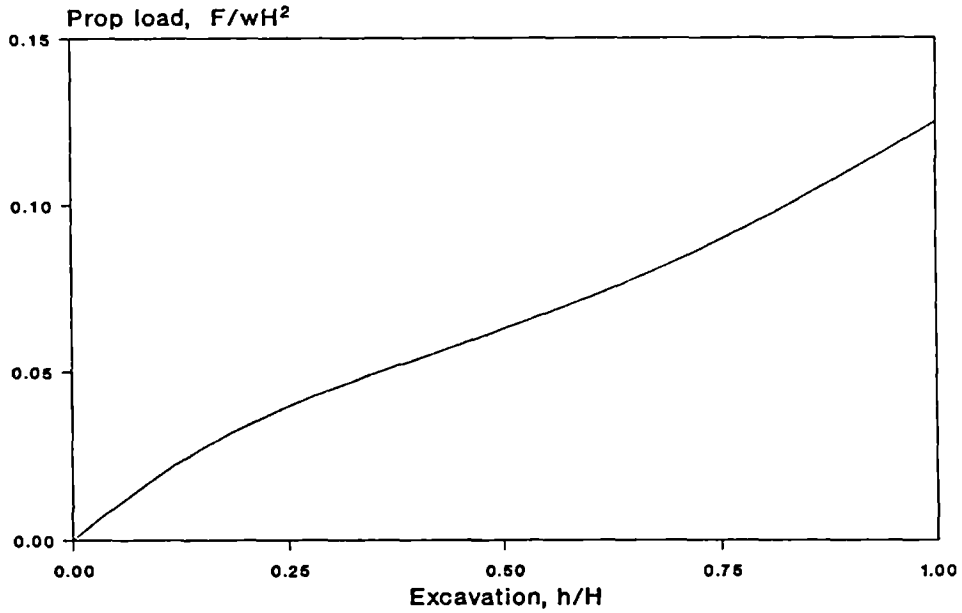

Fig. 4.10 Prop load against excavation

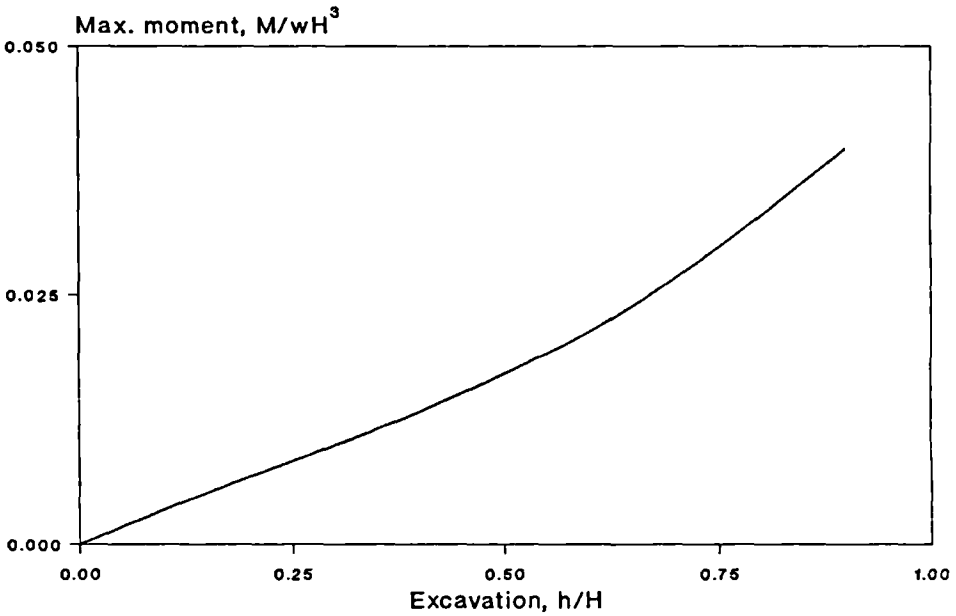

Fig. 4.11 Maximum bending moment against excavation

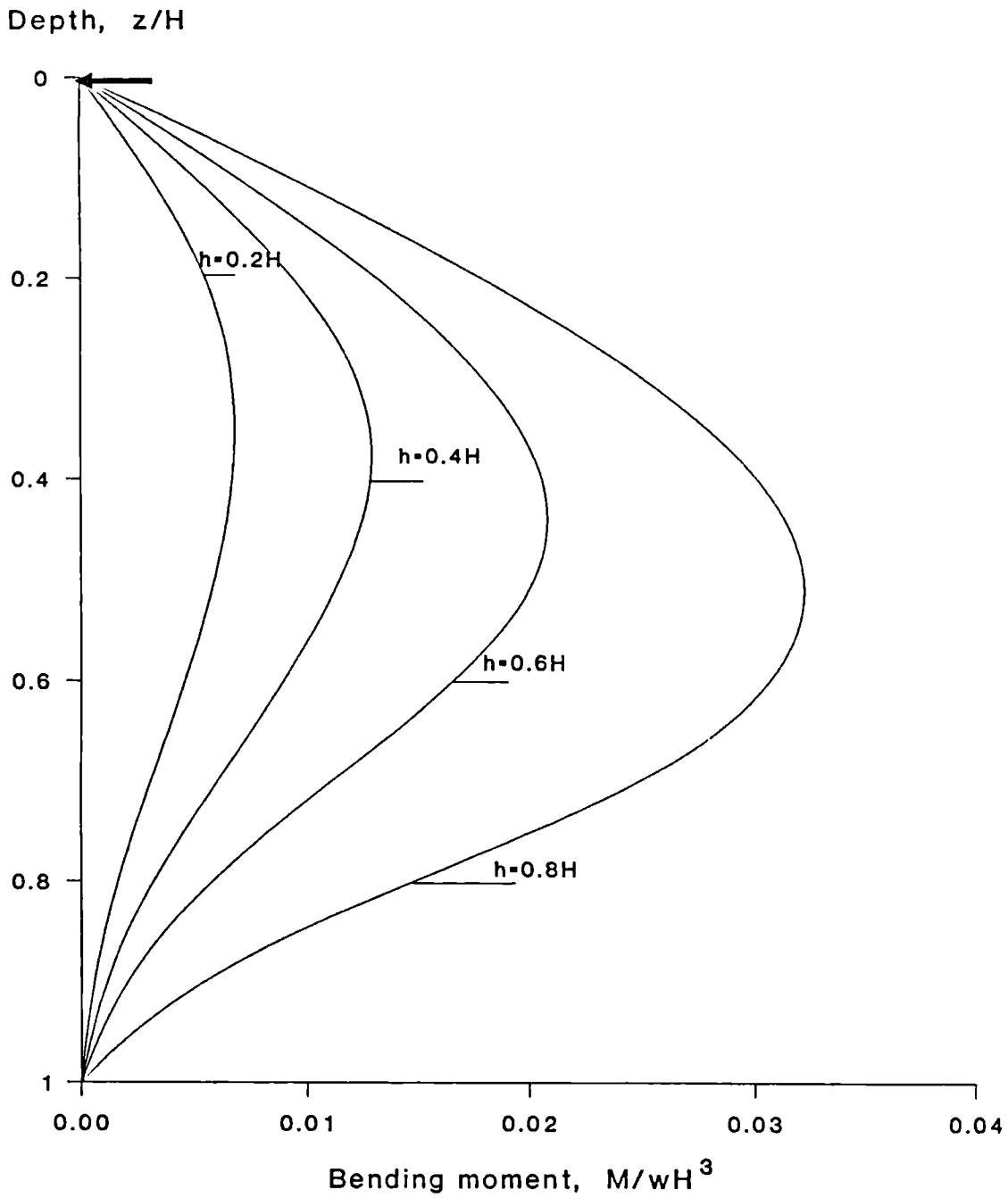

Fig. 4.12 Bending moment diagram for the mobilised strength method

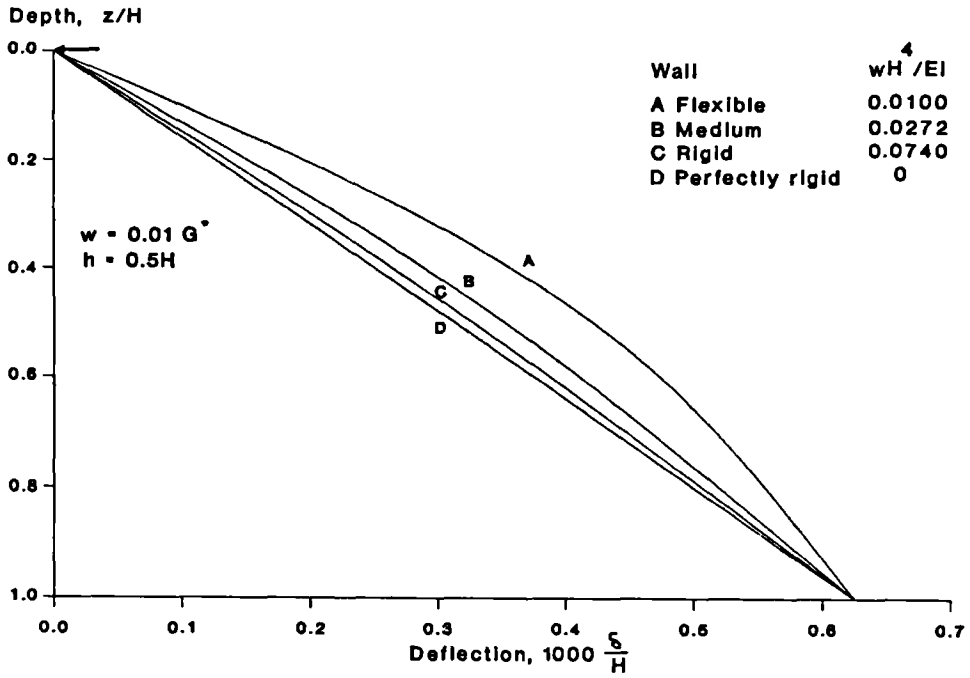

Fig. 4.13 Wall deflections for walls of different flexibility

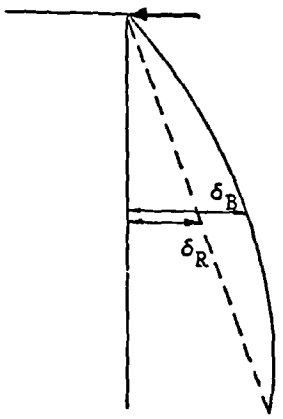

Bending factor

$$\beta = \frac{(\delta_B - \delta_R)_{max}}{\delta_R} \times 100\%$$

Fig. 4.14 Definition of bending factor

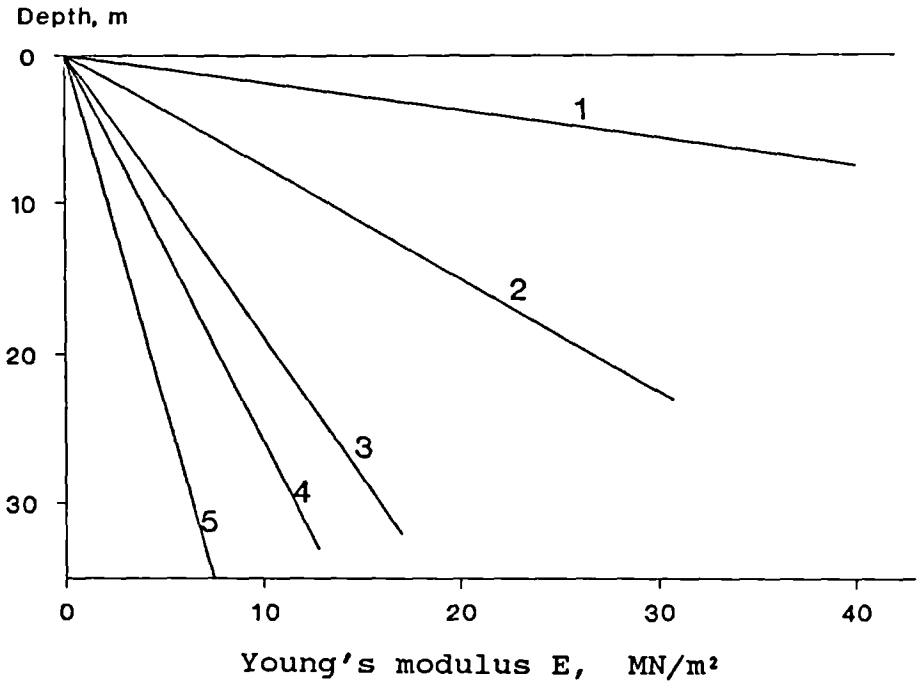

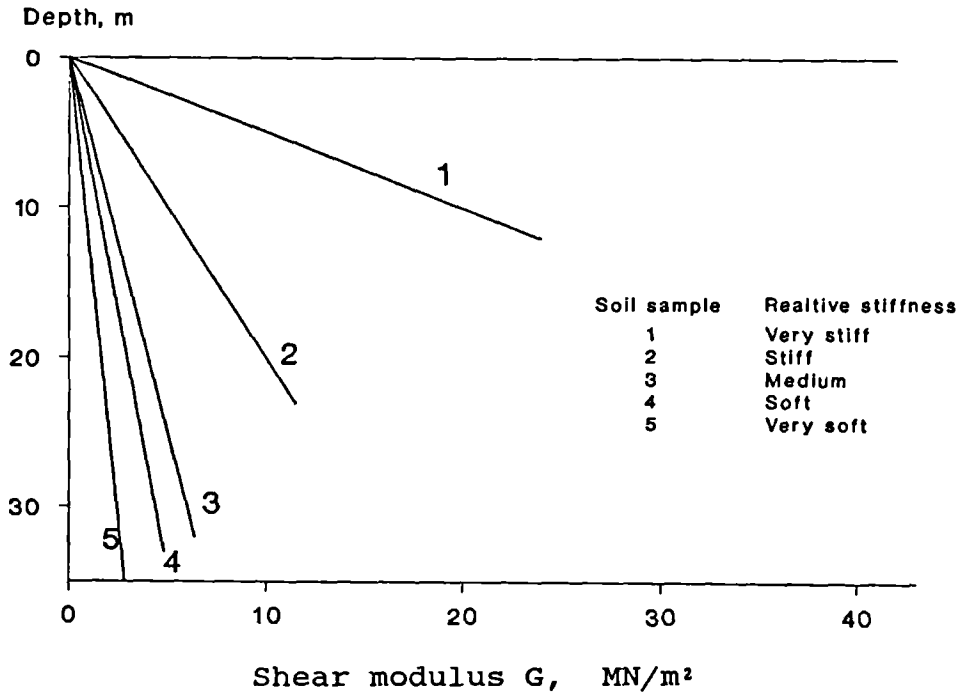

Fig. 4.15 Different soil stiffness considered in the mobilised strength method

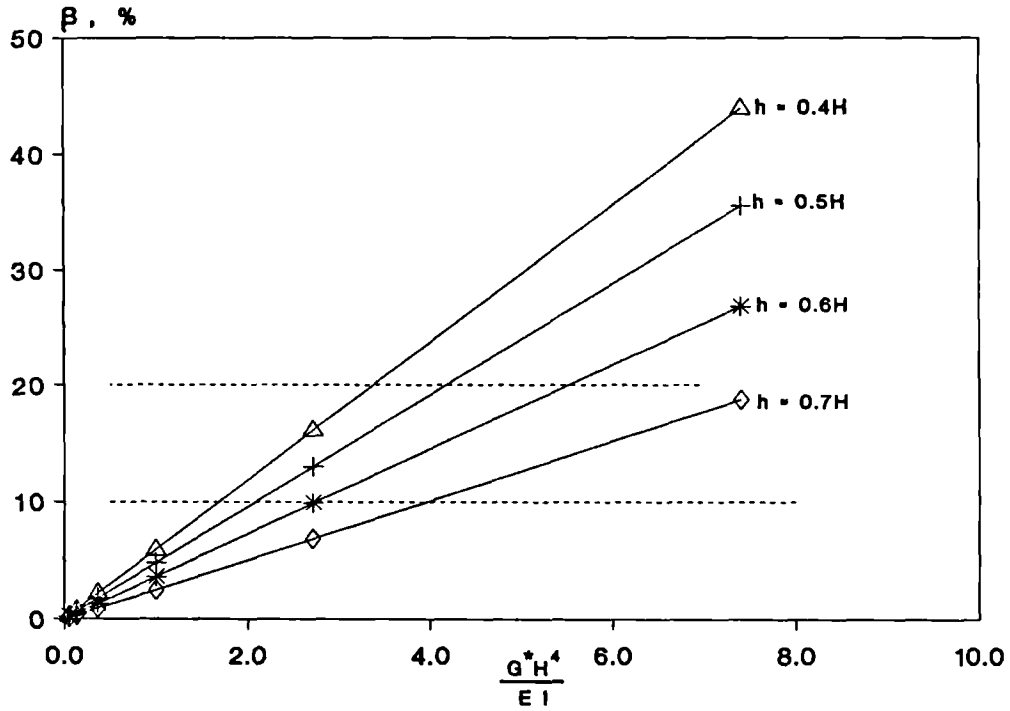

Fig. 4.16 Bending factor against flexibility ratio

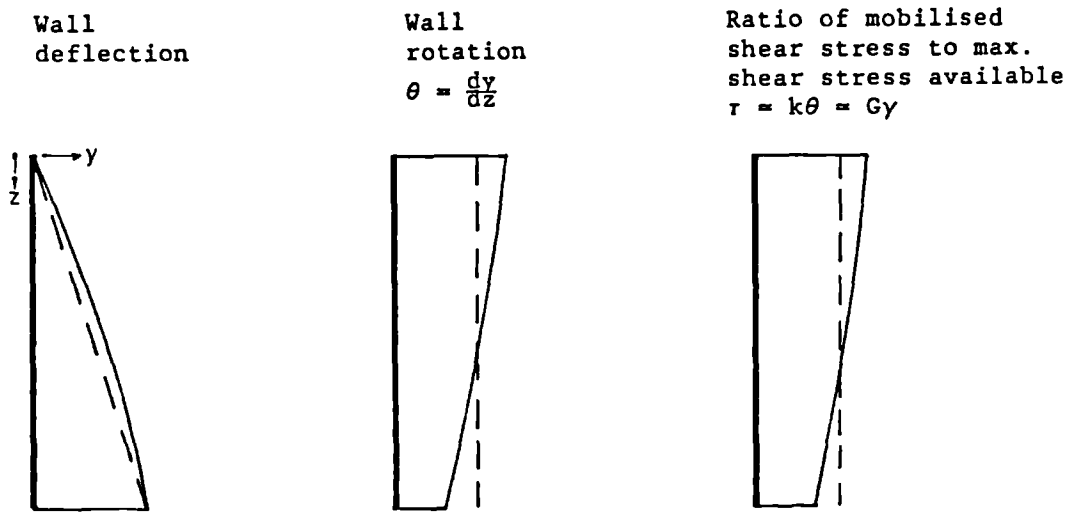

a. Rigid wall

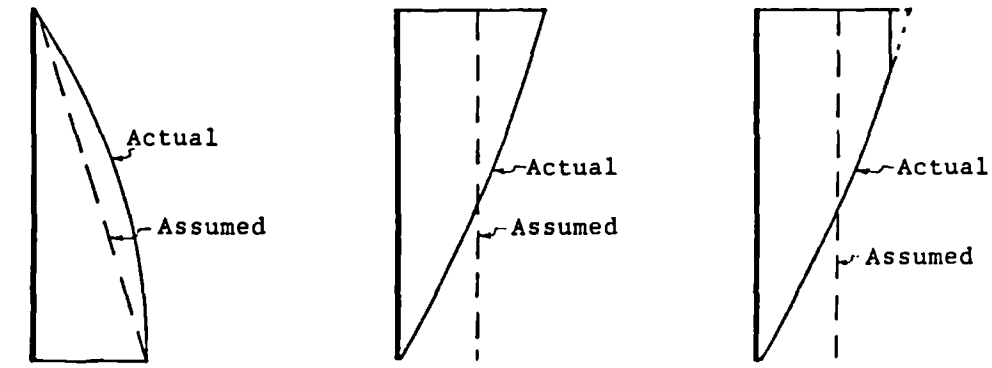

b. Medium rigid wall

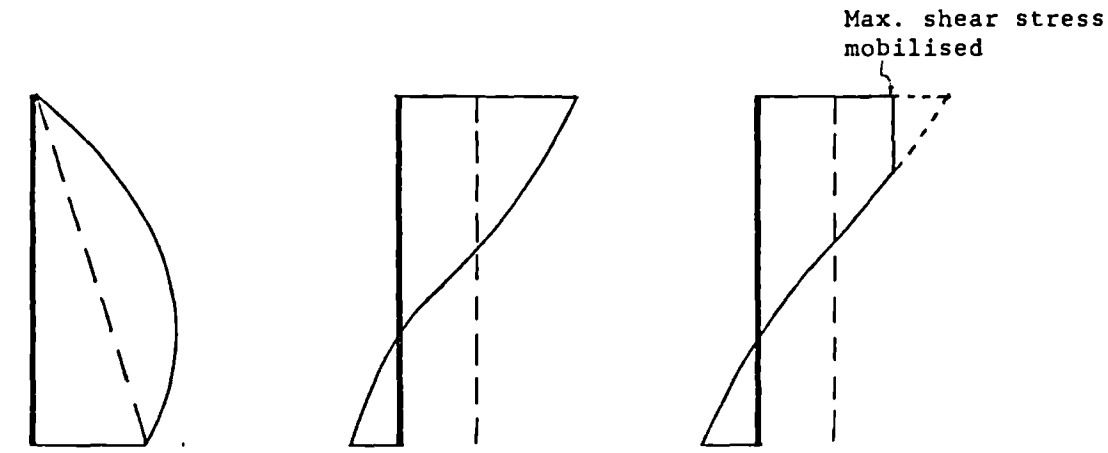

c. Flexible wall

Fig. 4.17 Implications of different categories of diaphragm wall

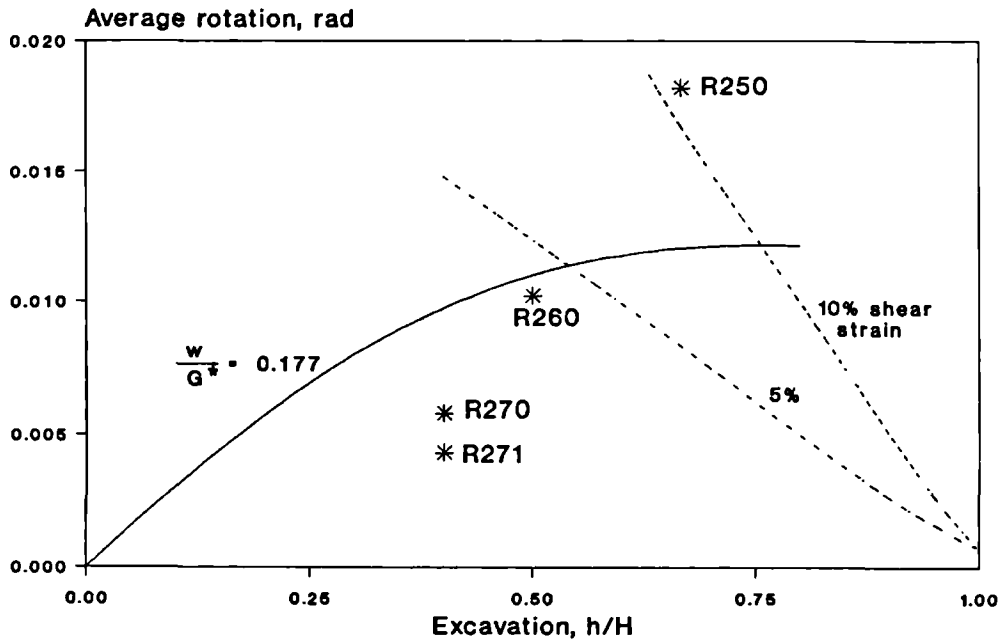

Fig. 4.18 Average wall rotation from finite element analyses against excavation

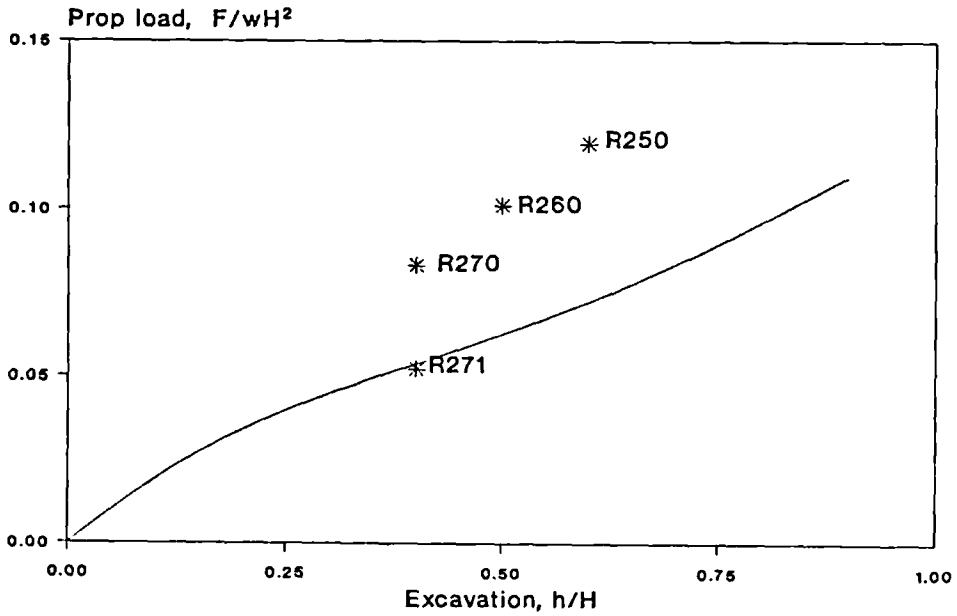

Fig. 4.19 Normalised prop loads from finite element analyses against excavation

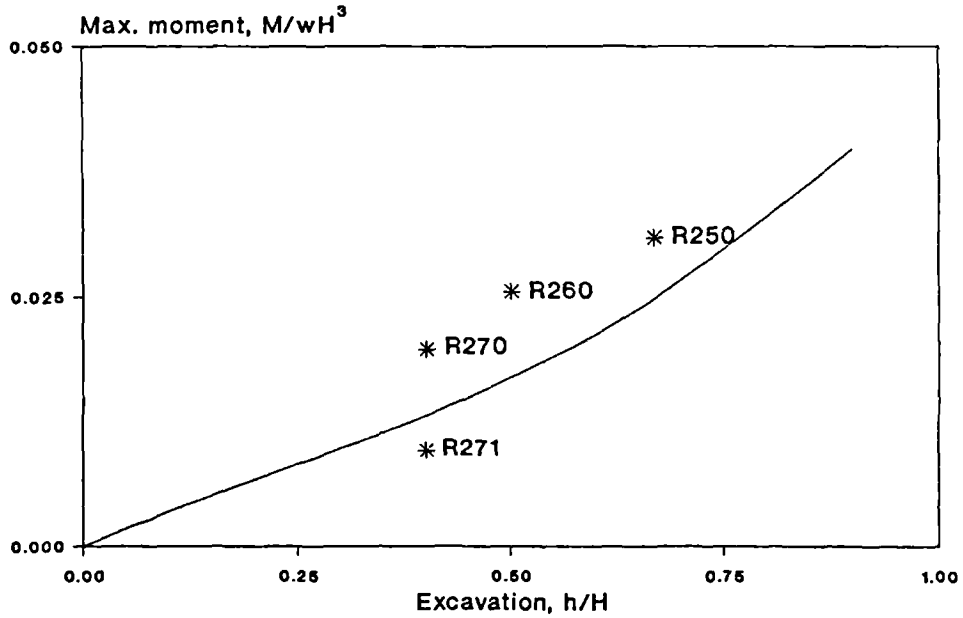

Fig. 4.20 Normalised maximum bending moments from finite element analyses against excavation

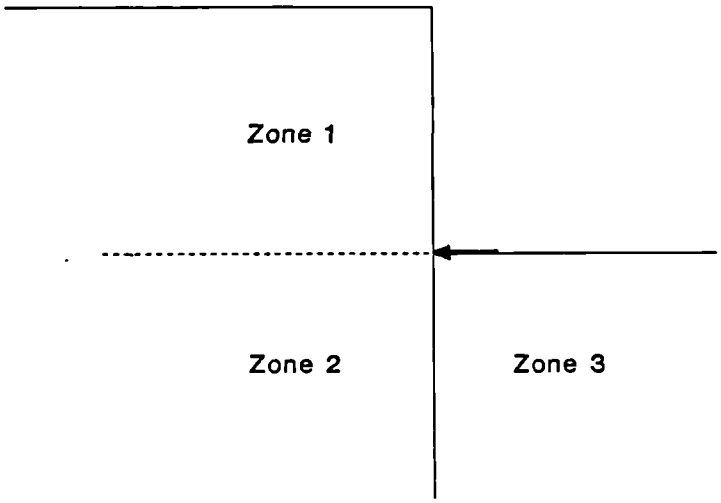

Fig. 5.1 Idealised zones of soil adjacent to a wall propped at dredge level

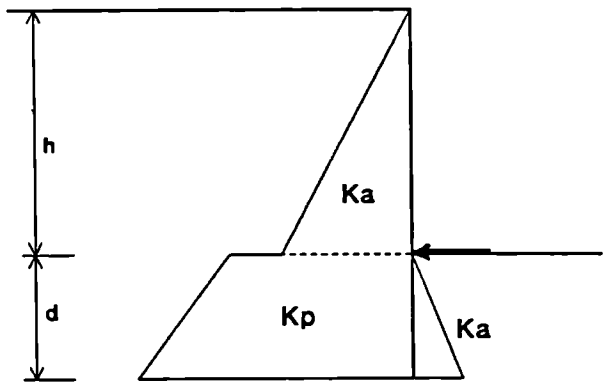

Fig. 5.2 Limiting soil stress distribution for a wall propped at dredge level of shallow embedment

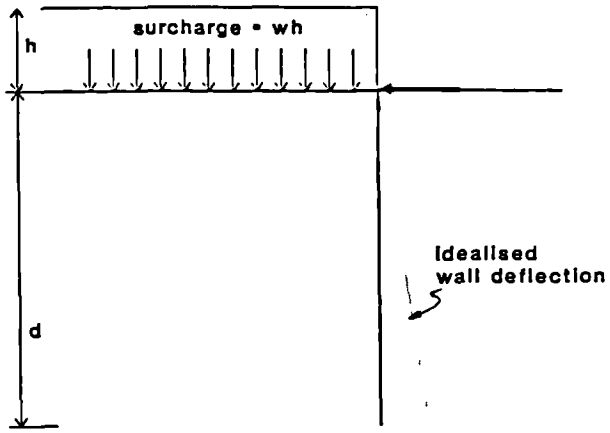

Fig. 5.3 Schematic representation for a wall propped at dredge level of deep embedment

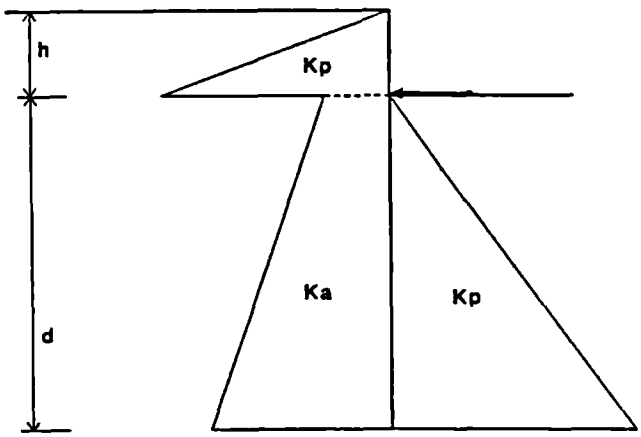

Fig. 5.4 Limiting soil stress distribution for a wall propped at dredge level of deep embedment

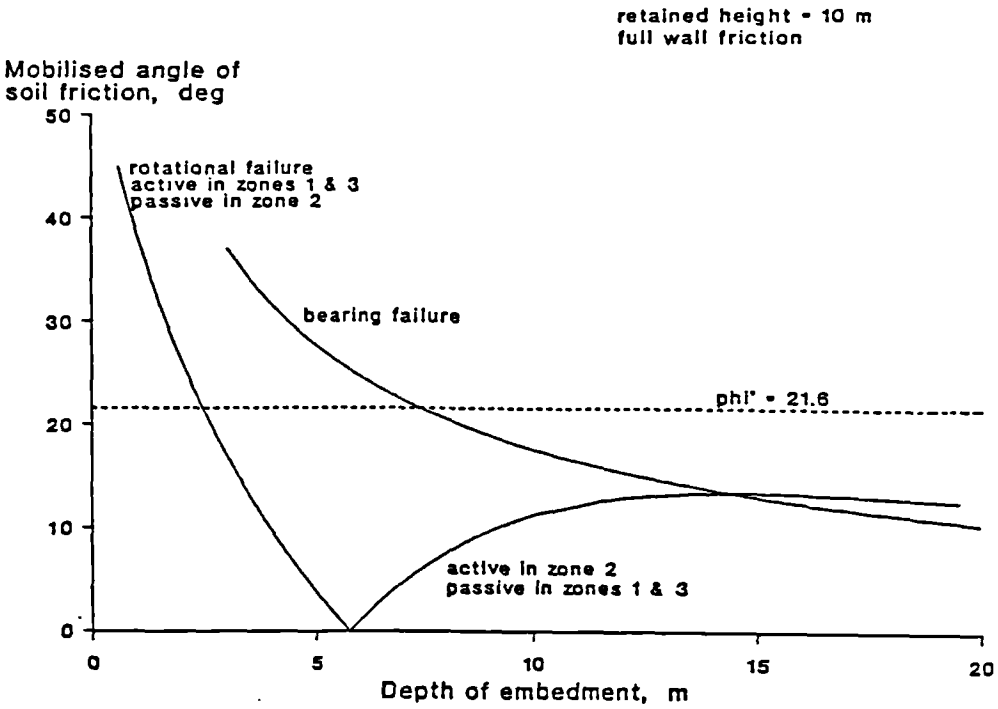

Fig. 5.5 Limiting mobilised angle of soil friction against depth of embedment showing the reversal of wall rotation

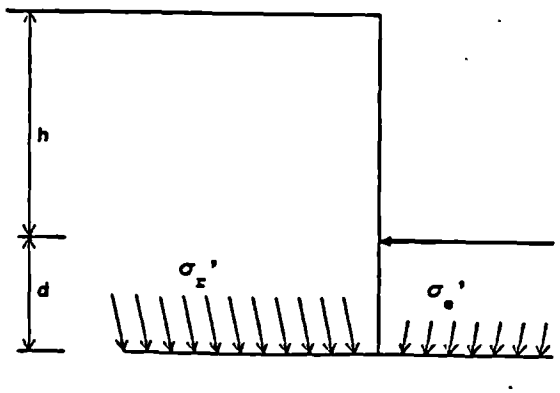

σ_r' = major principal stress on retained side
σ_e' = minor principal stress on excavated side
σ_r' & σ_e' are dependent on wall friction

For bearing failure:

$$\sigma_a' > \sigma_b' \frac{1+\sin\phi'}{1-\sin\phi'} \exp(\pi\tan\phi')$$

where
$\sigma_a' = \gamma(h+d) - u_t$
$\sigma_b' = \gamma d - u_t$
γ = unit weight of soil
u_t = pore water pressure at toe level

Fig. 5.6 Bearing failure criteria at toe level

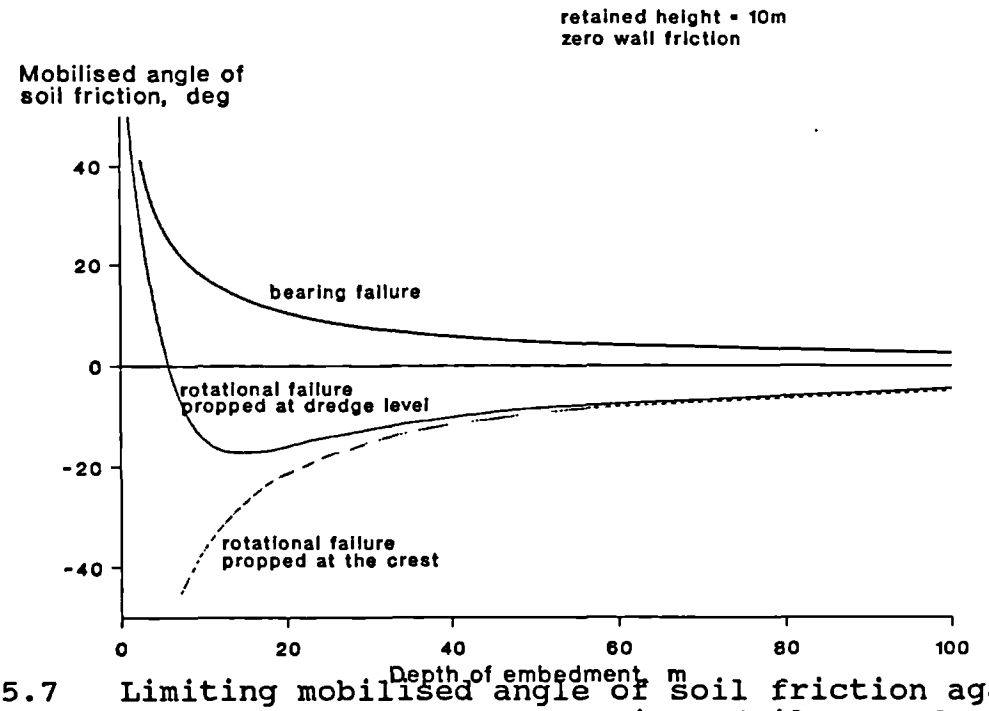

Fig. 5.7 Limiting mobilised angle of soil friction against depth of embedment for various failure modes

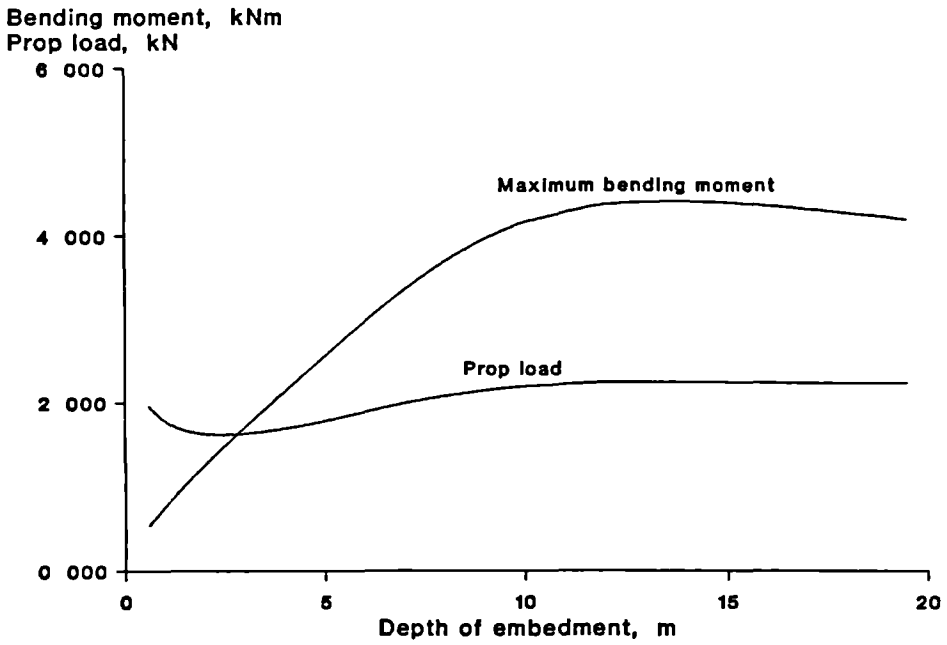

Fig. 5.8 Calculated maximum bending moment and prop load against depth of embedment

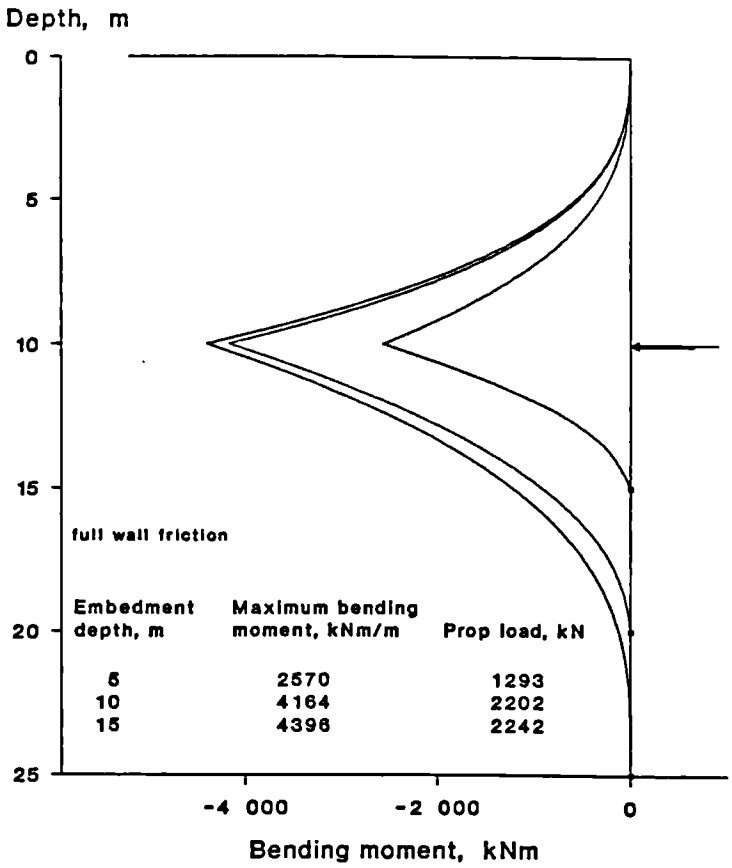

Fig. 5.9 Bending moment diagrams and prop load calculated from limit equilibrium method

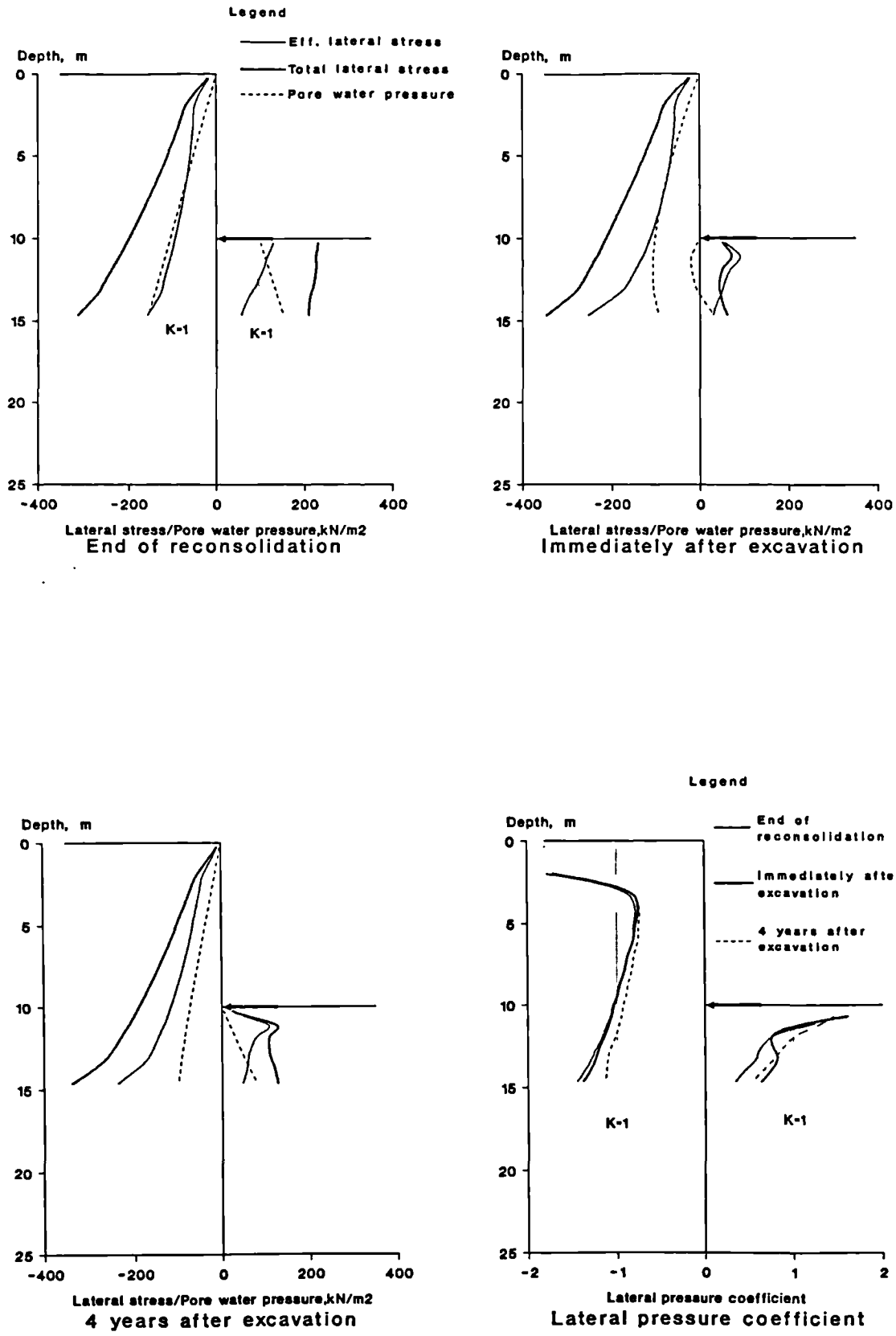

Fig. 5.10 Lateral stresses, pore water pressure and lateral earth pressure coefficients distributions for rigid wall of 5m embedment

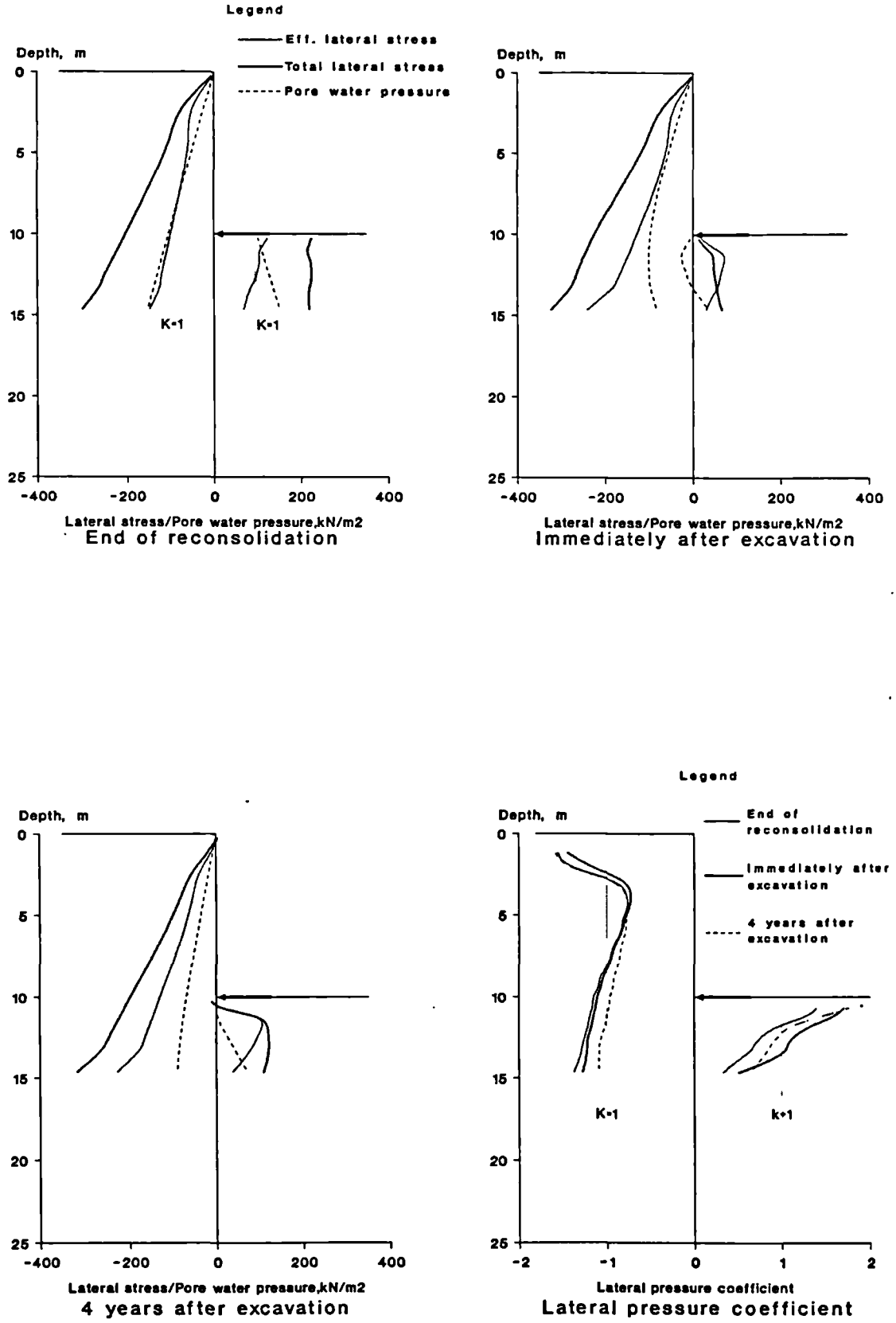

Fig. 5.11 Lateral stresses, pore water pressure and lateral earth pressure coefficients distributions for flexible wall of 5m embedment

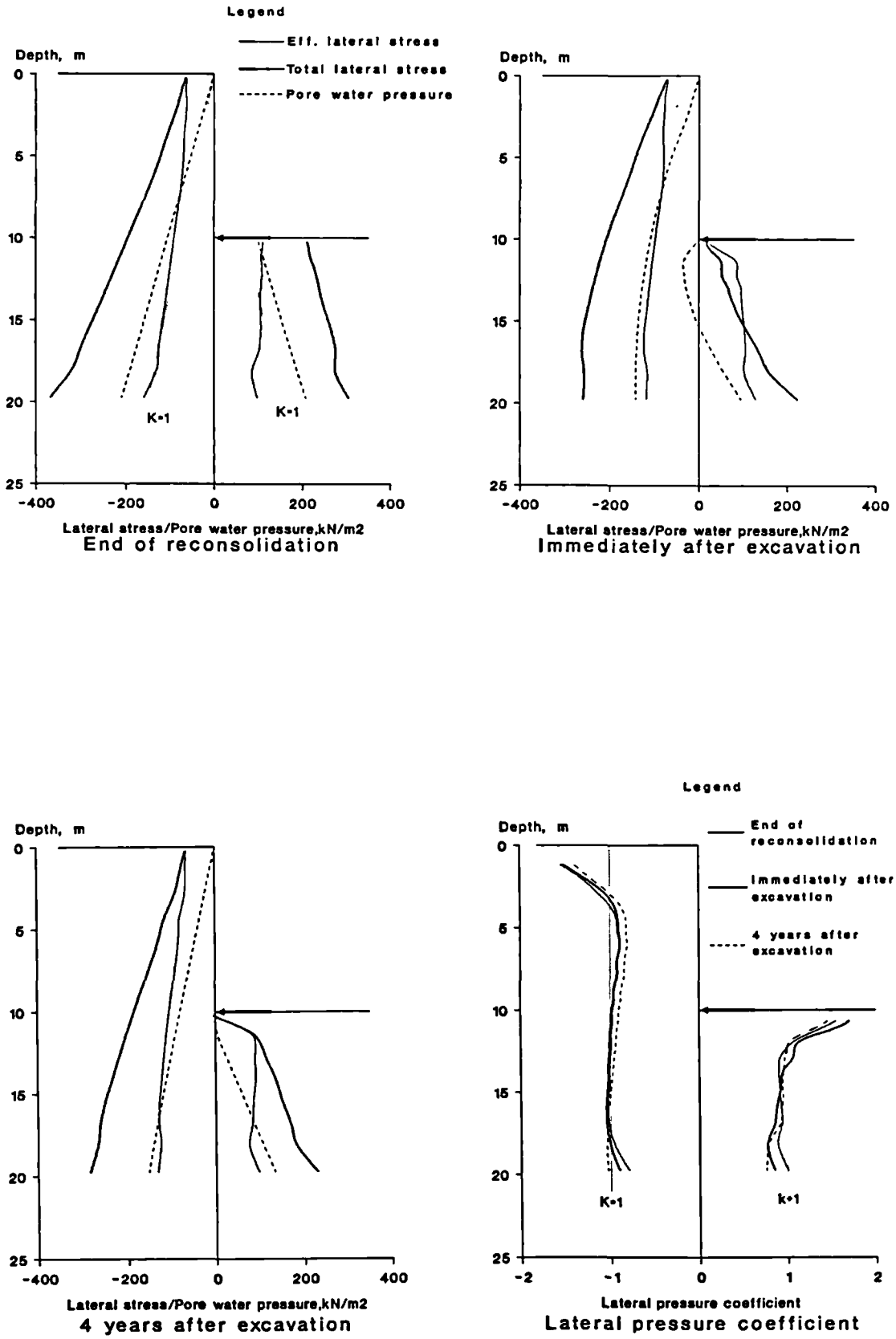

Fig. 5.12 Lateral stresses, pore water pressure and lateral earth pressure coefficients distributions for rigid wall of 10m embedment

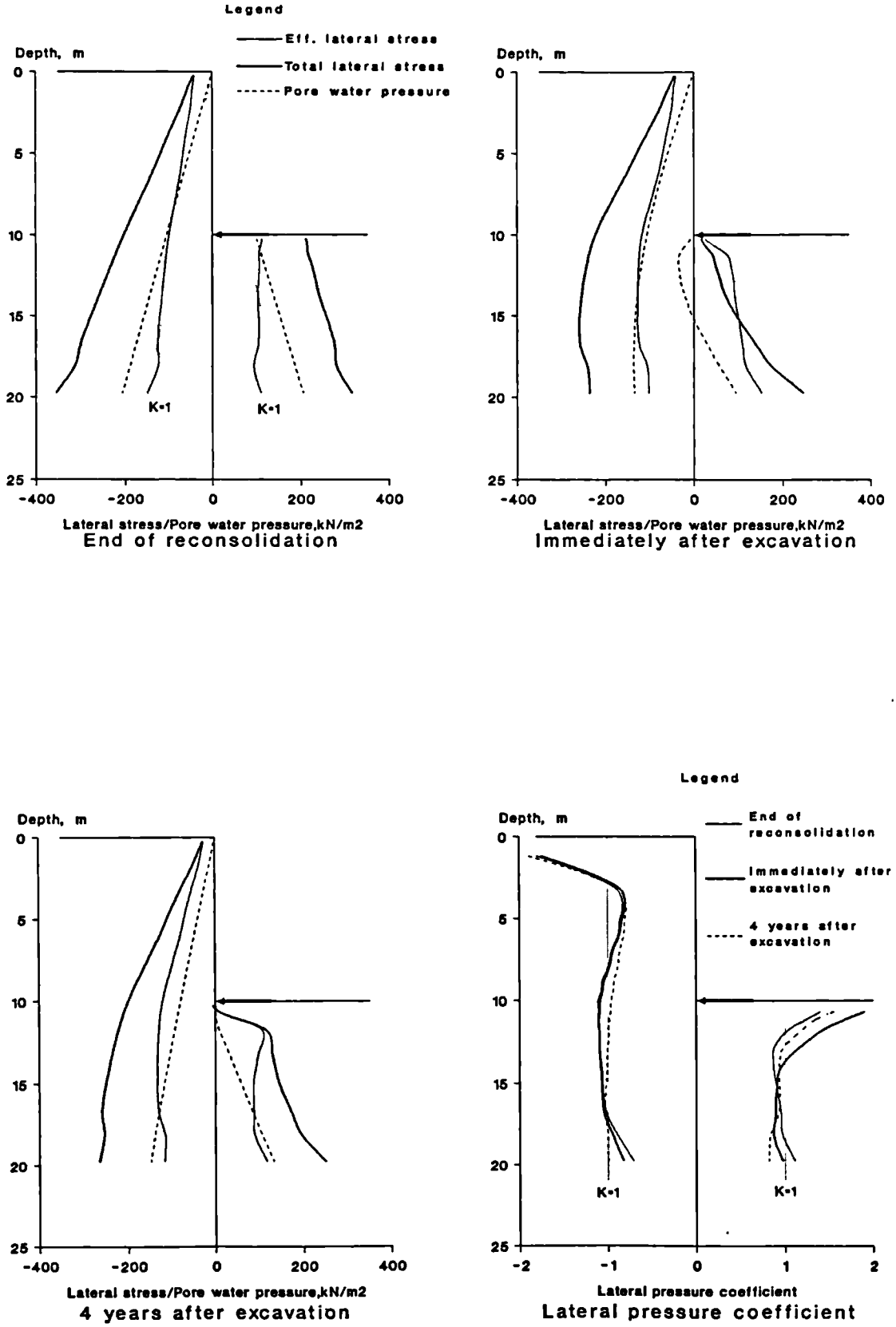

Fig. 5.13 Lateral stresses, pore water pressure and lateral earth pressure coefficients distributions for flexible wall of 10m embedment

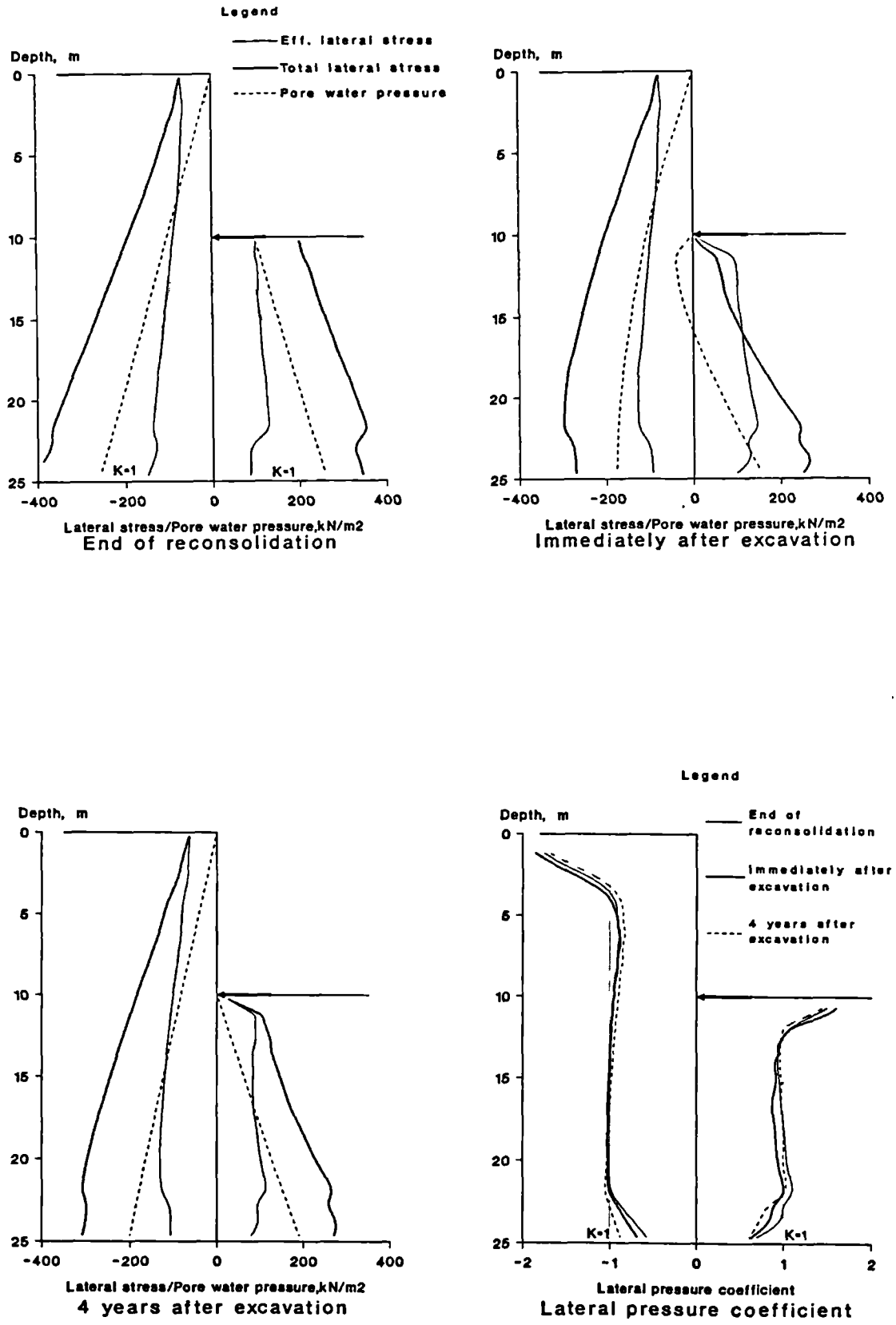

Fig. 5.14 Lateral stresses, pore water pressure and lateral earth pressure coefficients distributions for rigid wall of 15m embedment

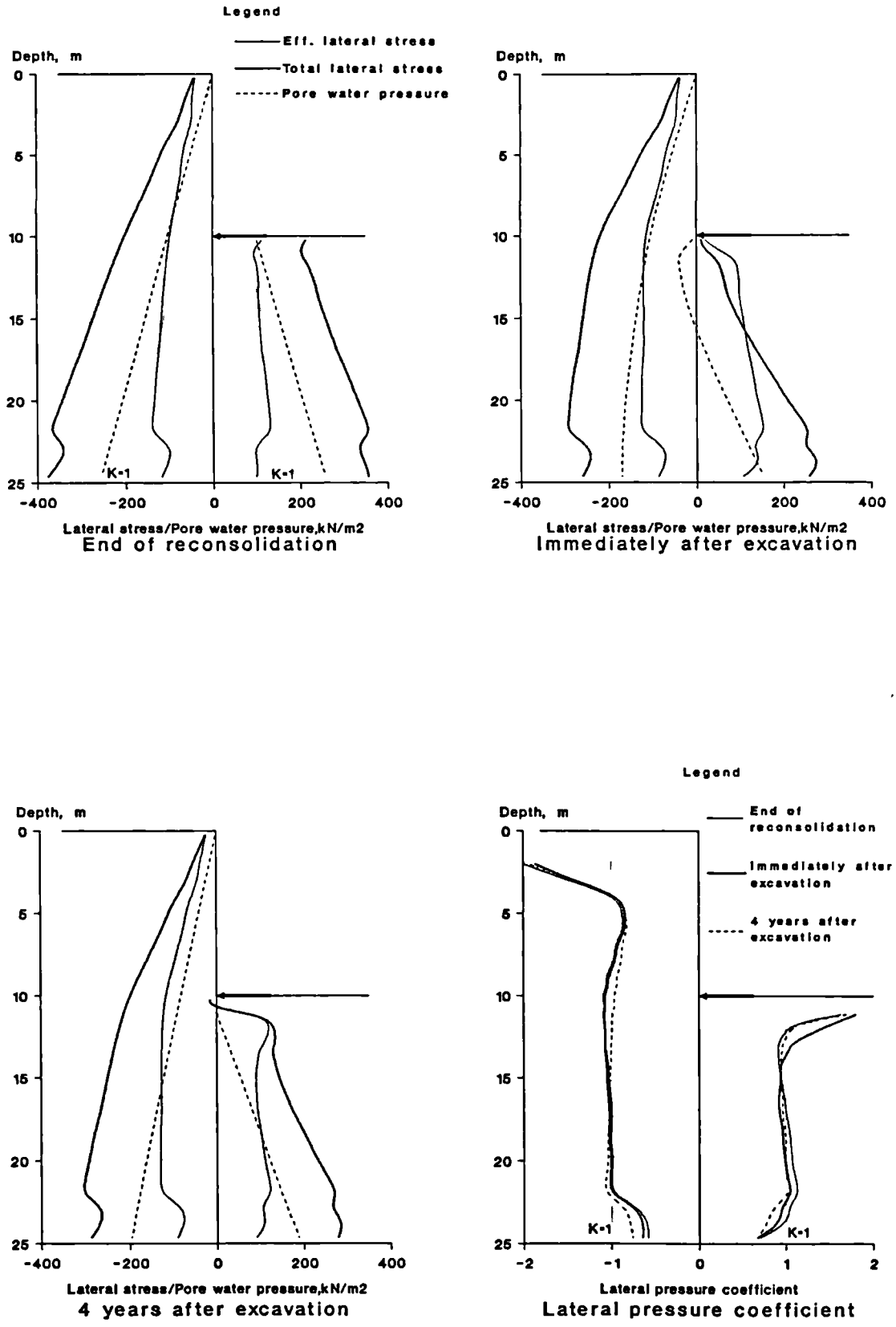

Fig. 5.15 Lateral stresses, pore water pressure and lateral earth pressure coefficients distributions for flexible wall of 15m embedment

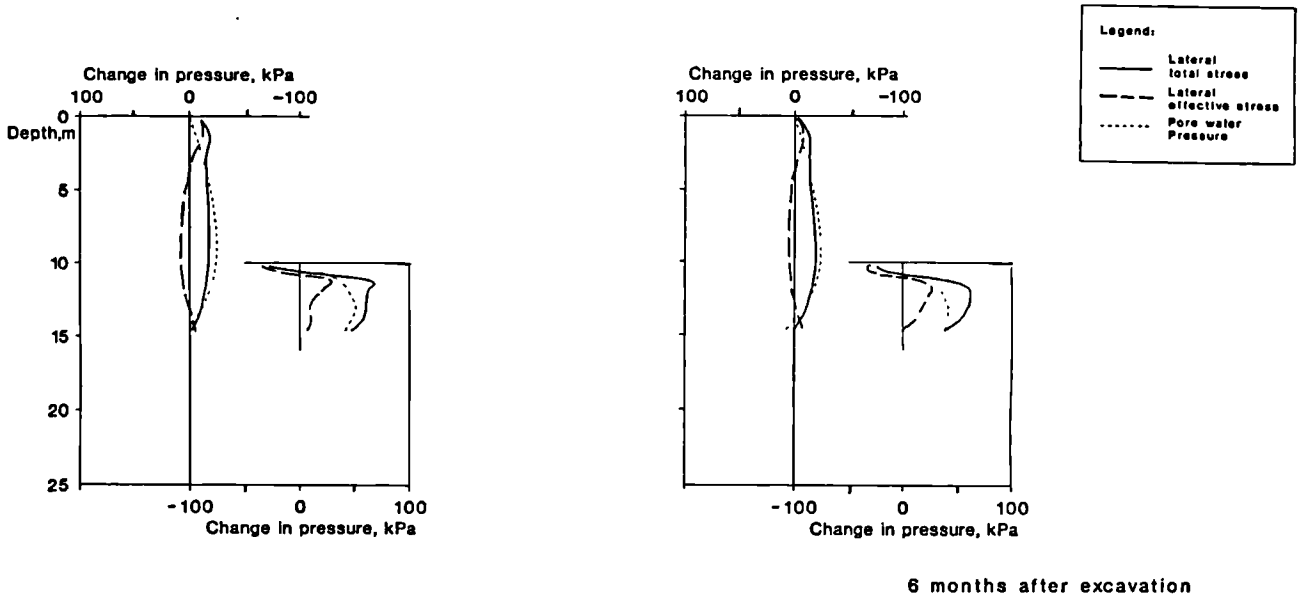

Fig. 5.16 Post-excavation changes in lateral stresses and pore water pressures for walls of 5m embedment

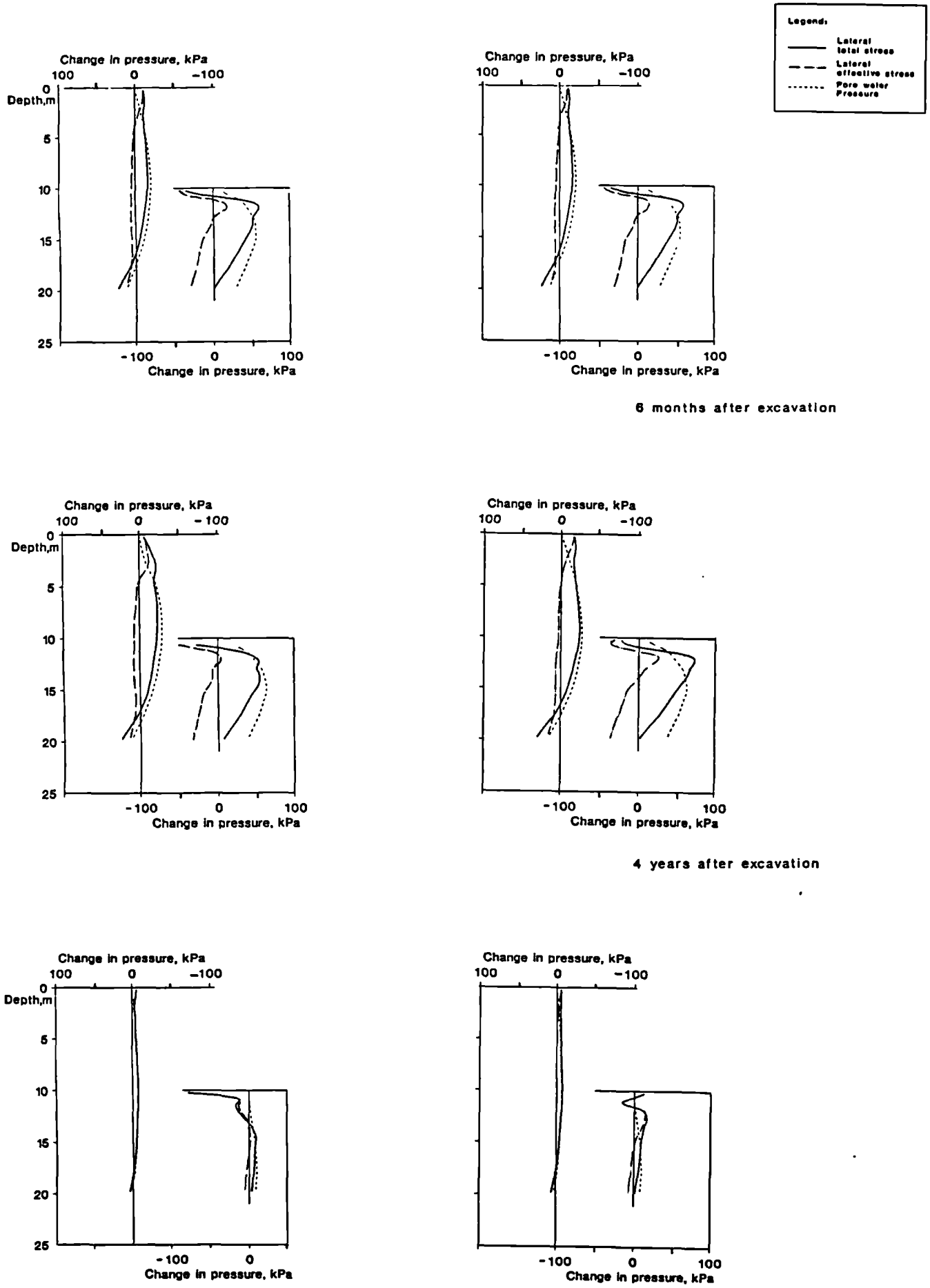

Fig. 5.17 Post-excavation changes in lateral stresses and pore water pressures for walls of 10 m embedment

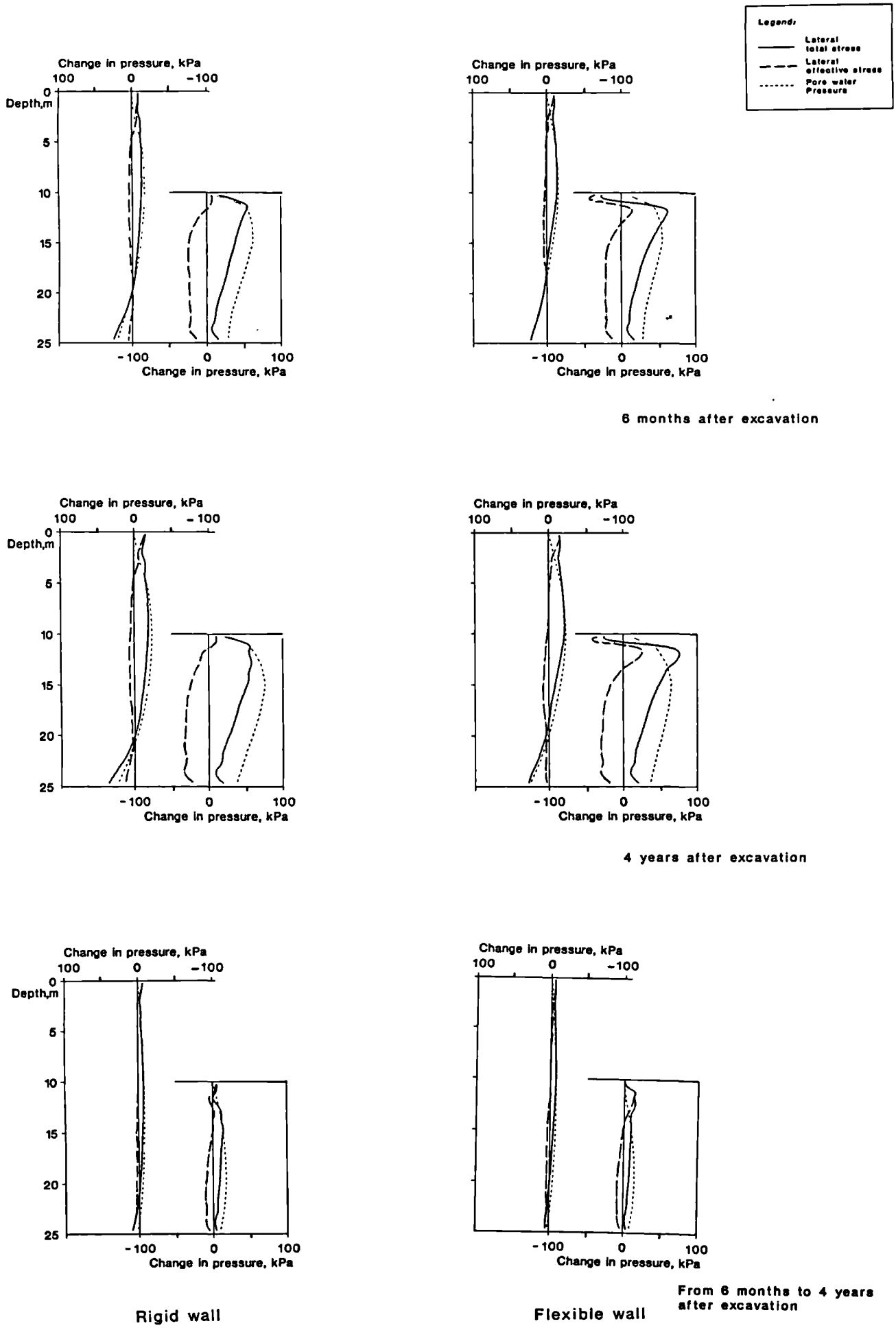

Fig. 5.18 Post-excavation changes in lateral stresses and pore water pressures for walls of 15m embedment

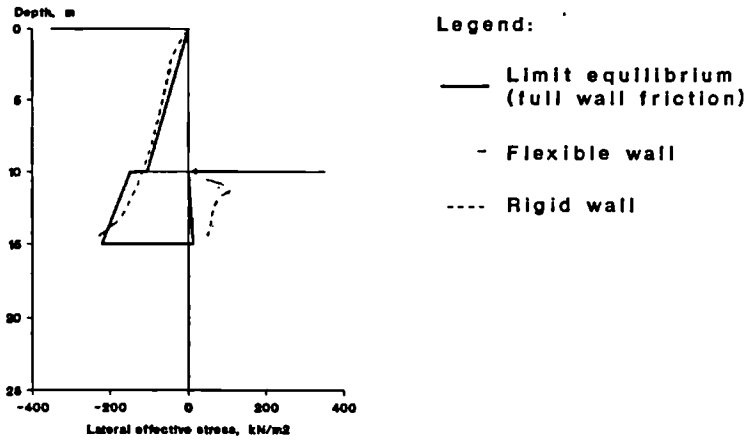

a. 5m embedment

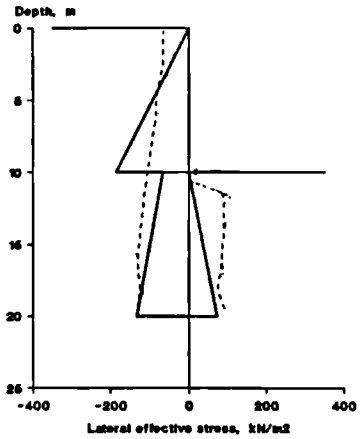

b. 10m embedment

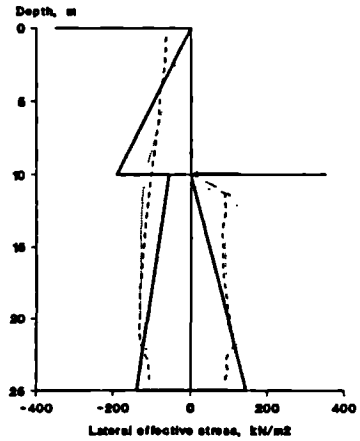

c. 15m embedment

Fig. 5.19 Comparisons of long term lateral effective stresses from limit equilibrium calculations and finite element analyses

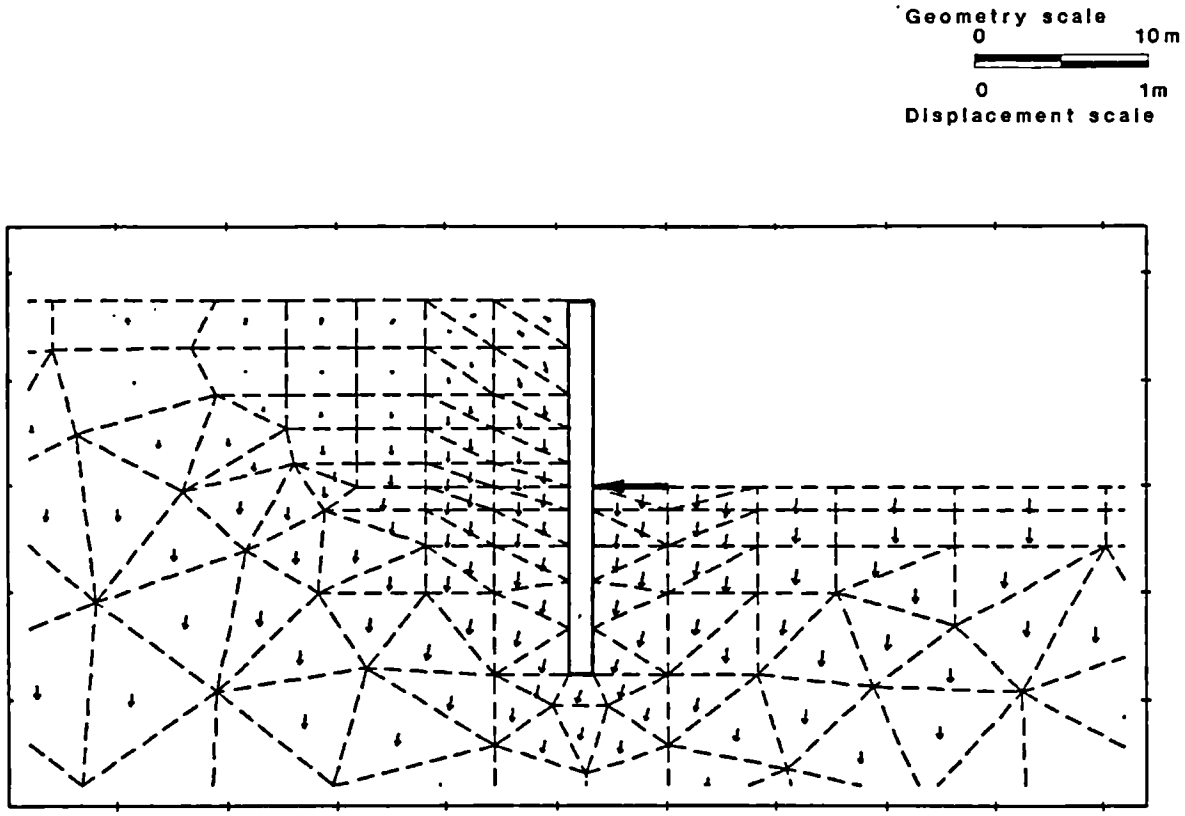

Fig. 5.20 Displacement vector diagram for a rigid wall of 10m embedment at the end of reconsolidation

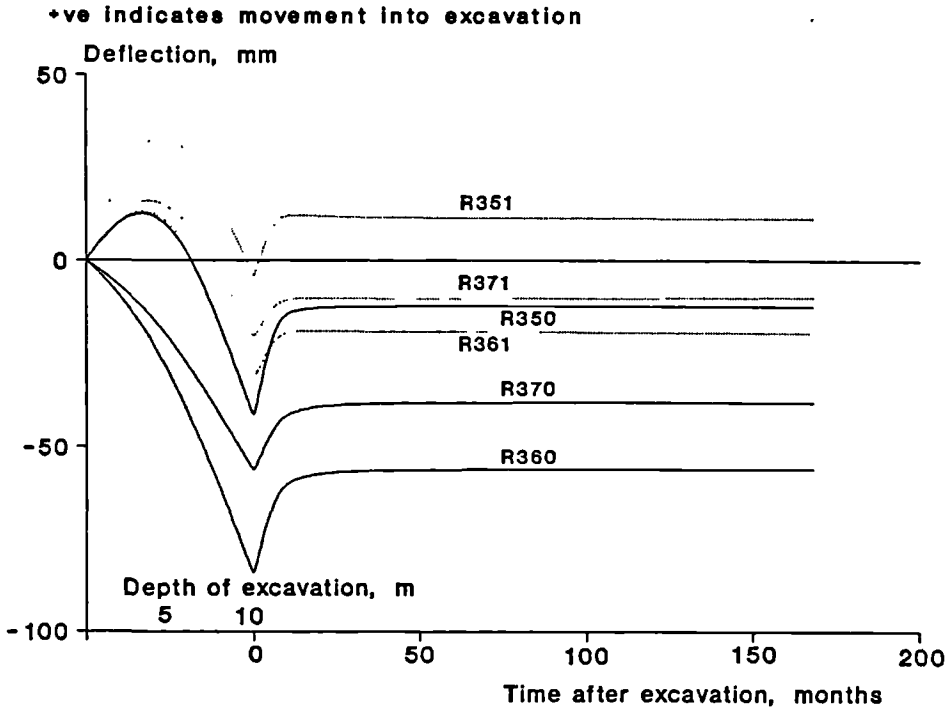

a. Crest deflection

Analysis	Embedment depth, m	Wall rigidity
R350	5	Rigid
R351	5	Flexible
R360	10	Rigid
R361	10	Flexible
R370	15	Rigid
R371	15	Flexible

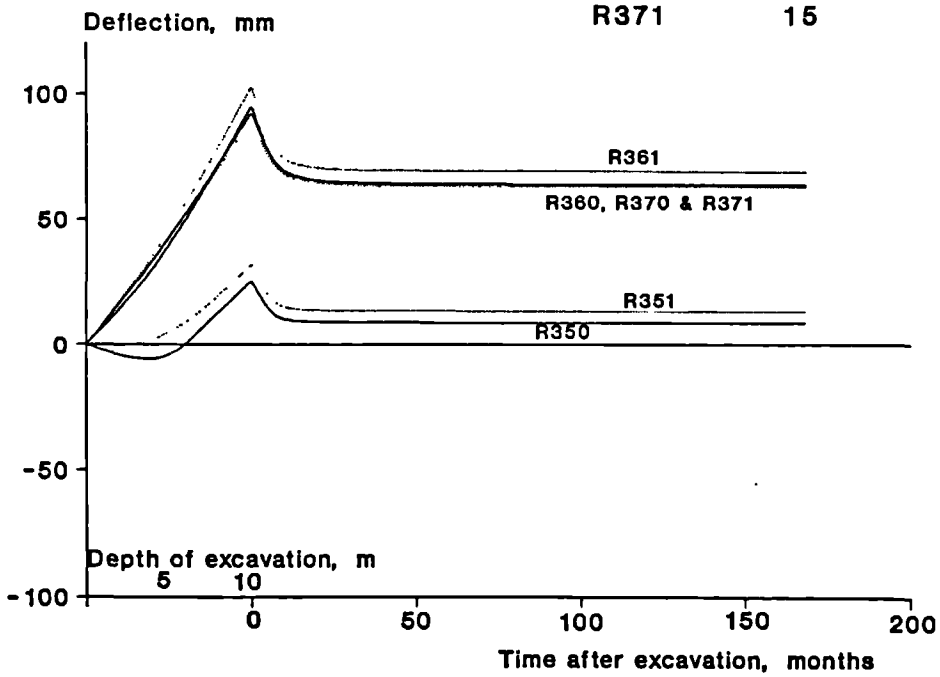

b. Toe deflection

Fig. 5.21 Computed crest and toe deflections against excavation and time for walls propped at dredge level

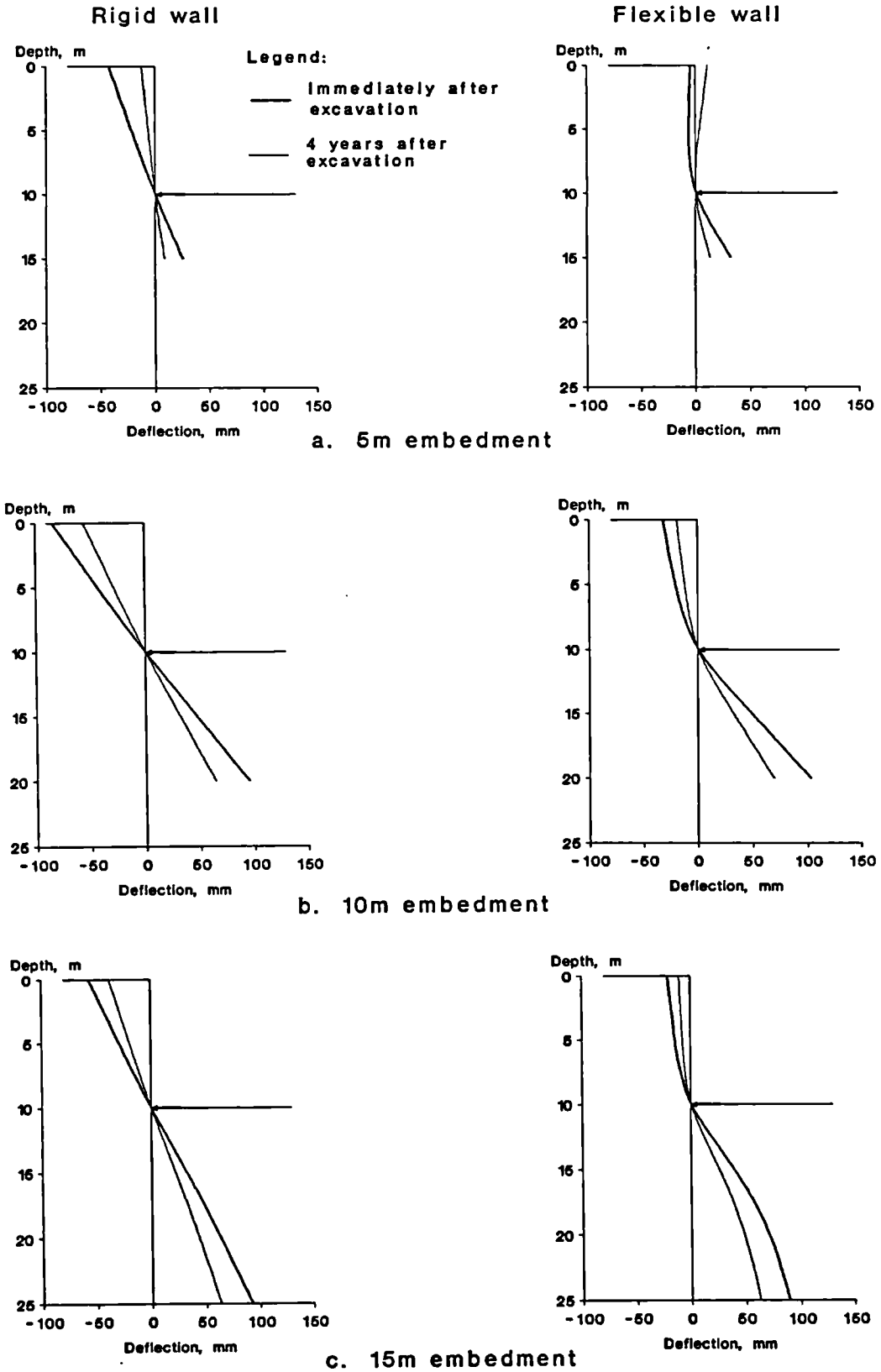

Fig. 5.22 Wall deflections for walls propped at dredge level

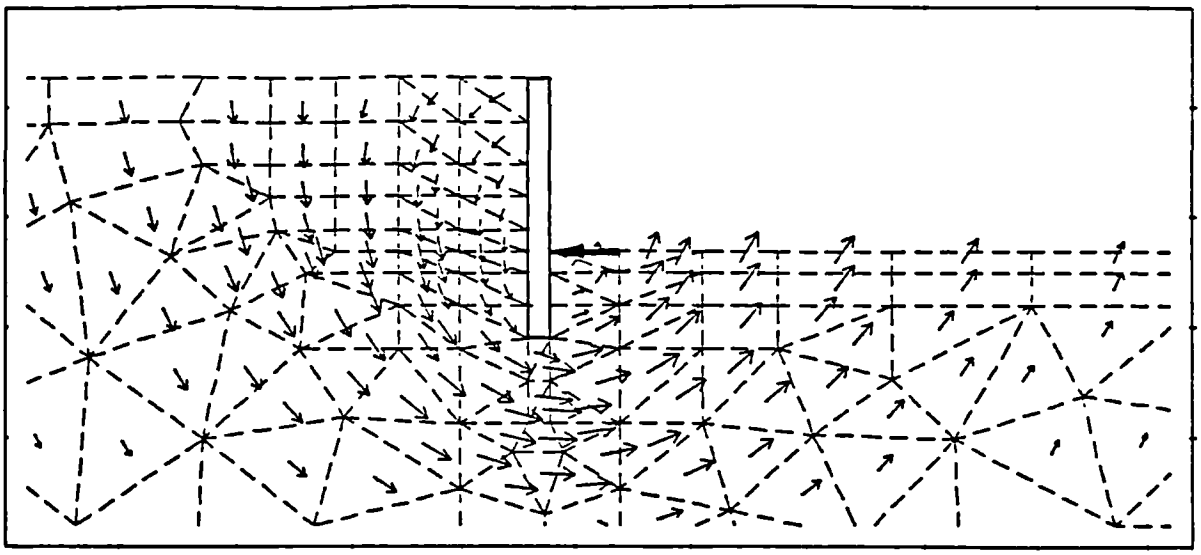

a. Immediately after excavation

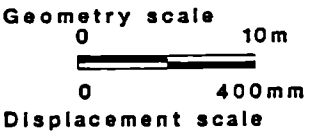

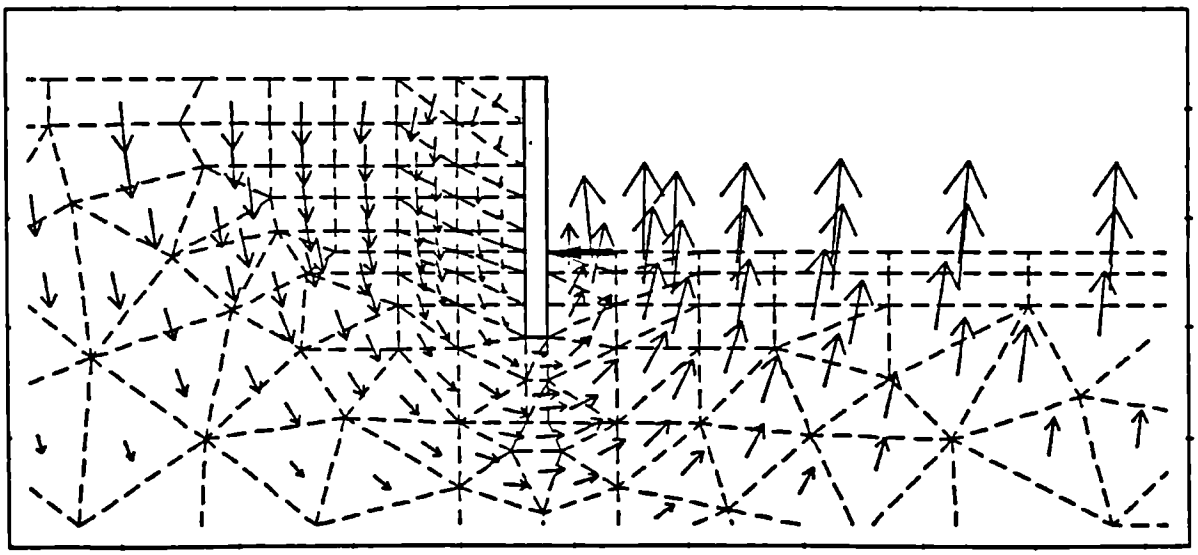

b. 4 years after excavation

Fig. 5.23 Incremental displacement vector diagrams for rigid wall of 5m embedment

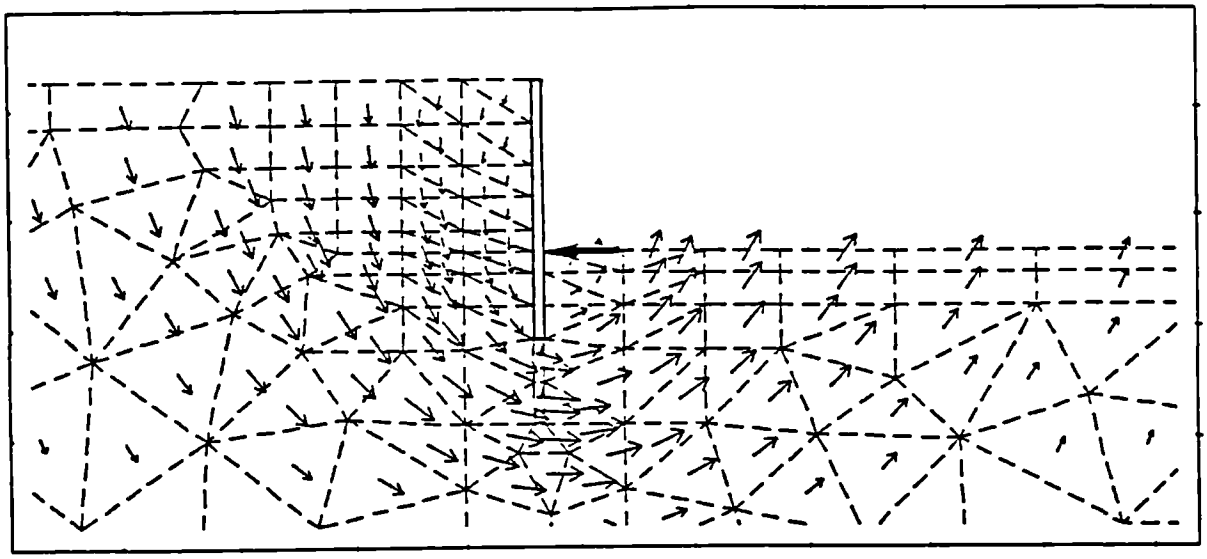

a. Immediately after excavation

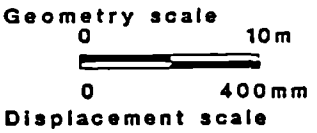

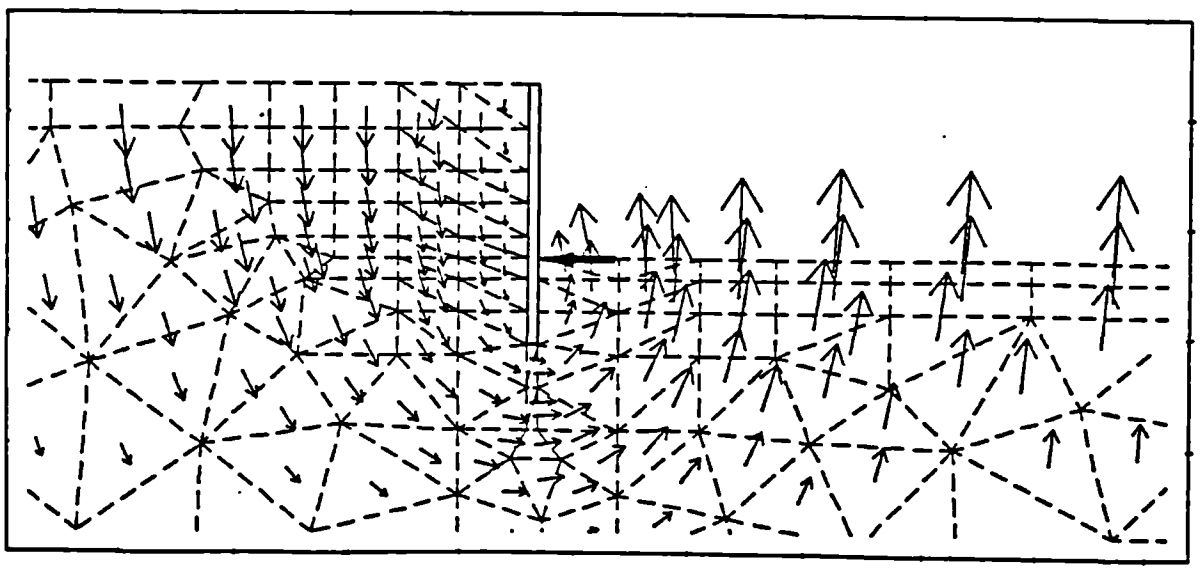

b. 4 years after excavation

Fig. 5.24 Incremental displacement vector diagrams for flexible wall of 5m embedment

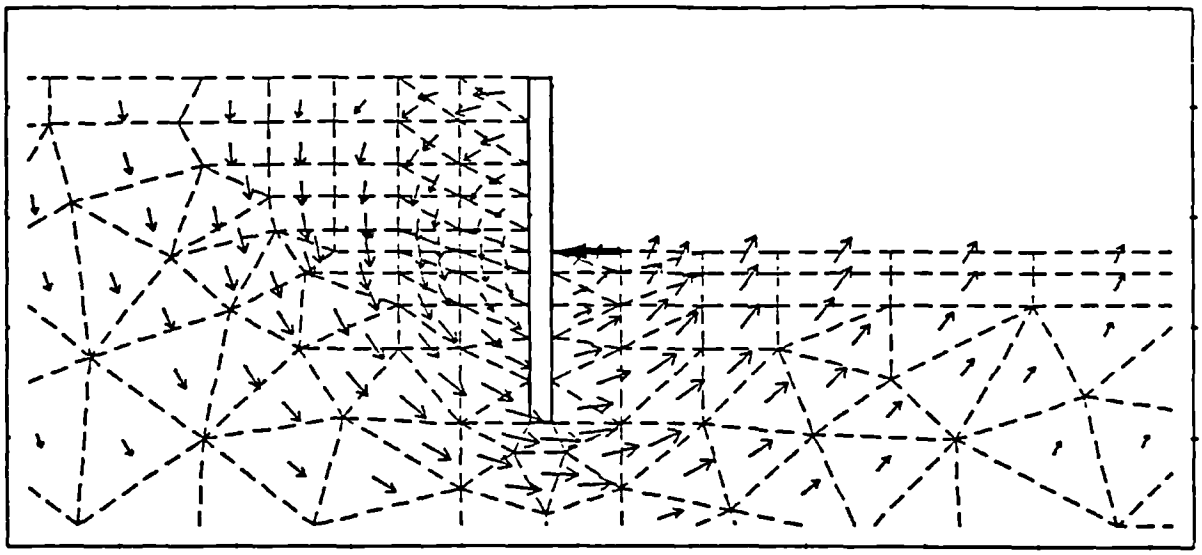

a. Immediately after excavation

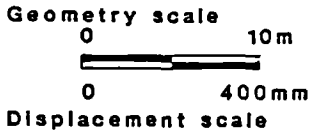

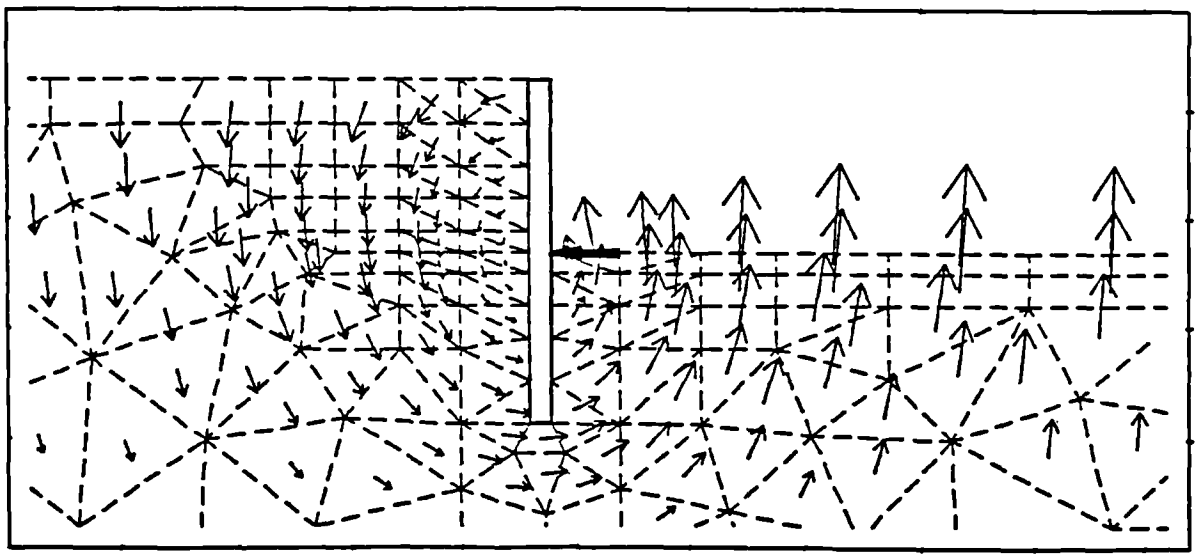

b. 4 years after excavation

Fig. 5.25 Incremental displacement vector diagrams for rigid wall of 10m embedment

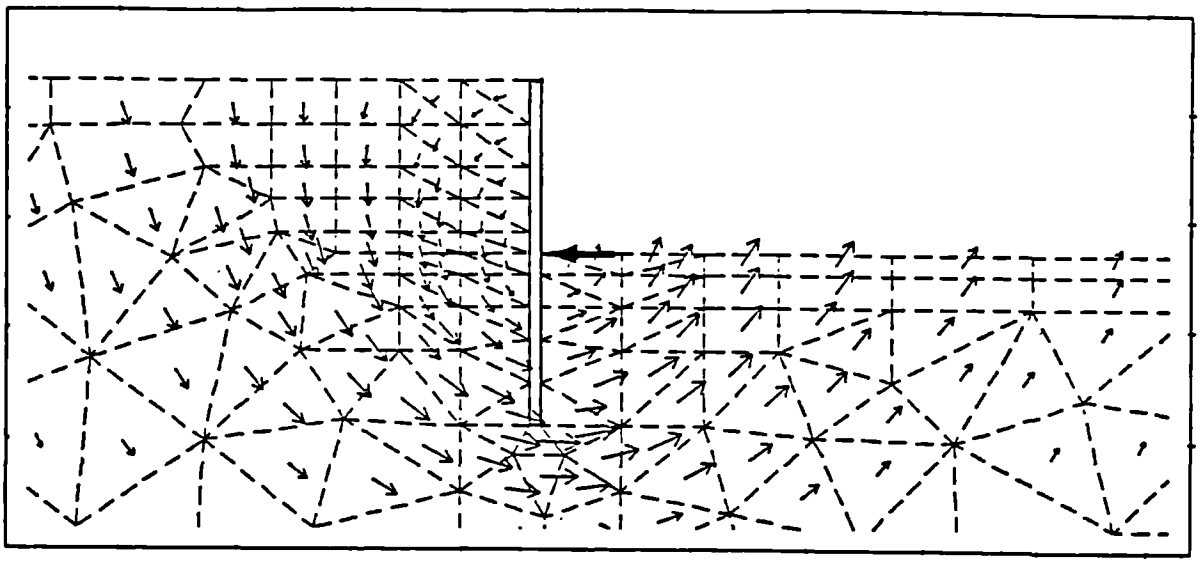

a. Immediately after excavation

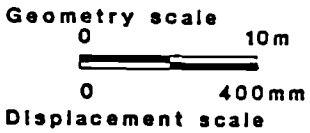

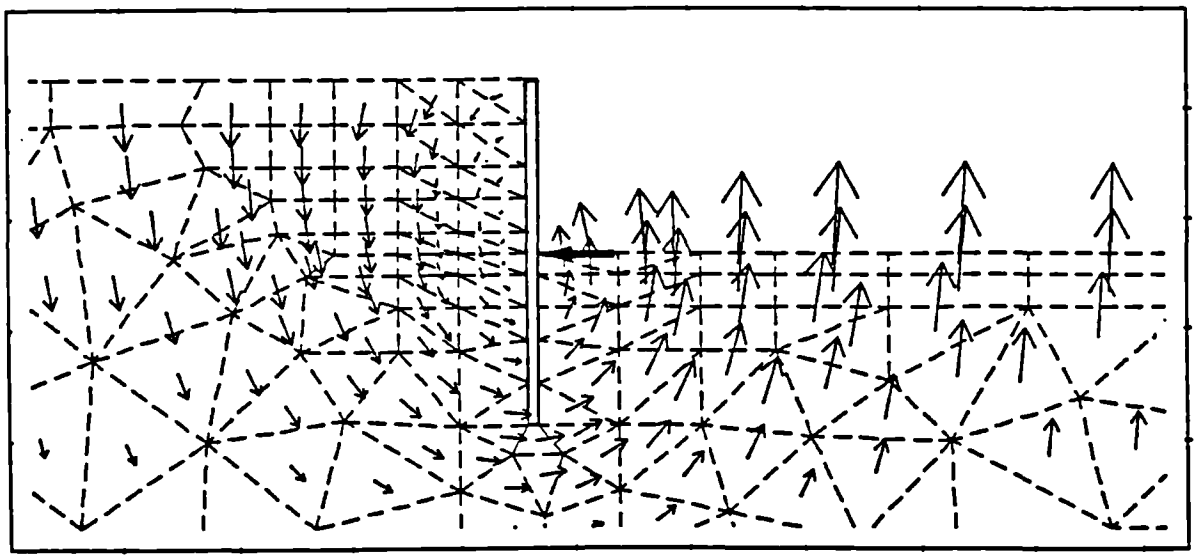

b. 4 years after excavation

Fig. 5.26 Incremental displacement vector diagrams for flexible wall of 10m embedment

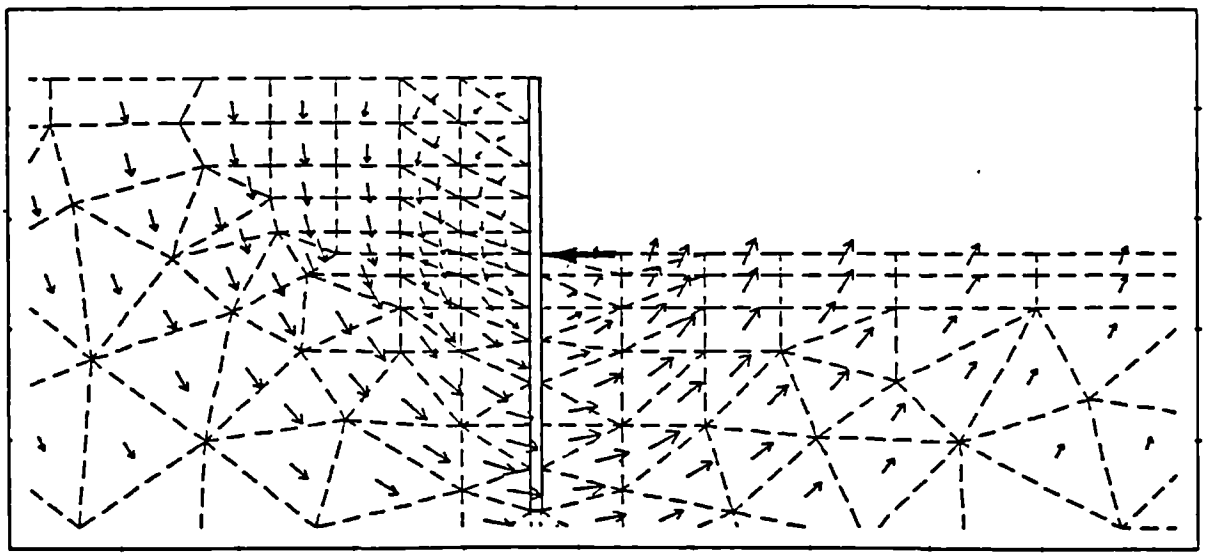

a. Immediately after excavation

Geometry scale
0 10m
0 400mm
Displacement scale

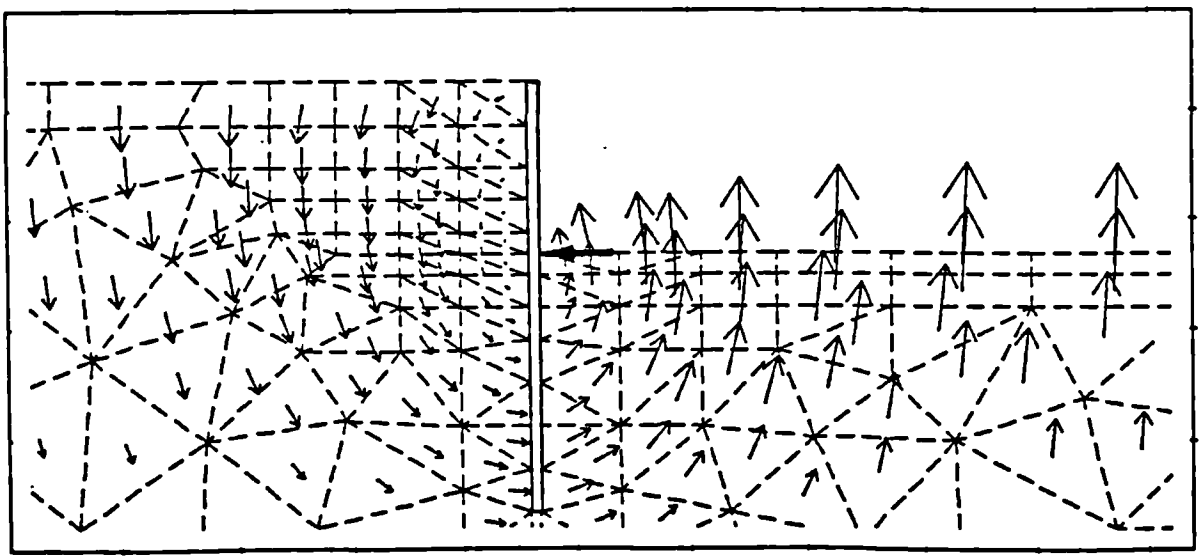

b. 4 years after excavation

Fig. 5.27 Incremental displacement vector diagrams for rigid wall of 15m embedment.

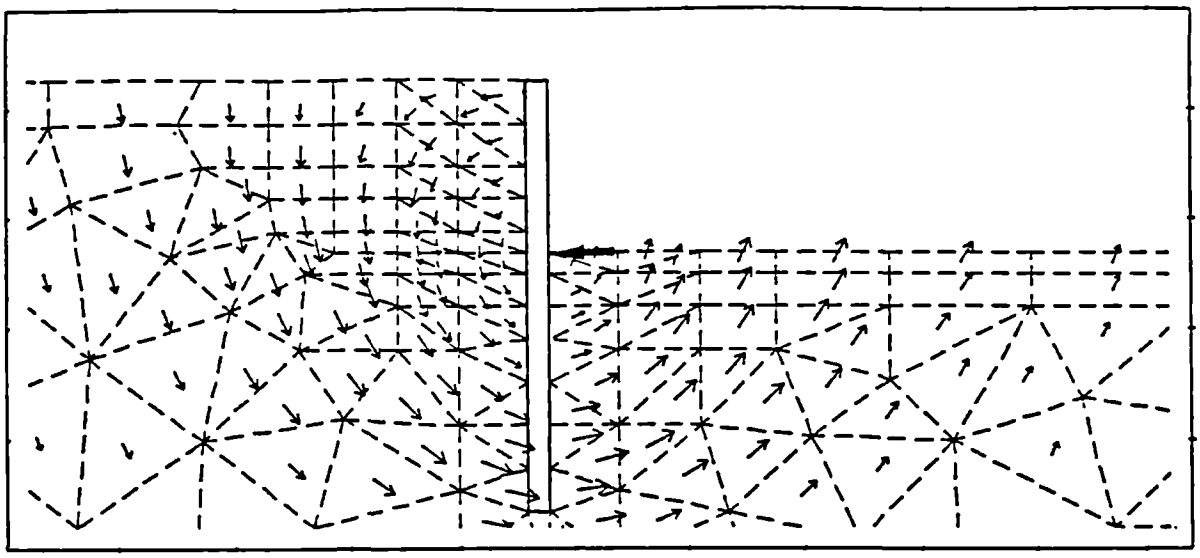

a. Immediately after excavation

Geometry scale
0 10m
0 400mm
Displacement scale

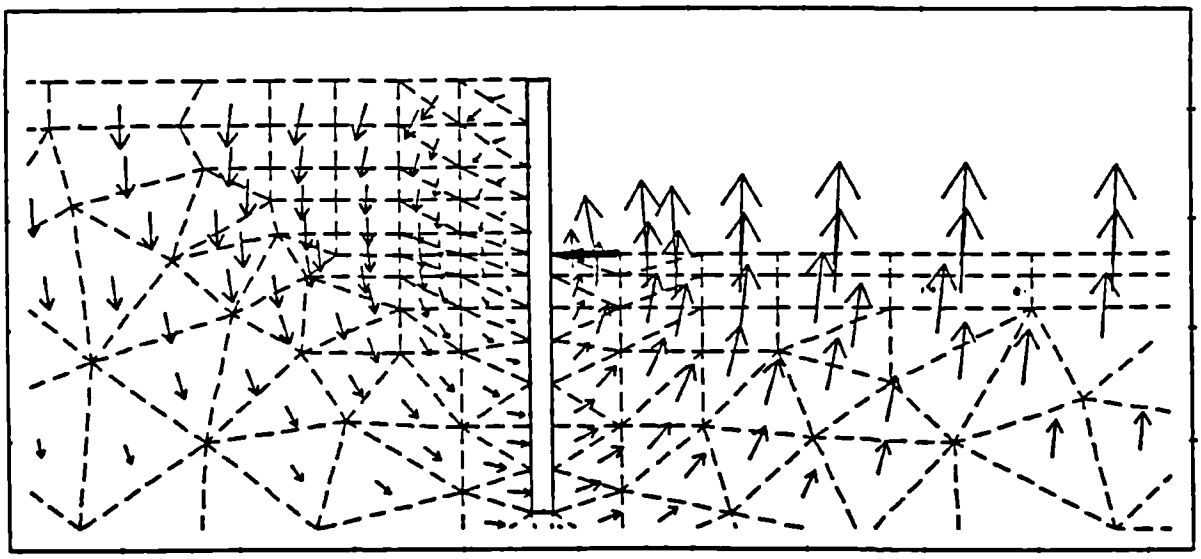

b. 4 years after excavation

Fig. 5.28 Incremental displacement vector diagrams for flexible wall of 15m embedment

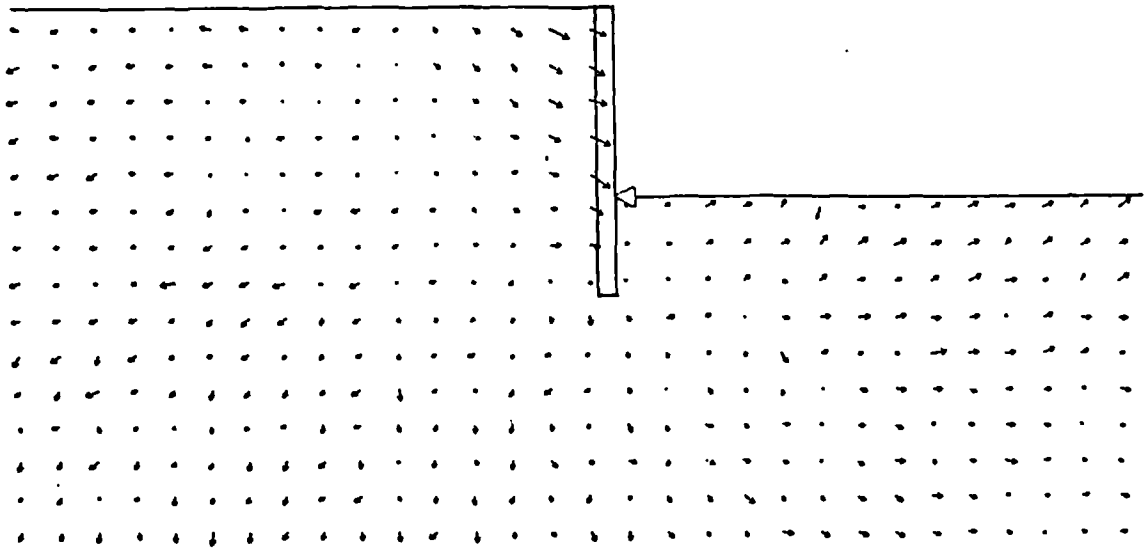

a. Soil movements during excavation, DWC17

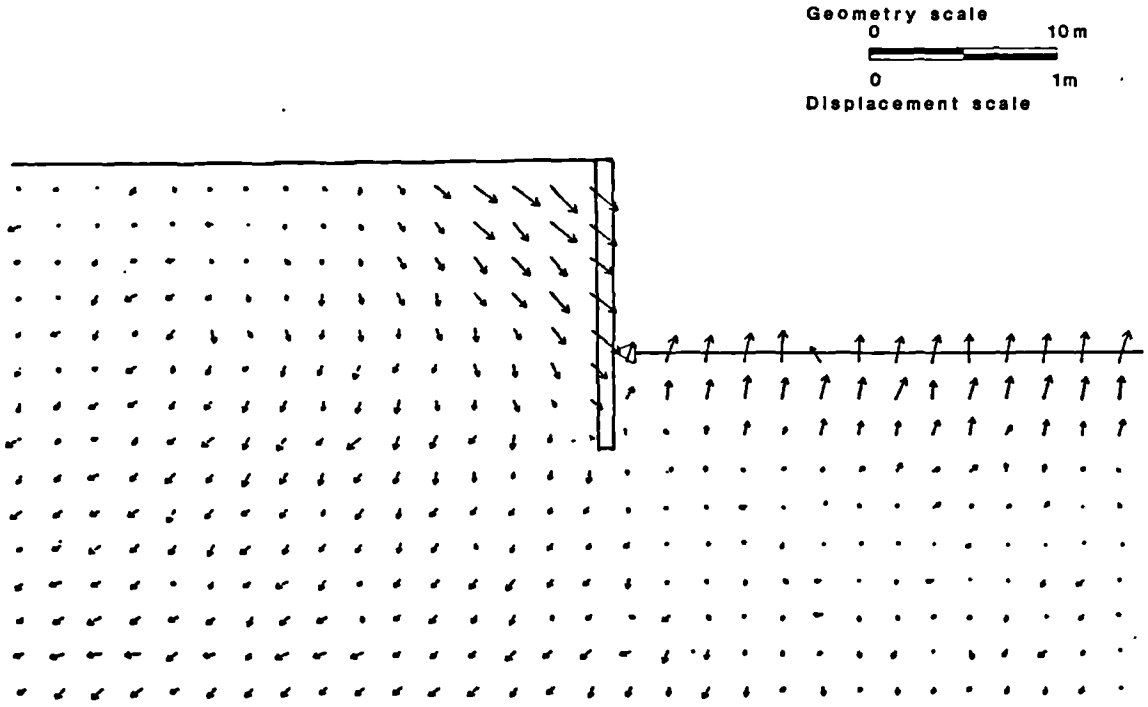

b. Long-term soil movements, DWC17

Fig. 5.29 Measured soil movements from centrifuge test, DWC17 (from Powrie, 1986)

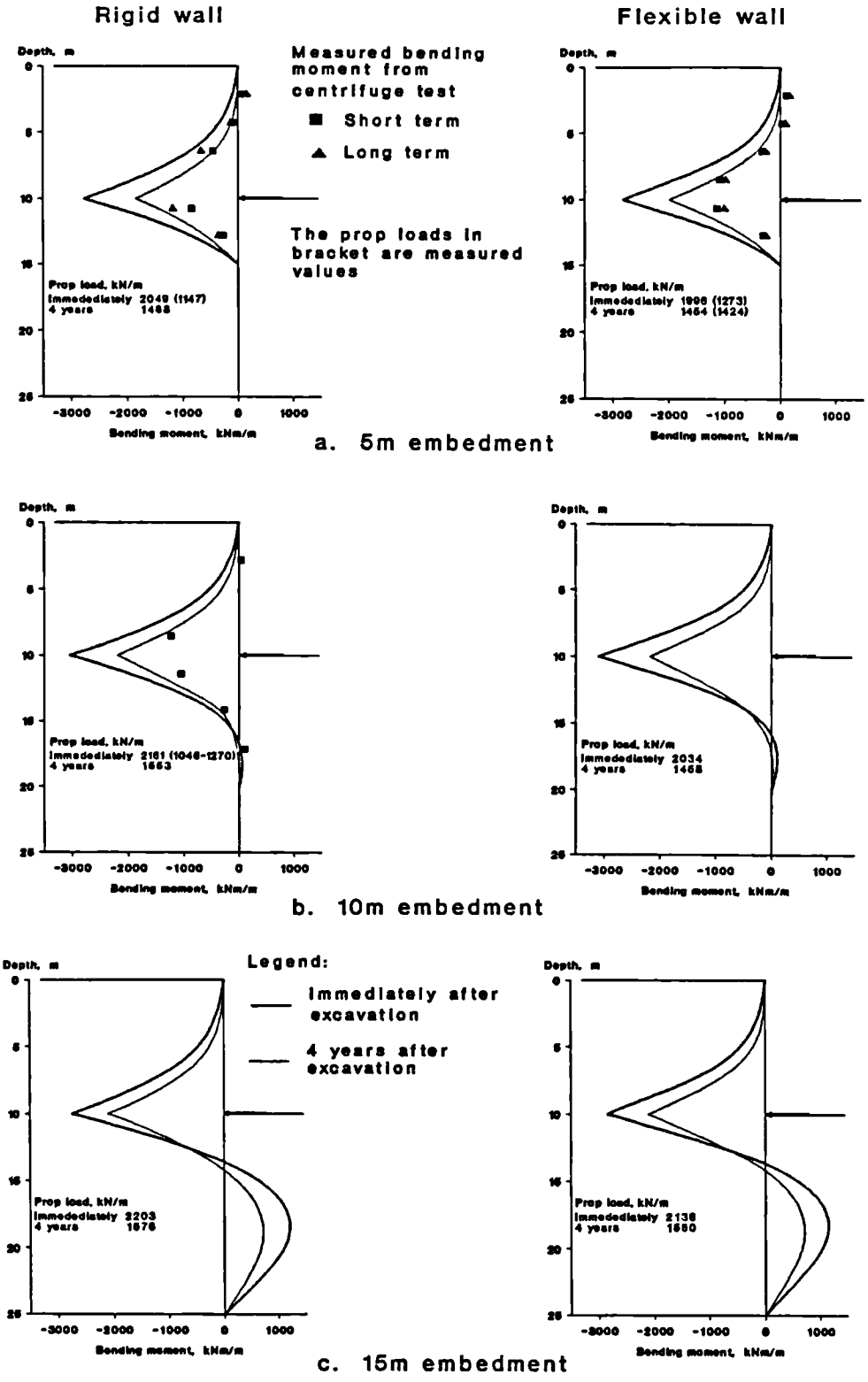

Fig. 5.30 Bending moment diagrams and prop loads for walls propped at dredge level

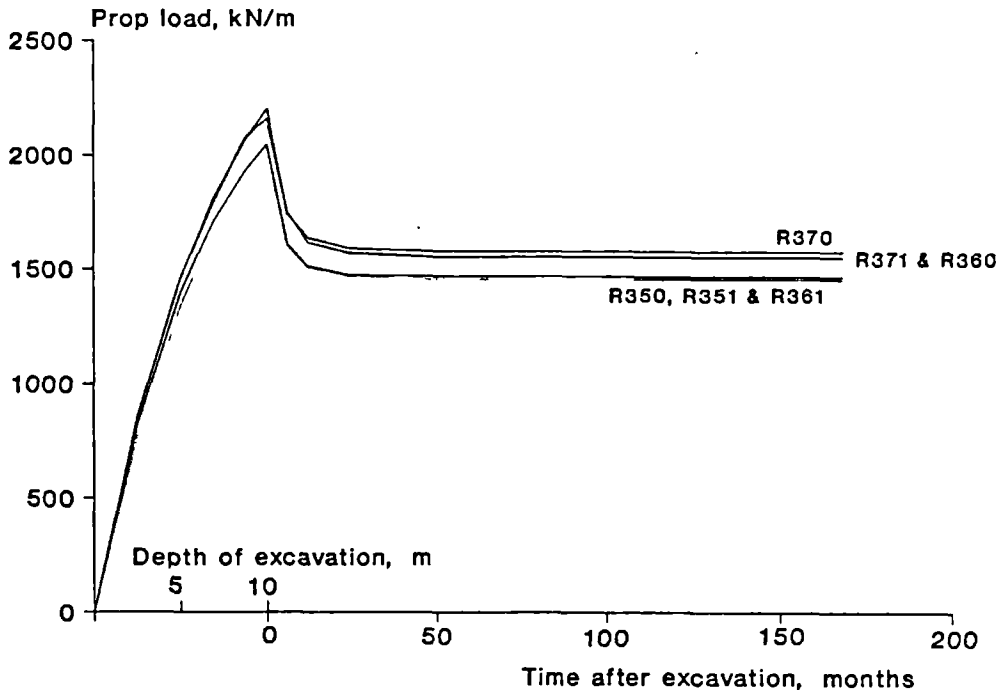

Fig. 5.31 Computed prop loads against excavation and time for walls propped at dredge level

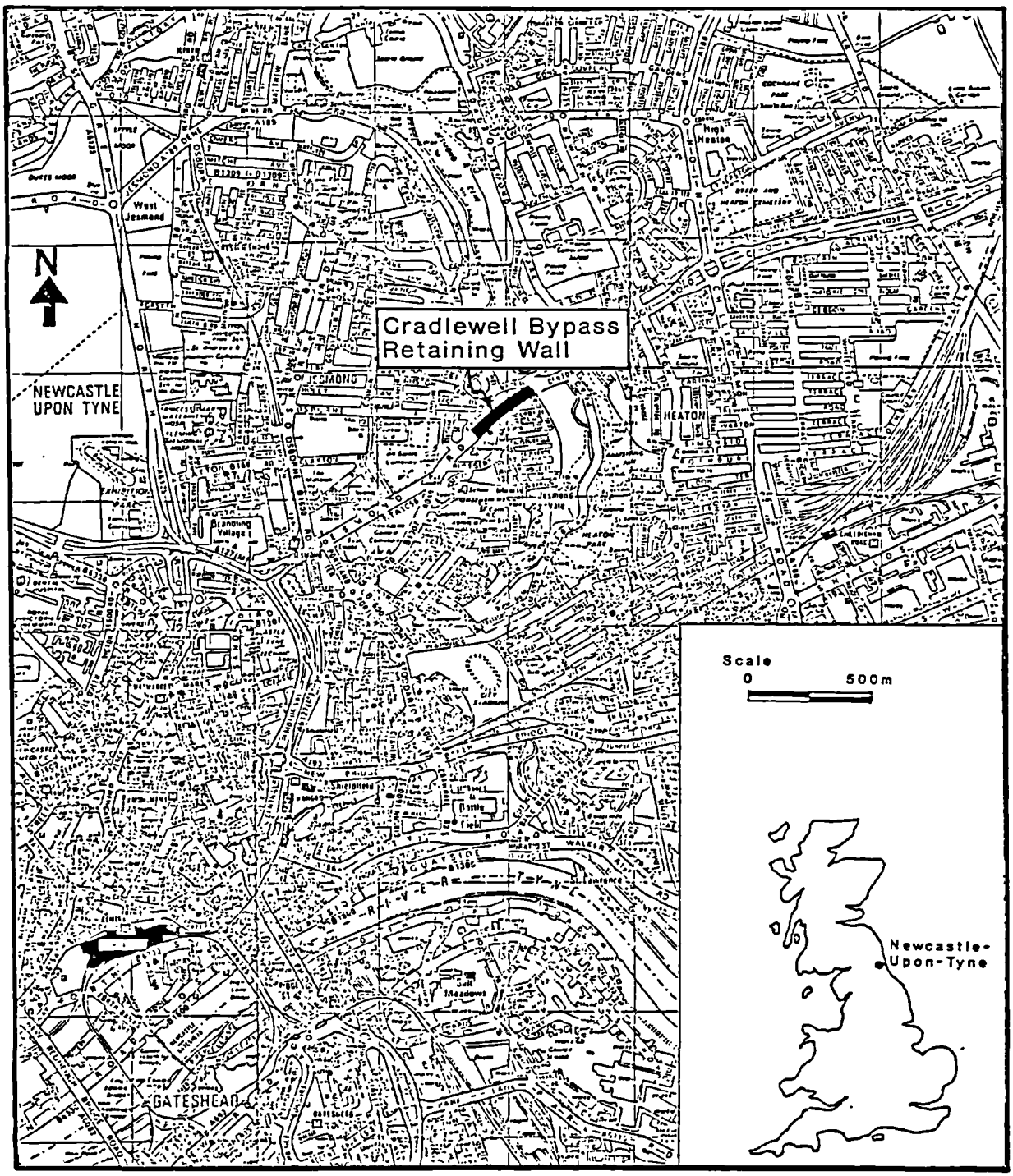

Fig. 6.1 Site location plan for the A1058 Cradlewell Bypass retaining walls

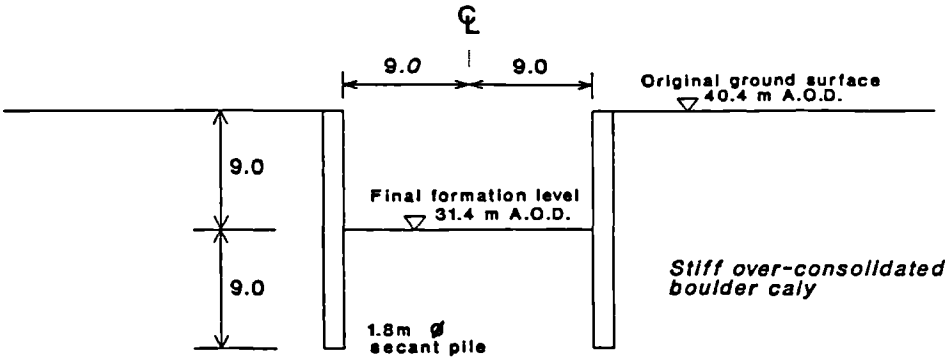

Fig. 6.2 Typical cross-section

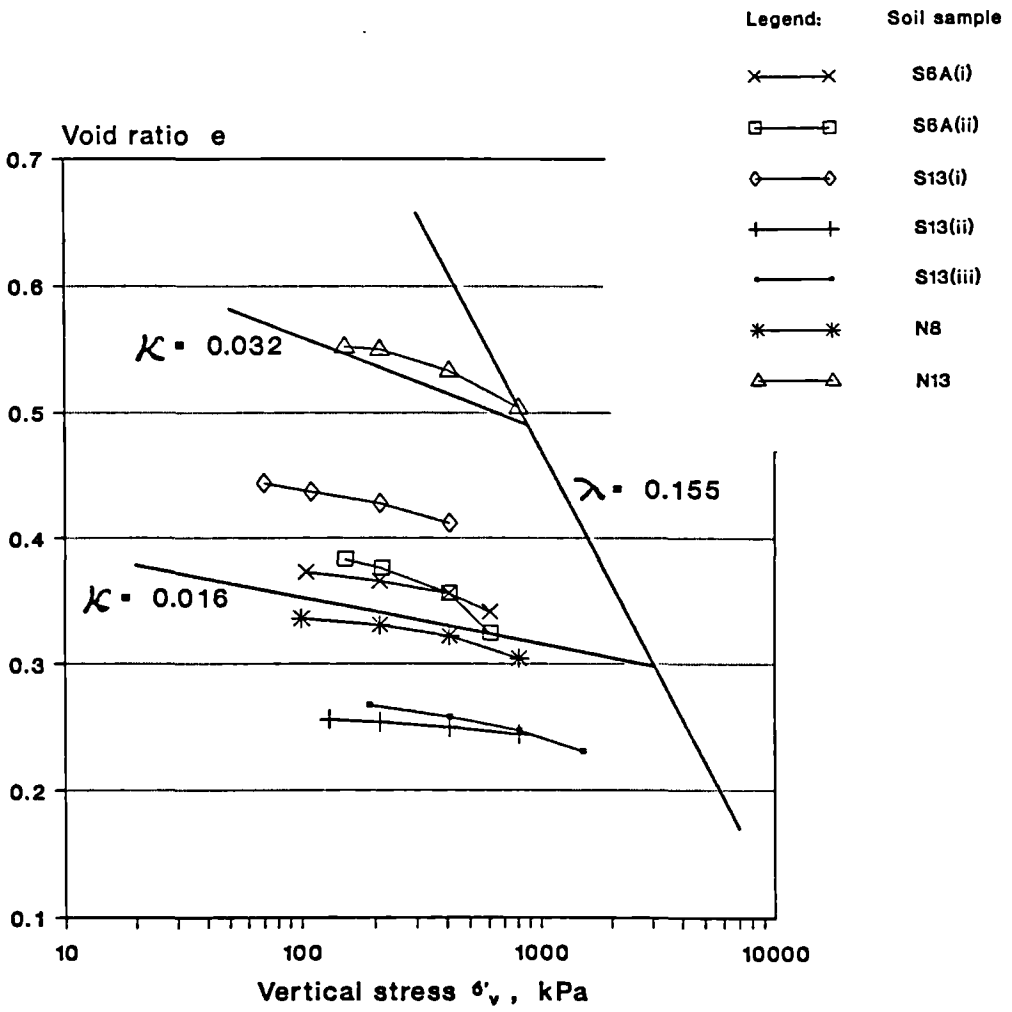

Fig. 6.3 Evaluation of soil parameters (data from oedometer tests of Tyneside Metro S.I., 1972)

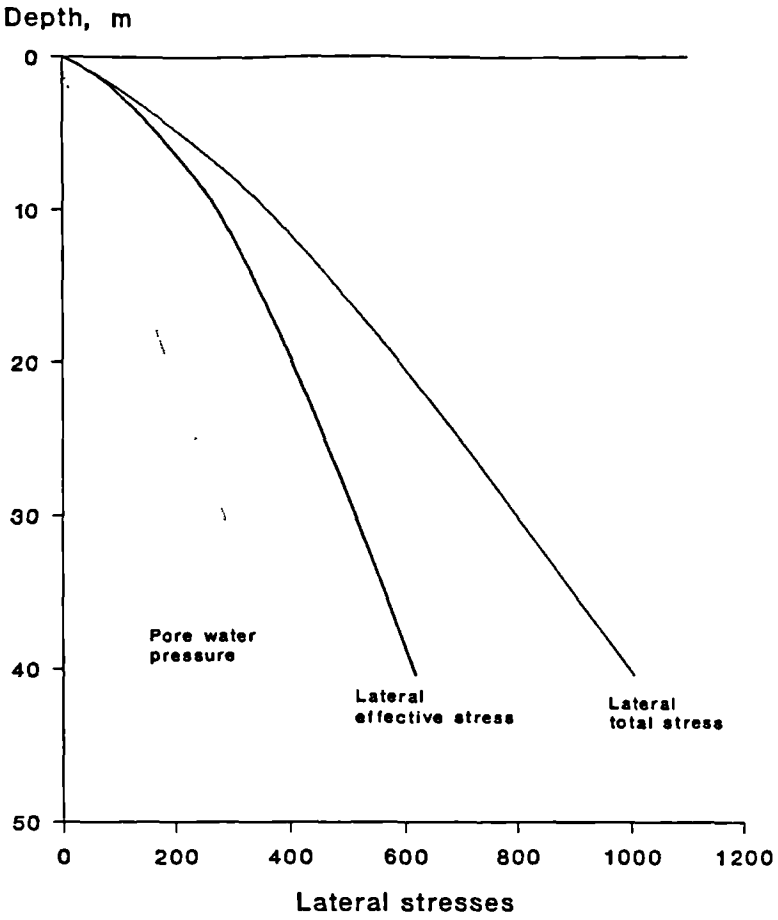

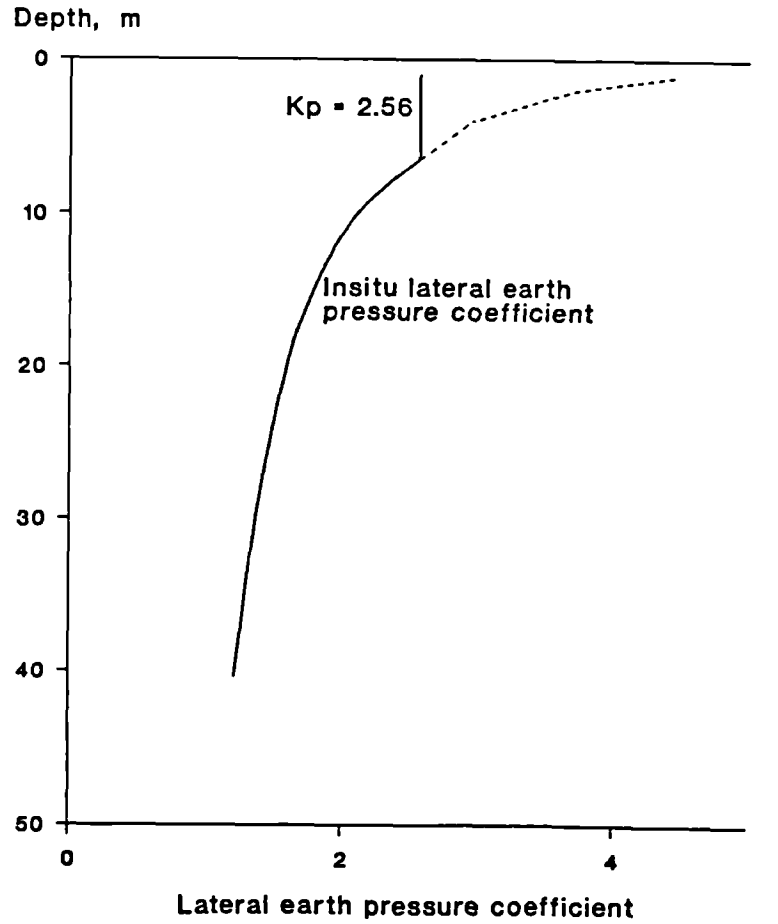

Fig. 6.4 Calculated insitu lateral stresses and earth pressure coefficient

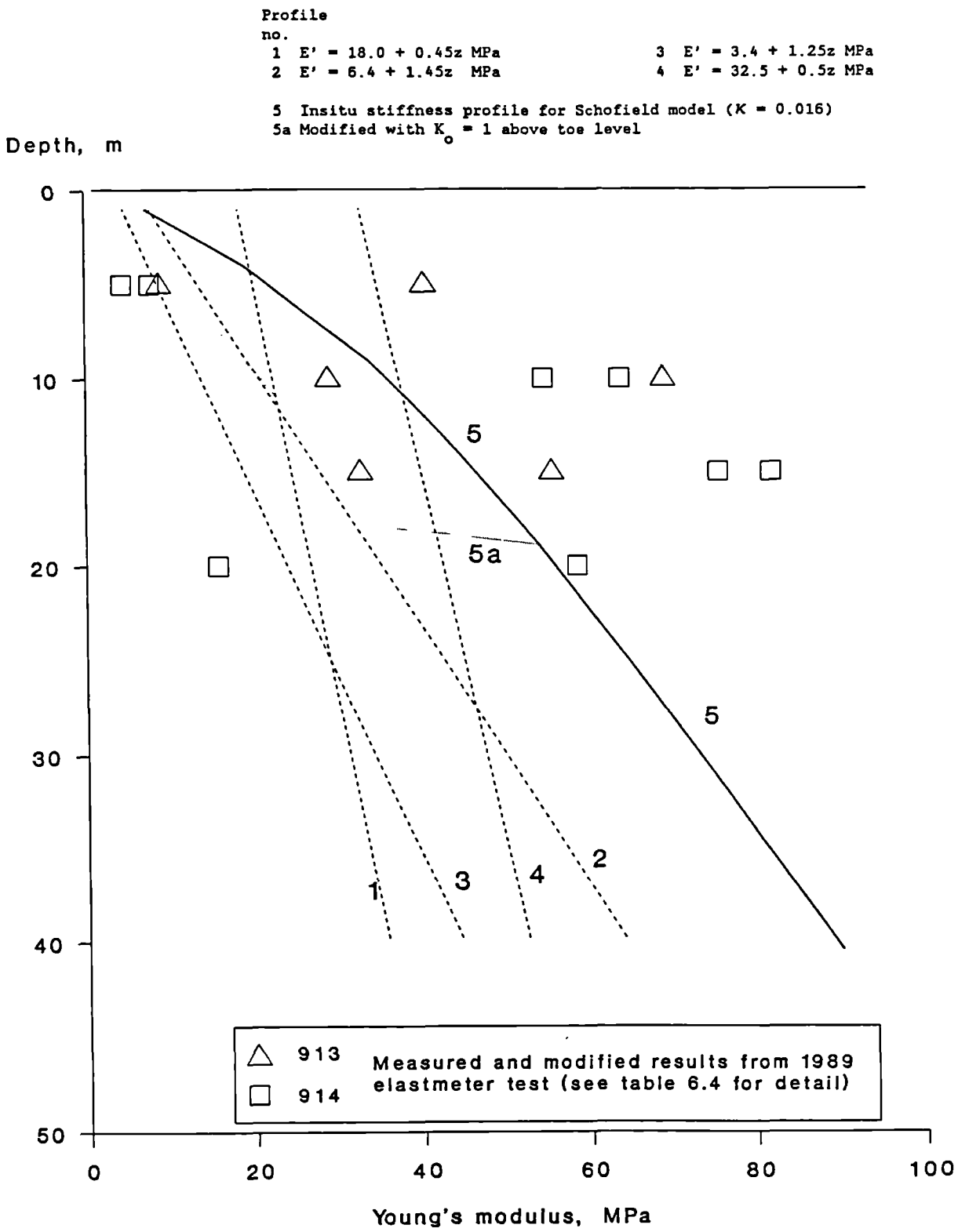

Fig. 6.5 Estimated insitu soil stiffness profiles by various methods

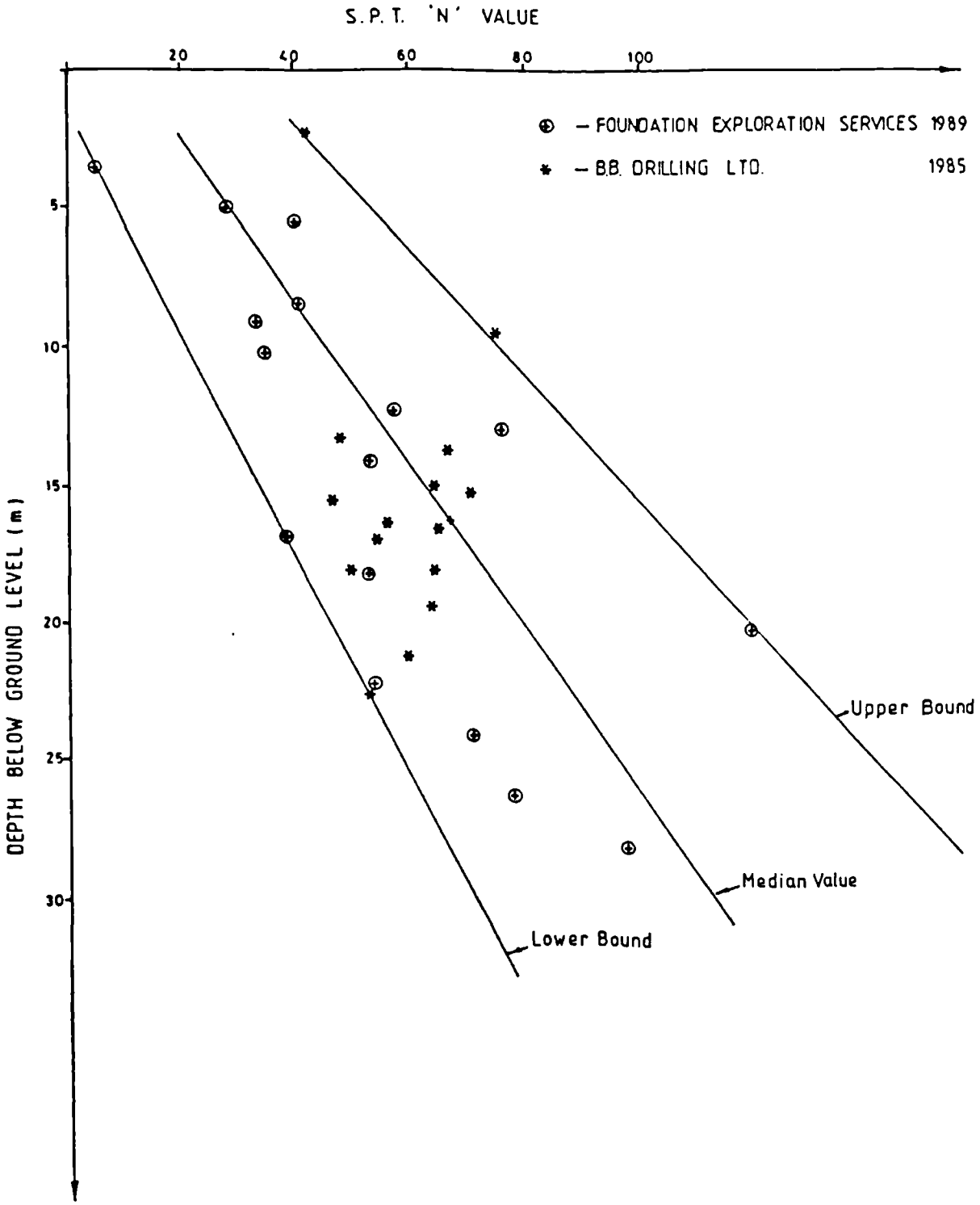

Fig. 6.6 Profiles of standard penetration test 'N' values (from figure 1, 1989 S.I.)

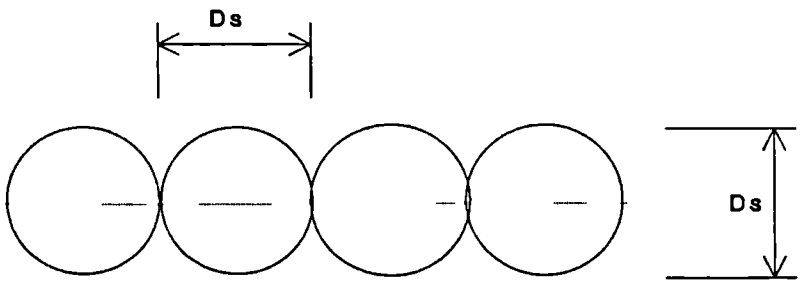

a. Secant pile

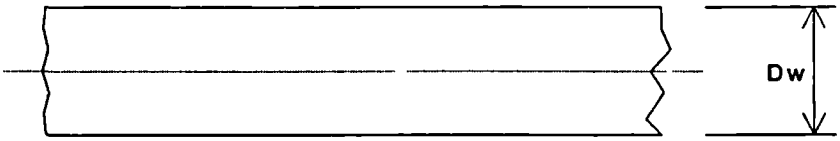

b. Diaphragm wall

For secant pile:

No. of piles per metre width = 1/Ds

2nd moment of area for circle = $\frac{\pi}{4}\left(\frac{D}{2}\right)^4$

2nd moment of area for secant pile wall = $\frac{1}{Ds}\ \frac{\pi}{4}\left(\frac{Ds}{2}\right)^4$

$= \frac{\pi}{64} Ds^3$ m^4/metre length

For diaphragm wall:

2nd moment of area = $\frac{Dw^3}{12}$ m^4/metre length

Therefore,

$$D_w = \left(\frac{12\pi}{64}\right)^{1/3} D_s$$

$$= 0.838\ D_s$$

Diameter of secant pile = 1.8m
Equivalent thickness of diaphragm wall = 1.5m

Fig. 6.7 Calculation of equivalent thickness for diaphragm wall

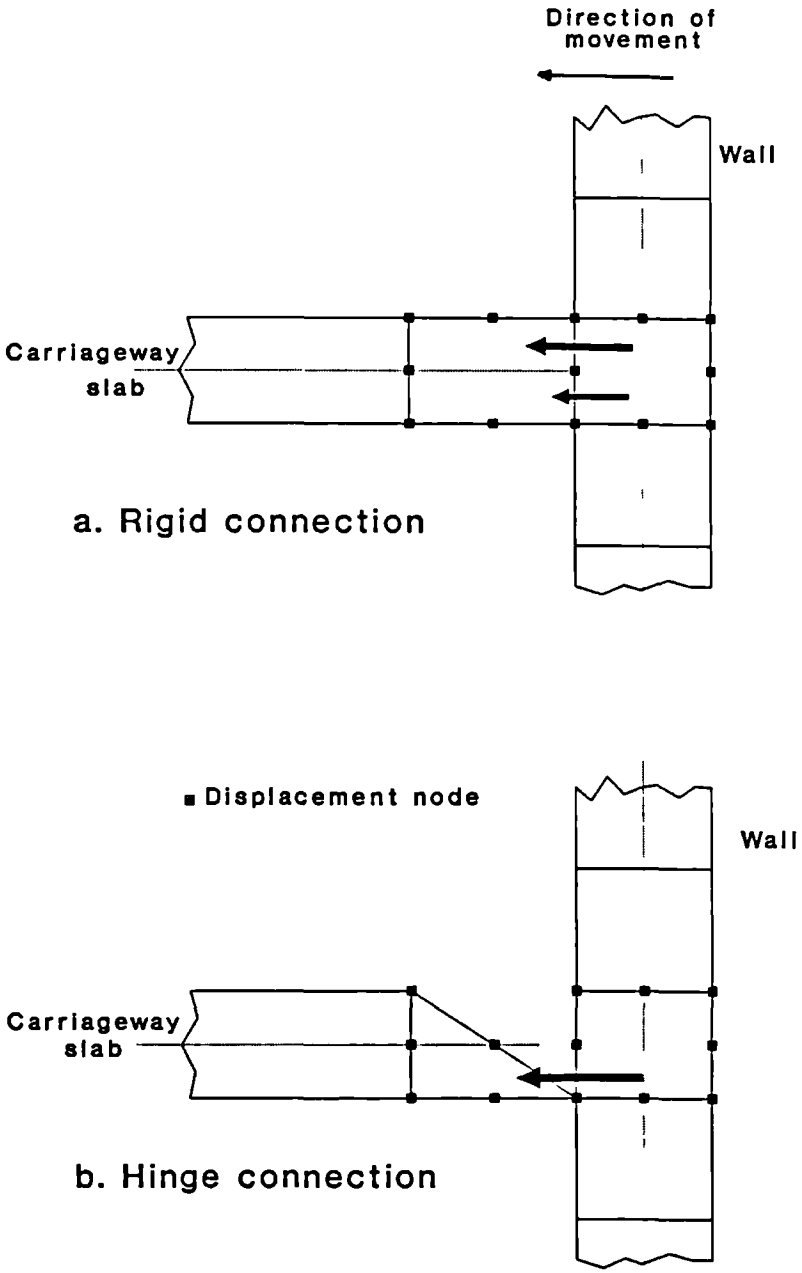

Fig. 6.8 Different connections between the retaining wall and the carriageway slab

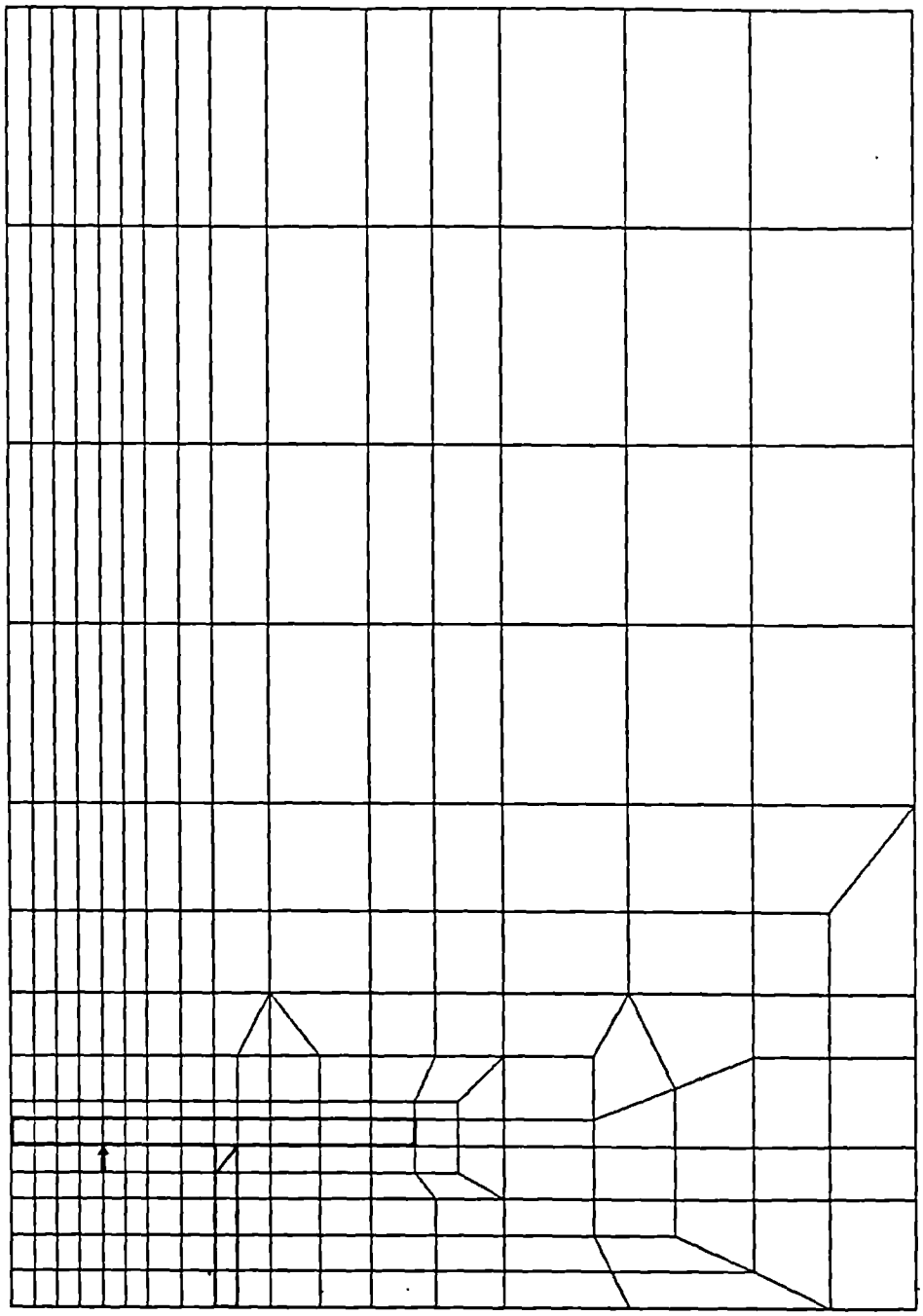

Fig. 6.9 Finite element mesh

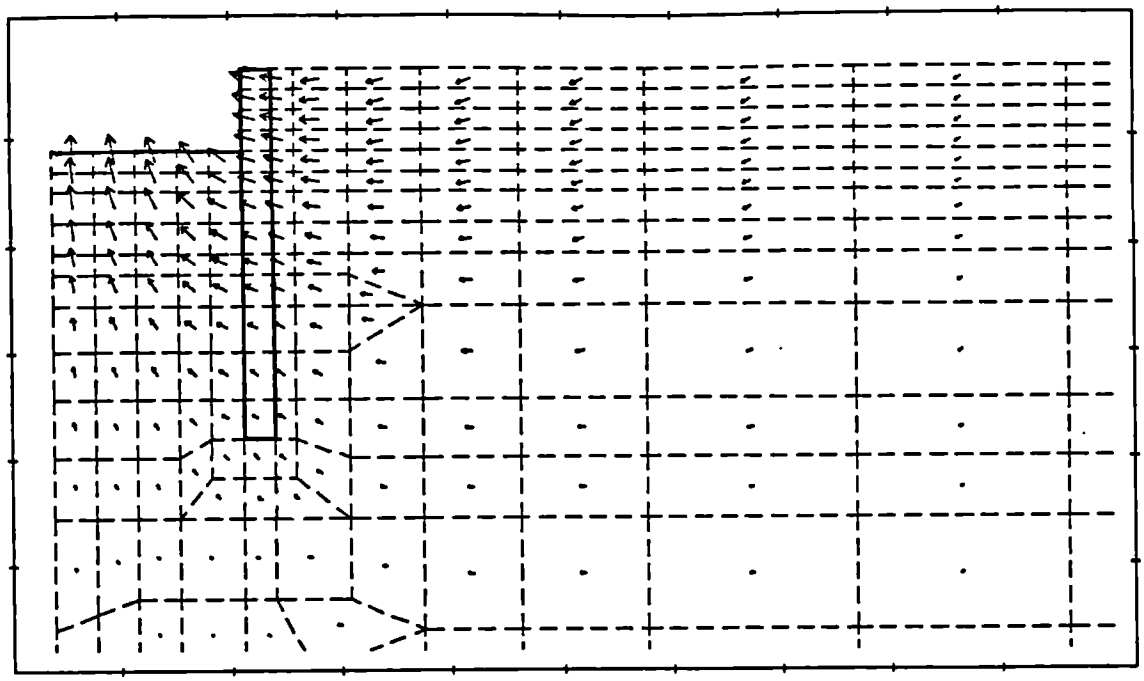

a. Stage 1

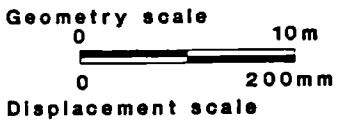

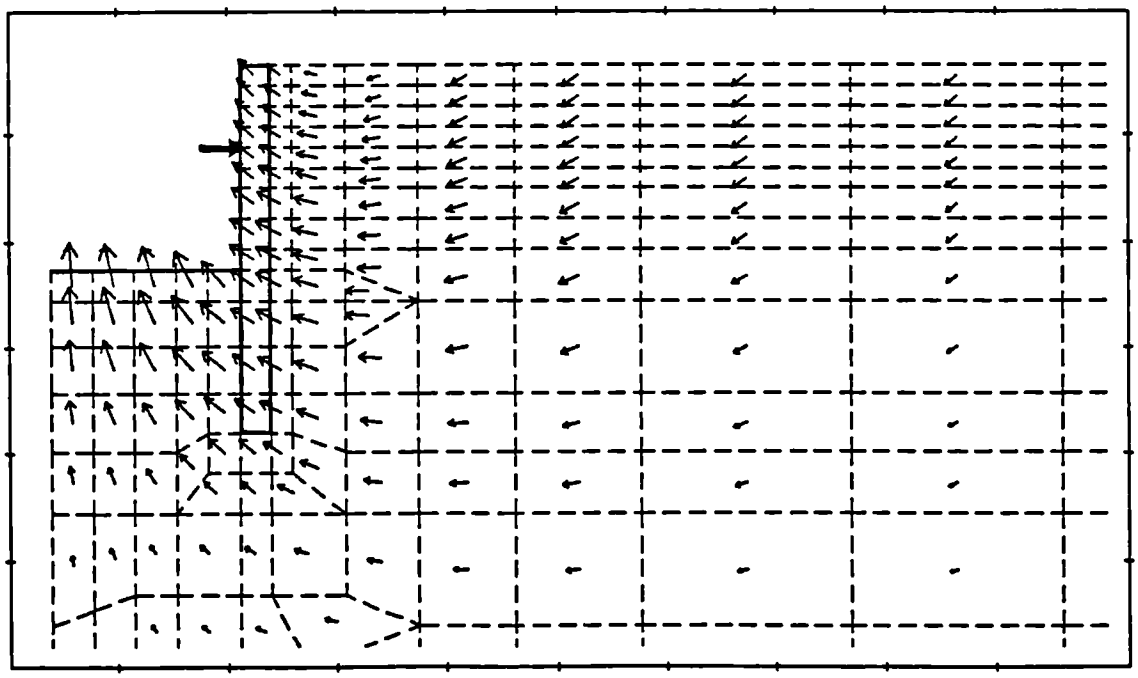

b. Stage 2

Fig. 6.10 Cumulative displacement vector diagrams

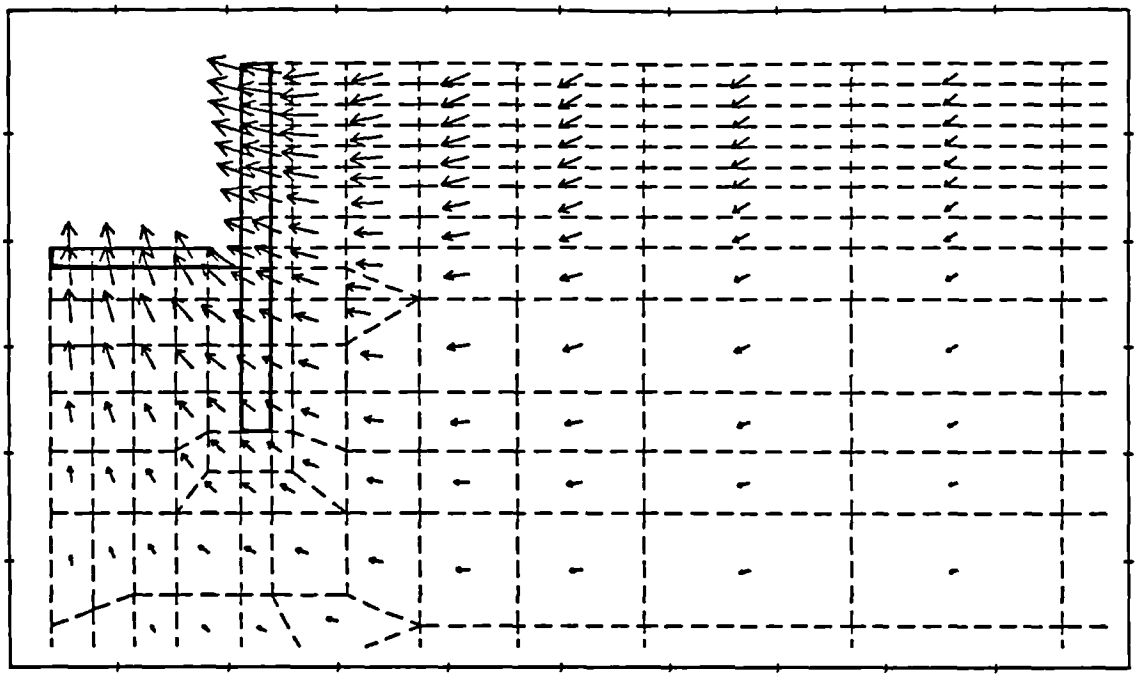

c. Stage 3

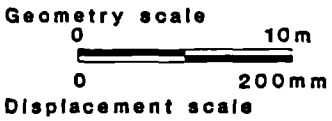

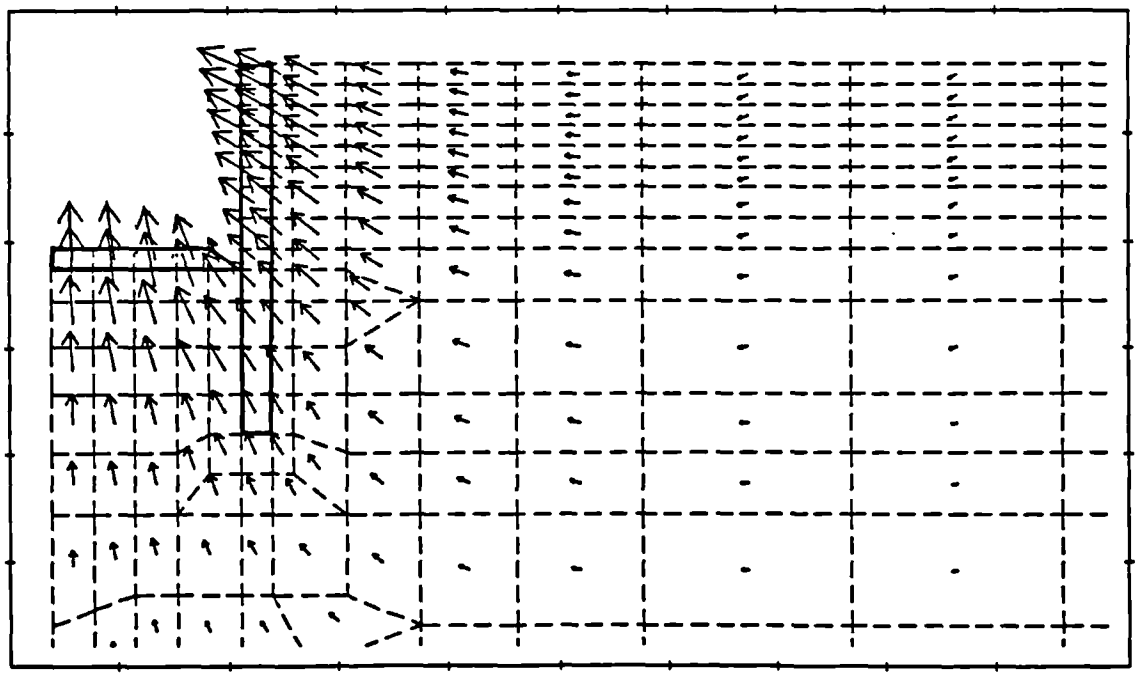

d. Stage 4 + 120 years

Fig. 6.10 Cumulative displacement vector diagrams

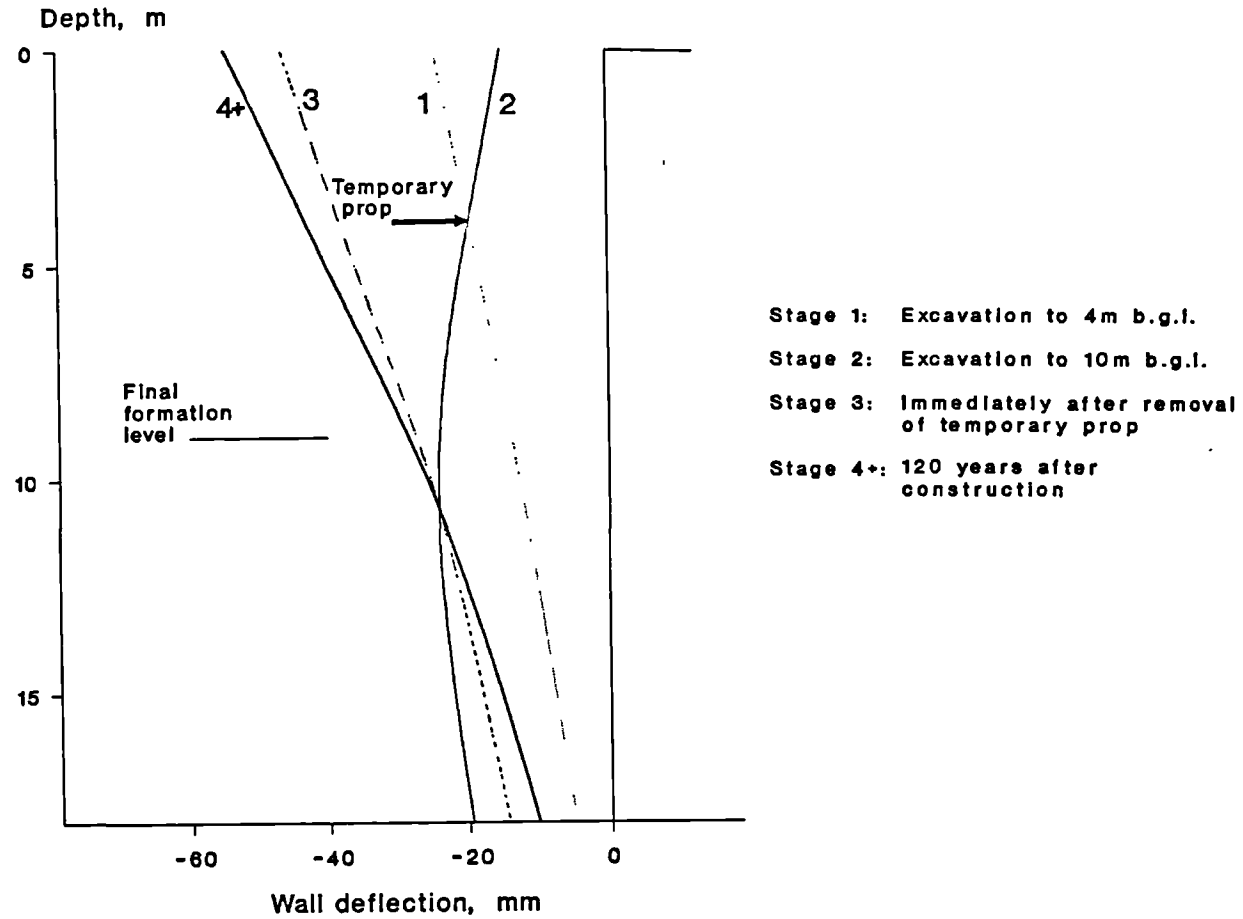

Fig. 6.11 Computed wall deflections at different stages

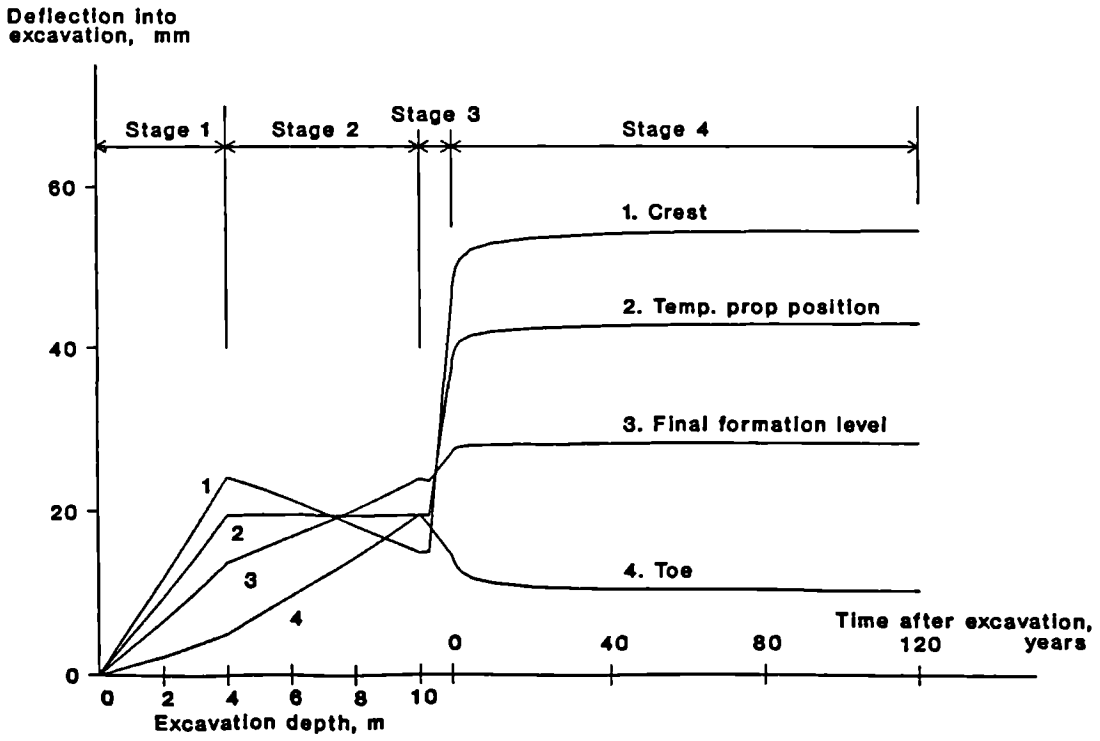

Fig. 6.12 Wall deflections against excavation and time

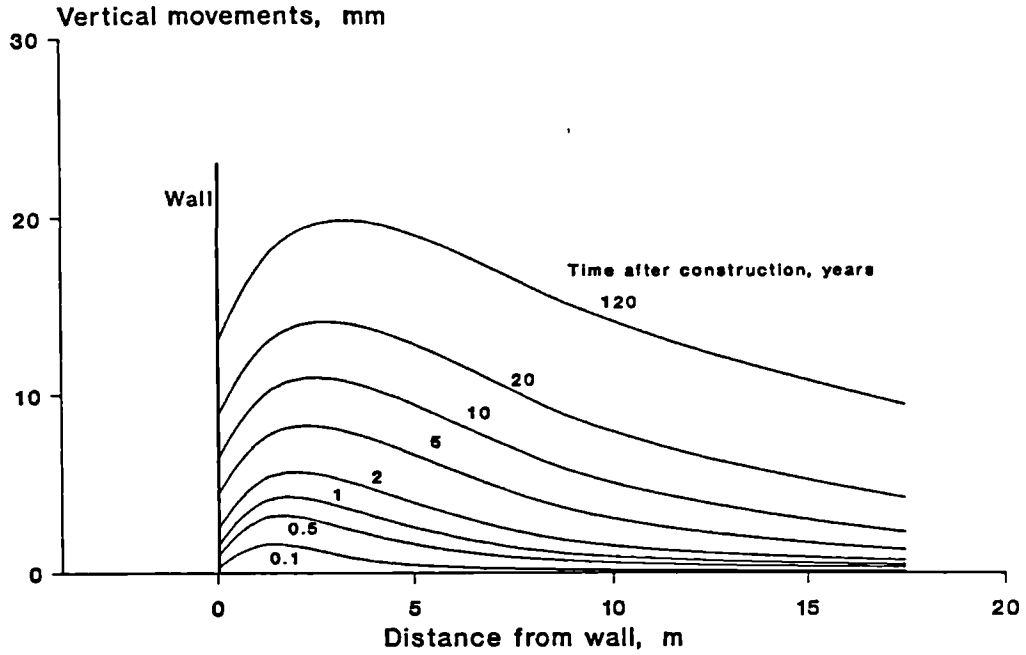

a. Vertical movements

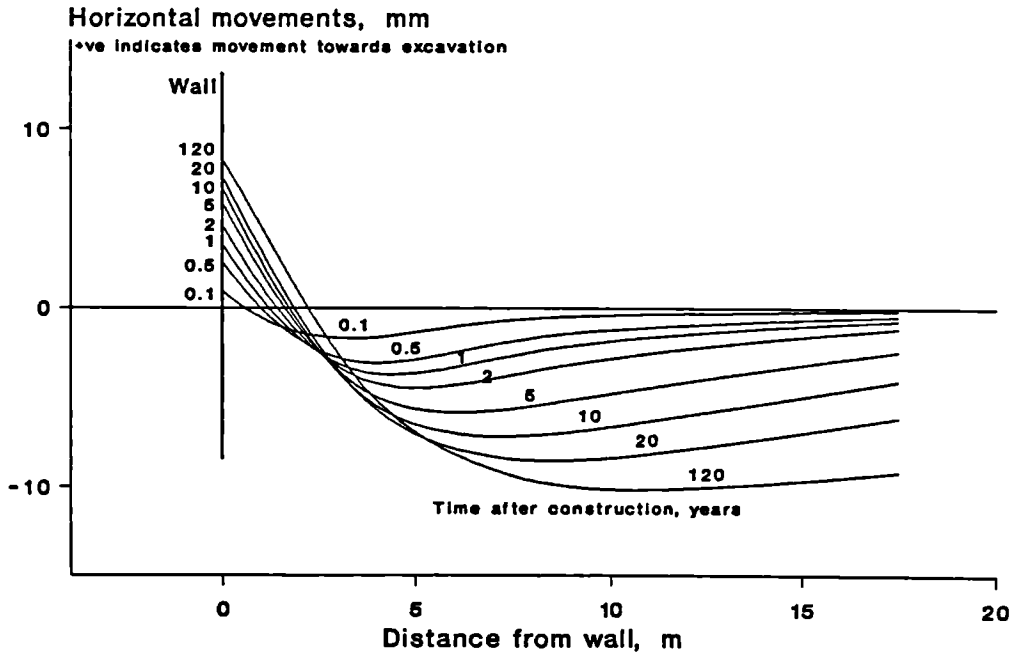

b. Horizontal movements

Fig. 6.13 Post-construction surface movements in retained soil

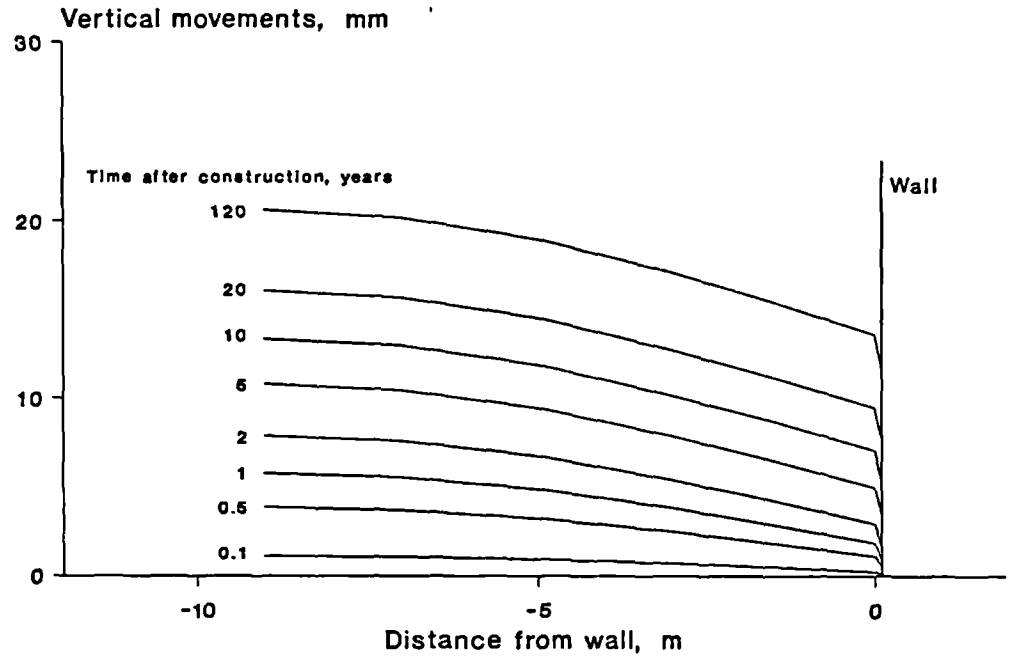

Fig. 6.14 Post-construction vertical surface movements on excavated side

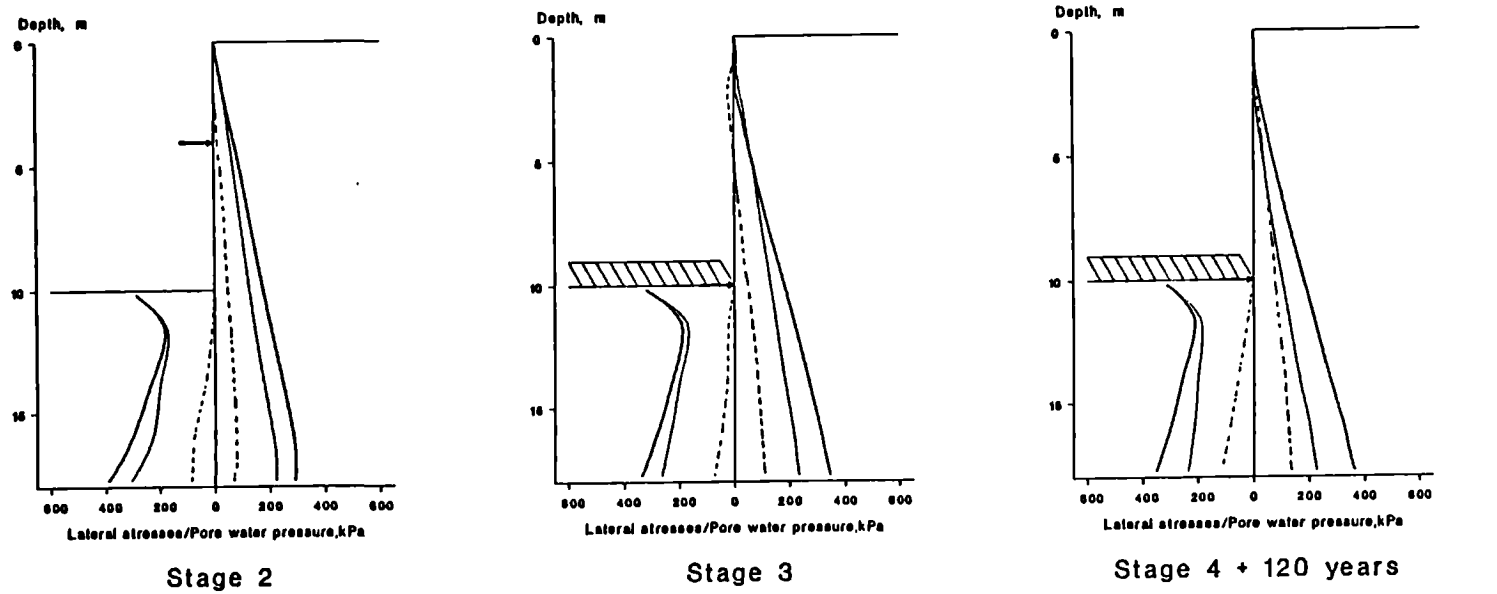

Fig. 6.15 Lateral stresses and pore water pressure distributions

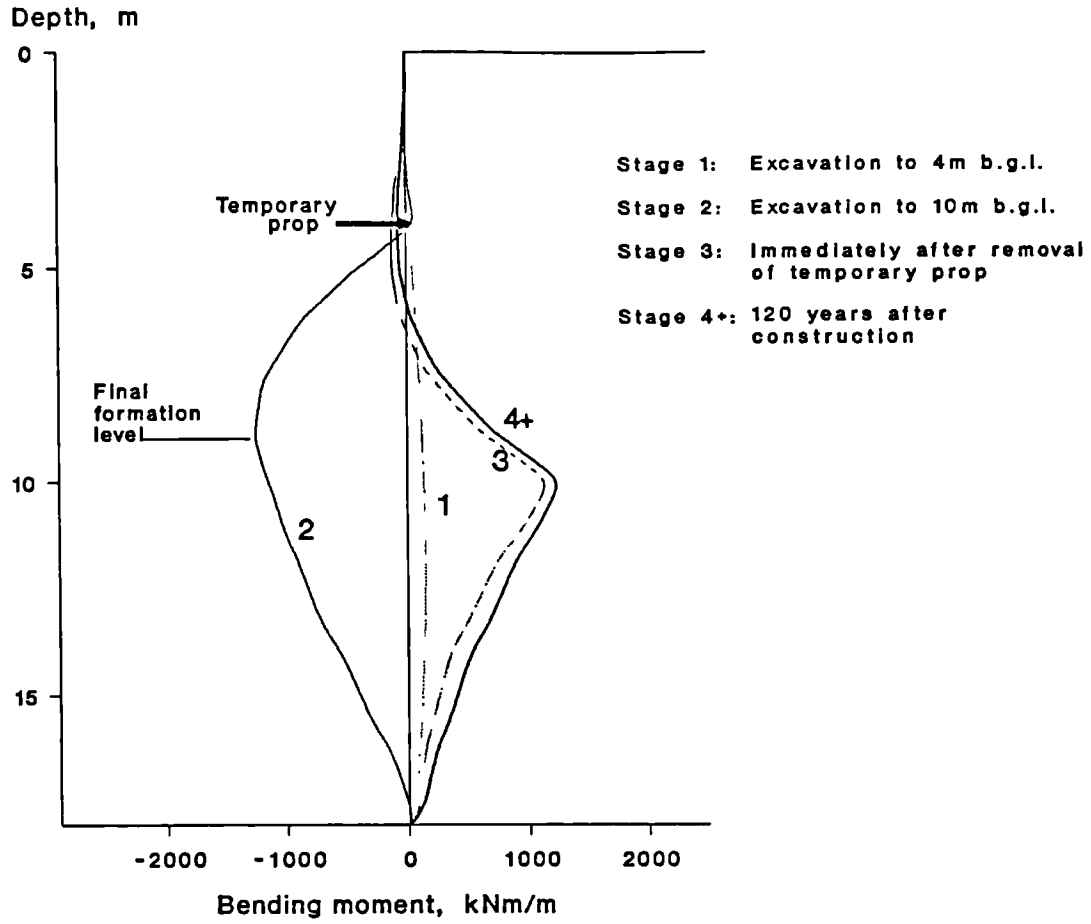

Fig. 6.16 Bending moment diagrams at various stages

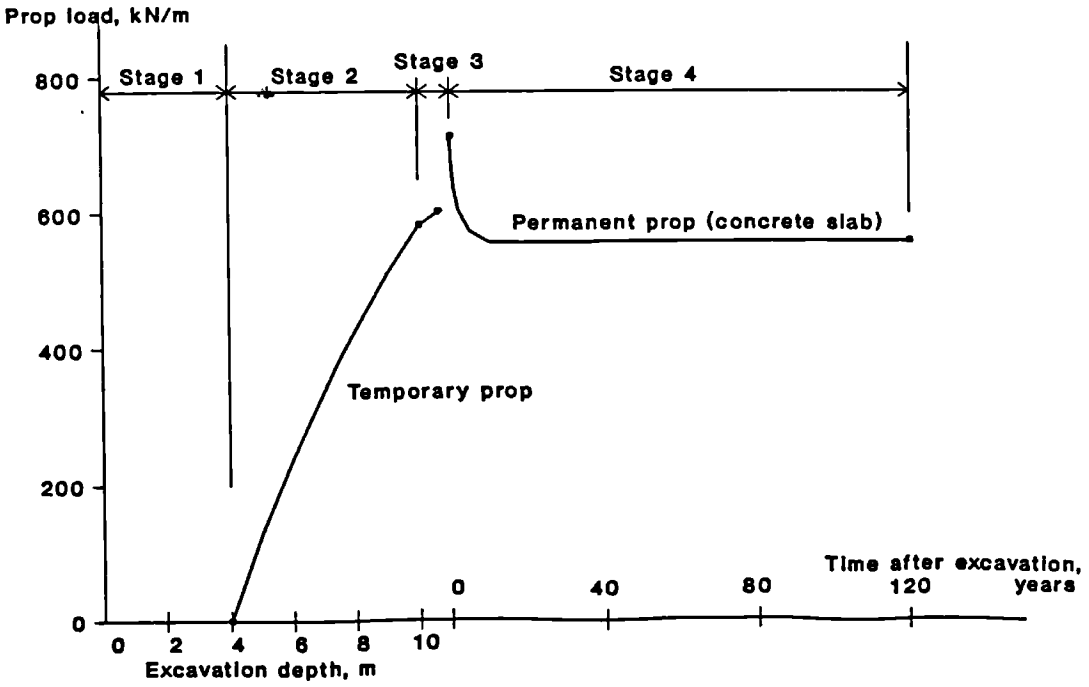

Fig. 6.17 Prop loads against excavation and time

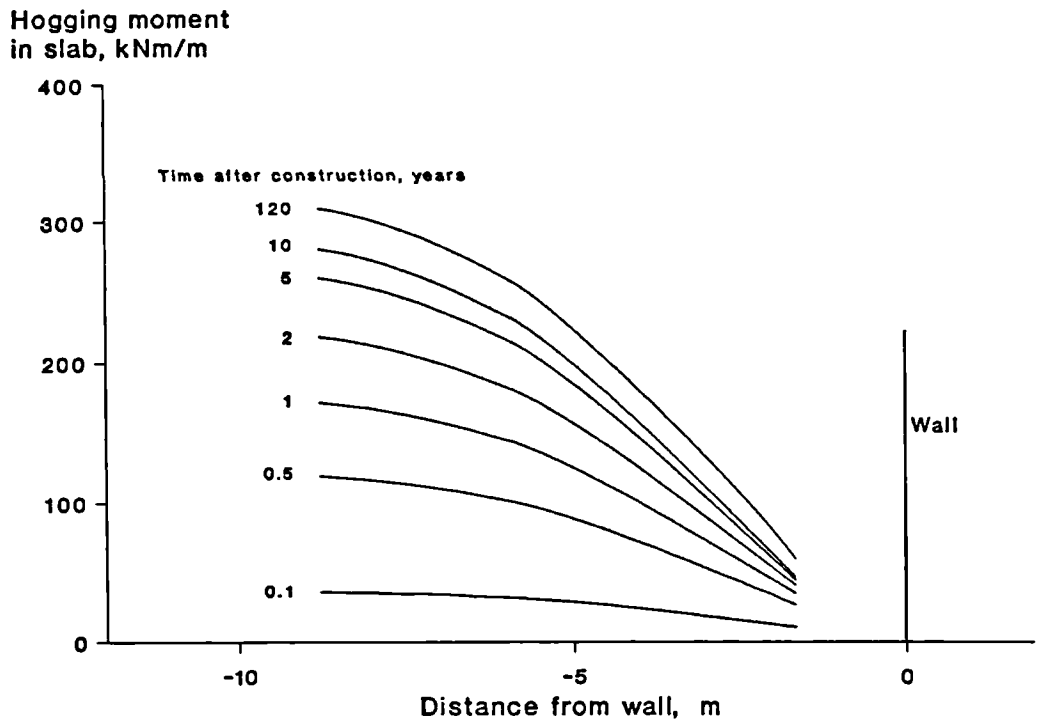

Fig. 6.18 Bending moments in carriageway slab

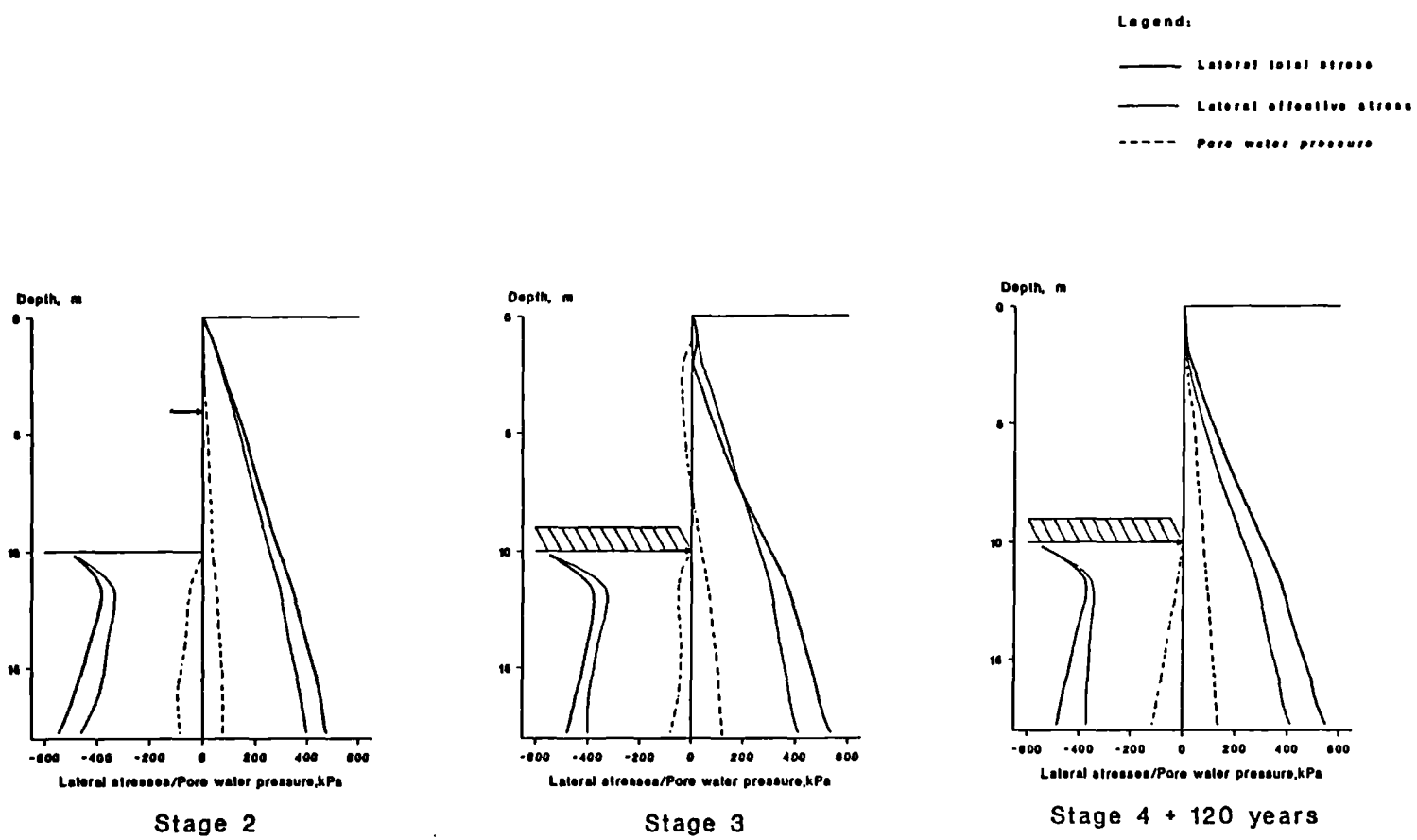

Fig. 6.19 Lateral stresses and pore water pressure distributions for case 2

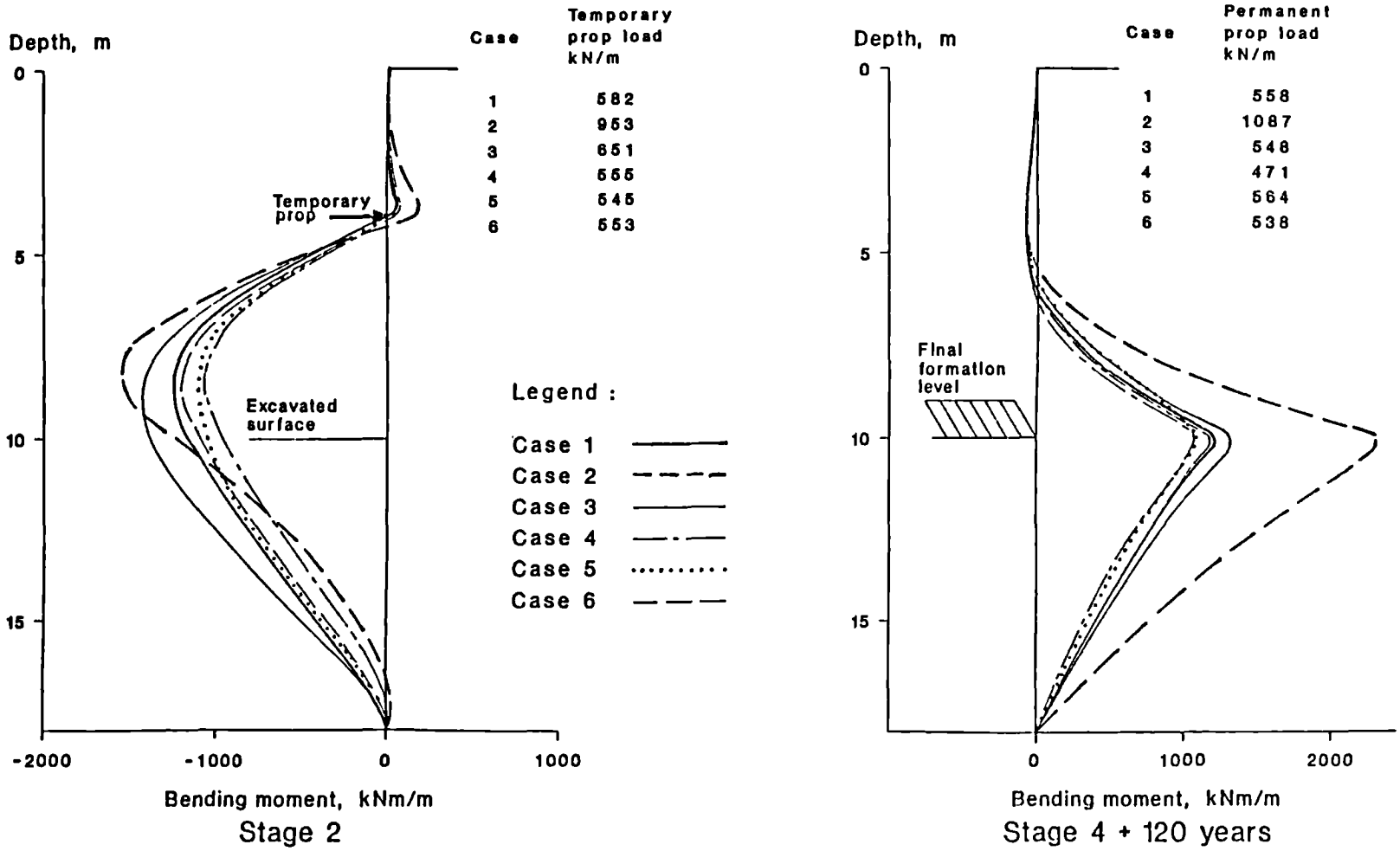

Fig. 6.20 Comparisons of wall bending moments

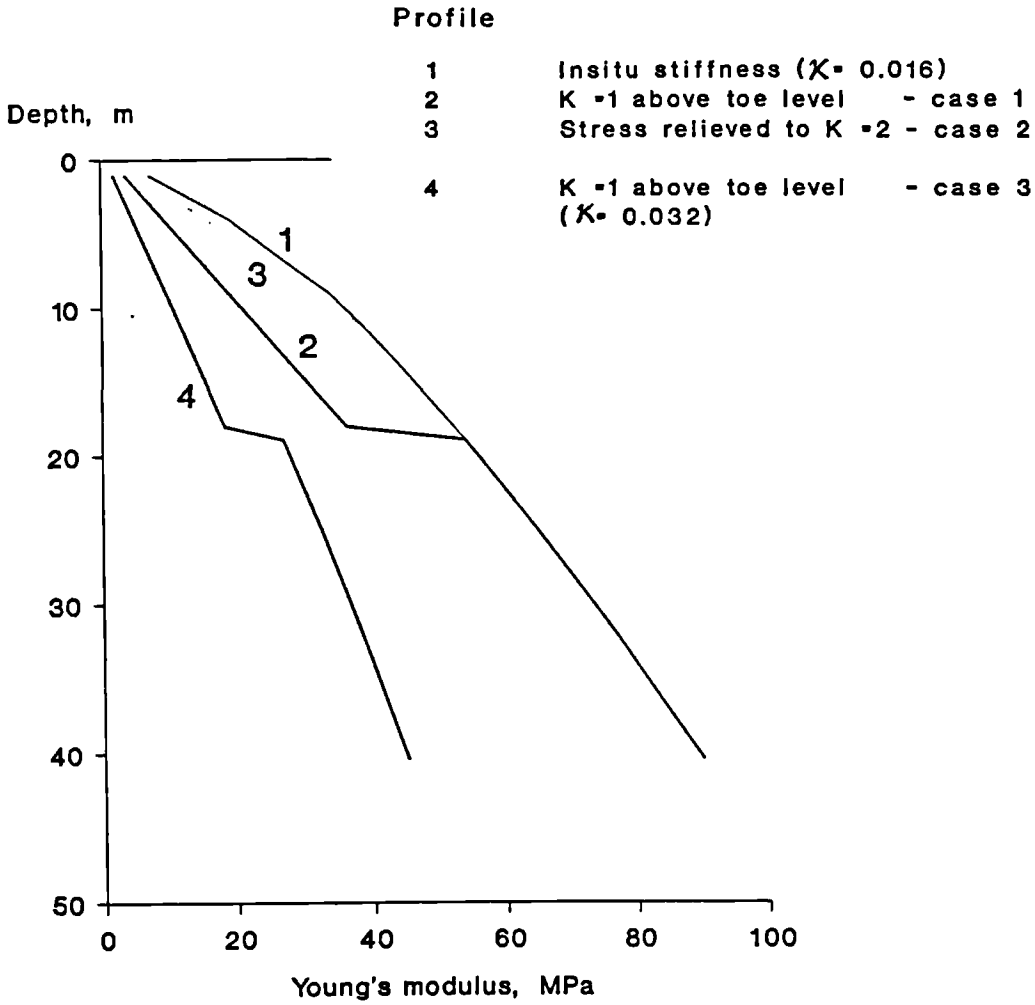

Fig. 6.21 Soil stiffness profiles used in finite element analyses

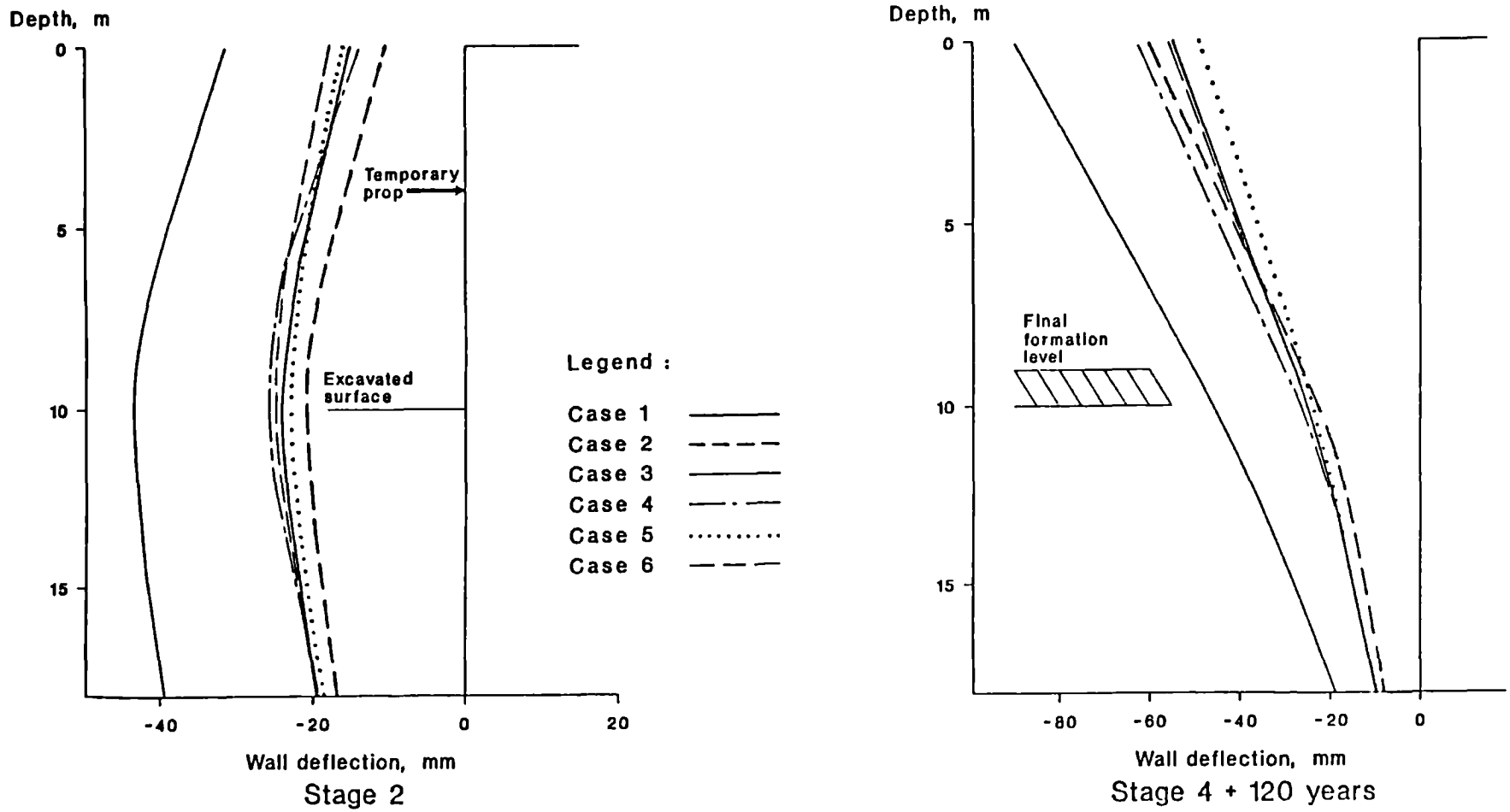

Fig. 6.22 Comparisons of wall deflections

APPENDIX A

CALCULATION OF BENDING MOMENTS

APPENDIX A - CALCULATION OF BENDING MOMENTS

In modelling diaphragm walls using 8-node linear strain quadrilateral elements, the finite element program CRISP offers four alternative methods of calculating the wall bending moments. These will be discussed in the following sections and the difficulties associated with each will be highlighted.

A.1 Method 1 - Internal Stresses

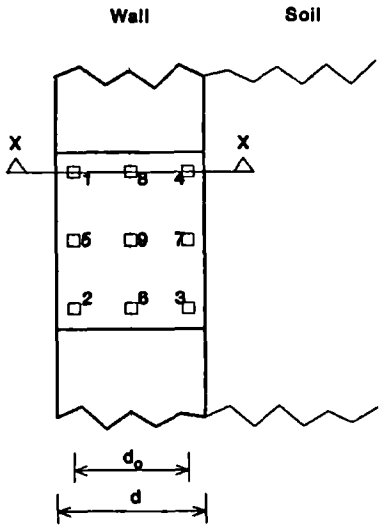

Fig. A1 Integration points of wall element

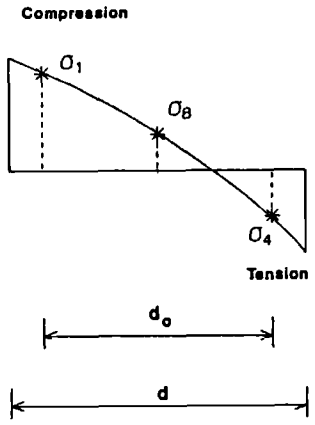

Fig. A2 Longitudinal stress across section X

This method makes use of the longitudinal stresses in the wall elements which are calculated directly from the finite element analysis (fig. A1). At any depth, the longitudinal stress across the wall element is as shown in fig.A2. The bending moment is then calculated according to standard engineering beam theory:

$$M = \int_{-d/2}^{d/2} \sigma \, y \, dy \quad \text{per unit width} \qquad \ldots\ldots (A1)$$

σ is assumed to vary linearly across the section and the distribution is determined by the stresses at the outermost integration points (i.e. points 1 and 4) and extrapolated to the wall surfaces. In such case:

$$M = \frac{(\sigma_1-\sigma_4)}{d_o} I \qquad \text{per unit width} \qquad \ldots.(A2)$$

where I = 2nd moment of area = $d^3/12$ per unit width

$d_o = 0.7746\ d$

hence $$M = 0.1076(\sigma_1-\sigma_4)d^2 \qquad \text{per unit width} \qquad \ldots.(A3)$$

In centrifuge modelling, as listed in table 2.3, the linear dimension will have to be multiplied by n (increased gravity level) to achieve the prototype scale whereas the stresses are identical in both situations. Therefore the prototype bending moments for centrifuge modelling are:

$$M = 0.1076(\sigma_1-\sigma_4)(nd)^2 \qquad \text{per unit width} \qquad \ldots.(A4)$$

In order to verify both the ability of the program CRISP to model bending behaviour and the validity of the method for calculating the bending moments, a series of analyses was carried out on a prismatic beam with standard end fixity and loading conditions, as shown in fig. A3.

In each analysis, L=10m, d=1m but the beam was modelled using different numbers of elements, resulting in different element aspect ratios (l/d). It can be seen from fig. A4c that the bending moments computed from the patch tests (case 3) - i.e. shortening the length on one side of the beam and extending on the other - using any number of elements were within 2% of those calculated from the beam theory, showing that the program is capable to handle the pure bending behaviour to a reasonable accuracy. In other tests, the results (fig. A4a & A4b) showed that if too few

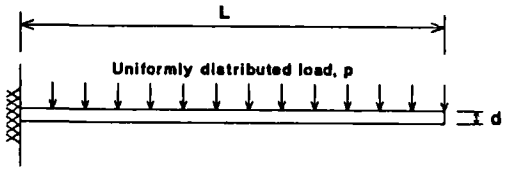

a. Case 1 : Cantilever

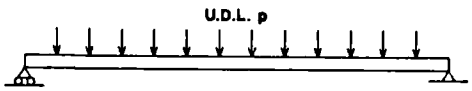

b. Case 2 : Simply support

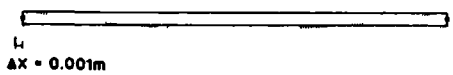

c. Case 3 : Patch test

Fig. A3 Tests on bending behaviour

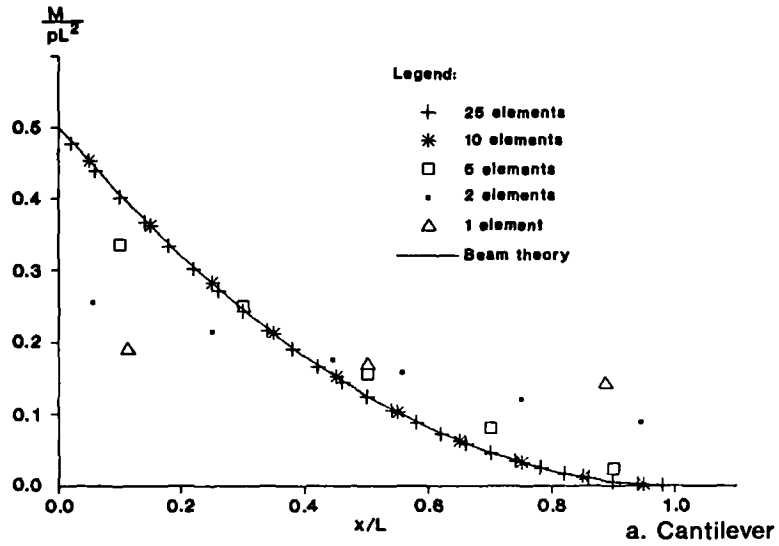

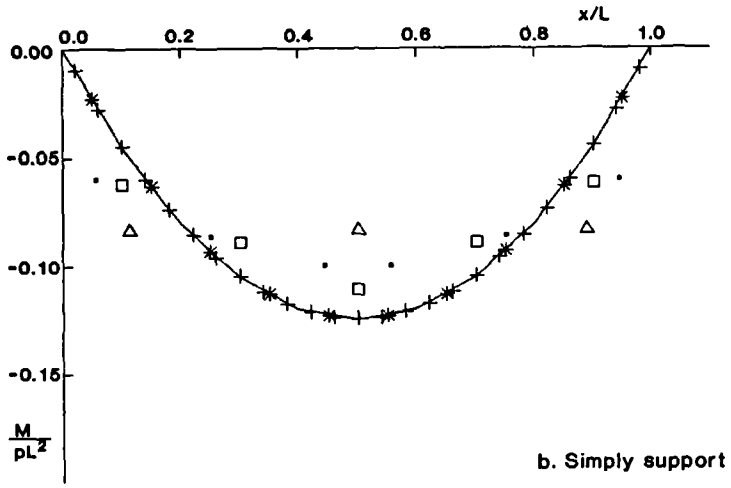

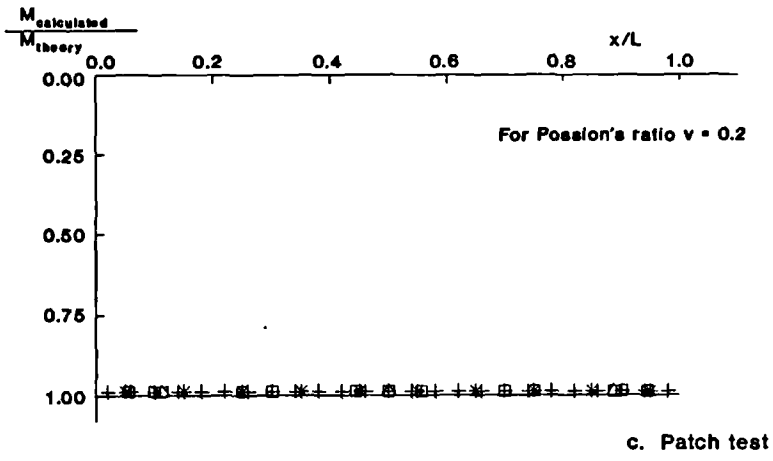

Fig. A4 Comparisons of theorectical and calculated bending moments

elements were used (1 or 2 elements), there could be a large discrepancy between the calculated and the theoretical values. Since the beam was modelled using linear strain quadrilateral elements, the displacement within each element was in the form of second order polynomial ($\delta = \int \epsilon \, dx$). However it is well known that the displacements of a uniformly loaded beam are a function of degee 4 (Case & Chilver, 1971): thus the substantial discrepency is understandable .

The results also showed that the bending moments calculated using 10 elements were very close to the theorectical values (within 1%), so that it is not justifiable to increase the number of elements further.

Although the program can calculate bending moments in isolated beams if sufficient elements are used, the applicability of this method to diaphragm walls is still uncertain. In beam theory, it is assumed that the stress is linearly distributed and the neutral axis is at the middle of the beam (unless there is an axial load). However, it is more usual that the stresses across points 1, 8 and 4 (see fig. A1) in the wall are non-linear. It may perhaps seem more appropriate to establish a stress function relating the stresses at these points and integrating the function to produce the bending moments using equation A1. On such basis, with a quadratic function and Simpson's rule for integration, the results did not show any improvement, in fact a larger discrepancy was obtained with the bending moments oscillating along the wall depth from the values calculated using beam theory. The reason for this is unclear.

A.2 Method 2 - External Stresses

This method uses the stresses at the integration points in the soil elements nearest the wall (fig. A5) to establish the horizontal stress distribution (fig. A6) acting on the

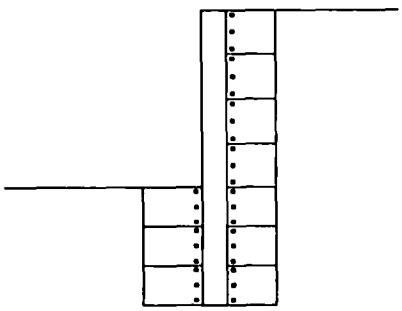

Fig. A5 Intergartion points used in method 2

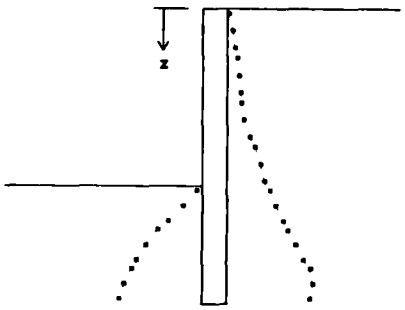

Fig. A6 Lateral stress distribution

wall surface. If the shear stresses at the soil:wall interface are ignored, the bending moment at depth 'a' will be:

$$M = \int_0^a \sigma_h \, (a-z) \, dz \qquad \text{per unit width} \qquad \ldots.(A5)$$

Again there are different methods for the integration of equation A5. The first and simplest is to assume linear stress distribution between adjacent integration points and integrate using the trapezious rule. Alternatively, Simpson's rule may be used for a quadratic expression, but calculations showed that this did not produce a significant better result. The last method involves fitting a (n-1)th degree polynomial (n is the number of points available) to the stresses concerned, taking into account the sigular points, such as the prop location or the level of the

excavated surface. Then the bending moments are calculated by analytical integration of the function. Unfortunately, although this calculation was substantially longer than the first approach, the results were in fact the worst of all three methods in comparison with the results from beam theory.

There are some sources of error associated with this method. Firstly, since the soil is "attached" to the wall, there will inevitably be shear stresses acting on the wall surface, therefore a factor due to the shear has to be added to equation A5:

$$M = \int_0^a \sigma_h \, (a-z) \, dz - A \quad \text{per unit width} \qquad \ldots.(A6)$$

At the near face (fig. A7), A=0, whereas at the far face:

$$A = \int_0^a d \, \tau \, dz$$

It can be seen that the bending moments are not unique across the section. If the bending moments at the centre of the wall are concerned:

$$M = \int_0^a \sigma_h \, (a-z) \, dz - \int_0^a d/2 \, \tau \, dz \quad \text{per unit width} \qquad \ldots(A7)$$

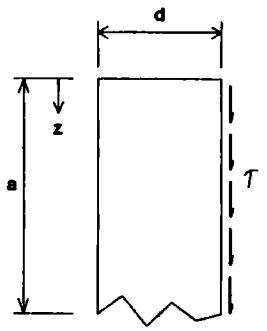

Fig. A7 Shear stress on wall surface

The error in bending moment in the top half of the wall may not be significant, since the shear force is small. Although the lever arm (d/2) for the shear component is small, the shear forces (on both sides of the wall) near the toe are substantial and lead to significant non-zero bending moments if this effect is ignored.

The term due to shear also contributes to the problem of bending moments on the wrong side of the wall for cantilevered section. For example, assume the horizontal stresses are equal to the vertical stresses (K=1) and increase linearly with depth and the soil:wall friction is δ and c=0. At depth 'a' (fig. A8), the bending moment will be:

$$M = \gamma a^3/6 - \gamma a^2 d \tan\delta /4$$

If d=1m, γ=20kN/m^3, δ=15°,

$$M = 3.33a^3 - 1.34a^2$$

and $M = 0$ when $a = 0.4$m

This implies the longitudinal stresses in the wall will be tensile on the excavated side for depths above 0.4m.

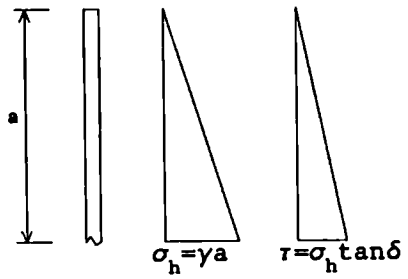

Fig. A8 Idealised stress distribution

Another source of error is the fact that the integration points are some distance (depending on the size of the elements) away from the wall. The stress variations in this vicinity may be large, and even a small distance can be significant. Sometimes, if triangular elements are used for the soil, the mid-side integration points are not in the same vertical plane as the other points. Also in displacement approach finite element analysis, the stresses in the elements are deduced by differentiation of the calculated nodal displacements and are therefore less accurate (Gunn, 1990). Any errors in the stresses will be compounded in the calculation of the bending moments progressively down the wall.

A.3 Method 3 - Stresses in Interface Elements

All the analyses in this dissertation were carried out with slip interface elements placed between the soil and the wall. Hence, in theory, the bending moments can be calculated, similarly to method 2, from the normal stresses in these elements. Since the slip elements are nearer the wall, it should yield better results. However, attempts to use this method for calculating the bending moments produced some unpredictable results, probably due to the way in which the stiffness matrix is formulated - assigning some artificial stresses ($\tau_{max}=\sigma_n'\tan\phi'$ and $\sigma_n'=0$ when slipping occurs and tension is developed) in the next load increment once the limiting values are exceeded. Therefore, this method is not used.

A.4 Method 4 - Differentiation of Nodal Displacements

It is also possible to calculate the bending moments by differentiating the wall displacements with respect to the depth ($M = -EI\ d^2y/dz^2$). This can be done by numerical differentiation but the the accuracy is obviously dependent

on the number of displacement points available. The results are particularly inaccurate near the two ends of the crest and the toe. For the same number of points, it was found that a 3-point forward or backward difference method could give reasonable solutions in comparison with the results obtained from beam theory in most circumstances and a higher order differentiation again did not guarantee better results.

A.5 Conclusion

Although each of the methods outlined above has its own drawback, it seems that using the stresses in the wall elements, i.e. method 1, can produce reasonable results with relatively less effort. Throughout this dissertation, the first method with a linear stress distribution across the section was used in calculating the bending moments, but separate checks were often carried out using the second method to ensure that the two values were in reasonable agreement.

REFERENCES

REFERENCES

1. AL-TABBAA,A. (1987)
   Permeability and Stress-Strain Response of Speswhite Kaolin, PhD Thesis. Cambridge University

2. ATKINSON,J.H. & BRANSBY,P.L. (1978)
   The Mechanics of Soils. McGraw-Hill

3. BICA,A.V.D. & CLAYTON,C.R.I. (1989)
   Limit Equilibrium Design Methods for Free Embedded Cantilever Walls in Granular Materials. Proc. I.C.E., Part 1, Vol. 86

4. BJERRUM,L., FRIMANN CLAUSEN,C.J. & DUNCAN,J.M. (1972)
   Earth Pressures on Flexible Structures.
   Proc. 5th European Conf. Soil Mech., Vol. 2, Madrid

5. BOLTON,M.D. (1979)
   A Guide to Soil Mechanics. Macmillan

6. BOLTON,M.D., BRITTO,A.M., POWRIE,W & WHITE,T.P. (1989)
   Finite Element Analysis of a Centrifuge Model of a Retaining Wall Embedded in a Heavily Over-consolidated Clay.
   Computer & Geotechnics, Vol. 7

7. BOLTON,M.D. & POWRIE,W. (1987)
   The Collapse of Diaphragm Walls Retaining Clay.
   Geotechnique, Vol. 37, September

8. BOLTON,M.D. & POWRIE,W. (1988)
   Behaviour of Diaphragm Walls in Clay Prior to Collapse.
   Geotechnique, Vol. 38, March

9. BOLTON,M.D., POWRIE,W. & STEWART,D.I. (1985)
   Diaphragm Walls in Clay, Progress Report.
   Cambridge University

10. BOLTON,M.D., POWRIE,W. & SYMONS,I.F. (1989/1990)
    The Design of Insitu Walls Retaining Over-consolidated Clay, Part 1 & 2. Ground Engineering, Vol. 22, Nov.,Dec. & Vol. 23, March

11. BRITTO,A.M. (1988)
    Private Communication.

12. BRITTO,A.M. & GUNN,M.J. (1987)
    Critical State Soil Mechanics via Finite Elements.
    Ellis Horwood

13. BURLAND,J.B. & HANCOCK,R.J.R. (1977)
    Underground Car Park at the House of Commons: Geotechnical Aspects. Structural Engineer, Vol. 55, February

14. BURLAND,J.B., POTTS,D.M. & WALSH,N.M. (1981)
The Overall Stability of Free and Propped Embedded Cantilever Retaining Walls. Ground Engineering, Vol. 14, July

15. CAQUOT,A. & KERISEL,J. (1948)
Tables for the Calculation of Passive Pressure, Active Pressure and Bearing Capacity of Foundations. Gauthier-Villars

16. CARDER,D.R. & SYMONS,I.F. (1989)
Long-term Performance of an Embedded Cantilever Retaining Wall in Clay. Geotechnique, Vol. 39, December

17. CARTER,J.P., SMALL,J.C. & BROOKER,J.R. (1977)
A Theory of Finite Elastic Consolidation.
Int. J. Solids & Structures, Vol. 13

18. CP2 (1951)
Earth Retaining Structures. British Standard Institution

19. CORSON,C.M. (1987)
Retaining Wall Design Program for BBC Micro-computer, Final Year Project. King's College, University of London

20. COULOMB,C.A. (1776)
Essai sur une Application des Regles des Maximic et Minimis á Quelques Problems de Statique Relatif á L'architecture. (Tests on the Application of Upper and Lower Bound Theories to Engineering Problems). Mem. Acad. Royal Prés. (Divers Savans)

21. DANIEL,D.E. & OLSON,R.E. (1982)
Failure of an Anchored Bulkhead. Proc. A.S.C.E., J. Geotech. Engineering Div., Vol. 108 (GT10), October

22. FELLENIUS,W. (1927)
Erdstatische Berechnungen Mit Reibung und Kohasion und Unter Annahme Kreiszylindrischer Gleitflachen. (Static Calculations of Frictional and Cohesive Soils Assuming Circular Slip Surface).
Berlin

23. FINNO,R.J. & NERBY,S.M. (1989)
Observed Performance of a Deep Excavation in Clay.
Proc. A.S.C.E., J. Geotech. Engineering Div., Vol. 115 (GT8), August

24. FOURIE,A.B. (1984)
The Behaviour of Retaining Walls in Stiff Clay, PhD Thesis.
Imperial College, University of London

25. GUEST,D.R. (1990)
Experimental and Analytical Analysis of Reinforced Embankment on Soft Foundation, PhD Thesis.
King's College, University of London

26. GUNN,M.J. (1990)
Calculations of Bending Moments, Private Notes

27. HARR,M.E. (1966)
Foundations of Theorectical Soil Mechanics. McGraw-Hill

28. HUBBARD,H.W., POTTS,D.M., MILLER,D. & BURLAND,J.B. (1984)
Design of the Retaining Walls for the M25 Cut and Cover Tunnel at Bell Common. Geotechnique, Vol. 34, September

29. HVORSLEV,M.J. (1937)
Uber die Festigkeitseigenschaften Gestorter Bindiger Boden. (The Properties of the Ruptured Soil).
Igeniorvidenskabelige Skrifter A No. 45, Kobenhavn

30. IRONS,B.M. & AHMAD,S. (1980)
Techniques of Finite Elements. Ellis Horwood

31. JAKY,J. (1944)
The Coefficients of Earth Pressure at Rest. J. Soc. Hungarian Architects & Engineers, Budapest, October

32. JARDINE,R.J., POTTS,D.M., FOURIE,A.B. & BURLAND,J.B. (1986)
Studies of the Influence of Non-Linear Stress-Strain Characteristics in Soil-Structure Interaction. Geotechnique, Vol. 36, June

33. LI,E.S.F. (1986)
The Stability of Propped Embedded Retaining Wall in Frictional Soil, Final Year Project. King's College, University of London

34. MAYNE,P.W. & KULHAWY,F.H. (1982)
Ko-OCR Relationship in Soil. Proc. A.S.C.E., J. Geotech. Engineering Div., Vol. 108 (GT6), June

35. NAVFAC DM7 (1982)
Design Manual: Soil Mechanics, Foundations and Earth Structures.
U.S. Dept. of Navy, Washington D.C.

36. PADFIELD,C.J. & MAIR,R.J. (1984)
Design of Retaining Walls Embedded in Stiff Clays.
CIRIA, Report 104

37. POTTS,D.M. & FOURIE,A.B. (1984)
The Behaviour of a Propped Retaining Wall: Results of a Numerical Experiment. Geotechnique, Vol. 34, June

38 POTTS,D.M. & FOURIE,A.B. (1985)
The Effects of Wall Stiffness on the Behaviour of a Propped Retaining Wall. Geotechnique, Technical Notes, Vol. 35, June

39. POTTS,D.M. & FOURIE,A.B. (1989)
Comparison of Finite Element and Limiting Equilibrium Analyses for an Embedded Cantilever Retaining Wall.
Geotechnique, Vol. 39, March

40. POWRIE,W. (1986)
The Behaviour of Diaphragm Walls in Clay, PhD Thesis.
Cambridge University

41. POWRIE,W. & LI,E.S.F. (1989)
A1058 Cradlewell Bypass, Analysis of the Behaviour of the Holy Trinity Retaining Walls, Draft Interim Report.
Newcastle-Upon-Tyne City Council

42. RANKINE,W.J.M. (1857)
On the Stability of Loose Earth. Proc. Royal Society

43. REDULIC,L. (1935)
Ein Beitrag zur Bestimmung der Gleitsicherheit.
(An Essay on Definition of Slipping). Der Bauingenieur

44. ROWE,P.W. (1952)
Anchored Sheet-Pile Walls. Proc. I.C.E., Part 1, Vol. 1,

45. ROWE,P.W. (1955a)
A Theorectical and Experimental Analysis of Sheet-Pile Walls.
Proc. I.C.E., Part 1, Vol. 4

46. ROWE,P.W. (1955b)
Sheet-Pile Walls Encastré at the Anchorage.
Proc. I.C.E., Part 1, Vol. 4

47. SCHOFIELD,A.N. (1980)
Cambridge Geotechnical Centrifuge Operations, 20th Rankine Lecture. Geotechnique, Vol. 30, March

48. SCHOFIELD,A.N. & WROTH,C.P. (1968)
Critical State Soil Mechanics. McGraw-Hill

49. SCOTT,C.R. (1980)
An Introduction to Soil Mechanics and Foundations.
Applied Science Publishers

50. SITE INVESTIGATION REPORTS:
1966 S.I. for Coast Road Extension
1972 Tyneside Rapid Transport System S.I.
1985 Cradlewell S.I.
1989 Supplementary Cradlewell S.I.

51. SMITH,I.M. & BOORMAN,R. (1974)
The Analysis of Flexible Bulkheads.
Proc. I.C.E., Part 2, Vol. 57

52. SOKOLOSKII,V.V. (1960)
Statics of Granular Media. (English translation by JONES,D.H. & SCHOFIELD,A.N.). Pergamon Press

53. STEWART,D.I. (1990)
Forthcoming PhD Thesis. Cambridge University

54. STROUD,M.A. & BUTLER,F.G. (1975)
The SPT and the Engineering Properties of Glacial Materials. Proc. Symp. Engineering Behaviour of Glacial Materials, Birmingham

55. TAYLOR,R.N. (1984)
Ground Movements Associated with Tunnels and Trenches, PhD Thesis. Cambridge University

56. TEDD,P., CHARD,B.M., CHARLES,J.A. & SYMONS,I.F. (1984)
Behaviour of a Propped Embedded Retaining Wall in Stiff Clay at Bell Common Tunnel. Geotechnique, Vol. 34, Sept.

57. TERZAGHI,K. (1936)
The Shearing Resistance of Saturated Soil and the Angle Between the Planes of Shear. Proc. 1st Int. Conf. Soil Mechanics, Massachusetts

58. TERZAGHI,K. (1943)
Theorectical Soil Mechanics. John Wiley

59. TERZAGHI,K. & PECK,R.N. (1948)
Soil Mechanics in Engineering Practice. Johy Wiley

60. WEBB,C. (1989)
Precast Hinge Counters Clay Heave Under London's North Circular, Technical Report. Highways, June

61. WHITE,T.P. (1987)
Finite Element Calculations Involving the Yielding of Dilatant Soil, MPhil Dissertation. Cambridge University

62. WROTH,C.P. (1975)
In-situ Measurement of Initial Stresses and Deformation Characteristics. Proc. Speciality Conf. In-situ Measurement of Soil Properties, A.S.C.E., North Carolina

63. ZIENKIEWICZ,O.C. (1967)
The Finite Element Method in Structural and Continuum Mechanics. McGraw-Hill